# *Soil Moisture Estimation for landslide monitoring: A new approach using multi-temporal Synthetic Aperture RADAR data*

THOMAS CHARLIE JAMES BLISS

# Soil Moisture Estimation for landslide monitoring: A new approach using multi-temporal Synthetic Aperture RADAR data

Thomas Charlie James Bliss

Department of Geography

Durham University

Thesis submitted in partial fulfilment of the requirements for the University of Durham for the degree of Doctor of Philosophy

September 2020

# Declaration

I confirm that no part of the material presented in this thesis has previously been submitted for a degree in this or any other university. In all cases the words of others, where relevant, have been fully acknowledged.



Thomas Charlie James Bliss

September 2020

# Acknowledgements

They say it takes a village to raise a child. As I sit here working away in the quiet corner of a childhood friend's house, in the village in which I grew up, hundreds of miles from Durham, scrounging their internet and occasionally being brought sustaining cups of tea and words of encouragement, and look back at the many people in Durham and elsewhere who have supported me during the last few years of this project, that saying seems to be true of this thesis as well.

The biggest enablers of this thesis have been my supervisory team – Profs John Wainwright and Danny Donoghue at Durham University and Dr Colm Jordan at BGS. Their help has been essential in the production of this thesis and I'm exceptionally grateful for their unending patience, kindness and understanding during the last few years as I've wobbled my way through. It has been a pleasure to work with them and get to know them. Particular thanks must also go to Dr Andy Sowter at Geomatic Ventures, who patiently guided me through realistic approaches to processing the SAR data used in this project, and to Terri Freemantle at the Satellite Applications Catapult for her help. My thanks also to Prof Nick Rosser and Dr Dave Milledge for their comments at my progression review in 2015, which very much helped to refine the focus of this project. Thanks as well to the Natural Environment Research Council (NERC), who funded this PhD.

The staff of St John's College have played a huge part in supporting me through this thesis, whether it be in the pastoral support, friendship and guidance offered by the Senior Tutor's Office in Dr Mark Ogden, Jeanna Spencer, and Rev Susie Curtis; the support from Rev Prof David Wilkinson, and Angela Cook, or the employment given to me during my sabbatical in the maintenance team led by Alan Usher. Their prayers and practical support have been the foundation for these last few years.

A huge thanks also has to go to my willing fieldwork helpers – Dr Guy Paxman, Dr Victoria Smith, Dr Rebecca Smith, and Dr Hannah Joyce – for accepting my cake-based bribes to get them up painfully early each fieldwork day and for putting up with my terrible observational comedy on the drive to and from the field site and the antics of the sheep at the field site - a truly heroic effort! Thanks also to the members of the first cohort of the IAPETUS DTP for the camaraderie that made a very long training week on the freezing shores of Loch Lomond quite unforgettable and forged a supportive environment which many of us truly benefitted from!

Indeed, the IAPETUS DTP has been a significant part of my PhD experience, and I'd like to thank Danny and John for their roles not just as my supervisors, but also as DTP directors, for the thought and efforts they've put into making the DTP a valuable extension to the PhD experience. Particular thanks also to Prof Mark Allen, who excellently filled the director role between Danny and John's tenures, for his support over several cups of tea while things were particularly challenging.

Thanks must also be given to the super support staff in the Durham Geography department – thanks to Kathy Wood for her ability to sort any logistical conundrum I placed before her; to Merv Brown for helping me get my field kit together, often at short notice; and, last but not least, to Jean Swales who masterminded the production of the vast quantities of tea and toast in the Manley Room which fuelled much of the early production of this thesis.

The final throes of this thesis effort stand out particularly right now, and they have not occurred in the most stable of environments. So, thank you to Gemma, Joel, Toby and Archie Snape, the whole Lhermette family and Tricia and Adrian Pinington for variously hosting me, feeding me, keeping me sane, and providing me with internet access in the last push of this thesis, which coincided with a move and a pandemic! Thanks to the wonderful bunch of old-Johnians that is Will and Abi Deadman, Jonathan and Janet Berry, Ant Cooper, Ana Walpole and Edmund Waddelove for their prayers and for many adventures during the course of the thesis.

A huge thanks to Mum and Dad and the rest of my family. Mum and Dad have supported me hugely over the many years of being a student, with much patience and love. Thanks also to my extended family who were responsible for a large quantity of chocolate which arrived on my doorstep and was consumed during the last couple of months' final push!

Lastly, a massive thanks to my church family at St Nic's Durham, and, in particular, everyone who's been a member of the twenties and thirties community there who have prayed for me and this thesis every week for the past 5 years – from the fears of driving the behemoth that was the departmental Ranger, to the fiddlyness of SAR processing; all of these have been placed before God, and I am forever indebted to these people who have supported me in every situation and been my Durham family. They have pointed me back every time to the God who loves us more than we can imagine and has a plan for us, even when we can't see it for ourselves – to Him be the glory!

# Dedication

To Mum and Dad

and

In memory of a great friend, Ruth Trigger, who sadly died during the writing of this thesis.

*I lift up my eyes to the mountains — where does my help come from?*

*My help comes from the Lord, the Maker of heaven and earth.*

*He will not let your foot slip — he who watches over you will not slumber;*

*indeed, he who watches over Israel will neither slumber nor sleep.*

*The Lord watches over you— the Lord is your shade at your right hand;*

*the sun will not harm you by day, nor the moon by night.*

*The Lord will keep you from all harm— he will watch over your life;*

*the Lord will watch over your coming and going, both now and forevermore.*

*Psalm 121*

# Table of Contents

# List of Figures

.

List of Tables

# List of Abbreviations

AIEM – Advanced Integral Equation Model

ASI – Italian space Agency

BGS – British Geological Survey

CEH – Centre for Ecology and Hydrology

CRNS – Cosmic Ray Neutron Sensing

CSG – COSMO-SkyMed (Second Generation)

CSK – COSMO-SkyMed (First generation)

DEM – Digital Elevation Model

DTM – Digital Terrain Model

GCOS - Global Climate Observing System

HH – Horizontal-Horizontal Polarised SAR

HV – Horizontal-Vertical Polarised SAR

IEM – Integral Equation Model

InSAR – Interferometric Synthetic Aperture RADAR

LIA – Leaf Area Index

LiDAR – Light Detection and Ranging

NDVI – Normalised Difference Vegetation Index

SAR – Synthetic Aperture RADAR

SM – Soil Moisture

TDR – Time Domain Reflectometry

TLS – Terrestrial Laser Scanning

TSX – TerraSAR-X (SAR Platform)

VH – Vertical-Horizontal Polarised SAR

VV - Vertical-Vertical Polarised SAR

VWC – Volumetric Water Content

$\sigma^0$ – sigma nought – backscatter coefficient

# 1

# CHAPTER 1: INTRODUCTION

The Fifth Assessment Report of the IPCC (Stocker *et al.*, 2013) indicates that for a range of climate futures precipitation regimes will alter considerably, with extreme events more likely under several models. This has significant implications for the monitoring of precipitation-driven hazards at multiple scales worldwide. On account of these changing regimes and the need to better anticipate geomorphological responses to them, it is necessary for us to explore effective means of monitoring precursory conditions of hazard events and to assess those monitoring methods. Hydraulically driven mass movements of soil, accounted for an estimated 89.6 % of landslide fatalities globally in 2007 (Petley, 2008) and have the potential to damage infrastructure (Eriksson *et al.*, 2009), as well as built (Malone, 2004), and natural (Malamud *et al.*, 2004) resources. These mass movements are caused by a reduction in the material strength of the slope, the increased loading of a slope mass or a combination of both (Terlien, 1996), all engendered by changes in the moisture content of the slope mass and resulting in a reduction of the stability of the slope (Crosta and Frattini, 2001).

The monitoring of slope conditions prior to an anticipated precipitation event is important, as it enables assessment of the likelihood of slope deformation or failure from a precipitation event. That is, by knowing the moisture levels of the soil mass prior to further moisture potentially entering the soil mass, it is possible, when the thresholds for stability are known, to make informed decisions around whether slope failure is likely with further precipitation. Traditionally, the measurement of soil moisture has been undertaken in one of two ways – either remotely or *in situ* - where *in situ* capacitance-based probes are positioned in the soil mass at depths appropriate to the research being undertaken (Vereecken *et al.*, 2008) and / or destructive sampling (Schmugge *et al.*, 1980). Despite its advantages in enabling measurement at depth, this point-based methodology coupled with spatial interpolation is problematic even when dealing with field-scale monitoring due to

the high spatial heterogeneity of soil moisture (Giacomelli *et al.*, 1995); interpolated to catchment or regional scales it is an even less valuable means of assessing such a significant environmental variable (Wagner *et al.*, 2003; Santi *et al.*, 2013); in addition to this, the inefficiencies in terms of time and resources in taking measurements or implementing even small-scale built-in monitoring systems (Kornelsen and Coulibaly, 2013) and it becomes apparent that *in situ* monitoring approaches are limited in their appropriateness for assessing soil moisture, unless at the smallest of spatial scales, and impossible in any context where the site of interest is one that is not physically accessible, which is often the case. Therefore over the last few decades, remote sensing of soil moisture using a range of different aerial or satellite platforms has become increasingly common – originally in the form of optical or thermal sensing, but now, increasingly through RADAR platforms and, in particular, through the higher resolution Synthetic Aperture RADAR (SAR) platforms (Carlson *et al.*, 1994; Njoku *et al.*, 2003; Kerr, 2007). This thesis will focus on the capacity of one of the most recently launched X-band SAR constellations for use in monitoring soil moisture at a landslide test site.

SAR has particular potential as a technology for enabling remote sensing of the precursory conditions of major precipitation events. It is a form of active radar remote sensing that uses the motion of the sensing platform to increase the size of the effective aperture of the sensor, thereby increasing the resolution of the images it takes. It works by emitting a pulse of electromagnetic radiation at a surface and receiving this pulse back. The active nature of the sensor means that it achieves a higher resolution than passive systems. SAR has the advantage of not being affected by cloud cover, and its backscatter amplitude is directly affected by the dielectric constant of the soil it penetrates (Ulaby *et al.* 1986; Sabins, 1996). In light of the recent increase in short wavelength SAR platforms like Sentinel 1, COSMO-SkyMed, ALOS PALSAR, NovaSAR and ICEYE, and the much-improved revisit times these constellations provide for data acquisition when compared to earlier SAR platforms, SAR again represents an exciting tool, the potential utilisation of which for soil moisture estimation in complex settings has not been fully explored or defined through rigorous ground-truthed testing. Many of the recent constellations to be launched use the short X and S-band wavelengths, with these platforms offering much higher resolution images (~1m) than, for example, their C-band Sentinel 1 counterpart (~10m), but also are affected more by surface roughness (Hajnsek *et al.*, 2009). SAR has predominantly been used in landslide contexts for

the monitoring of slow-moving landslide events (Cascini *et al.* 2010) or the assessment of techniques to enable future deformation monitoring (Colesanti *et al.*, 2003; Strozzi *et al.*, 2005; Colesanti and Wasowski, 2006; Corsini *et al.*, 2006; Guzzetti *et al.*, 2009), rather than as a means of monitoring the causes of the deformations (Liu *et al.*, 2013).

In recent years constellations of SAR satellites have become more common, thereby reducing the trade-off between image resolution and return-times which had been an early stumbling block to SAR utility for environmental scientists (Kelly *et al.*, 2009). Despite the increased use of SAR in the environmental sciences for the monitoring of soil moisture, there continues to exist a significant challenge in estimating soil moisture, particularly at short wavelengths, and that is the impact of surface roughness on the backscatter return (Baghdadi *et al.*, 2002).

## 1.1 Problem setting

As established already, it is anticipated that hydraulically driven landslides are going to become a more common problem due to climate change. In situ monitoring of soil moisture is limited by the spatial coverage possible, and optical proxies for measuring moisture are limited by cloud cover and often low resolution imagery. Active aerial or satellite RADAR platforms are recognised as offering significant advantages over the more traditional optical or passive RADAR technologies (Kerr, 2007) by operating at all times of day and regardless of cloud cover, and by providing higher resolution imagery (Kerr *et al.*, 2010). Further to this, the development of constellations of satellites bearing active RADAR sensors has optimised the period between image acquisitions (Kelly *et al.*, 2009), thereby making active RADAR a commonly cited option for soil moisture monitoring (Ulaby *et al.* 1986; Shi *et al.*, 1991; Giacomelli *et al.*, 1995; Griffiths and Wooding, 1996; Sabins, 1996; Moran *et al.*, 2000; Gorrab *et al.*, 2016; Sekertekin *et al.* 2020).

There are, however, considerable challenges in monitoring soil moisture using SAR (Wagner and Pathe, 2005). Among these is the fact that other surface characteristics, like surface roughness (Ulaby *et al.* 1986) and vegetation cover (Wagner *et al.*, 1999; Hajnsek *et al.*, 2009; Capodici *et al.*, 2011; Santi *et al.*, 2012) impact upon the backscatter signal, such that it is hard to estimate the soil moisture component of the backscatter signal (Kerr *et al.*, 2010). Furthermore, the complex surface geometry of landslide-prone areas and the impact this geometry has on SAR backscatter (Njoku *et al.*, 2003), by causing image foreshortening and shadowing

together with changes in that slope surface geometry caused by landsliding or vegetation change between image acquisitions, potentially rules out the most common and simple soil moisture inversion approach: change detection.

At the time this project was begun, the majority of studies using high resolution SAR products had focussed on using them for soil moisture monitoring in agricultural contexts, not with a view to monitoring conditionally stable slopes. This thesis explores the appropriateness of using a high resolution single-polarised X-band Synthetic Aperture RADAR (SAR) product as a means of remotely sensing a primary precursory condition of slope failure – high soil moisture at a geometrically complex slow-moving landslide site. It uses Spotlight 2 data from the COSMO-SkyMed platform which became operational the year this project began.

## 1.2 Research Aim and Objectives

The aim of this project is to assess the extent to which the estimation of soil moisture at a conditionally stable / seasonally unstable slope is appropriate using single polarised X-band Synthetic Aperture Radar delivered through a satellite constellation. To meet this aim, the following objectives were established.

*Objective 1: To describe the relationship between surface soil moisture at a penetration depth equal to that of X-band SAR and moisture at depths closer to the failure plain and more representative of the wider soil mass.*

This objective is to assess whether X-band – the shortest wavelength commonly used in SAR applications – penetrates the soil to a depth at which estimated soil moisture is a useful indicator of the state of the soil mass. The surface-depth relationships explored in this objective feed into Objective 2.

*Objective 2: To assess the spatial variability of surface and subsurface soil moistures in the soil mass.*

This objective draws on the relationships found in Objective 1, exploring whether the spatial resolution of X-band Spotlight2 data is appropriate for the spatial autocorrelation of soil moisture in soils prone to landsliding.

*Objective 3: To explore the viability of using high resolution single-polarised X-band SAR for monitoring soil moisture on a geometrically complex site with limited a priori roughness knowledge.*

This objective explores how appropriate X-band SAR products are for soil moisture monitoring using high resolution imaging modes at a site that is geometrically complex, given that the majority of soil moisture estimation has been undertaken either in geometrically ideal (flat) conditions, or using large quantities of *a priori* data, or using multi-polarised imagery.

The thesis is structured so that Objectives 1 and 2, which relate to the understanding of the spatio-temporal relationships of soil moisture at multiple depths in the soil mass are examined in Chapter 4. Objective 3 is split across Chapters 5 and 6, with Chapter 5 focusing on an analysis of the coherence of the CSK data used in this project, and Chapter 6 exploring wider issues around the viability of constellation-based satellite imagery and its utilisation by different members of the academic community.

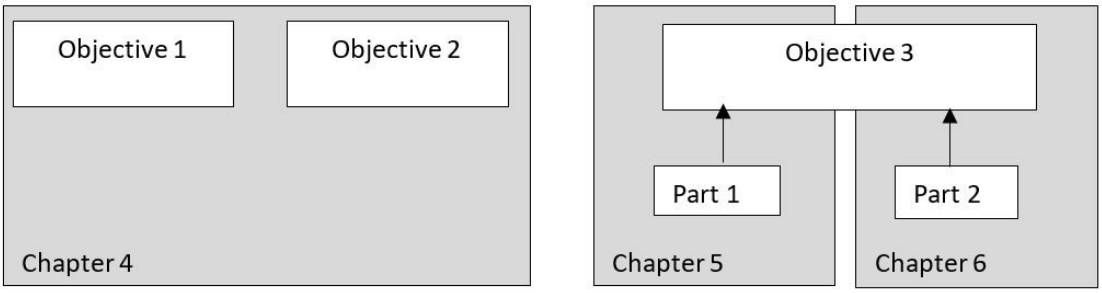


Figure 1.1 Schematic of Objectives within the thesis structure

## 1.3 Organisation of the Thesis

The thesis comprises of six chapters (2-7) beyond this introduction. The structure of the thesis is set out below, with a brief summary of each chapter and its contribution towards meeting objectives one to three.

Chapter 2 is a literature review that positions this thesis within the current state of knowledge and research. The chapter outlines the current state of knowledge on hydraulically driven landslides, the techniques used for monitoring those landslides, and the current uses and limitations of SAR for environmental monitoring. The gaps in the current state of knowledge are highlighted.

Chapter 3 describes the Hollin Hill landslide observatory, the research that has been undertaken at the site previously, the ground-truthing equipment used there for monitoring slope conditions, the context of soil moisture remote sensing at the site,

and the context for using COSMO-SkyMed (CSK) at the site. It sets out the methods used in processing the *in situ* and remote sensing data.

Chapter 4 presents the results and analysis of multi-depth *in situ* soil moisture monitoring undertaken at the Hollin Hill Landslide Observatory co-temporally with the CSK acquisitions explored in Chapter 5. This is followed by a discussion of the impacts of the spatio-temporal relationships displayed at the site and the implications these have to undertaking SAR processing in chapter 5, thereby meeting Objectives 1 and 2.

Chapter 5 presents the results of CSK image calibration and processing with respect to the measured *in situ* soil moisture data described in Chapter 4. In this chapter, Objective 3 is met and discussed.

Chapter 6 assesses the viability of using X band SAR to assess soil moisture. This is undertaken from two perspectives – that of this particular site, and that of the appropriateness of using X band for this particular task. These findings are contextualised by a comparison with the results from other X-band soil moisture studies.

Chapter 7 provides a summary of the discussions of the results presented in chapters 4, 5 and 6, outlines their novelty, and makes recommendations for future practice in this research area for different audiences.

## 1.4 Project history

This thesis is an individual piece of work undertaken between 2014 and 2020 under the supervision of Profs John Wainwright and Danny Donoghue at Durham University and Dr Colm Jordan at the British Geological Survey (BGS). The fieldwork was undertaken at the Hollin Hill Landslide Laboratory in North Yorkshire, which hosts *in situ* slope monitoring equipment implemented and maintained by staff at BGS. While this work sits in the context of other studies undertaken at the site by a variety of different researchers both working at and in collaboration with BGS, the experimental design, acquisition and processing of data from and relating to the Hollin Hill site was undertaken by myself. Where others have contributed to the project in the form of guidance, help or information, this has been directly referenced in the body of the text.

In 2015 a bid was successfully made for data through the UK Satellite Application Catapult, which issued a call for expressions of interest after forming an agreement

with the Italian space agency (ASI), from the newly-launched COSMO-SkyMed (CSK) constellation. The research for, design and specification of the application was undertaken by me, with minor revisions by the supervisory team prior to submission.

This thesis explores the utilisation of this data - the highest resolution X-band Spotlight2 imagery available to civilian projects, in the context of estimating soil moisture at a slow-moving rotational landslide (Jenkins *et al.* 2006) consisting of Lias-derived soils at the British Geological Survey's (BGS) Landslide Observatory at Hollin Hill in North Yorkshire, UK. Nine images, taken roughly one month apart, that were tasked for our project are used in this project in combination with measurements taken *in situ* contemporary with the imaging overpasses, are used in this project to assess the opportunities that high resolution X-band SAR provides in the context of monitoring hydraulically driven landslides.

This nine-month study was designed to enable evaluation of estimation techniques suitable for different stages of the phenological cycle through ground-based surface measurements. This project enables, through the use of empirical data, the uncertainty associated with the performance of X-band SAR for soil monitoring over different geomorphic and vegetated conditions to be assessed.

## 1.5 Novelty

The novelty of the project has, to some extent, already been stated, in that it uses SAR data from the COSMO-SkyMed (CSK) constellation, which became operationally shortly before the project began. Further novelty is provided by the characteristics of the field site chosen for the project. The Hollin Hill site opens up a new climatic and geomorphic avenue for CSK-soil moisture studies, which previously had been confined predominantly to semi-arid (Riccio *et al.*, 2012; Iacobellis *et al.*, 2013; Gorrab *et al.*, 2014), plain (Santi *et al.*, 2012) or high-mountain conditions (Paloscia *et al.*, 2014). The site enables the value of CSK data to be assessed in the context of an active slope setting, in a temperate climate using high-quality ground-truthing data, thereby taking the application of CSK to the next stage, through assessing solutions to real-world geomorphic problems. Furthermore, the utility of this site should not be underestimated. The landslide - a slow moving hydraulically driven rotational slide in Lias-derived soils - is representative of landslides found across Western Europe and the UK, with Lias-derived slides accounting for 15% of recorded landslides in the UK (Jones and Lee, 1994), and

seasonal rotational slides being the dominant landslide type in the UK and parts of Europe (Evans *et al.*, 2013; Pennington *et al.*, 2015). In addition to the active clay-dominant Lias soil, two other distinctive soil types are found at the surface of the site, with drainage properties that are quite distinct from each other. This enables studying a wider dynamic range of soil moisture values than would be possible in a more homogeneous study site.

## 1.6 Summary

To summarise, soil moisture estimation with SAR has been attempted since the 1950s, and has been achieved with some success in environments where confounding factors are well constrained. This thesis uses new SAR technology in a novel environmental context to explore whether soil moisture can be estimated at a geometrically complex landslide site, with limited *a priori* geometrical information, as a simulation of a likely scenario for monitoring of a realistic landslide hazard scenario. The project explores the spatio-temporal relationships of surface soil moisture at an active slow-moving landslide site between June 2016 and February 2017, the relationship between these and measurements at greater depths, and the implications of these for defining optimal CSK data processing.

## 1.7 Impact of Covid-19

It was originally envisaged that the scope of this project would be both broader and deeper in terms of the questions asked of the data and the extent to which the data was processed. Unfortunately, due to the COVID-19 pandemic and the impact this had on undertaking planned fieldwork, access to computing labs and supervision and its timing just as in-depth processing was about to be undertaken, it was necessary to redesign some of the analysis undertaken in this project, and to not undertake some.

Although the original design of the project is somewhat hampered by not being able to undertake the micro-scale surface roughness measurements intended, these limitations have provided the opportunity to ask questions that wouldn't have been asked, but that have value in that they reflect a research context that would not be uncommon for future CSK product users in settings where the data is being used for a range of hazard-specific applications – namely, situations where a lack of ground truthed surface roughness data at a scale close to that of the incident wavelength is to be expected. This might be where CSK data is being used to monitor precursory conditions of a rainfall event in an area where risk of landsliding or flooding is

recognised, but where accessibility or scale of the area has made micro-scale surface roughness impossible. The research has, therefore, been able to assess the viability of using CSK data for monitoring soil moisture in a context that would not be uncommon if wanting to use CSK for hazard assessment in areas where high quality a priori data isn't available. A discussion of what this means for the viability of using CSK for SM monitoring is given in Chapter 6.

There was also the intention of experimenting with the impact that applying different back-scatter – SM models to the data to assess how best to optimise processing of CSK data for SM estimation. Again, due to the limitations the pandemic presented in terms of accessing training to be able to do this, this was not undertaken. Chapter 6 does, however, explore the extent to which this limits the quality of the results presented in the thesis.

A full break-down of the methods and anticipated impacts the undertaking of them on the analysis of the data in this project is presented in Appendix 2.

# 2

# CHAPTER 2: LITERATURE REVIEW

This chapter introduces the literature on the areas of research which underlie this thesis, exploring the mechanisms and monitoring methods of hydraulically driven landslides, the state of understanding of landslide hydrology and then providing the context of SAR – its capabilities and challenges in being used for environmental remote sensing. Overall, this chapter positions the thesis in its broader context (Figure 2.1), preparing the ground for the Materials and Methods chapter (Chapter 3) and the discussions in Chapters 4, 5 and 6.

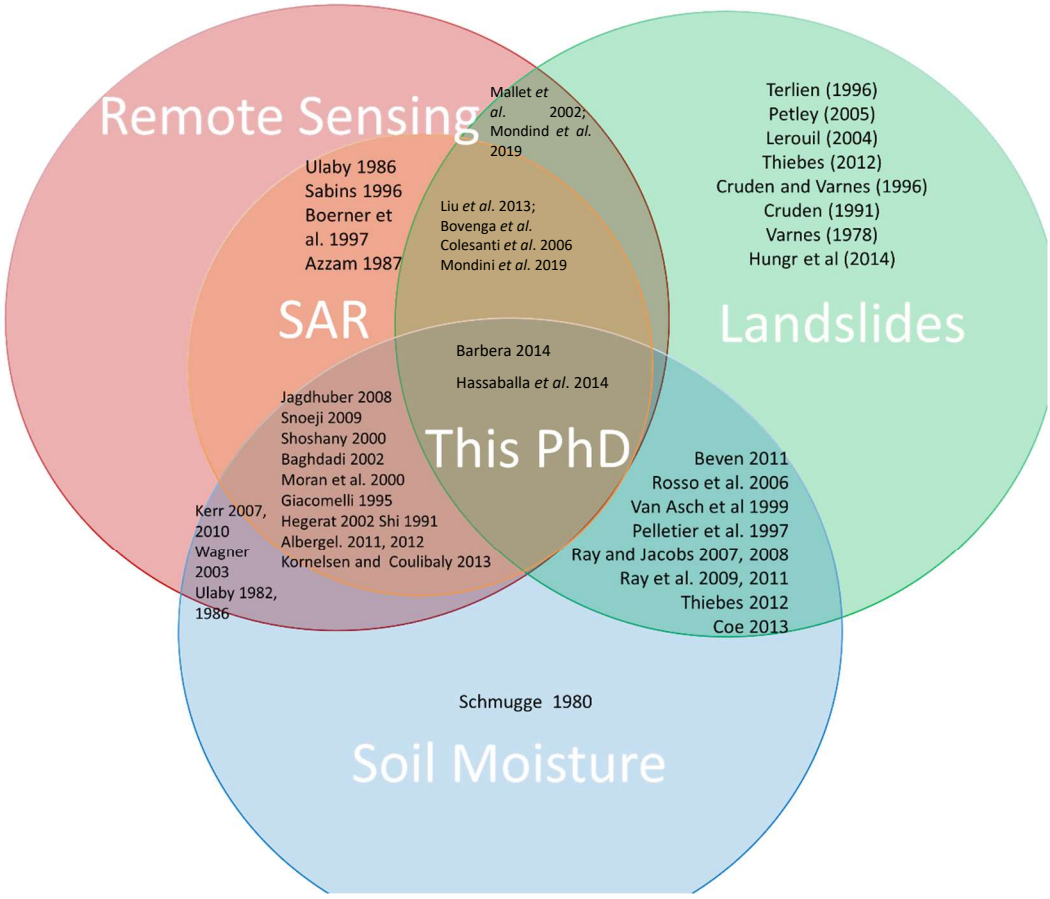


Figure 2.1 Conceptual Map of thesis context with selected references appended

## 2.1 Slope Processes

This section sets out the types of slope failures, the mechanisms behind these slope failures and the methods of monitoring causes of slope failures. Beyond the broad introduction to the topic, the focus is limited to reactivated, rainfall-induced landslides – the type encountered at Hollin Hill – the study site for this project.

### 2.1.1 Characterising Landslides

The term 'landslide' encompasses a range of different types of slope failure, but the overarching definition that is most often employed in research, and was adopted by the United Nations International Decade for Natural Disaster Reduction (IDNDR), is "the movement of a mass of rock, earth or debris down a slope" (Varnes, 1978; Cruden, 1991). A number of classification systems of landslides have been developed over the years (Skempton and Hutchinson, 1969; Varnes, 1978; Cruden and Varnes, 1996; Shroder *et al.,* 2005). Under Varnes' (1978) definition of landslide types, which provides a systematic set of descriptors for each of the possible landslide types and the adapted form (Cruden and Varnes, 1996), which is the most widely used system in the English-speaking world (Hungr *et al*., 2014), there are five kinds of slope failure - fall, topple, slide, flow and spread – which are further sub-categorised by the material characteristics – rock, debris or earth (see Figure 2.2) and rate at which that slope failure occurs (Brabb, 1991).

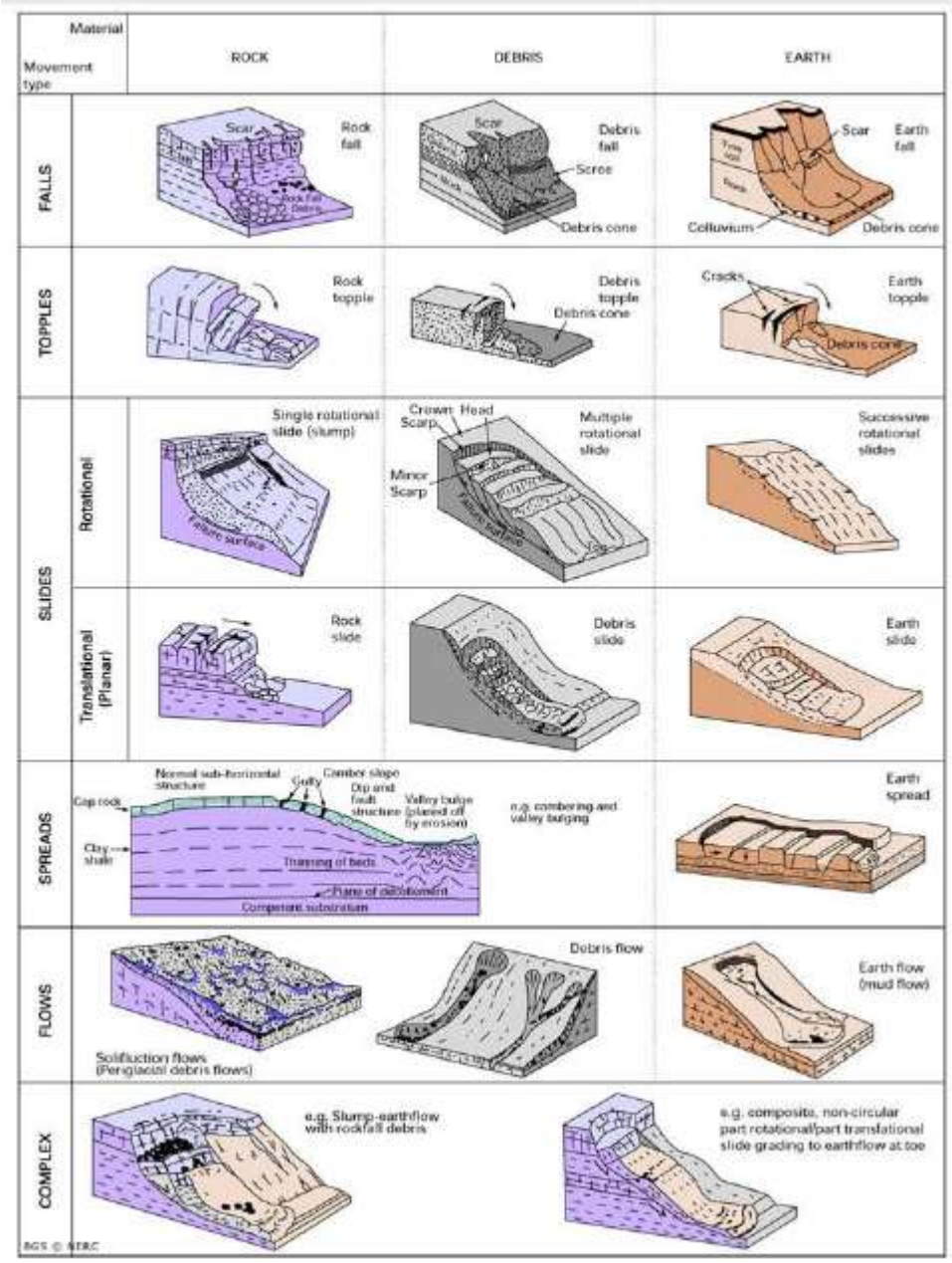


Figure 2.2 Landslides classifications by type and material. Source (BGS, 2015a) adapted from (Cruden and Varnes, 1996).

#### 2.1.1.1 Deformation Drivers

Slope deformations and failures are complex. It is, however, helpful at this stage to provide a simple summary of the underlying physics behind the process. If we consider the soil mass as a block on a slope (see Fig 2), its movement, or lack thereof, can be defined by the relationship between the downslope component and friction. That is, the block remains stable for as long as the driving forces remain less than the resisting forces. Without any external influences, like rainfall or weathering, which change the relative values of these two components, the system sits in stasis.

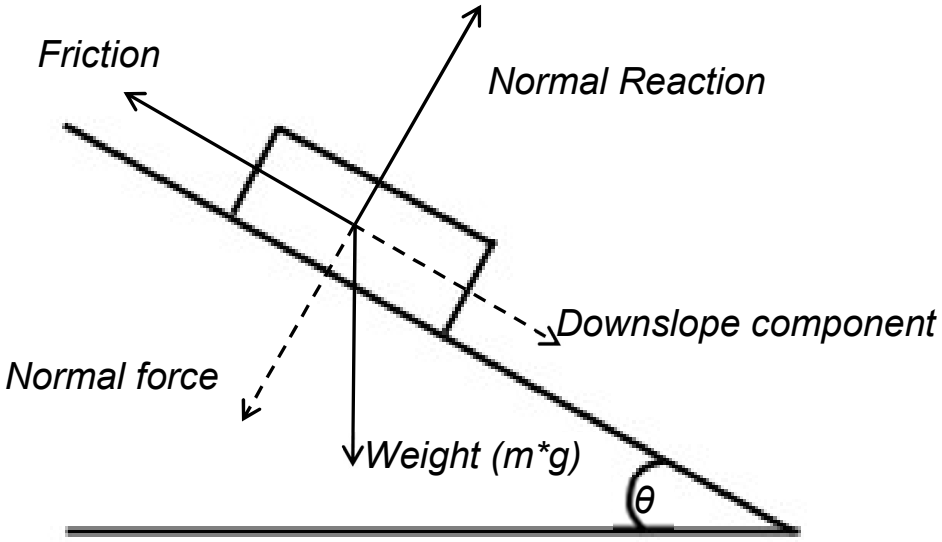


Figure 2.3 Diagram of forces acting on a mass on a slope. Adapted from(Kirk, 2003).

Movement at the slip surface in reactivated landslides, like the Hollin Hill landslide, occurs when the shear stress exceeds the shear strength along the slip plain, as defined by the Mohr-Coulomb relationship (Craig, 1995). This stress relationship was described by (Terzaghi, 1950) in adapting the Coulomb (1776) equation:

$$T_f = T_o\,(\sigma - u)tan\varphi \qquad [2.1]$$

where To is the cohesive strength of the soil, σ is the normal stress on the slip plane, $u$ is the pore pressure and φ is the angle of internal friction. Slope failures occur when $T_f$ is greater than a slope-specific threshold value. As such, landslide acceleration occurs when effective stress (Picarelli, 2007) or changes in material properties occur (Skempton, 1985; Terzaghi *et al.*, 1996). The Mohr-Coulomb equation has been further adapted to include two-dimensional slope geometry, thereby enabling estimation of the factor of safety ($F$) for any point on the slope where the block thickness and pore pressures are known (Morgenstern and Price, 1965; Sarma, 1979):

$$F = \frac{c' + (\sigma_n - u).\tan\phi}{\sigma_n.\sin\alpha,\cos\alpha} \qquad [2.2]$$

$$\tau = \sigma_n.\sin\alpha.\cos\alpha \qquad [2.3]$$

where, $\sigma_n$ is the normal stress, u is the pore-water pressure and $\sigma_n$-$u$ the effective stress, as defined by (Terzaghi, 1936), α is the angle of the slip plane and $\varphi$ is the angle of internal friction. It should, however be noted that there are limits to the utility of this infinite slope model.

Landslides can have many causes, whether they be geological, anthropogenic, or morphological (Cruden and Varnes, 1996), but normally just one driver (Varnes, 1978). There are thought to be four main drivers of reactivated landslide motion – raising of groundwater through precipitation, tectonic activity, drainage-line blocking (Chatwin, 1994), and anthropogenic action (Schuster and Highland, 2007). It is, however, difficult to ascertain a threshold for slope deformation to result at (Rosser, 2010). For, it is possible for slope failures to occur without noticeable input drivers (Froude, 2011). This can be due to the slope sitting near to the failure threshold, thereby meaning that only a small input is required to move it into the failure envelope (Rosser, 2010). Alternatively, a much larger than modelled trigger can be required to cause failure (Gerrard and Gardner, 2000), for it is well recognised that there is not, necessarily, a proportional relationship between the magnitude of a trigger and its impact on slope stability (Phillips, 2006).

External drivers act to decrease the slope's internal coefficient of friction over time (Brunsden and Thornes, 1979; Wieczorek, 1996). These processes are, predominantly, environmentally driven and, in particular, hydraulic (Pelletier *et al.*, 1997), with there being a strong relationship between increased rainfall and increased slope failures in the UK (Figure 2.4). One of the primary causes of the reduction of internal slope friction is the increase in water content of the slope (Casagli *et al.*, 1999). In shallow, soil-based landslides, infiltrated moisture acts as a lubricant between soil particles, also reducing the stability of the slope. At the same time, the increase in water within the slope increases the mass of the soil mass (Brand, 1981; Ray and Jacobs, 2007), thereby increasing the stress on the slope, while also reducing the stress-bearing characteristics of the slope as water cannot sustain shear stress (Thiebes, 2012), thereby reducing the stability of the slope. Once the cumulative effect of these factors crosses a slope-specific threshold, slope failure activates (or reactivates).

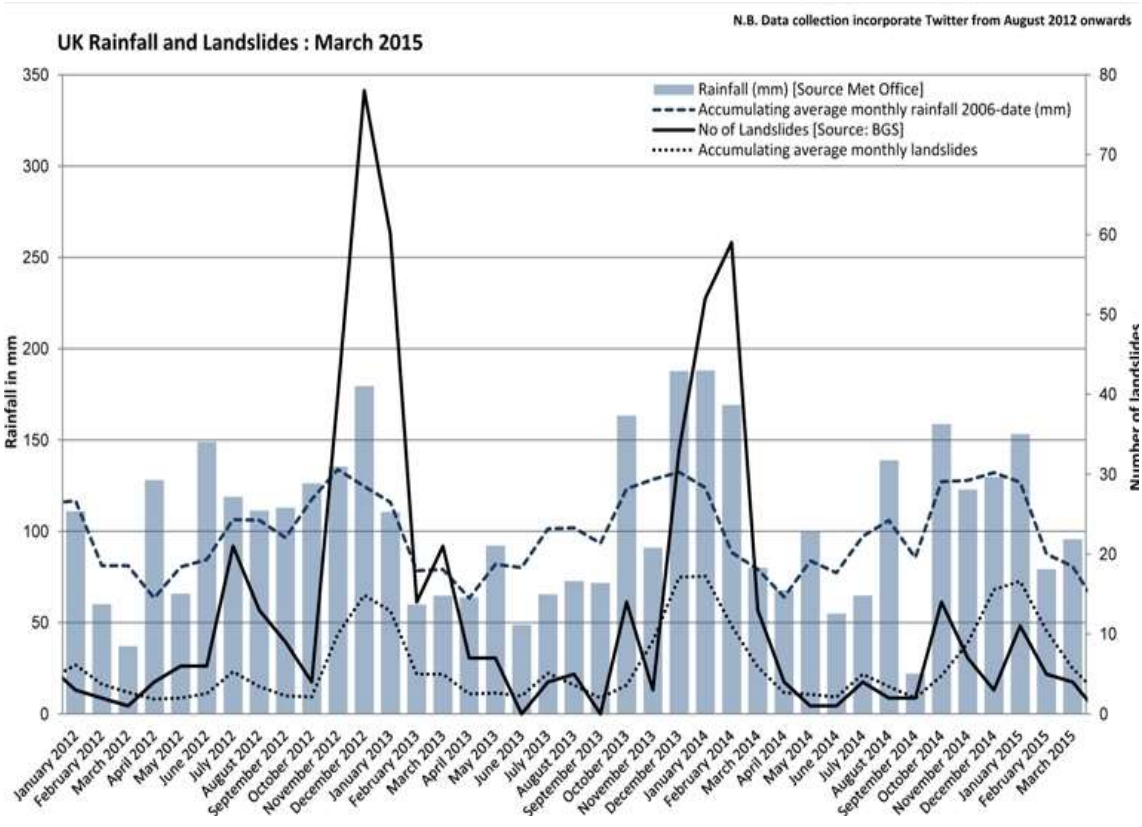


Figure 2.4 Chart relating rainfall and landslide numbers in the UK between January 2012 and March 2015 (BGS, 2015b).

The complexity of associating measured hydrological drivers of slope deformation can be seen in the results of empirical studies of the roles of pore pressures (Allison and Brunsden, 1990; Matsuura, Asano and Okamoto, 2008) and rainfall intensity and duration (Caine, 1980; Wieczorek, 1987; Dahal and Hasegawa, 2008) on slope instability. Indeed, several empirical studies have found that there is a non-linear relationship between landslide acceleration and pore pressure (Skempton, 1985; Corominas *et al.*, 2005; González *et al.*, 2008; Matsuura *et al.*, 2008). Likewise, studies have shown that the same pore pressure values have caused different landslide accelerations (Bertini *et al.*, 1984; González *et al.*, 2008). This has, therefore, been interpreted as meaning that although deformation is related to changes in effective stress due to pore pressures, it is also modified by changes in shear strength due to the way particles behave during shearing or restoration of material strength during periods of inactivity (Angeli *et al.*, 2004), thereby reducing the possibility of reactivation (van Asch *et al.*, 2007).

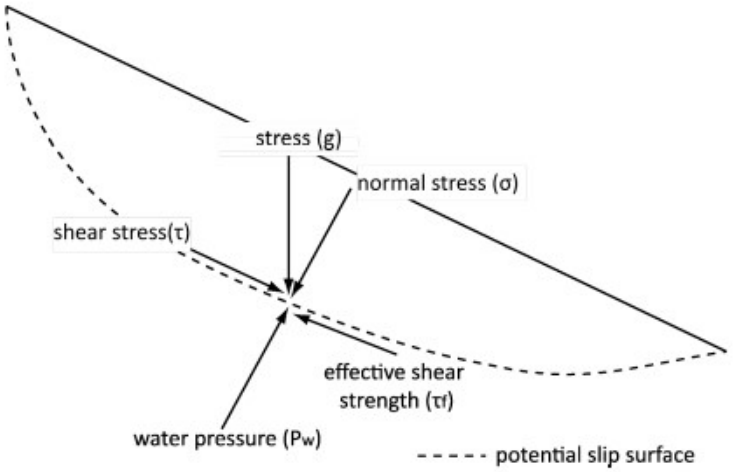


Figure 2.5 Forces acting on a potential failure plane. From (Froude, 2011) adapted from (Selby, 1983).

Given the Mohr-Coulomb relationship and multiple empirical studies (Bhandari, 1988; Allison and Brunsden, 1990), it is clear that hydrological triggering (Terlien, 1996) through pore pressure is a key driver of rainfall-induced landslides. It must, however, be noted that there are other factors, like the shear strength, the hydrogeology, especially the difference between the permeability of the sliding mass and the routes for surface water into the slip surface through surface cracking or other surface discontinuities (Corominas *et al.*, 1999; van Asch *et al.*, 2007) that make attempts at predicting slope behaviour difficult.

#### 2.1.1.2 Summary of landslide overview

This section has shown that there is great complexity in the interpretation of slope stability due to the heterogeneity of slope materials, conditions and drivers. It has shown that there is a variety of means of measuring and categorising slope stability and that the relationship between external hydraulic drivers and slope stability is not simple.

## 2.2 Monitoring Landslides

Monitoring of slopes tends to fit into one of two categories – monitoring the drivers of deformation, or monitoring deformation itself. Monitoring of landslide movement can be undertaken using a variety of different sensor types. The following section outlines core philosophies of *in situ* and then remote sensing monitoring techniques.

### 2.2.1 Monitoring Deformation

Extremely slow and slow moving landslides, like the one focused on in this study, have variable movement rates (Petley *et al.*, 2005), though poor spatial and temporal resolution of monitoring of slopes have led to them being interpreted by some as moving at a steady rate (Petley *et al.*, 2005). One of the causes of the poor spatial resolution mentioned by Petley is that subsurface displacement monitoring can be expensive due to equipment costs, is labour intensive in its deployment and, to some extent destructive of the material it is used to monitor, and does, necessarily, produce point data, which require extrapolation to enable full-slope monitoring. Equipment that is often used include inclinometers, extensometers, and Time Domain Reflectometry (TDR) (Kane and Beck, 2000; Huisman *et al.*, 2001). Table 11 sets out the main technologies applied to measuring slope displacement and their typical ranges and accuracies.

Table 2.1 Typical of representative accuracy values of various pieces of equipment used for landslide monitoring. Source: (Malet, Maquaire and Calais, 2002).

| Method | Use | Results | Typical range | Typical accuracy |
|---|---|---|---|---|
| Micrometer screw-level | Angular displacement | *da* | 0.1 rad | 4.10−4 rad |
| Fissurometer | Differential movement of compartments | *dD* | <20 mm | ±0.1 mm |
| Levelling vernier pole | Opening of small cracks | *dD* | <200 mm | ±0.5 mm |
| Short-base extensometer | Opening of cracks | *dD* | 25–450 mm | ±0.1 mm |
| Invar distance-meter | Displacements of moving targets | *dD* | Up to 40 m | ±0.1 mm |
| Wire extensometer | Displacements of moving targets | *dD* | Up to 100 m | ±0.5 mm |
| Tacheometric level | Variation of altitude | *dZ* | Variable | 20 mm |
| Electro-optic distance-meter | Displacements of moving targets | *dD* | 1–10 km | 7 mm±1–5 ppm |
| Geodetic station | Displacements of moving targets | *dX, dY, dZ* | 1–10 km | 3 mm±1–5 ppm |

### 2.2.2 Remote sensing of Deformation

An alternative to *in situ* monitoring is remote sensing. There are various remote sensing approaches to monitoring slope movement. LiDAR (Light Detection and Ranging) and TLS (Terrestrial Laser Scanning) are particularly effective at this, with InSAR (Interferometric Synthetic Aperture Radar) also being widely used (Krieger *et al.*, 2007; Eineder *et al.*, 2009; Liu *et al.*, 2013). In many cases, however, particularly in the case of InSAR, deformation is only assessed after a major event due to the complexity of tasking satellite acquisitions in near-real time for non-emergency events.

There are various remote sensing approaches to monitoring slope movement. Terrestrial options most commonly used are LiDAR and TLS (Wagner and Pathe, 2005; Evans *et al.*, 2013; Jebur *et al.*, 2014); these are particularly effective. Airborne and Satellite-based approaches to deformation monitoring used to be based predominantly on photogrammetry, but the development of multi-polarised SAR platforms has enabled InSAR to be a successful tool for measuring deformation (Bovenga *et al.*, 2012; Colesanti and Wasowski, 2006; Krieger *et al.*, 2007; Liu *et al.*, 2013). Likewise, the reduction in revisit time for single-polarise SAR platforms has made surface displacement assessment possible through comparing the change in phase between images (Massonnet and Feigl, 1998).

Table 2.2 Methods and representative accuracies of techniques for remotely sensing slope deformation. Adapted from (Malet *et al.*, 2002) .

| Method | Use | Results | Typical range | Typical accuracy |
|---|---|---|---|---|
| Terrestrial photogrammetry | Displacements of moving targets | *dX, dY, dZ* | <200 m | 40 mm |
| Aerial photogrammetry | Displacements of moving targets DEM comparison | *dX, dY, dZ* | Hflight<500 m | 100 mm |
| Radar interferometry (InSAR) | DEM comparison | *dX, dY, dZ* | Variable | 3–5 mm |
| DORIS | Displacements of moving targets | *dX, dY, dZ* | Variable | 2 mm |

### 2.2.3 Monitoring deformation drivers

There are well-attested challenges for monitoring landslides. Thresholds for hydraulic drivers of slope deformation can often only be calculated retrospectively (Caine, 1980) or through modelling, which, inherently, has limitations based on the quality of data and the amount of complexity that can be viably achieved (Wainwright and Mulligan, 2013). Likewise, precursory conditions can significantly influence the onset and scale of landslide activity, which some monitoring technologies like rain gauges cannot easily accommodate (Lacasse and Nadim, 2009). Indeed, various landslide catalogues and reports seem to show that landslide events occur in spite of or despite hydraulic inputs (Gerrard and Gardner, 2000). Despite the challenges associated with monitoring drivers and understanding the functional thresholds associated with slope failure, there is nevertheless a growing body of work focussing on the monitoring of deformation drivers (Barbera, 2014; Merritt, 2014; Uhlemann *et al.*, 2016).

#### 2.2.3.1 Remote Sensing of Soil Moisture

Despite continued use of *in situ* soil-moisture probes in landslide studies (Merritt *et al.*, 2013), there has been limited work on remotely sensed surface soil moisture and its relationship with slope instability. However, recent works by Ray & Jacobs, (2007, 2008); Ray *et al.*, (2010), investigating the relationship between remotely sensed soil moisture and landsliding events in three different sites – Colorado, US; Leyte, Philippines; and Dhading, Nepal – have shown that, in these three cases, there is a temporal link between raised soil-moisture values and landslide occurrences. The research used AMSR-E data – passive microwave data, whose soil moisture product is available at 25 km resolution – downscaled to 1 km grids. The development of this technique through these papers has focussed increasingly on Colorado, in particular, and the relationship between remotely sensed soil moisture (which applies to, at most, the top 5 cm of the soil column), and the underlying soil moisture values. The earlier papers (Ray and Jacobs, 2007, 2008), highlight that the relationship between rainfall and soil moisture is not as clear-cut as the relationship between rainfall and landsliding.

Various studies have used measurements of the wetness of slopes as proxies for slope stability. A common approach has been that of using moisture indices derived from optical satellite imagery, like LandSat or MODIS (e.g. Western *et al.* 2002; Yang *et al.* 2013; Zhang *et al.* 2015), which have largely proved to be successful, though, as with all optical products, are affected by cloud cover (Kerr *et al.*, 2010). Coe (2012) investigated the correlation between a soil-moisture proxy and the rate of movement of the deep-seated, groundwater controlled, Slumgullion landslide in Colorado. In this, he found a strong correlation between MDBI index and landslide movement.

In addition to remotely sensed proxies of soil moisture, there are *in situ* techniques. There are two main types – quasi-point measures of soil moisture, which use a capacitance probe inserted in the soil mass to measure the impedance of the soil mass (Delta T Devices, 1999), from which the volumetric soil water can simply be calculated (Archer *et al.*, 2016). These sensors can be used at multiple depths and are able to be set up to provide automated acquisitions (Kuras *et al.*, 2009; Fersch *et al.*, 2018).

### 2.2.4 Relating surface soil moisture and slope deformation

The partitioning of incident precipitation on a slope - that is, into the soil mass or as runoff (Beven, 2011), - and the demonstration of the current state of saturation in

the soil mass is determined by near-surface soil moisture (Albergel *et al.*, 2012; Taylor *et al.*, 2012; Kornelsen & Coulibaly, 2013; Kerr, 2007). Given the importance of gauging the current state of a soil mass in advance of a precipitation event, whether this be in the context of preparing for hazards like flooding (Western *et al.*, 2004) or landslides (Coe, 2012), or for making ecosystem or agricultural decisions (Schmugge *et al.*, 2002), monitoring of this parameter is important (Teuling and Troch, 2005; Robinson *et al.*, 2008; Seneviratne *et al.*, 2010; Legates *et al.*, 2011). To this end, the importance of surface soil moisture in the hydrological process has recently been acknowledged by the Global Climate Observing System (GCOS), who made it a key climate variable for monitoring (GCOS-138, 2010).

Soil moisture has two roles to play in the modelling of landslide activation. First, it can be a direct input to models. Second, as mentioned above, it can act as a proxy of slope conditions, defining the extent to which those conditions will change. That is, a high surface soil moisture reading indicates an increased water-driven stress impacting on the slope, but also, that further infiltration into the slope at that point is going to be minimised, with an increasing amount of incoming water being partitioned into overland flow (Beven, 2011). Later work has focussed on modelling the relationship between surface soil moisture and deeper soil moisture, particularly in the unsaturated zone, using a Variable Infiltration Capacity (VIC) model. This model uses an adapted form of the Infinite slope stability model to model water and energy fluxes within the soil mass (Ray and Jacobs, 2007; Ray *et al.*, 2010), in particular using remotely sensed soil moisture as an input for dynamic two-layer soil-mass values.

It should be noted that although surface soil moisture is important in partitioning incoming rainfall, it is not just surface moisture that has an impact on slope stability, but deeper moisture as well (Leroueil, 2004; Vereecken *et al.*, 2008). A challenge within the modelling component of this project will be to establish how these two (or more) zones relate in the context of slope failure. A further interesting point to consider in the context of linking surface and subsurface soil moisture stores is that several studies into soil-moisture modelling have found that under certain conditions, for example clayey soil (Leroueil, 2004), that subsurface pore pressures are not necessarily linked to surface moisture.

## 2.3 Landslide Hydrology

The route water incident to a soil mass takes is determined by several things, including material porosity, surface angle and the hydrophobicity of the material. Additional to these, and important in this study is the moisture content of the material. For, as Horton demonstrated (Horton, 1933), if the material is saturated incident water is unable to infiltrate and forms overland flow. Within the slope, there are similar, though more complex, relationships between the wetness of a material and the routing of water through it.

One of the main challenges for using surface soil moisture as an input to landslide monitoring is, necessarily, the vertical disjuncture between what is measured at the surface and the conditions near the key failure plane; that is, the fact that moisture measured by SAR systems is in the top 5 cm of the soil profile (Pelletier *et al.*, 1997), while the failure plane typically sits considerably deeper, normally sitting between 1 and 4 m below the surface for translational slides in soils (Milledge, 2008) like the one being focussed on in this project.

As already examined, pore water pressure is a driver of slope deformation. The assumption within hillslope hydrology models is that water flow occurs from high to low pressures, as demonstrated by Darcy, and that these hydraulic gradients are related to topography (Tetzlaff *et al.*, 2008). Key characteristics that have been identified for the calculation of flow accumulation within the slope include: slope steepness, surface topography (Quinn *et al.*, 1991), sediment thickness, hydraulic conductivity and upslope contributing area. The sensitivity of soil saturation to these parameters is not well understood, despite multiple studies. Gallart's studies in Vallcebre, Spain – a slow-moving predominantly clay landslide with higher rates of motion at the top of the slope than the bottom, like Hollin Hill - found that while topographic index was a reasonable predictor of saturation patterns, sub-grid conditions like topography, soil characteristics, non-topographic flow pathways and dynamic water flow) were as important in controlling saturation (Gallart *et al.*, 1994; Gallart *et al.*, 1997, 2008; Latron and Gallart, 2007).

### 2.3.1 Preferential flow

Traditional hydrological models assume that soils act as continuous porous media. However, increasingly, empirical studies are showing that there is significant preferential routing of water through soil masses. This routing occurs through discontinuities in the pore structure, in the form of macropores caused by roots and

animal burrowing (Beven, 1981; Sidle and Swanston, 1982; Pierson, 1983; McDonnell, 1990). This preferential flow is particularly important in the context of landslides, where mass movement has a tendency to produce surface and sub-surface fracturing and discontinuities, causing uneven routing of water to the soil mass and slip plane, causing local variability in pore pressures and thereby shear stress. This is particularly of interest in the case of the Hollin Hill landslide, where the upper portion of the landslide is characterised by multiple, deep (~0.5 m) fissures, and a deeper scarp scar (~1 m), which, it is hypothesised, enables preferential flow into this part of the slope.

Studies of the significant heterogeneity in hillslope responses to rainfall events have revealed significant complexities in subsurface flows (McDonnell, 1990; Hutchinson and Moore, 2000). Traditionally, surface topography has been considered as a primary input to modelling of flow routing, however, some studies have found that in certain cases bedrock topography or discontinuities can provide a much better parameter for calculating spatial saturation patterns (e.g. (Freer *et al.*, 2002), where saturation of a uniform, shallow soil, was shown to be controlled by the topography of the granitic bedrock).

Preferential flow is well recognised as being a key challenge to hydrological modelling, though, the effects on slope stability can vary, with pipe flow, for example, in some cases, improving slope stability, because it provides efficient flow routing away from an area, thereby limiting pore pressure build-up (Pierson, 1983). Conversely, they enable increased flow into a less well connected area of the slope, thereby raising pore pressures in that area and reducing slope stability (McDonnell, 1990). While the spatial distribution of pipes is poorly understood, it is conjectured that, at smaller scales, they may have a greater impact on spatial soil saturation than traditional topographical controls (Hutchinson and Moore, 2000).

## 2.4 Slope processes Summary

This section has set out methods of landslide activation and reactivation, examined approaches to modelling slope motion and moved on to examine the underlying hydrological processes that drive instabilities and philosophies of modelling these. It has shown that it is critically important to understand soil moisture at scales key for monitoring slope deformation potential. Having assessed the studies that have undertaken this, and their challenges involved in *in situ* monitoring of this parameter, and the integration of the inherently quasi-point nature of *in situ* soil

moisture measurements, the focus of this chapter now turns to SAR and the opportunities that it offers for improving the monitoring of soil moisture at scales meaningful for landslide- and other hazard-related monitoring.

## 2.5 SAR

This section introduces and discusses Synthetic Aperture Radar (SAR) and its use in environmental remote sensing, highlighting methodological developments and challenges in the utilisation of the data.

### 2.5.1 Introduction to SAR

Synthetic Aperture Radar (SAR) is a high resolution radar imaging technology used for remote sensing of earth surface properties from either aerial or spaceborne platforms (Curlander and Mcdonough, 1991). SAR is an active sensor – that is, one that both emits and receives pulses of microwaves, as opposed to passive systems which just receive background microwave radiation (Kerr *et al.*, 2010). The system emits in the microwave band of the electromagnetic spectrum, and has, therefore, the ability to image during both the day and the night; with the ability to also penetrate cloud and, dependant on wavelength, rain (Ulaby *et al.*, 1986), SAR has been seen to represent an important technique for imaging earth surfaces across multiple disciplines ranging from agricultural science to oceanography (Jordan, 1980; Paloscia *et al.*, 2014).

To achieve its characteristic high resolution, which can be defined as "the minimum separation between two objects of equal reflectivity that will enable them to appear individually in a processed radar image" (Olsen, 2007), the platform effectively uses its own movement along its orbit to increase the effective size of the antenna, by receiving the backscatter signal from the surface at a point a distance from the initial point of emission (Sabins, 1996), using a small antenna and a broad beam. The Doppler effect and processing techniques are used to create a resolution akin to the very narrow beam used by Real Aperture Radar (RAR) to achieve fine spatial resolution narrow beam (ibid.). The Doppler principle says that there is a difference between the frequency of wave emitted and wave received if there is a change in velocity between the source and the observer (ibid.) and is applicable to all harmonic wave motion, including microwaves. The resolution of SAR is an order of magnitude improvement on that of Real Aperture Radar (RAR) sensors; in the case of satellite applications, the resolution of RAR is in the order of 100s of meters, whereas SAR resolution is in the 10s (Jordan *et al.*, 1991) or even 1s (ASI, 2009) of meters.

In terms of image product size and resolution, the resolution of the image and the swath width of the image are inversely proportional (Sabins, 1996), that is, the larger the swath width, the coarser the resolution of the image. For example, COSMO-SkyMed offers a 1m resolution for its Spotlight2 Mode with a swath width of 10km, whereas, in its ScanSAR mode, it has a resolution of 100m, but a swath width of 200km (ASI, 2009).

To produce an image, the SAR system emits an electromagnetic (EM) pulse at a specific wavelength, for a specific duration (a chirp). The chirps sent are timed such that they alternate with the returning energy pulses to the antenna; this is because in SAR systems the same antenna sends and receives. To prevent interference between the outgoing and incoming pulses, a duplexer blocks each circuit in turn when the other is operating; i.e. when the transmitter emits, the receiver is blocked and vice versa (Sabins, 1996).

Each pixel of SAR data contains complex data, with the phase angle, polarisation, and amplitude of the backscatter return in each pixel value. Early SAR usage, focussed on the amplitude values. While amplitude is still an important part of SAR processing - and is the component this thesis has focussed on - two other components of the returning signal are increasingly being used – phase and polarisation - with phase being of particular importance in Interferometric SAR (InSAR) (Hansen 2001; Massonnet and Souyris 2008), which has been widely used in producing digital elevation models (DEM) and in monitoring surface deformation following earthquakes or landslides (Massonnet and Feigl 2008), and polarisation being used in soil moisture estimation (Ouchi, 2013; Shi *et al.*, 2021) – particularly of vegetated surfaces (Jagdhuber *et al.*, 2008; Hajnsek *et al.*, 2009; Martone *et al.*, 2010).

The scene being imaged is illuminated in the look direction, which is orientated normal to the azimuth direction. Unlike visual imaging, radar imaging records backscatter values as a function of time, not distance because time can be measured more precisely. The amplitude of the return signal is a function of the interaction between the surface and the incident pulse (Sabins, 1996); surface properties influencing this include dielectric constant, surface roughness and orientation of features (like hillslopes or buildings); pulse properties might include the wavelength, polarization and depression angle of the incident energy (Sabins, 1996), which are discussed later in this chapter.

### 2.5.2 The history of SAR to the present day

The first SAR experimentation was undertaken in 1952, using an airborne (Wiley, 1985), with the first spaceborne system – SEASAT – being launched in 1978 (Jordan, 1980). Development of techniques and principles was undertaken through airborne SAR and the Shuttle Imaging Radar (SIR) missions, with SIR A and B being L-band HH polarisation sensors (Granger, 1983) – B having the ability to change incidence angles through a moveable antenna, and C (slightly later in 1994) offering fully polarimetric data at X, C and L-bands (Jordan *et al.*, 1991). Follow-up platforms were introduced by several space agencies from the early nineties; in 1991 the ERS1 SAR spaceborne platform was launched (Attema, 1991), JAXA launched JERS-1 (Nemoto *et al.*, 1991; Shimada, 2006), RADARSAT-1 (Raney *et al.*, 1991) was also launched and their follow-up platforms, ALOS-PALSAR (Rosenqvist *et al.*, 2007) and RADARSAT-2 (Moon *et al.*, 2010) respectively.

In recent years the focus has increasingly been on the development of systems capable of producing higher resolution imagery – in the order of meters or tens of meters - as evidenced in the development of recent SAR satellites like ALOS PALSAR 2, Sentinel 1, TerraSAR-X, TanDEM-X and COSMO-SkyMed generations 1 and 2, ICEYE and NovaSAR-S (Rosenqvist *et al.*, 2007; Attema *et al.*, 2009; Torre & Capece, 2011; Torres *et al.*, 2012; Cohen *et al.*, 2016), with full polarisation capability being common. Another development in SAR imaging capabilities seen in recent missions is a change of tack from developing single satellites with multiple sensors on them to much smaller and lighter satellites carrying just a SAR sensor. This significant reduction in weight (in some cases a whole order of magnitude in scale), has enabled multiple satellites, to be sent up at once and arrayed in constellations (Ouchi, 2013). This constellation approach has enabled the revisit time of SAR platforms to be much reduced – from the 24, 35, and 46 days of RADARSAT-2, ENVISAT-ASAR, and ALOS-PALSAR respectively, to the 7 hours (dependant on location and imaging specifications) offered by COSMO-SkyMed generation 1 (CSK) (ASI, 2009).

### 2.5.3 Geometry and terminology of RADAR processes

It is useful at this stage of the thesis to outline the main terminology and physics underlying SAR imaging. To summarise, there are 6 main bands (though K band is sometimes split into two) (Table 2.3) within the microwave section of the electromagnetic spectrum which are used for radar imaging. The band letters were assigned randomly in World War 2 and do not follow alphabetically (Sabins, 1996).

The microwave spectrum extends from 0.3GHz and 100cm to 100GHz and 0.3cm respectively. For remote sensing the most common bands used are the longer wavelength band, L (15-30 cm), the compromise band, C (3.8-7.5 cm) and the short wavelength X-band (2.4-3.8 cm) (Ulaby, Moore and Fung, 1981).

Table 2.3 Wavelengths and Frequencies of the bands making up the microwave portion of the electromagnetic spectrum. Source: (Sabins, 1996).

| Band designation | Wavelength (cm) | Frequency (GHz) |
|---|---|---|
| **K** | 0.8-2.4 | 40-12.5 |
| **X** | 2.4-3.8 | 12.5-8 |
| **C** | 3.8-7.5 | 8-4 |
| **S** | 7.5-15 | 4-2 |
| **L** | 15-30 | 2-1 |
| **P** | 30-100 | 1-0.3 |

The relationship between frequency and wavelength is defined by the following formula:

$$\lambda = \frac{30}{v} \quad [2.3]$$

general equation:

$$c = \lambda * v \quad [2.4]$$

where $c$ is $(3*10^8)$ ms-1, $\lambda$ is wavelength in cm, and $v$ is frequency in GHz.

2.5.3.1 Backscatter

Backscatter is the energy returned to the RADAR sensor after each pulse from the sensor. The backscattering coefficient is expressed as:

$$backscattering\ coefficient = \frac{Energy\ received\ by\ sensor}{Energy\ reflected\ isotropically\ by\ surface} \quad [2.5]$$

Although the value is normally negative, it is possible for it to be positive on occasions where surface geometry (e.g. a concave surface) serves to funnel the incident energy back to the antenna, for example in the case of a double bounce or dihedral scatterer or an urban area.

Radar images are predominantly interpreted through the backscatter coefficient – $\sigma^0$ - of each pixel (Ulaby, Moore and Fung, 1986). The value is measured in dB and is calculated through:

$$\sigma = \sigma^0 A \quad [2.6]$$

where σ is the backscattering cross section, $\sigma^o$ is the backscattering coefficient of the cell and A is the area of the cell (as defined by the azimuth and ground-range resolutions). The $\sigma^0$ value is most affected by two key components – surface geometry and the dielectric constant of the material. The dielectric constant is almost directly proportional to soil moisture (Engman, 1991).

In general, backscatter values can be classified thus (Sabins, 1996):

> Very high (above -5dB) – Urban; slopes toward emitter; very rough surface; steep incidence angle; dihedral scatterers
>
> High (-10 - 0dB) - rough surface; dense vegetation
>
> Moderate (-20 - -10 dB) – medium density vegetation; agricultural crops; moderately rough surfaces
>
> Low (below -20dB) - smooth surface; calm water; road; very dry terrain

#### 2.5.3.2 Pulse geometry

How the incident pulse interacts with the medium it meets is defined by multiple characteristics – geometry of the pulse, geometry of the surface, and the material properties of the surface. This section will expand on the role of each of these, in turn.

#### 2.5.3.3 Polarisation

The polarisation of the electromagnetic pulse is best defined as being "the behaviour in time of the wave field vector...observed at a fixed point in space" (Azzam and Bashara, 1987). This applies to both the electrical and magnetic components of the EM wave, which oscillate perpendicular to each other and their direction of movement. The polarisation of the overall EM wave is the vector resultant from the two vector components which make up the EM wave. The axis of oscillation can be either vertical or horizontal (V or H). When it is reflected by a surface most of it keeps that polarization. This is called 'parallel polarized' imagery and is referred to as HH or VV, depending on what the orientation of the original incident radiation was. Part of the pulse can be depolarised, however, when it encounters an abrupt or gradual change in refractive index, magnetic permeability, permittivity or conductivity (Boerner *et al.*, 1997). The return from this is referred to as cross-polarized - HV or VH.

2.5.3.4 Incidence Angle

The incidence angle is the angle measured from the vertical at which the radar beam is incident to the surface. It is smaller at the near-side, than it is at the far-side of the imaged area. The average incident angle quoted for an image product is measured from the mid-line of the image. It is generally assumed that all ground surfaces are horizontal (Sabins, 1996), however, when the imaged surface is sloped, the inclined surface angle impacts the equivalent incident angle (Figure 2.6). To incorporate surface geometry into incidence angle calculations on a pixel-by-pixel basis, a high resolution DEM can be used.

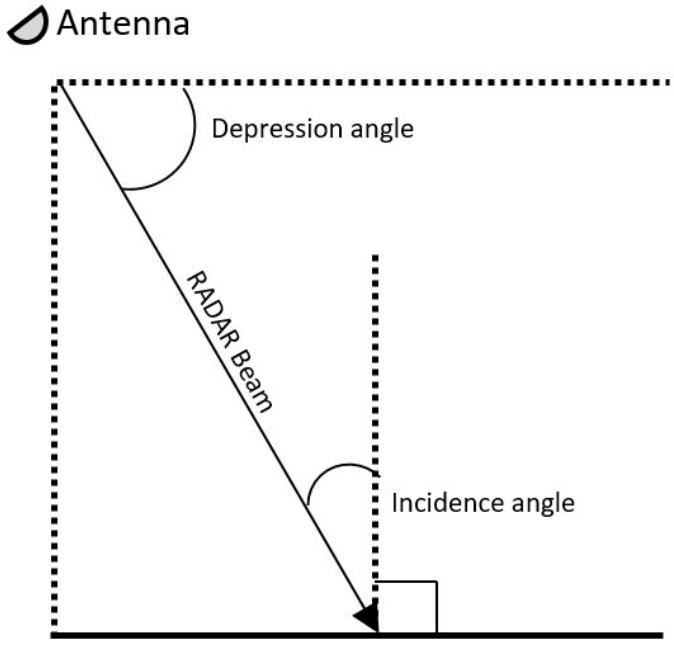


Figure 2.6 Diagram of angular relationships between depression angle and relative surface angle. Adapted from: Sabins. 1996.

There have been several theoretical and empirical studies of the impact of incidence angles on the backscatter values on different surface types (Figure 2.7) (Sabins, 1996). The relationships are complicated, with the polarisation and wavelength of the pulse both impacting on the return values (Ulaby *et al.*, 1982; Dobson *et al.*, 1985; Peplinski *et al.*, 1995).

2.5.3.5 Surface angle effects

The geometry of the imaged surface also has an impact on the backscatter values (Sabins, 1996). For example, a hillslope facing toward the satellite will have higher backscatter values than a flat surface due to two geometric characteristics. First, because the surface is tilted towards the radar, more of the incident ray is reflected

back to the sensor. Second, because the look angle foreshortens the slope (Shimada, 2010), so a larger area of the slope contributes to a pixel's backscatter total. Conversely, a slope tilted away from the sensor will have lower backscatter returns for the same reasons, with the additional challenge of potentially being shadowed by facing slopes.

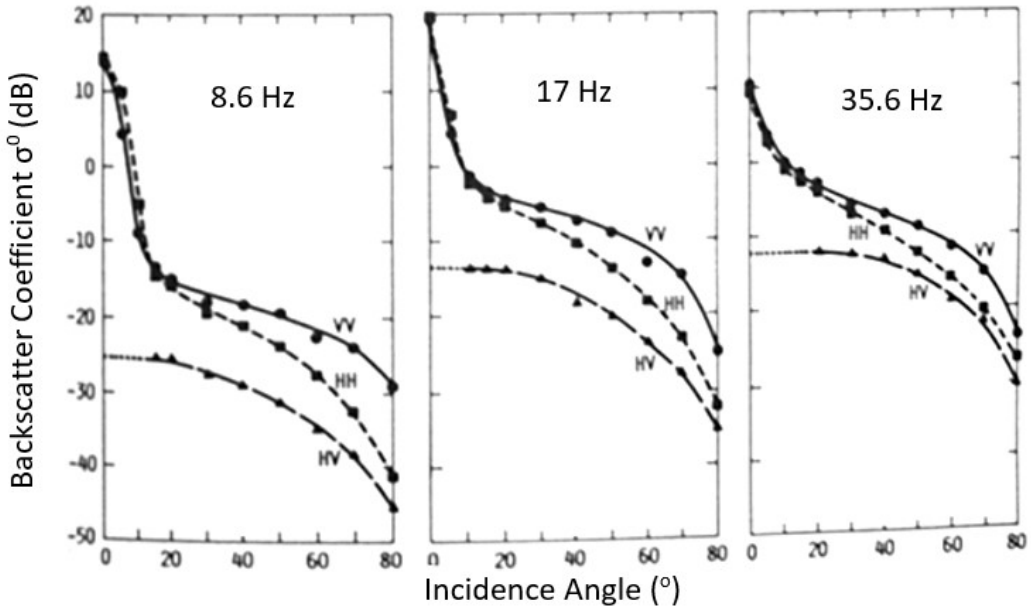


Figure 2.7 Relationship between backscattering coefficient and angle of incidence at different frequencies and polarizations when incident with dry tarmac (n.b. it is assumed that HV polarization has the same values as VH). Source: Ulaby *et al.* 1986.

#### 2.5.3.6 Surface Roughness

Backscatter is affected by multiple surface conditions, in particular, surface roughness. Different surface roughnesses have different reflectance properties. For example, flat water bodies, provide little or no backscatter because the radiation bounces off in the opposite direction to the incident beam. Rough surfaces like bare soil and lightly vegetated surfaces have higher backscatter values than water, as more of the incident beam is reflected back. Vegetated fields have higher values, and forests even higher due to volumetric and dihedral scattering. The highest backscatter values are from buildings in urban areas, particularly if they are aligned orthogonal to the line of sight of the satellite. When the radiation hits a smooth surface, some energy is scattered in all directions, but most is reflected away. As roughness increases, so the amount of backscatter returning to the receiver increases.

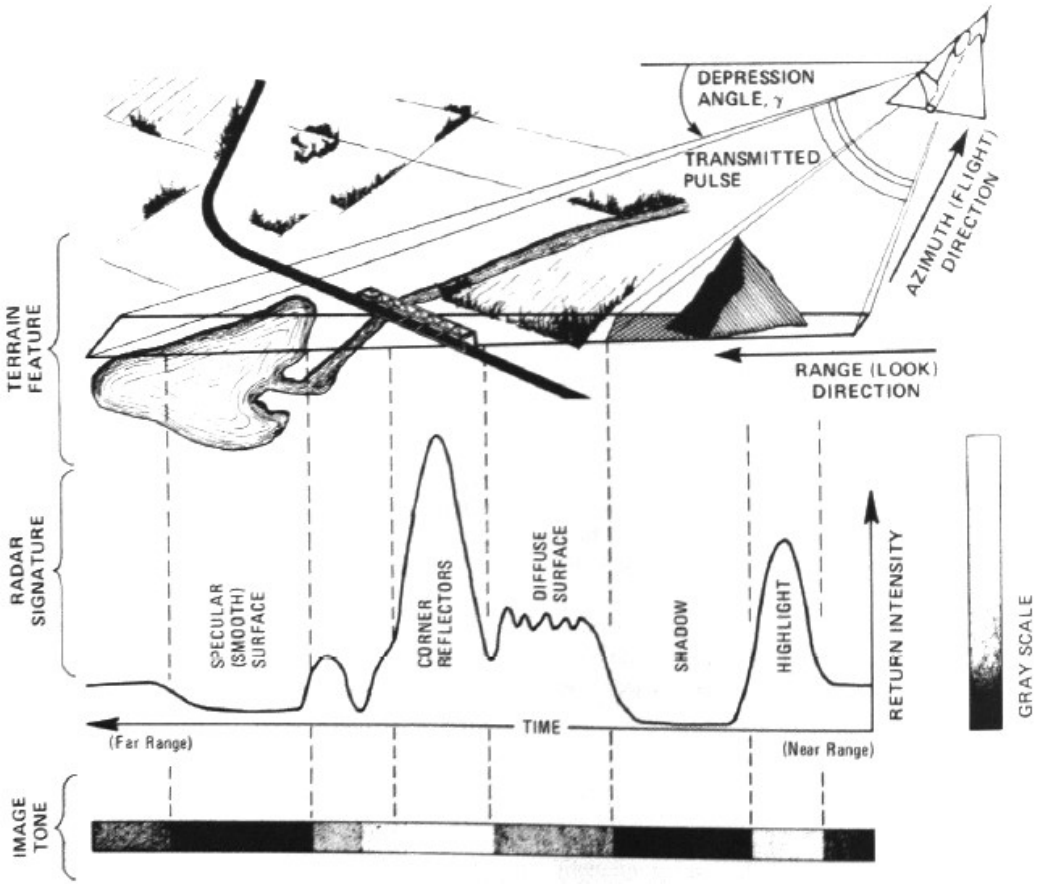


Figure 2.8 Impacts of surface material and geometry on backscatter returns. From Sabins 1996.

The effective roughness of a surface is defined by the wavelength of the incident pulse and the actual roughness of the surface. For, at different wavelengths, surface roughness resolves differently; what might present a very rough surface at X-band, would be effectively smooth at C or S-band; the effective roughness of a surface is defined by the Raleigh equation:

$$h < \frac{\lambda}{8 \sin} \qquad [2.7]$$

where h is vertical relief, λ is wavelength and γ is depression angle – the complement of the incident angle – of the sensor. The rougher the surface, the greater the backscatter. The longer the wavelength, the less the effective roughness of the same surface.

## 2.6 Soil Type

Although it might be thought that grain size of the soil would impact upon the effective surface roughness of the soil, the wavelengths used in SAR are sufficiently long that the variation in grain size makes them effectively smooth (Mironov *et al.*,

2004). However, soil type can impact the backscatter due to the effective dielectric constant of it. For, given that it is the dielectric constant of a medium that impacts the backscatter from that material, it is the amount of free water that a soil contains that mainly impacts its backscatter values. The dielectric constant is affected by grain sizes (Hallikainen *et al.*, 1985; Mironov, 2004; Srivastava *et al.*, 2009), with sandy soils having a higher concentration of free water than clay soils, which is why the correlation between moisture and backscatter coefficient is stronger in sandy soils than clay soils (Mironov *et al.*, 2004) as in sandy soils more water dipoles are free to align with the incident electromagnetic waveform (Engman and Chauhan, 1995).

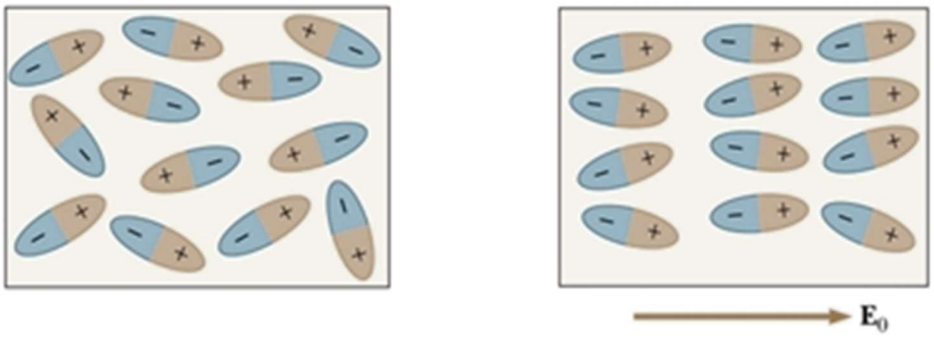


Figure 2.9 Orientation of polar molecules with and without the presence of an electric field. From (Serway *et al.,* 2000).

In interpreting SAR data using amplitude, the problem of equifinality is considerable. For, it is possible that the same amplitude value could be achieved through multiple different surface conditions, made up of different combinations of roughness, wetness, and contributory factors from neighbouring pixels.

## 2.7 Image resolution

The spatial resolution of the image is defined by the dimensions at ground level of the cell formed by range and azimuth resolutions. The range and azimuth resolutions are determined by both the imaging mode and the wavelength of the sensor.

Range resolution is determined by the depression angle and the pulse length – the length of time over which the pulse is emitted; measured in micro seconds (μs). It is converted from time to distance by multiplying by the speed of EM:

$$R = \frac{tc}{2\,\mathrm{co}} \qquad [2.8]$$

where, $t$ is the period of the pulse emission, $c$ is the speed of light ($3 * 10^8$ $ms^{-1}$) and $\gamma$ is the depression angle from the sensor. At different depression angles the same two points can be either resolved or not resolved based on their distance from the antenna. That is, it is possible for two objects of the same size to be differentially resolved on the basis of their distance from the azimuth. To improve the resolution, pulse length can be reduced, but this reduces the amount of energy emitted, and therefore, the amount of energy received back. This is an important consideration for the design of projects using SAR, for the size of features desired to be resolved needs to be considered when the resolution of the imagery chosen and also any post-processing of the imagery is designed.

Azimuth resolution is determined by the width of the terrain 'illuminated' by the beam. To be resolved, targets must be further apart than the width of the beam. Beam width is not constant. Rather, it increases with distance from the antenna. Azimuth resolution is higher for shorter wavelengths. Beam width is inversely proportional to antenna length (5.1).

$$R = \frac{0.7 * S * \lambda}{D} \quad [2.9]$$

where $S$ is slant range distance, $\lambda$ is the wavelength of the pulse and $D$ is antenna length.

Antenna length is limited due to the restrictions on transporting the system into orbit in the case of satellites.

Over recent years the resolution of images has increased considerably due to the increased use of shorter wavelength imaging platforms like TerraSAR-X, NovaSAR and COSMO-SkyMed. In Spotlight mode – the highest resolution imaging mode common to satellite platforms – images are available at resolutions smaller than 1 $m^2$ (Paloscia *et al.*, 2012; ASI, 2016; Cohen *et al.*, 2016).

## 2.8 Image calibration and correction

This section sets out the some of the necessary considerations when using SAR data. SAR imagery has quite different properties to the optical imagery. To be able to use the complex data in the image, it is necessary to calibrate and correct the image before being able to interpret it. This section outlines some of the steps considerations necessary in this.

### 2.8.1 Calibration

Before entering the operational phase, all SAR sensors undergo a period of imaging calibration and validation using ground-based targets with known parameters to ensure that sensors are well calibrated (Calabrese *et al.*, 2008; Grimani *et al.*, 2008). This is particularly important in the context of the ever-growing number of constellation satellites, where inter-calibration across the constellation is key for the delivery of appropriate products across the constellation.

### 2.8.2 Absolute backscatter returns

To be able to calibrate reflectance values for the SAR images it is necessary to have points of known reflectance value in the image (Gray *et al.*, 1990). Conventionally, these points are provided through the placement of trihedral corner reflectors. Trihedral corner reflectors are formed of three conducting plates intersecting at right angles (Figure 2.10), the reflectance of which, if its relative alignment to the satellite overpass is known, can be calculated (Ulaby *et al.*, 1982) (Figure 2.11) and thereby used as a known value within the image from which other values in that image can be cross-calibrated. The orthogonal structure of the trihedral corner reflector ensures that the reflected waves exit in the same direction as the original incident waves entered (Shaeffer *et al.*, 2004), meaning that it functions as a perfect reflector and appears very bright in the image (Sabins, 1996).

A comparison of the backscatter returns from corner reflectors, or other structures which produce a double bounce, can be used to inter-calibrate images from one or more satellite sensors to ensure good calibration between them (Baghdadi *et al.*, 2015). On the whole, most calibration work is undertaken by satellite operators prior to entering the operational phase, though it is becoming apparent that for some constellations there might be a need for product users to assess the inter-calibration of the imagery delivered to them (Baghdadi *et al.*, 2015; Gorrab *et al.*, 2015).

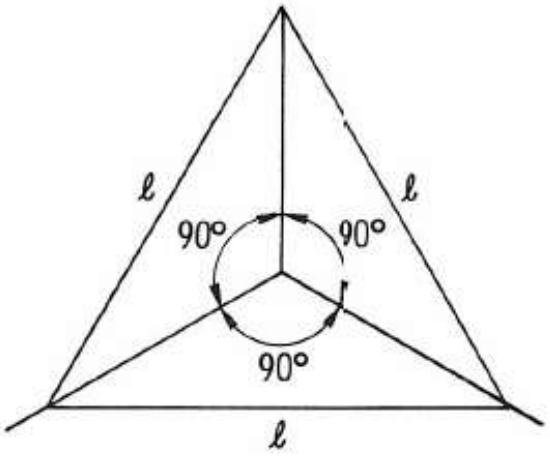


Figure 2.10 Diagram of orthogonality of a trihedral corner reflector. From (Ulaby *et al.*, 1982).

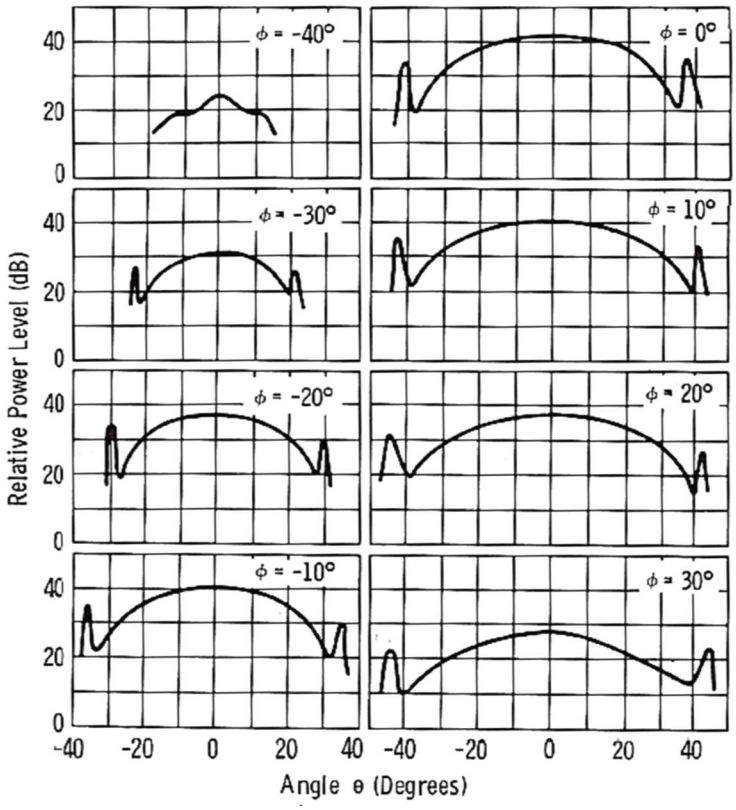


Figure 2.11 Relative power level (dB) of corner reflector backscatter at different incident and planar angles, with reflector side length 61cm and wavelength 1.25cm. From (Ulaby *et al.*, 1982)

### 2.8.3 Correction

Depending upon the product type ordered by the end-user, some correction procedures may need to be undertaken prior to use of the data. The majority of image providers (ASI, 2009) or their over-arching organisations offer extensive advise and often tools (ESA, 2020) for the appropriate means for undertaking any correction or post-processing. This section briefly sets out a couple of the corrections most commonly necessary to be undertaken with SAR data that has been provided with minimal processing undertaken by the provider.

### 2.8.4 Geometry

Side-looking radar systems producing slant-range displays compress the near-side features relative to the far-side features. The transformation used to correct for this is

$$G = H\left(\left(\frac{1}{sin^2\gamma}\right) - 1\right)^{0.5} \quad [2.10]$$

where, $G$ is ground-range distance, $H$ is the height of antenna and $\gamma$ is the depression angle of the sensor. This produces an image which assumes the ground is horizontal, and makes no allowance for topographic variations (Sabins, 1996). To account for topography, high resolution digital elevation models (DEMs) are used to calculate the local incidence angle on a pixel-by-pixel basis, and therefore correct the backscatter return value appropriately, with studies having found that using the highest resolution DEM product available to be the optimal approach (Baghdadi *et al.*, 2002). The European space Agency (ESA) have produced a tool within their SNAP software to enable this to be undertaken.

## 2.9 Speckle

Speckle is the product of irregular constructive and destructive scattering caused by scatterers in nearby pixels. On account of this constructive and destructive scattering (Fig 4.1), two adjacent pixels with very similar scatterers in them can have markedly different scattering signature. Two philosophies of how to mitigate the effects of this interference, and therefore to allow the estimation of soil moisture at a pixel-by-pixel basis, predominate – non adaptive and adaptive spatial domain filters.

### 2.9.1 Non-adaptive Spatial Domain Filters

Spatial Domain speckle filtering uses a moving kernel, which assigns a new value to the central pixel of the kernel. There are two kinds of non-adaptive filters - mean and median filters. These calculate the mean or the median respectively of the kernel area and assign it to the middle pixel. Each has different advantages and disadvantages. Mean filtering is good for smoothing the data but loses some of the image definition. It is, however, better at maintaining the radiometric qualities of the pixel. Median filtering is better at preserving texture than the mean filter, but modifies the radiometry of homogeneous areas. While being good at removing spot noise, this also means that it can often remove narrow linear features.

### 2.9.2 Adaptive Spatial Domain Filters

Adaptive filters, like non-adaptive ones reduce the impact of speckle but are also better at maintaining edge information. To do this, they exploit local statistics in the moving window.

#### 2.9.2.1 Lee Filter - Minimum Mean Square Error

The Lee filter is a weighted sum of the observed central pixel and the mean of the window values. The weighting coefficient is a function of heterogeneity in the window, which is measured with the coefficient of variation.

$$R = I_c * W + I_m * (1 - W) \quad [2.11]$$

where, $W$ is the weighting function $W = (1 - \frac{C_u^2}{C_i^2})$, $C_u$ is the noise variation coefficient $\sqrt{(1 - effective\ number\ of\ looks)}$, $C_i$ is the image variation coefficient $\sigma / l_m$, $I_c$ is the central pixel of the filter window, $I_m$ is the mean intensity in the filter window, σ is the standard deviation of intensity within the filter window.

#### 2.9.2.2 Frost Filter - Minimum Mean Square Error

Like the Lee filter, the Frost filter uses the MMSE approach. It does, however, differ on one fundamental point, namely, that it uses the measure of local heterogeneity to adapt the size of the kernel window. That is, the greater the local heterogeneity, the smaller the kernel window.

$$R = \frac{(P_1 * M_1 + P_2 * M_2 + \cdots + P_n * M_n)}{(M_1 + M_2 + \cdots + M_n)} \quad [2.12]$$

where, $M = e^{-AT}$ and $A = DampFactor * C_i^2$, $M$ is the weighting value, $T$ is the Euclidean distance between the centre pixel and the neighbouring pixels and *DampFactor* is the exponential damping factor.

#### 2.9.2.3 GAMMA MAP Filter - Maximum A Posteriori

This assumes that the values of the scene underlying the speckle has a gamma distribution.

It functions similarly to the enhanced Lee filter, but with a different filtering model for heterogeneous areas. It minimises the loss of texture better than the Frost and Lee filters for gamma-distributed areas (oceans, forested and agricultural areas). Where there is not a gamma distribution, it leaves the original pixel value.

$$R_f = (B * I_m + \sqrt{D})/(2 * A) \quad [2.13]$$

## 2.10 Remote sensing of soil moisture

There have been various approaches to monitoring soil moisture from space. Initially, the fact that wet soil is darker than light soil was utilised in optical surveys (Kerr *et al.*, 2010). Optical surveys then developed to using vegetation indices as proxies of soil moisture (Carlson *et al.*, 1994; Dubois *et al.*, 1995; Chauhan *et al.,* 2003). However, the presence of cloud cover, in particular when wetting was occurring, provided a significant problem for optical imaging methods, especially in the context of hazard assessment. Heat has also been used, for, wet soils have a higher thermal inertia and lower temperature than dry soils. So, thermal inertia monitoring has been tried (Kerr *et al.*, 2010). However, being, again, an optical measure, it also is affected by the factors affecting other optical approaches – atmospheric effects, masking by clouds, the opacity of vegetation covers. There were also problems with the method itself – it only measures the very surface of the soil, which is mainly affected by atmospheric conditions – wind cooling the soil – rather than soil processes (Kerr *et al.*, 2010). Other approaches include passive microwave sensors, which, while they have good return times, are limited in their utility for many applications by their low spatial resolution - in the order of tens of km (Sabins, 1996; Olsen, 2007; Kerr *et al.*, 2010; Kornelsen and Coulibaly, 2013).

Soil moisture estimation by SAR is not limited by many of the challenges optical imagery has. It is based on the linear relationship between the dielectric constant of the soil and the amplitude of the backscatter response (Engman, 1991). The dielectric constant is a phenomenon caused by water molecules aligning themselves

with incident electromagnetic waves on account of their dipolar arrangement (Serway *et al.*, 2000). At radar wavelengths, the dielectric constant is 3-8 for dry rock and soil. For water it is about 80 (Schmugge *et al.*, 1980; Sabins, 1996; Schmugge *et al.*, 2002); consequently, for wet soil, the value can be over 25, which, in some cases, can be approaching an order of magnitude greater than the dry soil value for the same point. The relationship between radar backscatter and volumetric soil moisture is "strong, positive, linear and independent of scale" (Shoshany *et al.*, 2000). The most common way to relate soil moisture and the dielectric constant is through one of three empirical curves derived by Hallikainen *et al.* (1985), Dobson *et al.* (1985) and Peplinski *et al.* (1995). When microwaves hit a surface, they can either be absorbed (attenuated), scattered, reflected or can penetrate and be further absorbed or scattered. Wilheit (1978) and Newton *et al.* (1982) have shown that the depth to which radar penetrates is equal to a couple of tenths of a wavelength.

To calculate the impact of the soil moisture on backscatter, the contribution from surface geometry needs to be accounted for either through elimination, measurement or modelling. There have been four different approaches to this problem – change detection, physically based theoretical models, empirical models or polarimetry. For, surface roughness has a large impact on backscatter; indeed, it is so significant that Baghdadi *et al.* (2002b) showed that roughness has a greater impact on the SAR response than soil moisture – a finding which has since been replicated (Gorrab *et al.*, 2015). This impact on backscatter makes it a prime area of interest in soil moisture retrieval, (Verhoest *et al.*, 2008) and one whose characterisation continues to create significant challenges for those seeking to estimate soil moisture (Wagner and Pathe, 2005).

Characterising surface roughness at a field scale is difficult. There are various methods of measuring roughness during field studies including pin profilometers at multiple scales (Álvarez-Mozos *et al.*, 2006) or laser profilometers (Davidson *et al.*, 2000, 2001; Mattia *et al.*, 2003). The heterogeneity of this parameter at a field scale means, however, that the extrapolation of these data at a field scale limits the accuracy of soil moisture retrieval when these extrapolated roughness values are extrapolated (Srivastava *et al.*, 2008).

### 2.10.1 Relative soil moisture estimation (change detection)

Change detection is probably the most common soil moisture estimation technique in used in modern studies that focus on soil moisture estimation itself, rather than

methodological improvements to soil moisture estimation (Moran *et al.*, 2000; Wagner *et al.*, 2003; Kerr *et al.*, 2010; Albergel *et al.*, 2012; Sportouche *et al.*, 2012; Ouellette *et al.*, 2017; Zhu *et al.*, 2019; Mattia *et al.*, 2020; Punithraj *et al.*, 2020; Zakharov *et al.*, 2020). Change detection mechanisms compare backscatter signals from two or more co-located images of the same location to calculate the change in dielectric constant of the soil (Ulaby *et al.*, 1986; Sabins, 1996). This method works on the assumption that one component of the backscatter – the surface roughness – remains constant between the two scenes, meaning that any change on a pixel-by-pixel basis is caused by a change in soil moisture (Moran *et al.*, 2000; Albergel *et al.*, 2012). Long repeat times (~1 month) can, however, limit its theoretical efficacy (Kerr, 2007), due to changes in vegetation during that time, although vegetation modelling or *in situ* characterisation field studies undertaken concurrent with SAR acquisition significantly improve the viability of it as a method (Hegarat-Mascle *et al.*, 2002; Wagner *et al.*, 2003). The primary advantage of change detection as a technique is that it is relatively computationally light and requires minimal *in situ* measurement, additionally, it requires much less detailed, or no, *a priori* knowledge of the site than the approaches set out in the next sections; however, the disadvantage is that it requires multiple images of the same geometry (although some recent studies (Sahebi and Angles, 2010; Wang *et al.*, 2011; Zhu *et al.*, 2018) have sought to utilise different geometries to enhance change detection methods), and gives a measure of *relative* moisture rather than absolute.

### 2.10.2 Physically based theoretical models

Physically based models account for the dielectric constant of the scattering surface. The disadvantage of these models is that they require *a priori* knowledge of surface roughness. Fung's (1994) Integral Equation Model (IEM) is the most well-known of these and is based on the Physical Optics Model (POM) (Born and Wolf, 1980; Song *et al.*, 2009) and the Small Perturbation Model (SPM) (Dubois *et al.*, 1995; Engman and Chauhan, 1995); several improvements and developments along the same theory have been proposed more recently (Baghdadi *et al.*, 2002; Song *et al.*, 2009).

### 2.10.3 Empirical models

Empirical models use the empirical relationship between soil moisture and the Normalised Radar Cross Section (NRCS), making them, therefore, generally limited to the location of the dataset they are developed at (Baghdadi *et al.*, 2002). More recently, empirical (Oh *et al.*, 1992; Dubois *et al.*, 1995) models or model extensions have been developed. These have the advantage of allowing inversion with dual

polarised observables, but have the disadvantage that they are based on regression coefficients from a specific test site, and therefore require re-calibration for each different location used. Somewhat bridging the gap between the theoretical and empirical models is the semi-empirical model developed by Shi *et al* (1991.

### 2.10.4 Semi-Empirical models

Semi-empirical models solve the problem of requiring *a priori* knowledge of surface roughness that theoretical models have, and the site specific problems of empirical models by combining characteristics of each – empirically based models and scattering theories (Oh *et al.*, 1992, 2002; Dubois *et al.*, 1995; Shi *et al.*, 1997; D'Urso and Minacapilli, 2006; Oh *et al.*, 2013; Kweon and Oh, 2014). The three most commonly used of these models are defined particularly in the polarisations required. Of the three earliest, and most often cited approaches to dealing with the surface roughness problem, there are three different philosophies: Oh *et al.*'s models (1992; 2002) require fully polarimetric data, Dubois *et al.*'s (1995) require dual-polarisation data, and Shi *et al.*'s (1997) only require single polarisation data. More recently, however, the research group Oh works in has moved to looking at the potential for using single-polarised SAR for soil moisture estimation (Oh *et al.*, 2011; Kweon *et al.*, 2013; Oh *et al.,* 2013; Kweon and Oh, 2014).

### 2.10.5 Polarimetry

Almost all recently launched SAR satellites are capable of producing data in multiple polarisations, some as single-polarised products, others as multi-polarised products. The increasing availability of multi-polarised products has led many to focus on this method for assessing soil moisture as the multi-polarised returns enable better assessment of surface geometries and scattering methods (Jagdhuber *et al.*, 2008; Hajnsek *et al.*, 2009; Martone *et al.*, 2010; Reigber *et al.*, 2013; Wang *et al.*, 2017).

Mathematical decompositions using fully-polarised SAR have significant advantages over methods like the simple change detection approaches outlined above in terms of being able to invert for both soil moisture and vegetation by making use of the difference in backscatter in each of the four polarizations (HH, HV, VH, VV). Polarimetric SAR proponents use the different responses of surface features to different polarisations of EM energy to decompose backscatter responses. Each pixel in a PolSAR image has four 'receive' values attributed to it. These values stem from the nature of a PolSAR system, which sends out first one polarisation, then receives both polarisations back, then sends the other polarisation and receives both

polarisations back. That is, it emits horizontally polarised EM wave, receives the horizontally (HH) and vertically (HV) polarised backscatter, then emits vertically polarised EM wave, receives the horizontally (HV) and vertically (VV) polarised backscatter (Jagdhuber *et al.*, 2008).

## 2.11 X-band soil moisture estimation context

Having considered the processual complexities associated with utilising SAR data for soil moisture estimation, it is necessary to focus more closely in on the specific challenges associated with utilising the shortest wavelength SAR products, one of which – X-band COSMO-SkyMed Spotlight2 data – is central to this project. In recent years the X-band SAR sensors have been deployed on satellite missions, for example on TerraSAR-X and the COSMO-SkyMed first (CSK) and second (CSG) generations. The utilisation of X-band SAR for environmental sensing is a divergent approach from that previously undertaken, where longer wavelength sensors, like the C-band RADARSAT and L-band ALOS PALSAR had been preferred for environmental remote sensing due, in part, to the smaller impact surface roughness has on the backscatter return. Shorter wavelength platforms have, however, become more common, particularly, in the context of increased interest in the development of satellite constellations, as they provide high resolution SAR data, with the benefit of the short return period constellations offer.

Although constellations have minimised the required trade-off between resolution and return-periods, several studies undertaken early on in the operational phase of the CSK project have shown that there is some discrepancy in the backscatter returns between the four satellites that make up the constellation (Baghdadi *et al.*, 2015; Gorrab *et al.* 2015), as well as discrepancy between the CSK and TerraSAR-X sensors (Paloscia *et al.*, 2012; Sportouche *et al.*, 2012; Pettinato *et al.*, 2013; Gorrab *et al.*, 2014; Baghdadi *et al.*, 2015; Gorrab *et al.*, 2015).

Sensors using longer wavelengths have predominated in the field of environmental monitoring as backscatter returns are less impacted by surface roughness, and therefore, soil moisture is easier to estimate (Baghdadi *et al.*, 2002). Indeed, the majority of studies which have used X-band SAR for soil moisture estimation have found that the only soil moisture estimation method that is appropriate using a single-polarised product is change detection, which assumes surface roughness does not change between images (Notarnicola *et al.*, 2010; Gorrab *et al.*, 2015). Many SAR studies have utilised multi-polarised SAR data to enable more robust soil moisture

inversions to be undertaken, through the ability this data gives for the better estimation of the roughness component of the backscatter return (Jagdhuber *et al.*, 2008; Martone *et al.*, 2010; Reigber *et al.*, 2013).

## 2.12 X-band environmental sensing summary

The use of X-band SAR for environmental remote sensing is still relatively novel. Although the potential to undertake this research direction has existed since the understanding of the relationship between dielectric constant and the SAR backscatter response was understood some decades ago (Ulaby *et al.*, 1986), it is only in the last decade or so that X-band SAR platforms have become available for environmental researchers to use. Although research into how best to estimate soil moisture from SAR backscatter has been studied for decades (Kerr, 2007), and different processing protocols have been developed for different specific uses in highly constrained circumstances, there is even greater uncertainty as to the best way to estimate soil moisture from X-band and other short-wavelength SAR products, or, indeed, whether this is even realistically achievable (Wagner and Pathe, 2005). For, as methodologies stand at the moment, the majority view is that change detection, which has the limitation for time series studies that it assumes stationarity of vegetation and its associated roughness, is the best approach for estimating soil moisture. Not only does this approach limit the return period of images that can be used, it also only provides a measure of relative moisture, rather than a measure of absolute moisture, the utility of which, in the context of monitoring a driver of slope instability which is generally accepted as leading to instability at a specific threshold, is questionable.

## 2.13 COSMO-SkyMed review

So far this chapter has explored the general context, theory and usages of SAR imagery. The narrower context of this thesis is now considered by summarising the extent of research undertaken with COSMO-SkyMed imagery at the time this project was undertaken.

### 2.13.1 COSMO-SkyMed Usage

In designing this project, a summary of all published work using the CSK platform was undertaken. Many of the projects highlighted in this review were focussed on algorithm development and testing (Notarnicola *et al.*, 2010; Balenzano, *et al.*, 2011; Oh *et al.*, 2011; Kweon *et al.*, 2012, 2013; Kweon and Oh, 2014). These projects can be divided into two groups: SAR algorithm testing, with *in situ* ground truthing, or

inversion testing against modelled data (Fontanelli *et al.*, 2013; Iacobellis *et al.*, 2013). Another key theme emerging from the papers is that of vegetation monitoring (Capodici *et al.*, 2011; Mattia *et al.*, 2012; Santi *et al.*, 2012; Satalino *et al.*, 2012; Paloscia *et al.*, 2014) and soil moisture monitoring of bare (Santi *et al.*, 2011; Wang *et al.*, 2013; Gorrab *et al.*, 2014; El Hajj *et al.*, 2015; Gorrab *et al.*, 2015) or vegetated soil conditions.

Another subset of projects was focussed on examining COSMO-SkyMed's data in comparison to other sensors (Balenzano *et al.*, 2011; Santi *et al.*, 2011; Paloscia *et al.*, 2012; Paloscia *et al.*, 2012), in particular TERRASAR-X, for specific roles, or comparing the ability to use X-band for environmental sensing with another more commonly used band, like C (Notarnicola *et al.*, 2010) or L (Balenzano *et al.*, 2013), in specific contexts. These studies found there to be variation in the backscattering returns between the 4 satellites of the constellation, with Baghdadi *et al.* (2015) finding a variation of 1.6 dB between CSK3 and CSK4 images, CSK2 very similar to CSK3, and CSK1 1.1dB darker than CSK3.

### 2.13.2 Terrain and Vegetation

Of the 23 papers published, 13 have test sites situated on plains, one has a test site on plain and mountainous terrain (Paloscia *et al.*, 2012), one has mountainous terrain (Paloscia *et al.*, 2014), and one has hilly terrain (Ciervo *et al.*, 2011; Riccio *et al.*, 2012) (none of the papers express their AOI terrain quantitatively); the rest do not specify the terrain.

In terms of vegetation, seven of the papers focus on sites with bare soil (Oh *et al.*, 2011; Santi *et al.*, 2011; Paloscia *et al.,* 2012; Gorrab *et al.*, 2014; Kweon and Oh, 2014; Gorrab *et al.*, 2015), seven on agricultural fields featuring predominantly wheat, beet and sunflower crops (Balenzano *et al.*, 2011; Kweon *et al.*, 2012, 2013; Mattia *et al.*, 2012; Santi *et al.*, 2012; Fontanelli *et al.*, 2013; Iacobellis *et al.*, 2013; Paloscia *et al.*, 2014), two on grasslands (Wang *et al.*, 2013; El Hajj *et al.*, 2015), two on tree, shrub and rocky sites (Capodici *et al.*, 2011; Paloscia *et al.*, 2014), three are not specified (Notarnicola *et al.*, 2010; Paloscia *et al.*, 2012; Riccio *et al.*, 2012).

There are two main regions where research has been undertaken. Unsurprisingly, given the access conditions from the Italian Space Agency, and their provision of funding and data early on in the constellation's operational phase (Pettinato *et al.*, 2013), for studies exploring the capabilities of SAR, mainland Italy and Sicily are the most common regions; Australia is also used in several papers as a location

(Satalino *et al.*, 2012; Wang *et al.*, 2013). The two other countries covered in papers at that point were South Korea (Kweon and Oh, 2014) and Burkina Faso (Ciervo *et al.*, 2011; Riccio *et al.*, 2012). From the body of literature surveyed, revisit times ranged from 1 day (Gorrab *et al.*, 2014) to 1 month. The number of images used ranges from five (Capodici *et al.*, 2011) to 28 (Wang *et al.*, 2013).

This brief survey of the studies published using CSK data showed that there was a knowledge gap in the area of soil moisture estimation over sloped terrain in temperate climates. This gap, therefore, represented a fit with the survey site – Hollin Hill. Furthermore, the scope for long time series acquisitions as exhibited by the time series survey showed that there was potential to extend this study to investigate the appropriateness of SAR use during the whole phenological cycle. At this point, studies had relatively short time series, with the majority of projects targeting development of processing methodologies and algorithms or assessing the performance of CSK relative to other platforms, with only one (Fontanelli *et al.*, 2013) using data that spanned a year or more. Most papers used images collected over a period of one to six months.

## 2.14 Summary of SAR literature

Synthetic aperture RADAR is not a new technology, having been first experimented with in 1952. It is, however, a complex technology to use well in the context of environmental remote sensing. Setting imaging parameters appropriately to enable soil moisture estimation is becoming more possible through the development of high resolution satellite constellations and the shorter return times that they offer, thereby making change detection a more viable estimation technique, but it is still challenging given the heterogeneity and variability of surface geometries. Great attention has to be paid, therefore, to the system parameters by which imagery is gathered, and the appropriateness for use of these images.

Satellite missions are designed for a broad market (Wagner and Pathe, 2005), and therefore do not always provide the specific criteria which are most required by environmental scientists. Likewise, the questions which are asked through SAR data – particularly those which query soil moisture in poorly constrained geometric contexts – are often inappropriate or currently not possible to ask given the challenges posed by surface geometry in the estimation of soil moisture. So, although SAR has many theoretical benefits over optical or other passive remote sensing

technologies, there are also challenges in its use that are well recognised by the remote sensing community, though not necessarily well solved.

## 2.15 Literature review summary

This chapter has explored the literature surrounding this thesis project. It has shown the current state of remote sensing of landslide drivers, the challenges of relating remotely sensed slope characteristics with slope failure, and also set out the history, opportunities and limitations of use of SAR for environmental remote sensing. This will be the basis from which each of the next four chapters will build. First, in the Materials and Methods Chapter, Chapter 3, and then in the discussion undertaken in each of the next three chapters.

# 3

# CHAPTER 3: MATERIALS AND METHODS

This chapter describes the fieldsite, the extant and novel in situ data products used in this project and their acquisition and calibration, and then gives the context of SAR remotes sensing at the field site, before describing the SAR data product used in this project and the supplementary data sets which were used to calibrate this SAR data product.

## 3.1 Field Site

The study area is the 4.5 hectare Hollin Hill Landslide Observatory in North Yorkshire, England (Lat-Long 54.1106°N, 0.9602°W), (Figure 3.1), bounded to the North, East and South by arable land and to the West by mixed woodland, used for pasture and with an elevation of between 55 and 100 m AOD and an average gradient of 12°; to the south sits an ice-marginal drainage channel from the Devensian (Chambers *et al.*, 2008). The site features four slow to very slow moving reactivated rotational earth flows (Cruden and Varnes, 1996), comprising of four landslide lobes stretching across the face of the slope (Figure 3.2) initiating in Whitby Mudstone-derived soils – a clay-dominant regolith (Powell, 1984; Hobbs *et al.*, 2012) – and then moving to a translational flow (Varnes, 1978; Cruden and Varnes, 1996) over Staithes Sandstone. The site is highly susceptible to landsliding driven by seasonal soil-moisture variations (Jenkins *et al.* 2006; BGS, 2016) - a type highly representative of landslides across western Europe and the UK and accounting for a high proportion of landslides recorded in Britain (Foster *et al.* 2007; Gibson *et al.*, 2013), and is well representative of landslides in stiff clays (Uhlemann *et al.*), being made up of materials from the Lias Formation, which is recorded as having the highest incidence of landsliding of any formation in the UK (Jones and Lee, 1994). The site has an Oceanic (Cfb) Climate (Koppen, 1936), characterised by warm summers (June to August) and cold winters (December to February).

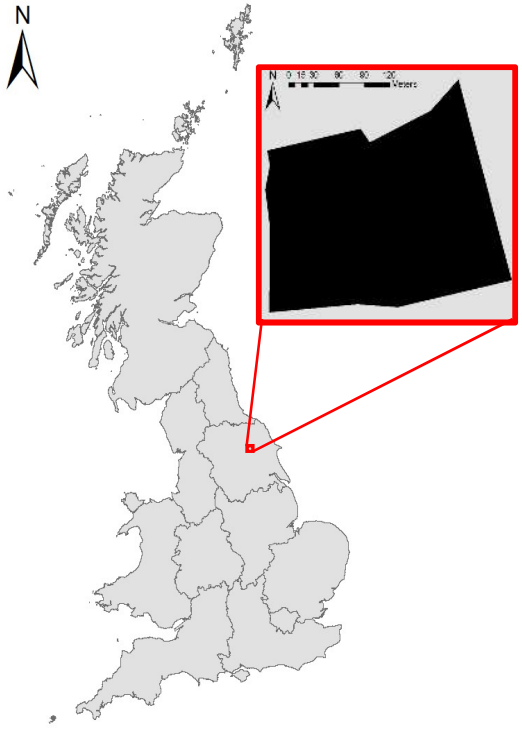


Figure 3.1 The Hollin Hill Landslide Observatory and its position in the UK


Figure 3.2a,b Interpretation of the Hollin Hill landslide features from (Chambers *et al.*, 2011) and optical imagery of the site from Google Earth (2020).


February 2017 – Eastern lobe back scarp cracking, from translational body, just East of cluster 2, looking N


January 2017 – Eastern lobe scarp and translational looking from 10m E of cluster 2, Looking NNW


November 2016 Eastern lobe from top of slope, looking SE


August 2016 – Eastern Lobe back scarp cracking, from translational body, just East of cluster 2, looking N

Figure 3.3a-d On-site images of the landslide

The Landslide Observatory, was set up in 2006 following reports from the farmer-landowner to the BGS that there was slippage of the slope (Jenkins *et al.* 2006). Although the landslide was originally reported in 2005, there is evidence of previous movement, with an inactive lobe underlying and extending beyond the current extent of the furthest East active lobe similar to that marked 'C' in Figure 3.4 which extends beyond the southern boundary of the site (pers. Comm. Archer 2014). The site has two primary benefits for the project, first an active BGS research presence, resulting in over a decade of high temporal resolution soil moisture and slope-deformation data, as well as continued real-time monitoring of these factors at sub-daily resolutions; and second, easy accessibility (~80 miles journey distance) from Durham University.

The site comprises of four landslide lobes of a poorly draining clay derived from Whitby Mudstone that overlies the more southerly Staithes Sandstone-derived soils. The Eastern-most lobe is the most active, with substantial cracking at the crown (Figure 3.2 and Figure 3.4), and sag ponds near the head of the lobe. The slide is rotational, transitioning to translational further down the slope.

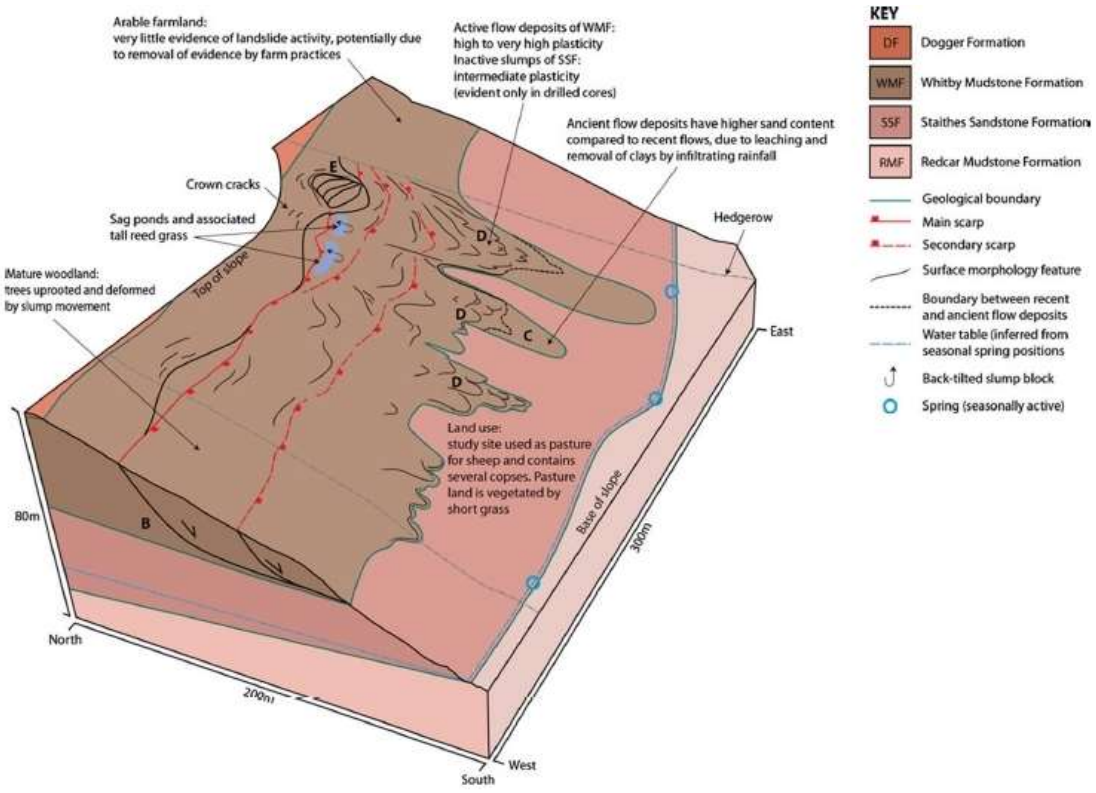


Figure 3.4 Diagram of Hollin Hill slope morphology. From (Merritt *et al.*, 2013).

## 3.2 Site Geology

Multiple geophysical studies of the site have been undertaken, including intrusive investigations through auguring and drilling (Figure 3.6a,b) (Gunn *et al.*, 2013), Electrical Resistive Tomography (ERT) surveys (Chambers *et al.*, 2008; Merritt *et al.*, 2013) have shown heterogeneity in the lithology of the site. The two core examples presented in Figure 3.6a,b shows the difference in the materials at two sites on the slope – Figure 3.6a shows the composition and potential slip lines in the clay of the active eastern lobe, and Figure 3.6b shows the composition of the materials near the foot of the slope in the sand. The lithologies and strength of the deposits shown in these figures shows the complexity of the slope. However, it is possible to summarise the general morphology of the slope thus: put simply, the site

is made up of four different underlying lithologies running in roughly east-west bands perpendicular to the line of the slope (Figure 3.5). The main body of the slope consists of Redcar Mudstone, overlaid by Staithes Sandstone, and Whitby Mudstone, the material properties of which are shown in Figure 3.7. All of these formations are part of the Cleveland Basin Lias Group and were laid down between the Toarcian and Sinemurian stages (Hobbs *et al.*, 2012) between 200–170 Ma ago (Knox *et al.*, 1991) and is made up of marine sediments (Powell, 1984). Lias deposits, and Whitby Mudstone in particular, are susceptible to slope instability (Jones and Lee, 1994). The material shows signs of significant weathering to destructuring with low strength to a depth of about 6m (Figure 3.6) (Gunn *et al.*, 2013).

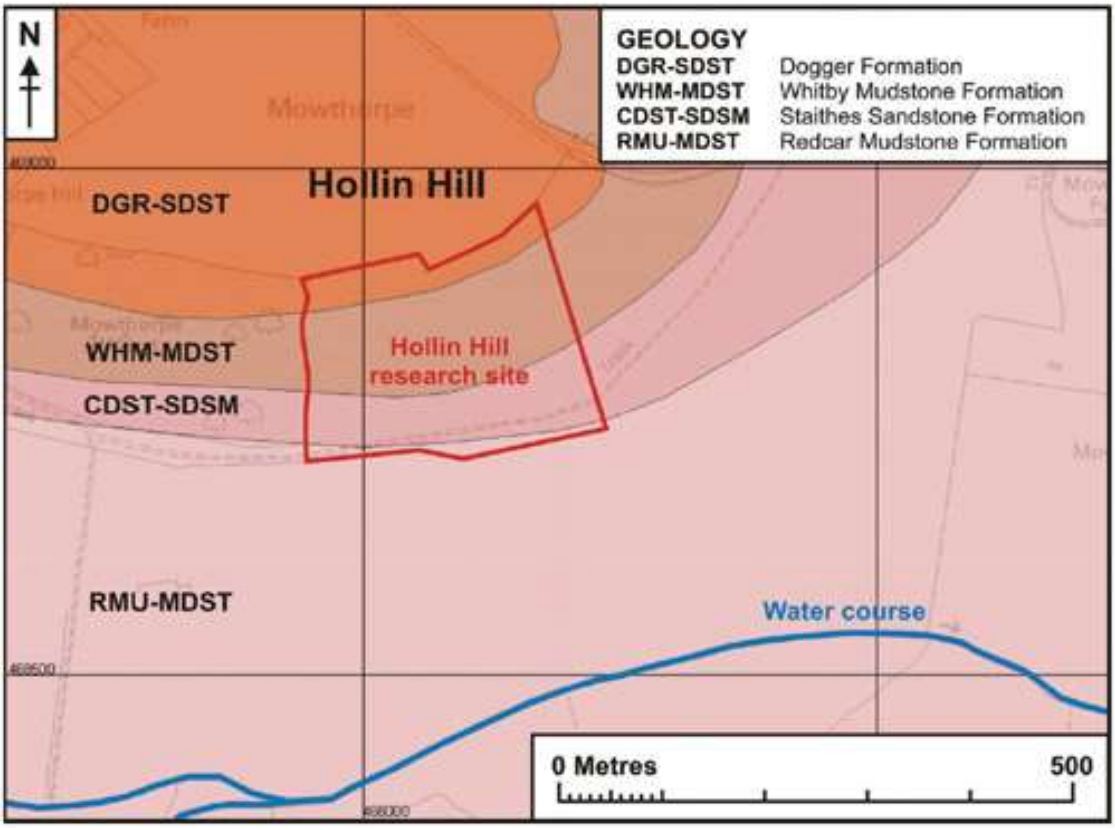


Figure 3.5 Bedrock Geology of the Hollin Hill Site. Source: (BGS, 2016)

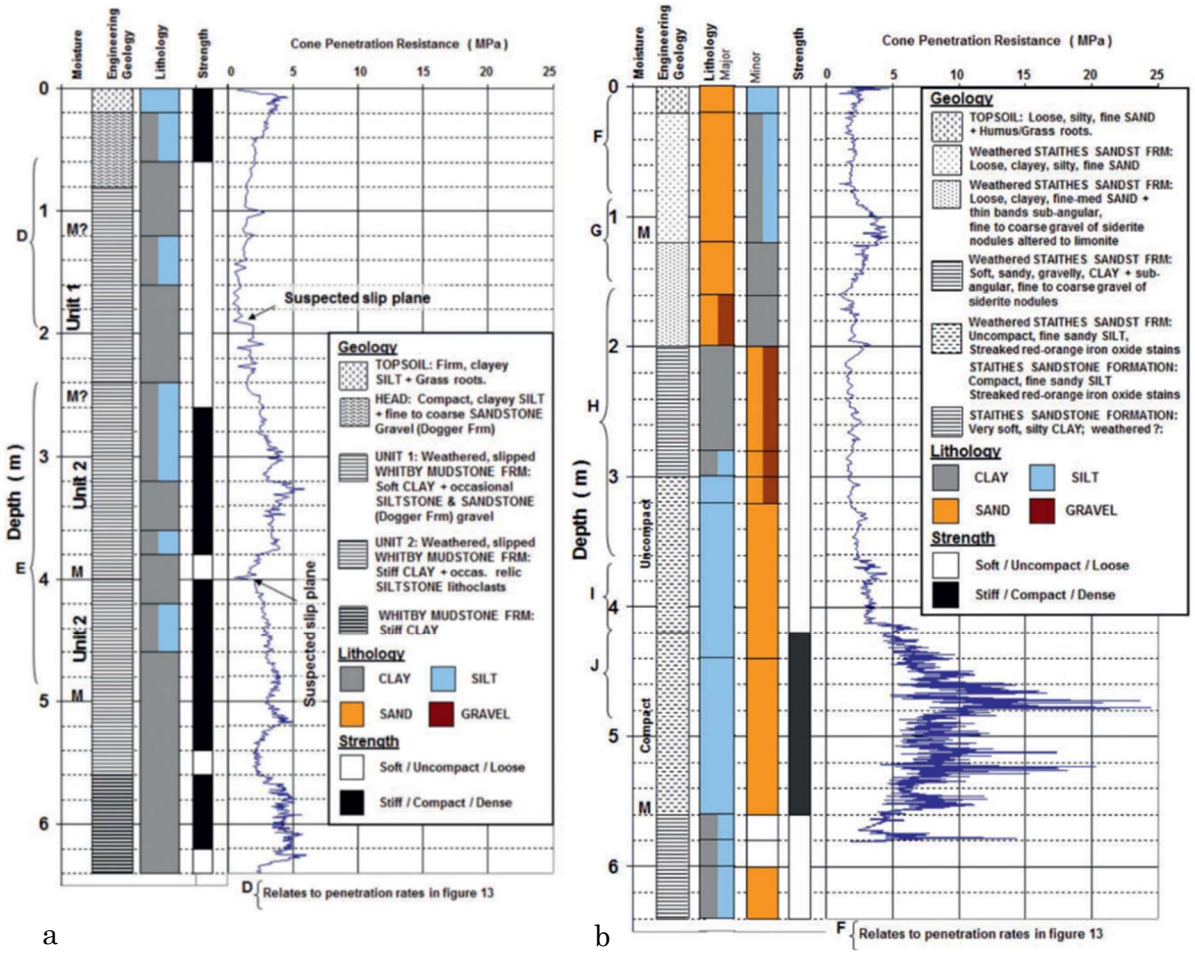


Figure 3.6a Log of a core taken by Gunn *et al.* (2013) in the main eastern lobe. Points marked with M indicate high moisture content and Figure 6b Log of a core taken by Gunn *et al.* (2013) in the main eastern rotational feature. Points marked with M indicate high moisture content.

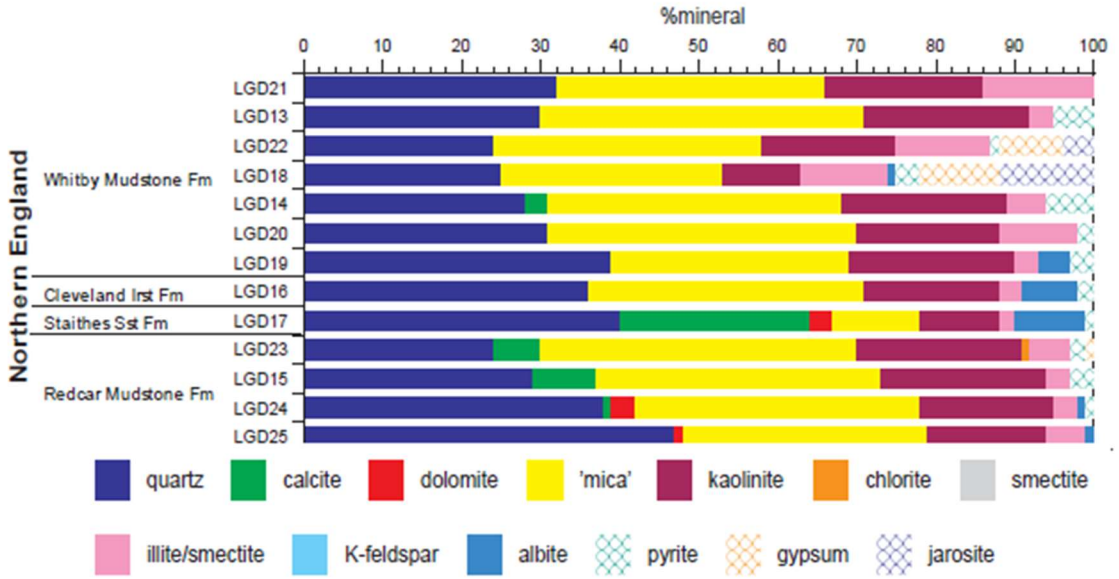


Figure 3.7 Percentage mineral composition of Lias materials. Adapted from: Hobbs *et al.*, (2012).

### 3.2.1 Glacial History

The site is thought to have been glaciated during the Anglian period, and to have been periglacial, with permafrost freeze-thaw during the Devensian coverage of the Vale of York (Gunn *et al.*, 2013), which is thought to have been the cause of the fissuring and shear zones of the site material (Jones and Lee, 1994; Gunn *et al.*, 2013). The valley floor to the south of the site is part of Sherriff Hutton Carr – an embayment from the Devensian period and the site of the ice-marginal Lake Mowthorpe (Chambers *et al.* 2011). The Vale of York is characterised by Lias Group formations, which are prone to instability (Jones and Lee, 1994; Foster *et al.* 2007; Merritt, 2014). Reconnaissance work by BGS of the area surrounding Hollin Hill has identified numerous similar rotational slides in the Lias-derived clays of the region (Figure 3.8) (Jenkins *et al.*, 2005).

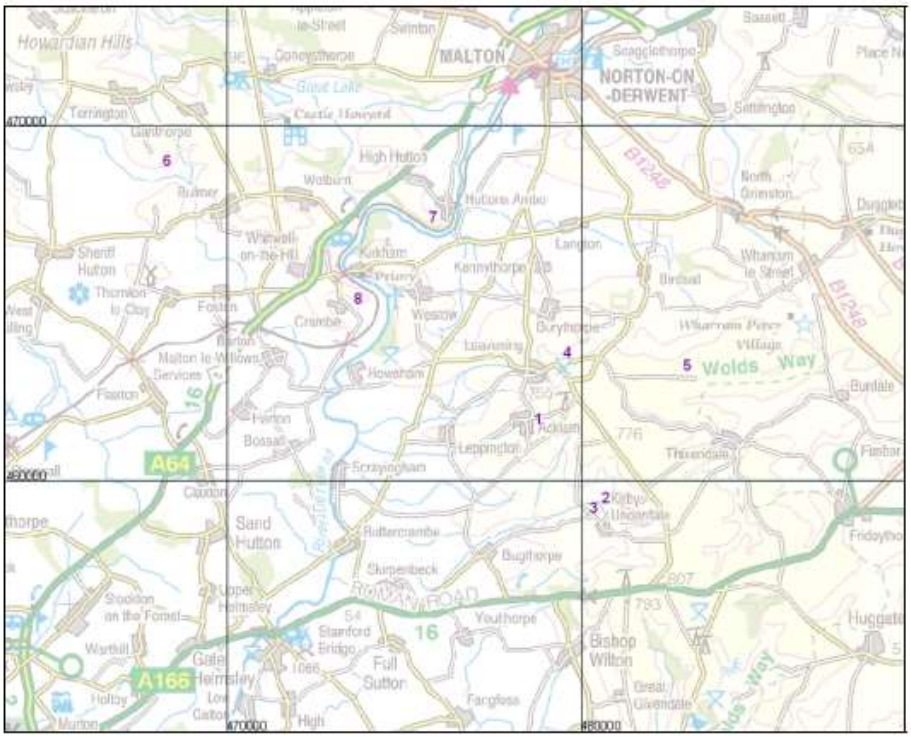


Figure 3.8 Locations of slide features in Lias formation found during BGS reconnaissance study. Hollin Hill is marked as location 6. From Jenkins *et al.*, (2005)

### 3.2.2 Soil

The soils associated with the lithologies outlined above are: the Hollin Hill escarpment is covered by a thin layer of head, ranging from 0.2 m at the head, to 1.3 m at the base of the slope (Chambers *et al.* 2011). This head is a clay with gravel, sand and silt inclusions and some organic inclusions, being made up of local materials and formed by a combination of surface processes like hillwash and soil

creep (Gunn *et al.* 2013). The Dogger Formation gives rise to free-draining sandy soil rich in gravel- to cobble-size rock fragments. The Whitby Mudstone is heavily weathered at the slope surface, forming a badly draining clay soil (Uhlemann *et al.*, 2016), which makes up the majority of the unstable lobes at the site. The Staithes Sandstone-associated soil is overlain with well-draining loam soil and a thin deposit of Aeolian sand over the periglacial head (Uhlemann *et al.*, 2016).

Investigation of the soil characteristics has been undertaken by the hydro-ecology team at BGS, and a simple, three-part soil classification for the site has been created. This map (Figure 3.9) of the soil types is used in the rest of the study as it recognises that, with the landslide being active, soil type boundaries cannot be neatly associated with the lithological boundaries. In particular, in the case of areas where the Whitby Mudstone has slid both recently and long ago, the clay of this formation now overlies some of the sand associated with the Staithes Sandstone section. Furthermore, in the case of the older slides, these clay and sand materials have been bioturbated, forming a distinct area of soil different from the other two types. The three types identified are: clay, sandy clay and sand (Figure 3.9), with the 'clay' class being the weathered Whitby Mudstone, the 'sandy clay' class being the bioturbated paleo- slip Whitby mudstone material and Staithes Sandstone, and the 'Sand' class representing the Staithes Sandstone-associated soil.

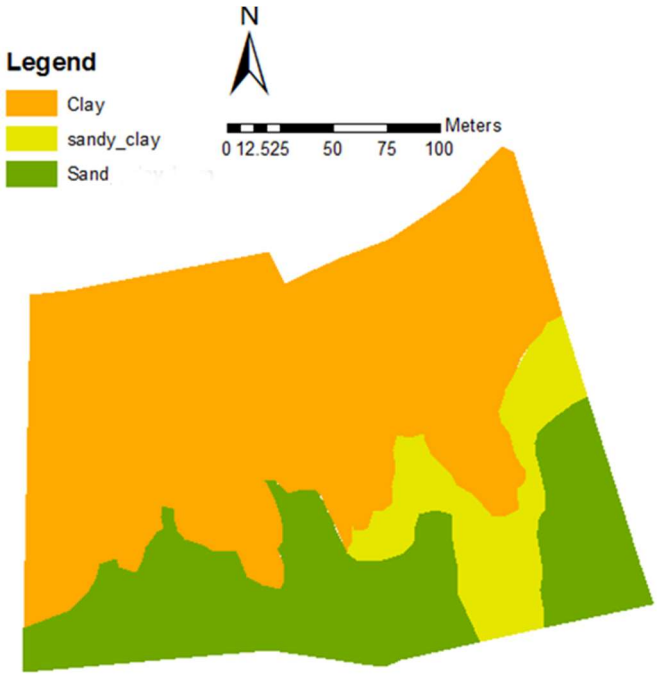


Figure 3.9 Map of soil types at Hollin Hill, where the mobile, upper clay slopes are orange, the sandy clay is yellow, and the sand is green.

### 3.2.3 Vegetation

The site can be classified as having a mixed vegetation regime, predominantly a grassed slope, with young, stand-alone deciduous trees that were planted in the early 2000s on the upper part of the western half of the slope, perhaps in an attempt to stabilise the slope. There are two distinctive vegetation zones at the site. The clay area of the is characterised by short, well cropped lush grasses, with occasional clumps of longer reeds, in particular in the area of the sag ponds on the Eastern lobe, and in areas just downhill of the surface cracking features, predominantly at the head of the slope (Figure 3.10). The clay-dominant area is well grazed by the herd of approximately 15 sheep resident at the site. The lower, sandy slopes are characterised by longer, more structured and clumpy grasses, the length of which varies throughout the year, and which, on occasion, are artificially cropped (Figure 3.11). This area is less favoured for grazing by the sheep.

June 2016 Upper slopes From cluster 2, NW

January 2017 From cluster B, looking NE

November 2016 Cluster A, looking N

February 2017 From Upper Eastern corner of site, looking W

Figure 3.10 Vegetation of the Clay of the site in June, November, January and February

August 2016 – From cluster H, looking W

November 2016 – From cluster H, looking W

December Cluster G, looking ESE

January 2017 Cluster 4 looking SW

Figure 3.11 Vegetation of the Sand of the site in August, November, December and January

### 3.2.4 Displacement Characteristics and Interpretation

As mentioned in section 2.1.1, it is rare that a landslide, unless it is a simple one, moves at the same rate and in the same way throughout the full mass of the slide. This is the case at Hollin Hill. There is evidence of more rapid movement at the head and the toe of the landslide, but with slower motion in the middle from the active breaking at the head scarp and the breaking up of the toe, with buckling of the surface in the middle portion of the slope. This discontinuity of slope motion can most simply be interpreted as being due to a shallower slope angle in the middle portion of the site – forming a natural terrace. The rate of movement of the slope changes episodically, with quoted rates varying from 0.5myr$^{-1}$ (Chambers *et al.*, 2011; Merritt *et al.*, 2013) to 3.5 myr$^{-1}$ (Uhlemann *et al.*, 2016), with most movement occurring during the wetter, winter months; this has been interpreted as being due to increased pore pressures in the slope material.

As was discussed in the section 2.1.1, slope stability in reactivated landslides is related to moisture content in the soil mass. It is posited that part of the cause for the landslide is the uneven rates of flow of water from the soil mass. The upper portion of the site is made up of clay derived from the Whitby Mudstone (Figure 3.12), which has the smallest pore spacings of the three soil types on the site and is, therefore, the slowest draining; whereas, the lower portion of the slope is more free-draining, having higher proportions of sand and silt. The most geomorphically active of these is the clay, which sits at the top of the slope, forming three distinct landslide lobes.

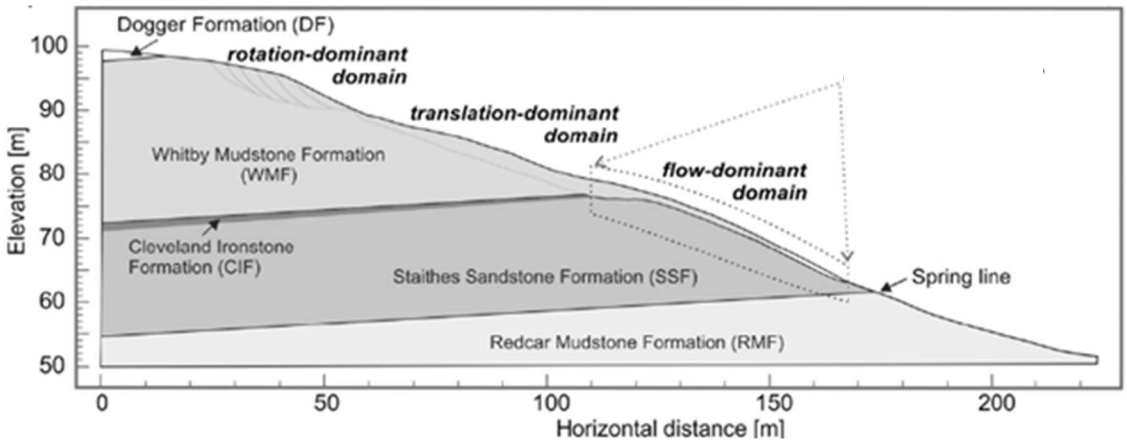


Figure 3.12 Cartoon of stratigraphy of the lithology of Hollin Hill and how this relates to slope failure. Source: Uhlemann *et al.* (2016).

### 3.2.5 Field site summary

Hollin Hill represents an exciting opportunity for the monitoring of soil moisture over a time series. The SensorNET and ALERT systems provide robust, automated collection of soil moisture and slope displacement data in near-real time, with robust calibration work having been undertaken by the soils and hydrogeology teams at BGS. The historic time series stretching back over six years is valuable in providing insight into processes at the site, as well as helping to inform the design of additional manual soil moisture measurement methods.

The site is also valuable in that the slide type and material types are similar to those of the most common slide types in the UK, and therefore make the findings in the following chapters potentially applicable to utilisation in other UK contexts for understanding and monitoring slope deformations.

The groundwater controlled slide is characterised by shallow rotational features at the top of the slope in the Whitby Mudstone Formation through to translational

movement over the Staithes Sandstone, forming four distinct active lobes across the site which extend to overlay the lower sandstone formations. The different lithologies which make up the slope provide significant opportunities for monitoring the interaction between soil moisture and slope stability, for example, how slopes drain, and how slope stability is impacted. Furthermore, the boundaries between the lithologies coincide with slope deformations and surface hydrological features, like surface ponding on the slope just below the Dogger-Whitby boundary and a spring-line at the Staithes-Redcar boundary. Geomorphologically, the main deformation features occur in the Whitby mudstone, as it accelerates down slope forming lobes.

## 3.3 Fieldwork methodology and data descriptions

This section describes the sets of in situ data created during the field campaign. The timeline of acquisitions is described, as are the data. In total, three *in situ* datasets are described – the shallow sub surface SensorNet soil moisture data, using the already extant SensorNet array, the deeper subsurface volumetric soil moisture data from CEH's CRNS COSMOS sensor, and a surface soil moisture data set that uses the SensorNET loci and additional loci – the establishment of which is described. The SAR data used are described in the final section of this chapter. The section begins with a description of the already extant sensing technologies that are utilised.

### 3.3.1 Already Extant *In situ* sensors

Prior to this project, Hollin Hill had two automated soil moisture-related sensor arrays. The SensorNET system is an array of 96 soil moisture sensors located in eight multi-scalar, nested clusters across the site, designed to enable multi-scalar soil moisture variation analysis (Lark, 2011; Marchant *et al.*, 2013). The COSMOS CRNS is part of a national array of sensors deployed by CEH since 2013 (Centre for Ecology and Hydrology, 2018) that monitor volumetric soil moisture.

#### 3.3.1.1 SensorNET

Hollin Hill has a semi-wireless array of 96 soil moisture sensors which have been measuring temperature and pore water pressure at a depth of 10 cm every 15 minutes since October 2011 to an accuracy of 2% (Marchant *et al.*, 2013). The sensors are located in clusters within the site, four in the clay soil, two on the sandy clay, and two on the sand (Figure 3.13). Each of these eight groups of sensors is made up of a multi-scalar nested design enabling multi-scalar soil moisture variation analysis to be undertaken (Lark, 2011), as demonstrated in Figure 3.14. The multi-scalar nested design was optimised by Lark *et al.* to enable robust assessment of soil

moisture variability at multiple spatial scales. In-depth discussion of the optimisation process can be found in Lark (2011). At each node of the SensorNET array is set a Decagon 5TE sensor at a depth of 10 cm. The 5TE measures apparent dielectric permittivity ($\varepsilon_a$) using an electro-magnetic field produced across the three prongs of the sensor to estimate the dielectric content of the medium it is in. The 5TE has a working range of 1 (air) to 80 (water) and with a soil-specific calibration, which was undertaken during this project, the sensor can achieve an accuracy of +-1 to 2% VWC (Decagon Devices, 2016).

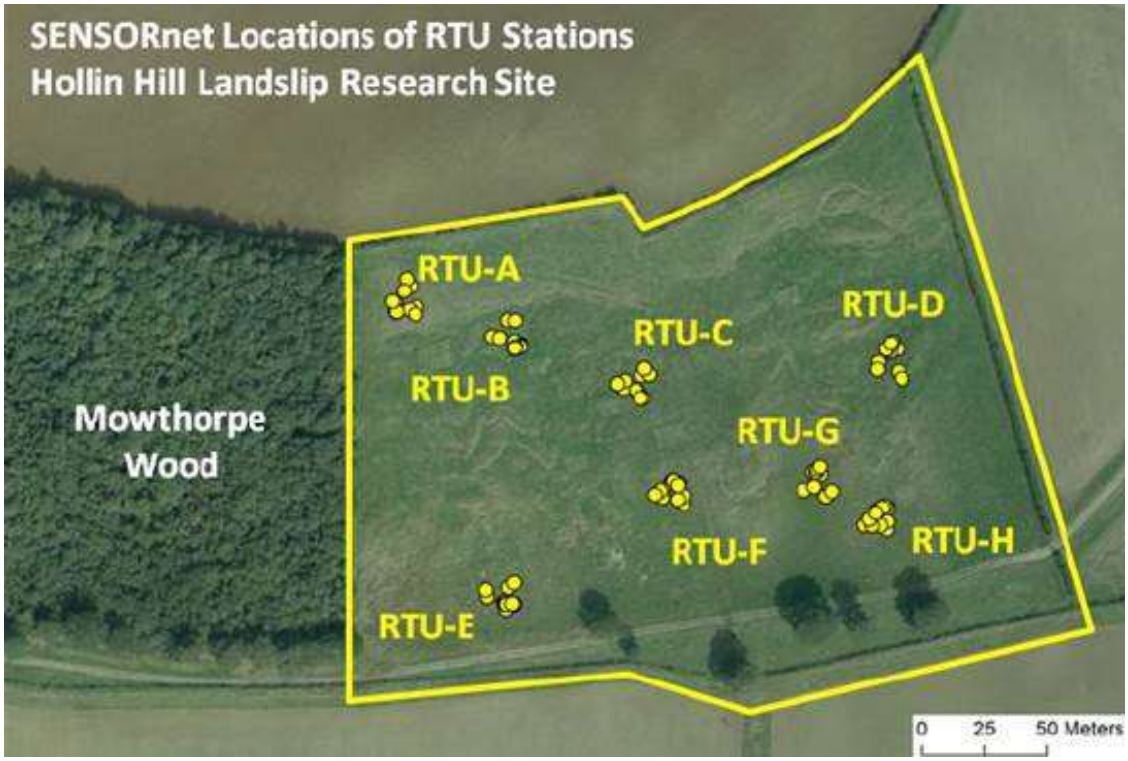


Figure 3.13 Location of SENSORNET clusters at the Hollin Hill Landslide Observatory. From BGS (2015a)

To achieve the quoted accuracy, soil-specific calibrations were undertaken by Nicole Archer at BGS using two methods – the first using three intact 6900 $cm^3$ cores of material – one for each soil type, with a 5TE implanted at 10 cm depth and data logger attached. These soil blocks were saturated, measurements taken, dried out and then measurements taken again. This is the preferred method as it does not disrupt the soil matrix structure. An additional calibration method was used however, as prescribed by Decagon where a soil sample is ground down, four litres of it is taken and repacked to the known soil bulk density. A raw reading (or dielectric permittivity) of the air-dried soil is taken and then a known quantity of water is added, this is then mixed well into the soil and again a raw reading taken, each time

also taking a small core of soil to estimate the gravimetric soil moisture. This was undertaken five times to create a calibration plot (Archer, pers.comm.) this methodology has since been published in (Archer *et al.*, 2016). Following Archer's calibration work, calibrated and raw values were provided to this project by Philip Meldrum at BGS.

The project design originally entailed using data from all eight SensorNET clusters to assess the subsurface spatial relationships, and also the relationship between surface and subsurface moisture. Following discussion with the SensorNET team at BGS, only data from three clusters – D, E and G has been provided to this project owing to issues with the sensors in the other clusters. It has also been noted by staff at BGS that while these three clusters are the more 'reliable' during the study period, there is potential that some sensors had errors during the period. It is important to note, therefore, at the outset, that all relationships and findings that are drawn must be done so with this caveat in mind, and, indeed, later, when the data are presented there is a comment on the criteria used to ensure only data appropriate to be used are. The three clusters, D, E and G correspond to each of the three soil types – Clay, Sand and Sandy Clay respectively. While these data are considered the most reliable from the site, there are multiple missing values (Table 4.1).

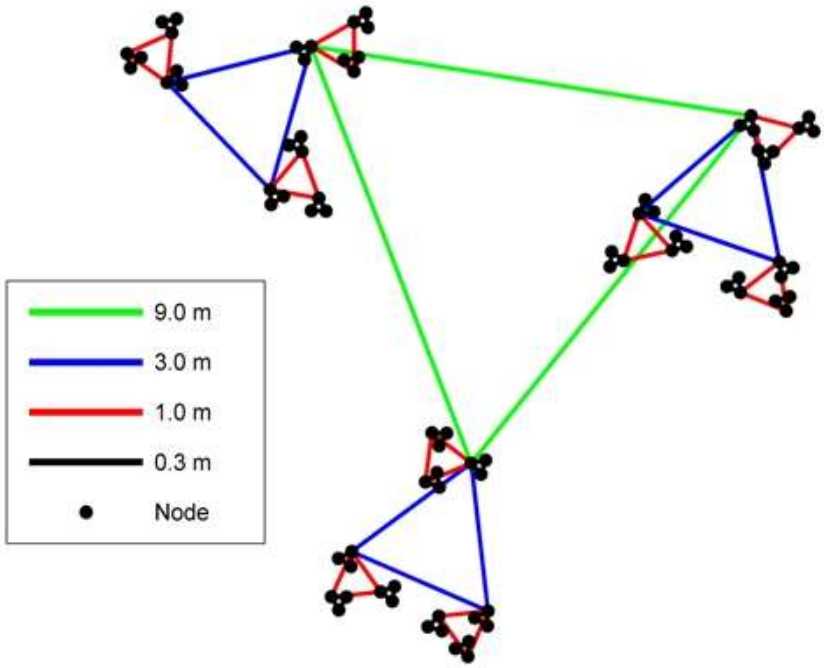


Figure 3.14 Cartoon of the multi-scalar design of the SensorNet array (Lark, 2011).

#### 3.3.1.2 COSMOS

CEH installed a COSMOS station at Hollin Hill in March 2014. The station has multiple automated environmental sensors, including a rain gauge, 3D Sonic anemometer, and a Cosmic Neutron Ray Sensor (CRNS) which measures the number of epithermal, or 'fast' neutrons at the soil surface, and from this Volumetric Water Content (VWC) is derived through a complex methodology set out in Centre for Ecology and Hydrology, (2018) and further expounded upon in Andreasen *et al.*, (2016), giving a soil moisture value over an area of up to 12 hectares and to a depth ranging from 0.4 m closest to the sensor, to 0.15 m furthest away from the sensor (Centre for Ecology and Hydrology, 2018). The distance over which the CRNS measures – approximately 200m (Centre for Ecology and Hydrology, 2018) is expected to easily accommodate the autocorrelation length of soil moisture, which can lie between 1 and 600 m (Western and Blöschl, 1999), but has been found to normally be about 30 to 60 m (Western *et al.*, 2004) The interpretation of CRNS data remains complex, and the behaviour of its outputs in relations to high soil moisture heterogeneity is to some extent still poorly understood (Köhli *et al.*, 2015). It does, however, if used circumspectly, allow an insight into soil moisture at greater depths than the SensorNET system allows for. The CRNS sensor provides data half hourly, with the average of the derived VWC value over the previous half hour provided, so as to minimise the effect of noise in the data, which can be considerable

(Centre for Ecology and Hydrology, 2018). The data used in this project is taken from the acquisition time of the CRNS that is closest to the time at which the ThetaProbe an SensorNet data were acquired. Because the CRNS system produces one data value for the area of its coverage at each acquisition, rather than the multiple points for both the SensorNet and ThetaProbe data, the number of data points - one per month, taken at 09:00 on the day of survey – is significantly fewer than the other two datasets, numbering nine values in all.

These two *in situ* systems, in combination with my own surface soil moisture monitoring (see Section 3.3.4) provide a strong basis of data against which to compare SAR soil moisture estimates, with the SensorNET data acting as a secondary ground-truthing mechanism for the SAR data analysis. The extant sensing technologies relevant to this project are shown in . This shows the technologies that were set up by the BGS shortly after they set up the Landslide Observatory at Hollin Hill in the mid-2000s to automatically monitor *in situ* slope conditions. The supplementary manual monitoring designed and undertaken for this project is shown in addition. Table 3.3 shows the SAR context at Hollin Hill prior to this project being undertaken – namely the Airborne NovaSAR emulator flights undertaken in June 2014 in conjunction with the UK Space Agency as part of a proof of concept test.

Table 3.1 Extant and novel sensing methods at Hollin Hill

| Extant/Previous Monitoring | Additional monitoring developed for this study |
|---|---|
| SensorNET (Lark 2011)<br>COSMOS CRNS array (Centre for Ecology and Hydrology, 2018) | Theta Probe array |

Table 3.2 Context of previous SAR work at Hollin Hill and the imagery commissioned for this project

| Previous SAR activities at Hollin Hill | Newly commissioned SAR imagery at Hollin Hill |
|---|---|
| Airborne SAR emulator (S and X band) (June 2014) | COSMO-SkyMed campaign (Spotlight2 X-band) |

### 3.3.2 *In situ* data summary

The Hollin Hill site has been a test-bed for automated contact-sensing (Vereecken *et al.*, 2008) of soil moisture for over a decade (Jordan, 2015; Archer *et al.*, 2016; Uhlemann *et al.*, 2016) and has more *in situ* monitoring equipment, and a greater density of monitoring points than any other site that has used CSK imagery. Only one project that was found in the literature, has used the combination of the ground truthing methods used in this study, and that used far fewer measurement locations (Fersch *et al.*, 2018) - the CEH CRNS sensor as part of the COSMOS-UK programme, which records volumetric soil moisture hourly. There is also an array of sub-surface TDR soil moisture sensors distributed across the site, which provides a denser *in situ* ground truthing dataset than that presented in any CSK projects published so far to the best of our knowledge.

### 3.3.3 Timeline of acquisitions

The fieldwork for this project was undertaken between June 2016 and February 2017, concurrent with the data acquisitions by the COSMO-SkyMed (CSK) constellation described later in this chapter. Although the experimental design aimed for satellite acquisitions being made on a regular, monthly, basis, due to satellite scheduling issues and failed acquisitions the time elapsed between images is not equal, with some images being considerably less than a month since the previous acquisition, and some being considerably more (Figure 3.15). Fieldwork was undertaken as close to co-temporally as safety permitted. CSK acquisitions occurred at 05:58 GMT and, due to late sunrises during the winter months, a start time of 09:00 was set for all fieldwork, to ensure the time between image acquisition and *in situ* measurements was similar across all datasets. Further to this end, clusters were visited in the same order on each field visit. Climatic data from each of the acquisition days shows that there was very little change in conditions between the satellite acquisition time and that at which *in situ* work was undertaken. No rain fell during that period on any occasion, and winds were, generally calm. The conditions at 0900 are, therefore, considered an acceptable proxy for those at 05:58. *In situ* surface measurements were taken with a Delta T industries Thetaprobe capacitance probe, recorded in notebooks, then entered into a spreadsheet, calibrated and entered into a GIS.

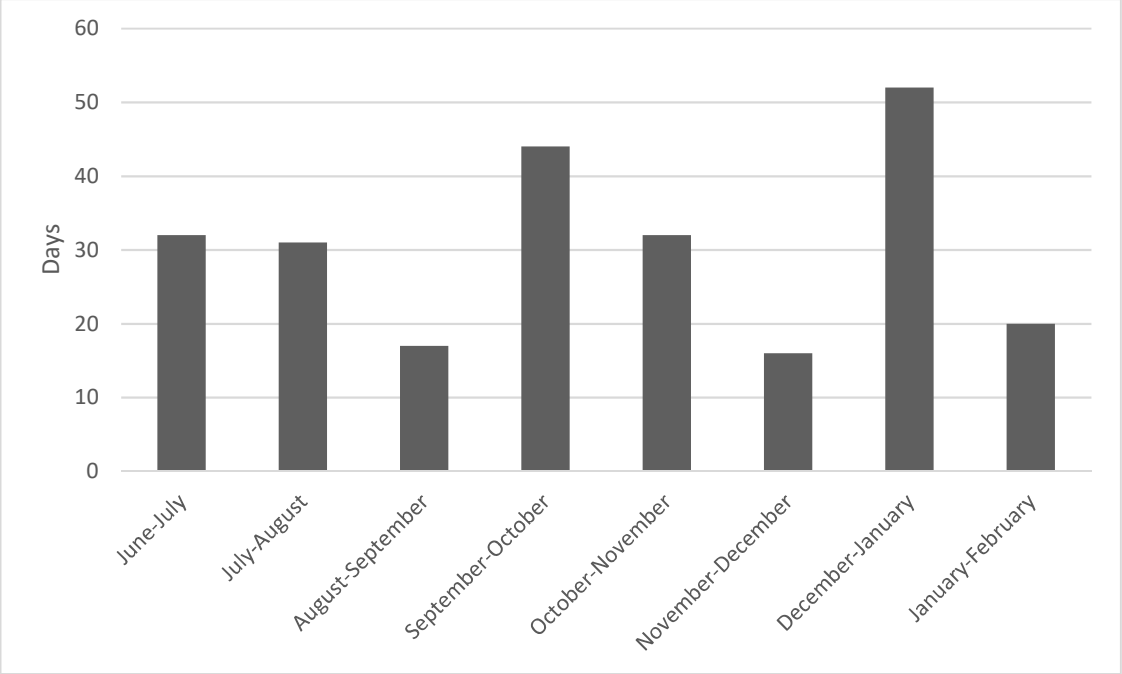


Figure 3.15 Interval between data acquisitions in days

For each month soil moisture readings were taken at the same locations, marked by plastic pegs at each of the clusters, and in the same order. This produced ~116 data points per acquisition, though with some variation. Notably, the early acquisitions – June and July – have fewer points (92 and 93, respectively) than the other months due to the difficulty of finding the original SensorNet marker pegs put in by BGS several years previously, many of which had degraded or been broken, and unfamiliarity with the site. Practice and increased familiarity with the difficult terrain of the site meant that during the course of the field campaign more data points were able to be taken.

Table 3.3 Count of surface readings by month

| Month | Count of Readings |
|---|---|
| **June** | 92 |
| **July** | 93 |
| **August** | 112 |
| **September** | 110 |
| **October** | 116 |
| **November** | 116 |
| **December** | 117 |
| **January** | 119 |
| **February** | 120 |
| **Total** | 995 |

3.3.4

### 3.3.4 Description, Acquisition and Calibration of surface data

The surface dataset is made up of 14 clusters of point loci. It uses the SensorNET node locations to form eight clusters (A-H) of 12 points in addition to eight points at each of six (1-6) additional clusters (see figure 3.16). The positioning of the eight SensorNET clusters across the site was designed to ensure that as many different soil type and slope angle characteristics of the site could be monitored as possible (Pers. Comm. Lark 2016). It was felt, however, that in order that the most might be made of the SAR data used in this project, and given the difficulties of using SAR over sloped and heterogeneous surfaces that additional sampling locations would enable better assessment of the SAR data product. Additionally, six more clusters of point locations were designed. Three categories were applied to assign cluster centroid locations – first, if an area had been previously identified from literature or a previous site visit as displaying specific slope or moisture characteristics that were deemed to be important for assessing the output of the SAR data; second, that the slope of the site, which was classified into 5 classes, should be represented proportionally; third, that, as far as possible, an even coverage of the site should be obtained to enable the most benefit from the SAR images to be had, through comparison with the best possible interpolated surfaces of *in situ* soil moisture. Using these criteria, six new cluster centroids were created, with eight nodes at each created, with distance and angle from the centroid randomly assigned by a simple Excel random number generator. The locations of these new points were marked in the field using a differential GPS (dGPS) and inert plastic pegs for ease of repeat-acquisition. The manual surface moisture dataset therefore consists of 14 clusters, eight overlaying the SensorNET clusters, six in new, targeted locations (Figure 3.16). Of particular note from these additional clusters is cluster 2, which was created at the sag ponds area to assess how wet the area was, with a view to assessing the capability of the COSMO-SkyMed sensor to enable estimation of such high soil moisture values. The rationale for this was two-fold. First, at the time most of the research into soil moisture estimation with CSK had been undertaken in Mediterranean areas, with minimal assessment of high soil moisture values, second, that this high-moisture area had been recognised by Jenkins *et al.* (2006b) as being a key determinant of instability of the lobe.

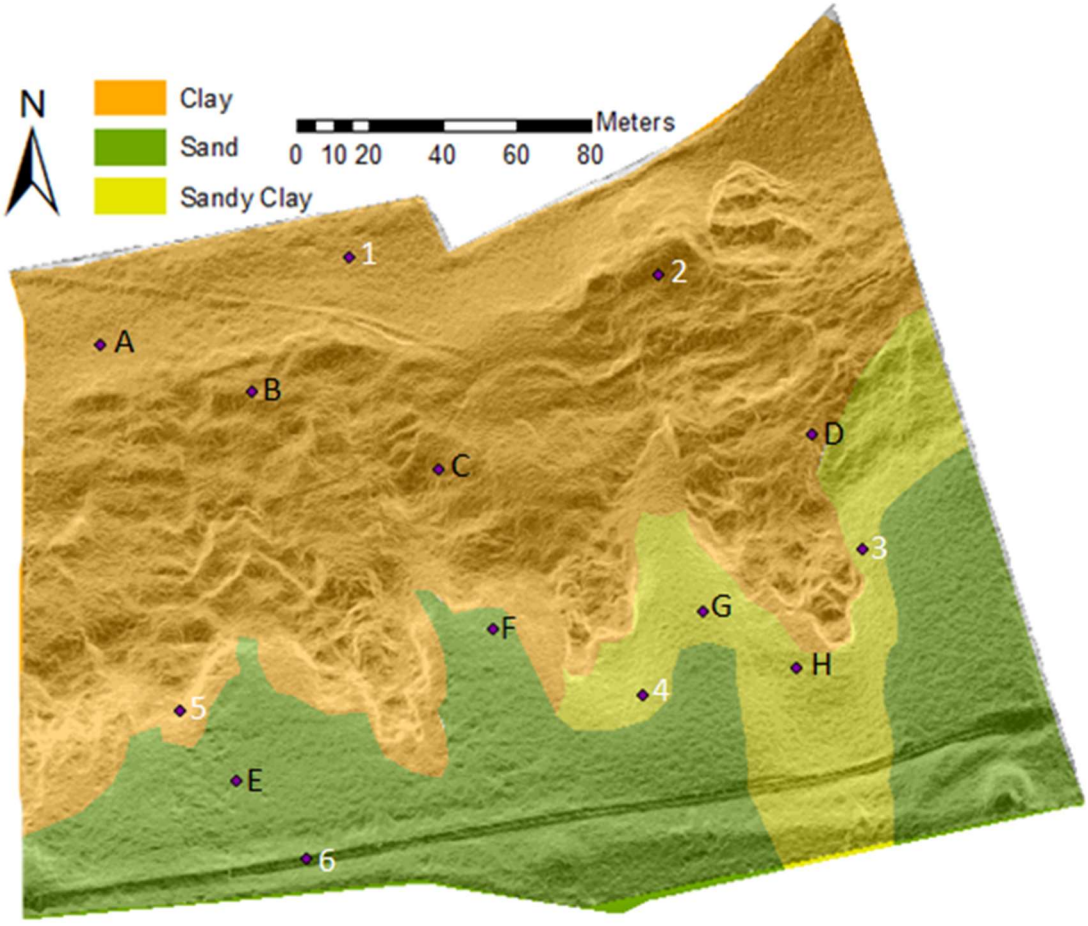


Figure 3.16 Location of SensorNET (A-H) and additional cluster (1-6) centroids

Surface soil moisture measurements were taken at these new locations, as well as each of the SensorNET node locations, using a Delta-T Theta Probe. The Theta probe is a hand-held probe measuring impedance, which can then be subsequently converted to soil moisture using soil-specific calibrations (Delta T Devices, 1999). The probe emits a 100MHz sinusoidal signal through four stainless steel rods, forming an array, which are placed vertically into the soil (Figure 3.17). The wetness of the surrounding soil influences the impedance of the array due to the dielectric constant – the impedance of the soil due to the current-carrying properties of water molecules (Delta T Devices, 1999). From the impedance of the array, the volumetric soil moisture can be calculated owing to the almost linear relationship between the square root of dielectric constant ($\sqrt{\varepsilon}$) and volumetric soil moisture ($\theta v$) (Delta T Devices, 1999).

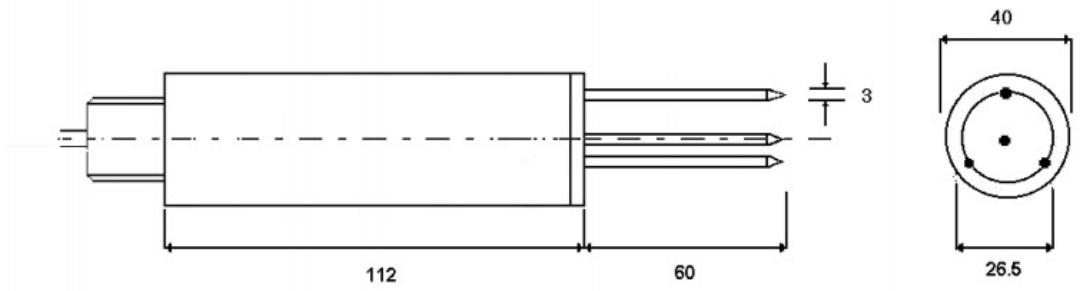


Figure 3.17 Theta Probe Design in plan and profile, showing size and arrangement of the four-pin array. All measurements in mm. Source: (Delta T Devices, 1999).

The surface data were collected by the ML2x soil moisture probe from Delta-T Devices, which measures the conductivity of the soil mass. In the field, readings in mV were read off the handheld Delta-T Devices HH2 moisture meter and written in field notebooks. To improve the accuracy of the calibration from the ML2x probe's mV reading to Volumetric Water Content (VWC) - which is quoted as 0.05 $m^3.m^{-3}$ when using Delta-T's supplied generalised calibrations - soil samples were collected from the site and calibration experiments undertaken. This calibration was undertaken by Nicole Archer, at BGS, following the prescribed procedure set out by Delta-T Devices (1999), which the company quotes as providing an accuracy of 0.01 $m^3.m^{-3}$ for the temperature range in which this study was carried out.

Research into the relationship between volumetric water content (θ) and the complex refractive index (equivalent to √ε (Delta T Devices, 1999)) shows that this relationship is linear (White *et al.*, 1994), with two coefficients, $a_0$ and $a_1$ being soil-specific. The relationship between √ε and θ is said by Delta-T Devices (1999) to be best described for the range of values in the dataset by (Eq. 3.1) – a third order polynomial.

$$\sqrt{\varepsilon} = 1.07 + 6.4V - 6.4V^2 + 4.7V^3 \qquad (R^2 = 0.998) \qquad [3.1]$$

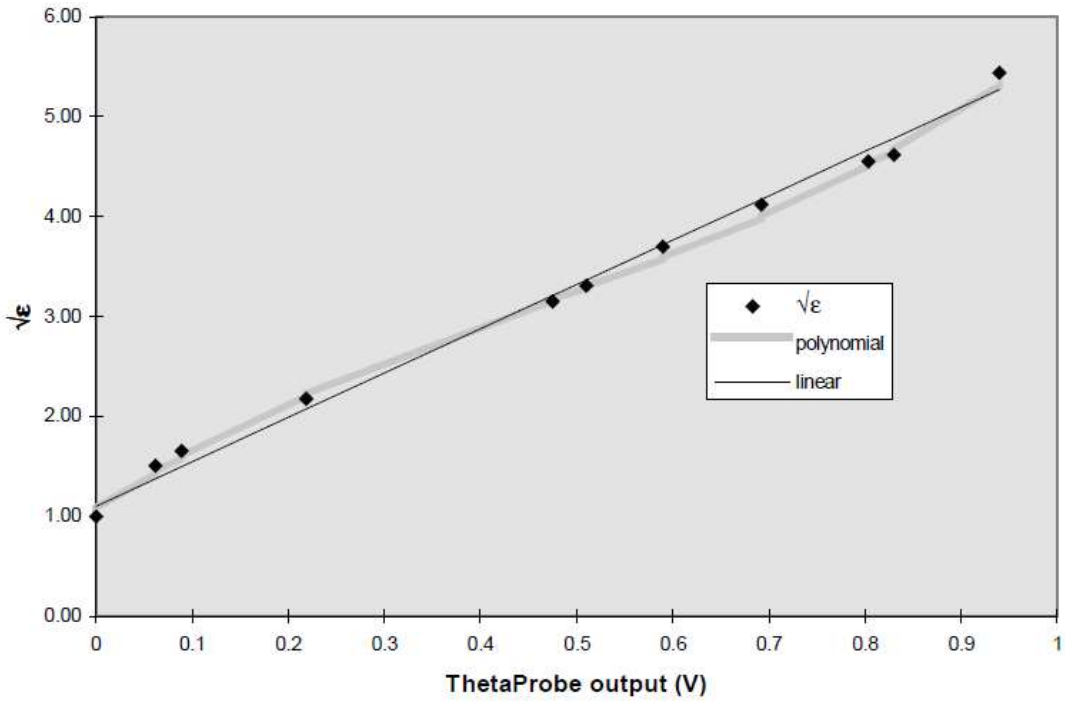


Figure 3.18 Relationship between ML2x output and √ε. From Delta-T, 1999.

To establish the values of $a_0$ and $a_1$ the following method was taken, which involved taking an undisturbed sample of each of the three different mapped soil types, measuring the volume (L) and then taking readings with the ML2x probe ($V_w$) and calculating $\varepsilon_w$ from

$$\sqrt{\varepsilon_w} = 1.07 + 6.4V_w - 6.4V_w^2 + 4.7V_w^3 \qquad [3.2]$$

The soil sample was then weighed ($W_w$), oven dried until $\theta \approx 0$, measured again with the ML2x ($V_D$), ) and $\varepsilon_0$ calculated (Eq. 3.3), and then weighed again ($W_D$).

$$\sqrt{\varepsilon_0} = 1.07 + 6.4V_D - 6.4V_D^2 + 4.7V_D^3 \qquad [3.3]$$

Volumetric water content of the original, pre-dried, sample is then calculated (Eq. 3.4):

$$\theta_w = \frac{(W_w - W_D)}{L} \qquad [3.4]$$

The second value required for soil-specific calibration is:

$$a_1 = \frac{\sqrt{\varepsilon_w} - \sqrt{\varepsilon_0}}{\theta_w} \quad [3.5]$$

The values for $a_0$ and $a_1$ for the three soil types, as calculated by Nicole Archer with samples taken from the site, are found in

Table 3.4 $a_0$ and $a_1$ values for the three soil types

| | $a_0$ | $a_1$ |
|---|---|---|
| **Sand** | 1.42 | 9.78 |
| **Sandy Clay** | 1.35 | 8.92 |
| **Clay** | 1.6 | 8.4 |

The calibration equation modifies Eq 3.2 with the results of equations 3.3, 3.4 and 3.5 to produce Eq 3.6:

$$\sqrt{\varepsilon} = \frac{(1.07 + 6.4V - 6.4V^2 + 4.7V^3) - a_0}{a_1} \quad [3.6]$$

Using the soil-specific calibration the error anticipated of each value is ±0.01 $m^3m^{-3}$, with the error stemming from errors in the MLx2 measurement. There are, however, other forms of error which might increase this value. It is supplied by Delta-T under the assumption that the probe is inserted exactly vertically into a uniform soil mass. This is highly unlikely to be the case given the presence of vegetation cover and the probability that some of the soil has been either aerated by slope movement or compacted by the sheep on site. The literature supplied by Delta-T estimates that the error associated with the soil mass structure or sampling method might range from 0.04 to 0.1 $m^3\ m^{-3}$.

## 3.4 Remote Sensing history and methods

### 3.4.1 Remote Sensing history at Hollin Hill

In June 2014 a two-day groundtruthing campaign was undertaken by a group from BGS, Durham University and Newcastle University as support for the Airbus Space and Defence Airborne SAR imaging campaign at Hollin Hill, which was a NERC-funded airborne simulator for the upcoming NovaSAR-S launch. The Airborne SAR campaign had two primary objectives, first to act as a test-bed for the NovaSAR-S platform which was due to be launched in 2016, second to investigate how concurrent S and X-band acquisitions perform in the context of soil moisture inversion. To achieve this, the Hollin Hill site was flown over with four different flight alignments while both sensors (S and X) were acquiring multi-polarised data (Figure 3.19). After

the first iteration of this flight plan, two 4x4 m quadrats were artificially wetted and *in situ* soil moisture measurements were taken shortly before a second iteration of the flight paths. A third overpass, and further wetting, had been scheduled, but this was not undertaken due to flight-time restrictions.

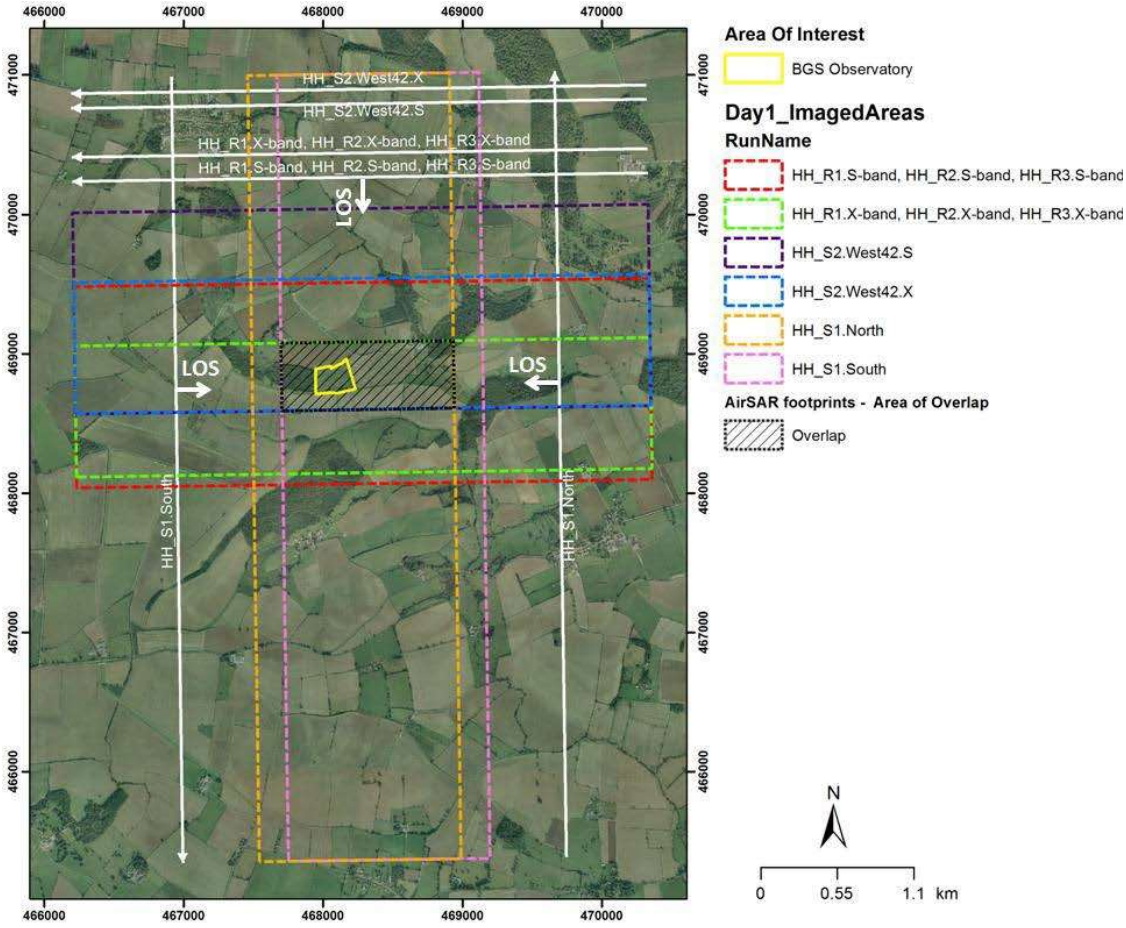


Figure 3.19 Intended Flight plan for aerial SAR campaign. Image by Colm Jordan.

The S-band component of the Airborne SAR campaign was designed to simulate the new NovaSAR-S sensor which launched in 2016. At the time it was envisaged that involvement in the Airborne SAR project would lead to further involvement with the NovaSAR data products during this PhD project through the Satellite Applications Catapult. The airborne SAR project was designed to utilise change-detection as a method for assessing the impact of soil moisture changes on backscatter returns at these two wavelengths, to enable evaluation of the potential for S-band to be used as a candidate for soil moisture inversion ahead of the NovaSAR-S launch in 2016.

Shortly after the airborne SAR field campaign was undertaken, the Satellite Applications Catapult created an agreement with the operators of the recently-launched X-band COSMO-SkyMed (CSK) platform – Agenzia Spaziale Italiana (ASI) - to provide low-cost access to their data products, creating a fine-resolution time

series dating back to 2011. It was anticipated that access to these two satellite-based data sources would provide the opportunity to assess the abilities of these high resolution, short wavelength, SAR sensors in soil moisture estimation. A bid was successfully made for data, with the findings from the Airborne SAR project informing the design of the CSK project.

A total of 136 images, across three processing levels – detected, detected improved, and Single Look Complex, were provided by Airbus Space and Defence following the field campaign. Significant issues occurred during the acquisition of the data due to flight path and tracking anomalies, which, upon examination of the data, made the utilisation of it, as had been intended, challenging, and following processing of the imagery within ENVI packages and discussion with the SAR specialists at BGS and Nottingham University, it was decided that little could be achieved by way of establishing the performance of the sensors for soil moisture estimation.

Despite the lack of utility of the Airborne SAR data for use in establishing the capabilities of S and X-band SAR for change-detection-based soil moisture inversion, the project does establish the research priorities and background to the CSK project this thesis has become. It has shown that Hollin Hill was recognised as being a very valuable site by Airbus Space and Defence, as well as the Satellite Applications Catapult, for the testing of novel soil moisture estimation techniques, both due to the extant SensorNET monitoring equipment, and due to the similarity of the site soil to many UK-based landslides and, therefore, the potential for its use as a test-bed for assessing the performance of remote sensing techniques in the context of hazard assessment. Having established the context of SAR usage at Hollin Hill the focus of this chapter now turns to the SAR data used in this project.

### 3.4.2 Research history summary

Despite the lack of utility of the Airborne SAR data for use in establishing the capabilities of S and X-band SAR for change-detection-based soil moisture inversion, the project does establish the research priorities and background to the CSK project this thesis has become. It has shown that Hollin Hill was recognised as being a very valuable site by Airbus Space and Defence, as well as the Satellite Applications Catapult, for the testing of novel soil moisture estimation techniques, both due to the extant SensorNET monitoring equipment, and due to the similarity of the site soil to many UK-based landslides and, therefore, the potential for its use as a test-

bed for assessing the performance of remote sensing techniques in the context of hazard assessment.

## 3.5 SAR data processing during this project

This section sets out the SAR data products used in this project, their parameters, and how they were processed to enable the meeting of Objective 3 in Chapters 5 and 6.

### 3.5.1 Data Summary

A time series of monthly Spotlight2 acquisitions was provided by ASI through the Satellites Application Catapult bidding process (Project: Corsair008). Nine COSMO-SkyMed Spotlight2 images, taken at approximately monthly intervals (Figure 3.20) between June 2016 and February 2017. COSMO-SkyMed is an X-band SAR satellite, and in Spotlight2 Mode has a pixel resolution of ~1m. Images were acquired in with the same parameters each time - HH (horizontal-horizontal) polarization – chosen because studies have shown that HH polarisation tends to be better than VV polarisation for soil moisture estimation (Balenzano, *et al.*, 2011) - at an incidence angle of 57° on an ascending path. Images were acquired by different satellites in the constellation depending on mission scheduling, and shows which of the four satellites was used in each acquisition. Images were acquired at 05:58 on each acquisition day – three hours before the *in situ* surface soil moisture readings were taken as described in the field campaign set out in previous chapter. On each occasion there was no rainfall between the satellite acquisition and fieldwork, and conditions were relatively mild and calm.

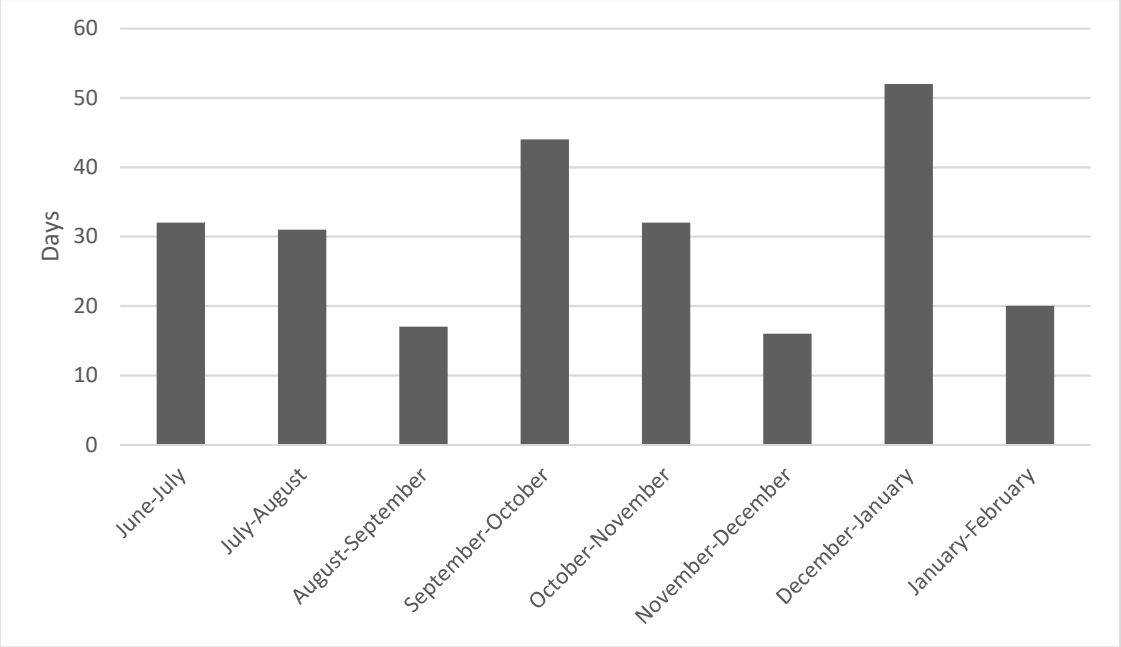


Figure 3.20 Period between image acquisitions

Table 3.5 COSMO-SkyMed satellite sensor used to acquire each image

| Month | Satellite |
|---|---|
| **June** | 2 |
| **July** | 4 |
| **August** | 4 |
| **September** | 3 |
| **October** | 4 |
| **November** | 3 |
| **December** | 4 |
| **January** | 3 |
| **February** | 1 |

### 3.5.2 Data Product

Nine single-polarised HH CSK images are used in this study. Data was acquired in the *Spotlight2* mode, which has 10x10 km² scene with a spatial resolution of approximately 1x1 m² single look – the highest resolution available from the constellation for non-military projects (Agenzia Spatiale Italiana, 2009), and the highest resolution commercially available SAR product at the time (Eineder *et al.*, 2009).

The CSK sensors are quoted as providing the following imaging quality parameters (Agenzia Spatiale Italiana, 2009):

- Peak Side Lobe Ratio (PSLR) ≤ -22 dB
- Integrated Side Lobe Ratio (ISLR) ≤ -12 dB
- Azimuth Point Target Ambiguity ≤ -40 dB
- Radiometric Accuracy ≤ -1 dB (single look)
- Radiometric Linearity ≤ -1.5 dB
- Radiometric Stability ≤ -1 dB
- Total Noise Equivalent (NE)°σ ≤ -19 dBm2/m2

ASI offer various levels of data processing for their standard products prior to delivery including multilooking, geocoding and terrain correcting (Agenzia Spatiale Italiana, 2009). It was felt that on the basis of the complicated geomorphology of the site that it was important that orthorectification should be able to be undertaken using a high quality digital terrain model (DTM), given the lack of information from ASI regarding the scale of the surface model they would utilise. This project, therefore, uses Level 1A Single-look Complex Slant (SCS) data. This complex format data is focussed in slant range azimuth with zero Doppler projection, with the data focused, weighted and radiometrically equalised. The processing stages that were performed by the Agenzia Spatiale Italiana (ASI) on the raw data to produce this level 1A product prior to delivery are (Agenzia Spatiale Italiana, 2009):

- frame synchronization
- transmission protocol removal
- packet data filed re-assembly
- data decompression
- statistics estimation
- data formatting
- gain-receiver compensation
- internal calibration
- data focusing

Table 3.6 Characteristics of products of different processing options provided by ASI. From: (ASI 2009).

| | LEV 0 | LEV 1A | LEV 1B | LEV 1C<br>LEV 1D |
|---|---|---|---|---|
| Swath [km2] | ~10 km x ~10 km | | | |
| Incidence angle [deg] | ~20° ÷ ~60° | | | |
| Polarization | selectable among HH or VV | | | |
| Product Size [MB] | 750÷1700 | 700÷1450 | 841 | ≤1682 |
| Equivalent Number of looks | NA | 1 | 1 | 1 |
| Ground Range resolution [m] | NA | ≤1.0 | ≤1.0 | ≤1.0 |
| Azimuth resolution [m] | NA | ≤1.0 | ≤1.0 | ≤1.0 |
| Geolocation Acccuracy | NA | | ≤25 | ≤25<br>≤15 |

### 3.5.3 Post-delivery CSK data processing

ASI provided the Spotlight2 Level 1A data in HDF5 format. This data was then processed, as per e-geos (a subsidiary of ASI) (e-geos, no date) and ESA guidelines in ESA's SNAP software. Images were calibrated and radiometrically corrected, and then terrain corrected. The terrain correction was undertaken with several scales of DEM, which are outlined later.

### 3.5.4 Software packages used

Data processing was undertaken in a number of software packages. Following guidance from ASI, the SAR images were calibrated and terrain corrected in ESA's SNAP software (ESA, 2020), while ArcGIS 10.5, QGIS 3.2.2 (Bonn) (QGIS.org, 2020) were used for spatial analysis, and ENVI Classic was used for filtering, with the Jamovi 1.2 (The Jamovi Project, 2020) environment for R being used for statistical analysis.

### 3.5.5 Additional data products utilised

To meet Objective 3, a study was undertaken to assess the impact on correlation between *in situ* VWC values measured by the Theta Probe and the backscatter return by the scale of the DTM employed for terrain correction, CSK imagery calibrated in SNAP was terrain corrected using five different resolutions of open source imagery (Table 3.7). The *in situ* surface VWC values were then plotted against the backscatter value of the corresponding pixel.

Table 3.7 Summary of data used for terrain correction

| Imagery | Spatial resolution | Date of acquisition | Source |
|---|---|---|---|
| **Environment Agency (EA) Lidar DTM** | 0.25m | 2012 | Environment Agency (via digimap) |
| **Environment Agency (EA) Lidar DTM** | 0.5m | 2012 | Environment Agency (via digimap) |
| **Environment Agency (EA) Lidar DTM** | 1m | 2012 | Environment Agency (via digimap) |
| **Environment Agency (EA) Lidar DTM** | 2m | 2012 | Environment Agency (via digimap) |
| **SRTM Interferometric terrain model** | 3 Arc Sec ~ 90m | 2000 | USGS |

## 3.6 Chapter Summary

This chapter has shown the unique opportunity Hollin Hill presents as a test site for assessing the performance of CSK soil moisture estimation due to the established automated *in situ* monitoring equipment at the site, the well-established interest in developing the site for monitoring slope deformation drivers, and the novelty that the site presents with respect to environments CSK had been used for soil moisture estimation. In addition to this, the data sets used in the following chapters of the thesis and their acquisition has been described.

# 4

# CHAPTER 4: FIELD-SCALE SPATIO-TEMPORAL SOIL MOISTURE RELATIONSHIPS AT HOLLIN HILL OBSERVATORY

## 4.1 Introduction

Soil moisture is recognised globally as a key parameter to assess for the enabling of monitoring and modelling of environmental hazards or challenges in the context of a changing climate (GCOS-138, 2010) however, it is also recognised as being both spatially and temporally variable. This chapter explores the spatio-temporal soil moisture relationships at the Hollin Hill Landslide Observatory and how these should inform the design and processing of SAR data products. Hollin Hill is a valuable test site for this undertaking as it has three distinct soil types, as well as complex slope geometries, which provide evidence of the spatial variability of soil moisture in different soil conditions. Three datasets were used in this study – manually taken surface (0-5cm depth) soil moisture measurements using a theta probe, shallow (~10cm depth) automated soil moisture measurements from the BGS SensorNET array, and deeper (15-40cm) soil moisture data from the CEH CRNS sensor. Between June 2016 and February 2017 soil moisture data was collected on a roughly monthly basis to coincide with COSMO-SkyMed acquisitions of the site. The soil moisture data collected on these occasions is used in this chapter to explore the spatio-temporal relationships exhibited in the three datasets, in the context of examining the value of using single-polarised high resolution X-band SAR data for moisture-driven landslide monitoring. Objectives 1 and 2, which were set out in the introductory chapter of this thesis are engaged with and their connotations explored.

This chapter presents the shallow sub-surface, deeper sub-surface, and surface soil moisture data, from the SensorNET array, COSMOS CRNS sensor, and the manual Theta Probe measurements described in the materials and methods chapter. Objectives 1 and 2 are then engaged with through analysis of these three datasets.

## 4.2 Description of the data

This section describes the three *in situ* moisture datasets and the methods used in their acquisition, calibration, and processing and begins with a brief description of the temporal context of the fieldwork.

This section begins with descriptive statistics of the shallow sub surface soil moisture data, as collected by those probes that were operational within the SensorNET array. Between 29 (February) and 33 (August) data points are available for each month (Table 4.1). Although these data are the best quality available for the period, an investigation of the minima and maxima caused concern. Only two months have positive minima (November and February), with the other seven months having technically impossible negative VWC values. Likewise, February has a maximum VWC value of 100 $m^3.m^{-3}$, which is also not possible.

Table 4.1 Descriptive statistics of raw data SensorNET data

| | Count | Missing | Mean | Median | Minimum | Maximum | Skewness | Kurtosis | Shapiro-Wilks |
|---|---|---|---|---|---|---|---|---|---|
| **June** | 32 | 4 | 25.8 | 28.6 | -2.1 | 56.1 | -0.0734 | -0.611 | 0.482 |
| **July** | 32 | 4 | 28.2 | 33 | -3.18 | 53.8 | -0.381 | -1.06 | 0.08 |
| **Aug** | 33 | 3 | 16.2 | 21.1 | -22.6 | 34.7 | -0.769 | 0.143 | 0.015 |
| **Sept** | 31 | 5 | 23.1 | 23.9 | -4.53 | 45.5 | -0.134 | -1.11 | 0.145 |
| **Oct** | 31 | 5 | 23.6 | 25.7 | -7.69 | 56.3 | 0.0711 | -0.629 | 0.336 |
| **Nov** | 30 | 6 | 39.1 | 40.3 | 3.9 | 85.7 | 0.134 | -0.389 | 0.663 |
| **Dec** | 31 | 5 | 32.9 | 33.9 | -2.86 | 82.8 | 0.289 | 0.385 | 0.803 |
| **Jan** | 30 | 6 | 37.9 | 41.6 | -15.9 | 63.2 | -0.93 | 0.993 | 0.067 |
| **Feb** | 29 | 7 | 45 | 45.5 | 12.5 | 100 | 0.71 | 1.2 | 0.228 |

The data were cleaned (Table 4.2) to remove negative VWC values and those above 80%, which, following discussion with the Hydrology team at BGS, reference to anticipated values for these materials in other studies (Gunn *et al.*, 2013), and engaging with the literature provided by Decagon (Decagon Devices, 2016) is deemed the upper expected limit for measurements from these sensors (Meldrum, Archer pers.comm.). With the data cleaned, there are between 28 (February) and 31 (June) data points for each month.

Table 4.2 Descriptive statistics of cleaned SensorNET data

| | Count | Missing | Mean | Range | Minimum | Maximum | Skewness | Kurtosis | Shapiro-Wilks |
|---|---|---|---|---|---|---|---|---|---|
| **June** | 31 | 5 | 26.7 | 53.66 | 2.44 | 56.1 | -0.0037 | -0.61 | 0.35 |
| **July** | 30 | 6 | 30.2 | 48.82 | 4.98 | 53.8 | -0.35 | -1.12 | 0.059 |
| **Aug** | 30 | 6 | 19.3 | 33.01 | 1.69 | 34.7 | -0.167 | -1.6 | 0.006 |
| **Sept** | 30 | 6 | 24 | 42.33 | 3.17 | 45.5 | -0.0708 | -1.24 | 0.059 |
| **Oct** | 29 | 7 | 25.8 | 53.13 | 3.17 | 56.3 | 0.265 | -0.722 | 0.097 |
| **Nov** | 29 | 7 | 37.5 | 71 | 3.9 | 74.9 | -0.136 | -0.828 | 0.464 |
| **Dec** | 29 | 7 | 32.4 | 54.64 | 4.26 | 58.9 | -0.179 | -0.973 | 0.445 |
| **Jan** | 29 | 7 | 39.8 | 55.76 | 7.44 | 63.2 | -0.376 | -0.875 | 0.229 |
| **Feb** | 28 | 8 | 43 | 61.5 | 12.5 | 74 | -0.0569 | -0.886 | 0.563 |

The summary histograms show an almost bi-modal distribution, quite distinct from the unimodal distribution of the surface data (Figure 4.5). Likewise, the shape of the violin plots (Figure 4.2) is more similar between monthly datasets than in the case of the surface data (Figure 4.6) Normal distribution cannot, however, be assumed for these data sets, owing to the Shapiro-Wilks values, with none meeting the $p<0.001$ normality criterion (Table 4.2). While this is unexpected, as one would expect to be drawing values from a global dataset that is normally distributed, the multiple modes, in the form of different soil types, within the dataset probably is interpreted as being the cause of this result.

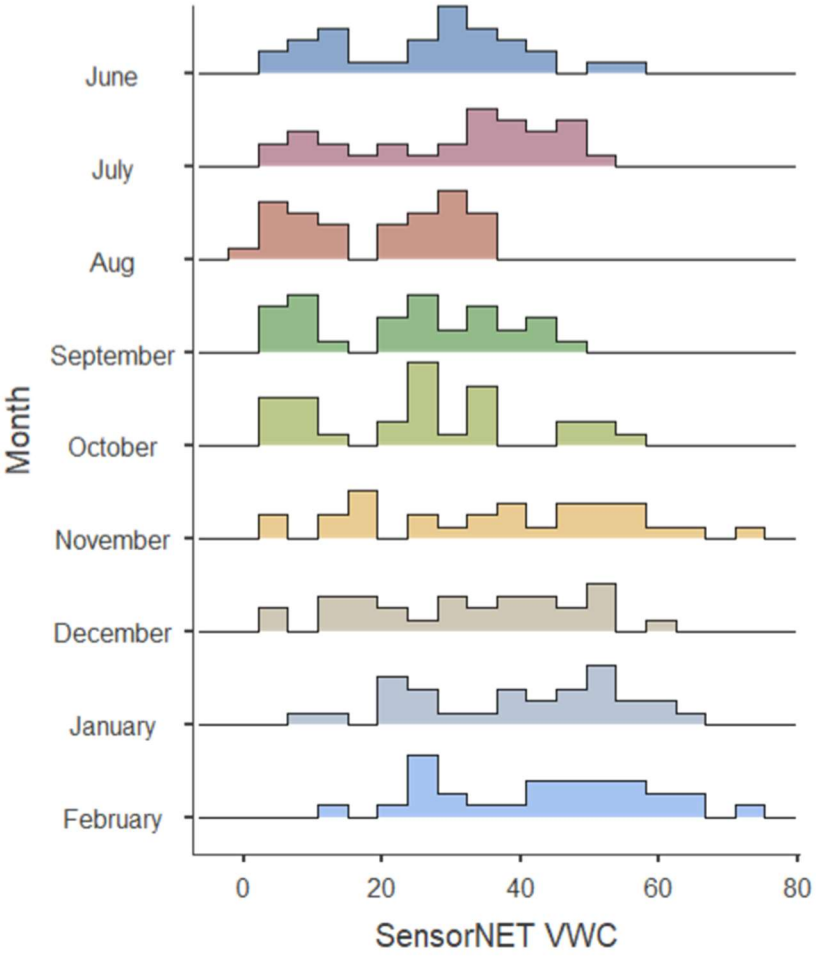


Figure 4.1 Histogram of cleaned SensorNET data

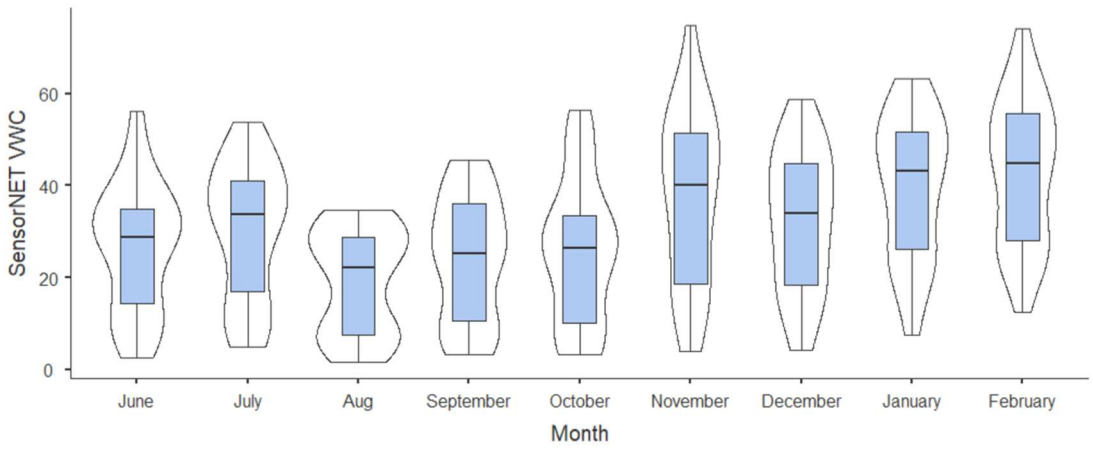


Figure 4.2 Box and violin plot of cleaned SensorNET data

### 4.2.1 Subsurface CRNS (COSMOS) Data

Brief summary statistics of the CRNS data are presented in Figure 4.3. Of note, is that the maximum value – 63.5 is higher than expected VWC values in literature (Centre for Ecology and Hydrology, 2018), and this should give greater confidence regarding the high values from the other datasets might be indicative of genuinely high moisture contents in the soil mass. These data are used in responding to Objective 1.

| | COSMOS |
|---|---|
| Mean | 44.5 |
| Median | 47.3 |
| Minimum | 31.0 |
| Maximum | 63.5 |
| Skewness | 0.289 |
| Kurtosis | -0.826 |
| Shapiro-Wilk p | < .001 |

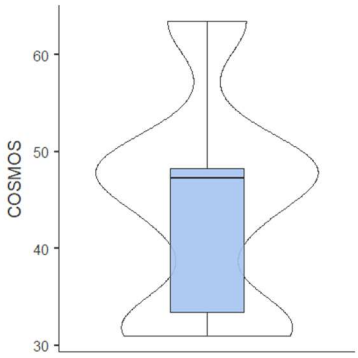


Figure 4.3 Descriptive statistics of COSMOS data

### 4.2.2 Descriptive surface spatial statistics

Using the full dataset - featuring data from all nine months, Figure 4.4 and Table 4.3 demonstrate that each of the three soil types exhibits a distinctive distribution of values. Sand is drier, more tightly clustered around the mean, and with a high density of data points around the mean. Clay is wetter, with a greater range of values and minimal peak to its histogram, showing its data points are well-spread across the dataset. Sandy clay is not as wet as clay and exhibits an unusual distribution of data points with an hour-glass type shape to the violin plot, with the 'neck' of the hour glass being just below the mean. None of the datasets exhibit a unimodal distribution. It is expected that this is due to the variability in soil moisture distributions throughout the period.

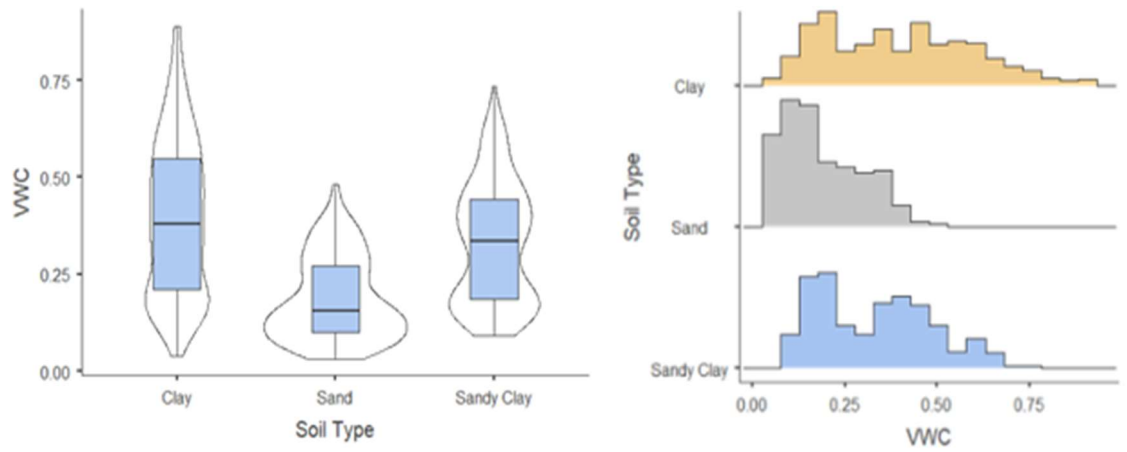


Figure 4.4 Histogram and Box and violin plots of VWC value distribution by soil type

Table 4.3 Descriptive statistics of VWC for each soil class

| Soil | Mean | Median | Minimum | Maximum | Skewness | Kurtosis |
|---|---|---|---|---|---|---|
| **Clay** | 0.395 | 0.379 | 0.038 | 0.889 | 0.321 | -0.776 |
| **Sand** | 0.187 | 0.155 | 0.032 | 0.483 | 0.628 | -0.629 |
| **Sandy Clay** | 0.328 | 0.334 | 0.093 | 0.733 | 0.338 | -0.904 |

All the soil types exhibit a positive skewness, with Clay and Sandy Clay being 'fairly symmetrical' and Sand being 'moderately skewed' (Bulmer, 1979). This is important to recognise as it give a measure of how far from a normal distribution that these samples are – and indicates that for each sample there is a distinctive distribution of data points. That is, that, for example, values for sand are strongly skewed towards lower values. The skewness standard error is low, with values ranging from 0.109 - 0.163 (Table 4.3), which indicates that it is possible to be confident in the skewness values.

All datasets have negative kurtosis values, showing that the tails of the distribution are of less weight that those found in a normal distribution, and showing that the 'outliers' are of minimal significance relative to the whole dataset. The implication of this is that fewer points sit in the tails of the data than in a normal distribution, so it can be interpreted that these points have minimal importance when considering methods of SAR processing.

### 4.2.3 Descriptive Surface Temporal Statistics

It was anticipated that through the nine months of these data the VWC levels would change, driven by seasonal variation in temperature and precipitation. Figure 4.5 and Figure 4.6 show this to be the case, with two distinctive shapes to the data being apparent. August, September and October are markedly drier than the other months, and have much tighter clustering of data points to the mean. The 'drier' months, as August-October are here defined, have smaller ranges and lower means than the other 'wetter' months.

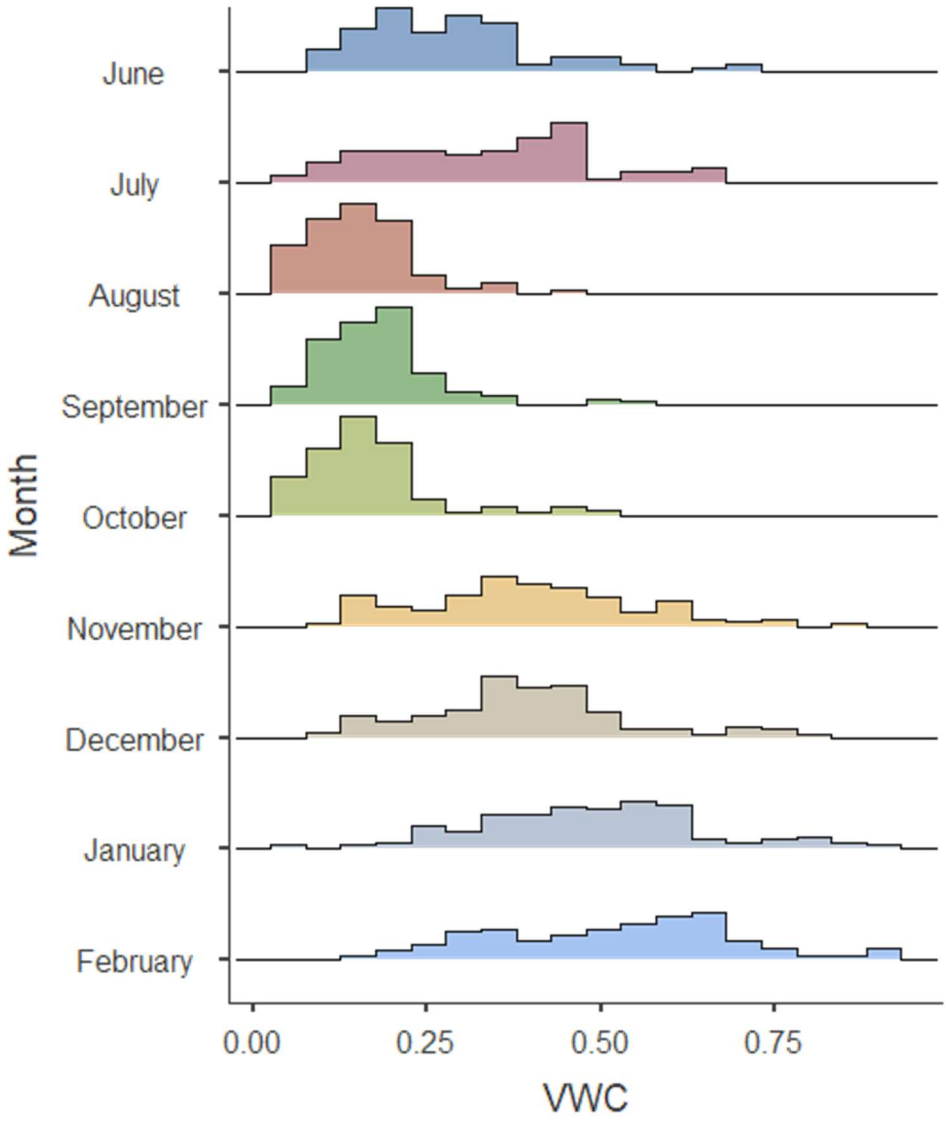


Figure 4.5 Histogram of VWC by month

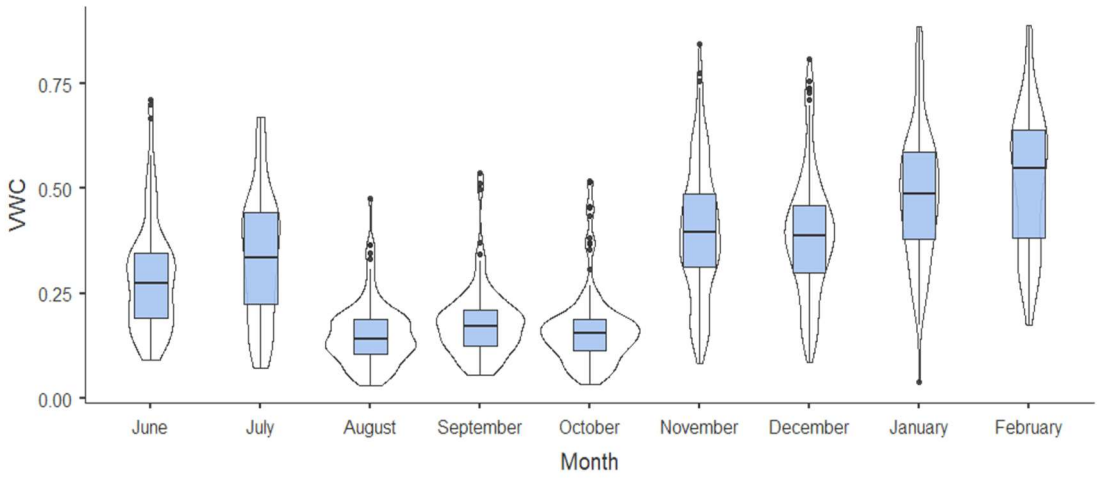


Figure 4.6 Box and violin plots of VWC by month

The skewness values (Table 4.4) show that all the data are positively skewed apart from February which is slightly negatively skewed, with a skewness value of -0.0262. The drier, August-October months are significantly more positively skewed than the wetter months. Of those wetter months, June is more positively skewed than the other months, with a skewness value of 1.06, compared to skewness values of 0.166 - 0.463 for the other 'wet' months. The standard error for all the skewness values sit within the range 0.209 - 0.251. The skew values indicate that data are weighted towards wetter values, which is significant both for our understanding of the distribution of the values at the site, but also in terms of remote sensing – that higher values have a greater weight.

Again, examining the kurtosis (Table 4.4), two distinct groups are seen within the data, with the drier months August – October exhibiting significantly greater kurtosis than the wetter months, with kurtosis values ranging from 2.82 to 4.85, showing that the outliers in these datasets are of significant weight relative to the main peak body of the dataset. As with the skewness assessment, June has a significantly different Kurtosis value to the other 'wetter' months, with a value of 1.25. Of the other 'wetter' months, July, November and February have negative kurtosis values of -0.631, -0.232 and -0.612 respectively, with December and January having low positive values of 0.337 and 0.247 respectively. The standard error of the kurtosis is similar across the months, with values ranging from 0.414 for November to 0.498 for June. This means that there are heavier tails, or more outliers in the drier months, than the wetter months. This indicates, therefore, that outliers are less significant in the wetter months.

Table 4.4 Descriptive temporal statistics

| Month | Mean | Median | Minimum | Maximum | Skewness | Kurtosis |
|---|---|---|---|---|---|---|
| **June** | 0.290 | 0.275 | 0.091 | 0.711 | 1.08 | 1.25 |
| **July** | 0.336 | 0.336 | 0.072 | 0.671 | 0.166 | -0.631 |
| **August** | 0.153 | 0.141 | 0.032 | 0.475 | 1.27 | 2.82 |
| **September** | 0.181 | 0.172 | 0.054 | 0.538 | 1.72 | 4.85 |
| **October** | 0.167 | 0.155 | 0.033 | 0.519 | 1.77 | 3.83 |
| **November** | 0.401 | 0.396 | 0.084 | 0.846 | 0.273 | -0.232 |
| **December** | 0.393 | 0.387 | 0.087 | 0.809 | 0.463 | 0.337 |
| **January** | 0.487 | 0.487 | 0.038 | 0.885 | 0.207 | 0.247 |
| **February** | 0.522 | 0.549 | 0.175 | 0.889 | -0.026 | -0.612 |

### 4.2.4 Descriptive Statistics by Cluster

Assessing the data at the next meaningful spatial scale down – clusters – shows that there are clear similarities within each soil type, and, likewise, dissimilarities soil type to soil type (Figure 4.7 and Figure 4.8). The most distinctive soil type by distribution is sand. The driest soil type, sand also exhibits the greatest clustering of values around the mean, and the smallest inter-quartile and absolute ranges of values. Clay and Sandy Clay have similar distribution profiles, although Clay has a greater absolute range of values and wider interquartile ranges. In the violin plots (Figure 4.7), Clay exhibits a narrow violin profile, whereas Sandy Clay has more incised and curved profiles. Looking at individual clusters, Cluster 2 is the wettest, with the greatest mean, minimum and maximum, at 0.587, 0.195 and 0.889 respectively. Cluster 5 exhibits a shape similar to that of the sand clusters in the violin plot and histogram, but it is most likely that this is caused by the steep, in some cases overhung terrain , rather than being representative of the VWC potential of the material at that location.

The data for the Sand clusters have positive skew (Figure 4.8 and Table 4.5 Descriptive Statistics by cluster, with clusters E and F being approximately symmetrical, with skewness values of 0.455 and 0.414 respectively, while cluster 6 is moderately skewed, with a value of 0.886. Sandy Clay also exhibits a positive skew to its data, though, apart from cluster 6 which has a skew of 0.59, to a lesser extent to Sand, with skew values from 0.0198 at G through to 0.282 at H. Clay clusters exhibit much less of a pattern in terms of skewness. Three clay clusters (C, 1, 2) have a negative skew, with 2 having the greatest negative skew at -0.267, which indicates that there are more higher values than lower values in the sample. The other four clusters have relatively strong positive skews, ranging from 0.331 for B to 0.763 at 5. It is significant that the negative skews are in the areas of the slope where

deformation is most apparent. The implication of this is that the sensing of higher values is important for SAR systems to be able to achieve.

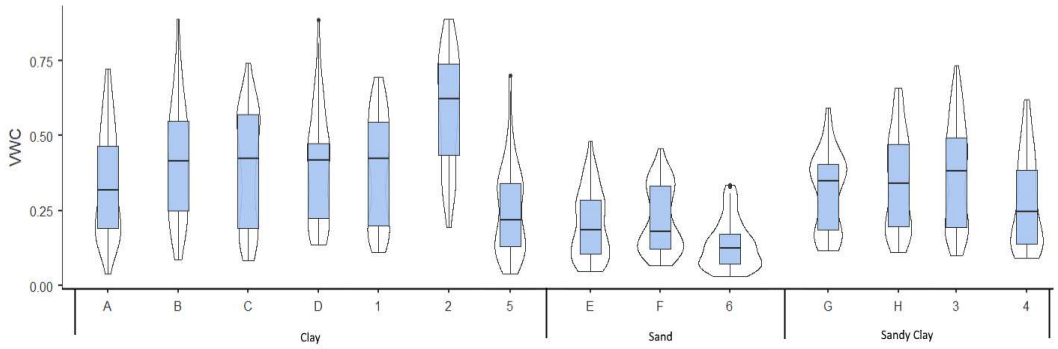


Figure 4.7 Box and violin plots of each cluster

Table 4.5 Descriptive Statistics by cluster

| Soil Type | Cluster | Number | Mean | Minimum | Maximum | Skewness | Kurtosis |
|---|---|---|---|---|---|---|---|
| **Clay** | A | 81 | 0.341 | 0.038 | 0.722 | 0.409 | -0.897 |
| | B | 76 | 0.414 | 0.085 | 0.889 | 0.331 | -0.482 |
| | C | 63 | 0.396 | 0.083 | 0.743 | -0.126 | -1.39 |
| | D | 70 | 0.391 | 0.138 | 0.885 | 0.47 | -0.365 |
| | 1 | 72 | 0.389 | 0.11 | 0.694 | -0.018 | -1.4 |
| | 2 | 72 | 0.587 | 0.195 | 0.889 | -0.267 | -1.03 |
| | 5 | 70 | 0.251 | 0.038 | 0.7 | 0.763 | 0.413 |
| **Sand** | E | 89 | 0.204 | 0.046 | 0.483 | 0.455 | -0.771 |
| | F | 64 | 0.22 | 0.066 | 0.456 | 0.414 | -1.22 |
| | 6 | 71 | 0.135 | 0.032 | 0.336 | 0.886 | -0.004 |
| **Sandy Clay** | G | 74 | 0.313 | 0.116 | 0.591 | 0.019 | -1.03 |
| | H | 76 | 0.346 | 0.111 | 0.66 | 0.282 | -1.07 |
| | 3 | 72 | 0.371 | 0.099 | 0.733 | 0.189 | -1.15 |
| | 4 | 64 | 0.278 | 0.093 | 0.621 | 0.59 | -0.826 |

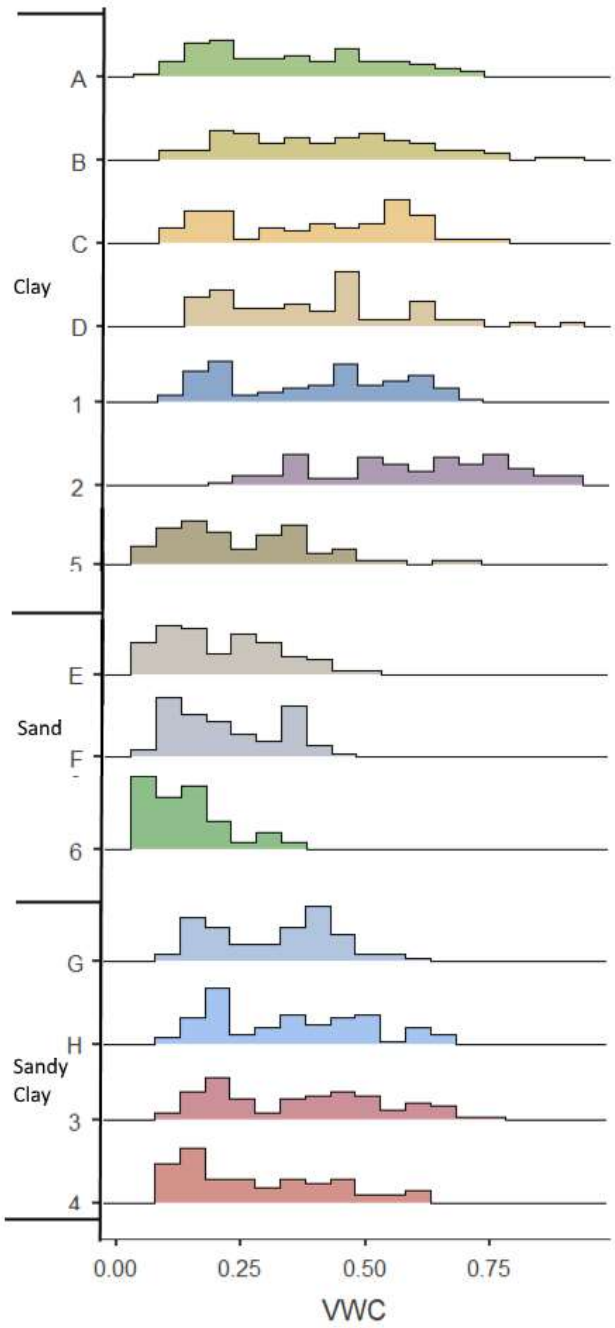


Figure 4.8 Histograms of each cluster

### 4.2.5 Surface soil moisture Descriptive Statistics – Comparing 'wet' and 'dry' data distributions

To gain a thorough understanding of soil moisture variability, the above cluster-by cluster analysis has been undertaken again but with the data split into 'dry' and 'wet' month categories, as these were found in the Descriptive Surface Temporal Statistics analysis (Section 4.2.3) to exhibit distinctive data distributions. Case studies of individual months were considered but the size of the dataset is insufficient to make meaningful assessments of moisture patterning.

The 'wet' dataset, with the notable exception of clusters 6 and G, exhibits a more even spread of data values within the range of values. This characteristic is apparent across soil types, though is less strongly pronounced in the sand class, where the violin diagram (Figure 4.9) shows more pronounced clustering around the mean than is evident in the other soil classes (again, with the exception of cluster G, which exhibits strong clustering around the mean).

In the 'wet' subset, trends around the overall wetness of clusters relative to each other are maintained in the 'wet' data, with, as expected, the clay class being, with the exception of 5, wetter than Sandy Clay or Sand. This relationship is maintained in the 'dry' subset, though to a lesser degree. In the 'dry' subset, cluster 2 is of note, given its high soil moisture values. These do not exist as occasional outliers as in the case of cluster B, but rather, account for the full dataset for that cluster.

Whereas the 'wet' subset exhibits narrow violins for the majority of clusters, the 'dry' subset exhibits greater clustering of data points around the mean. While this clustering is greater for Sand and Sandy Clay, it is also, to a lesser extent, present in the Clay clusters as well, with the notable exception, again, of Cluster 2, which has two clustering areas, one within the lower-mid quartile, and the other in the upper quartile.

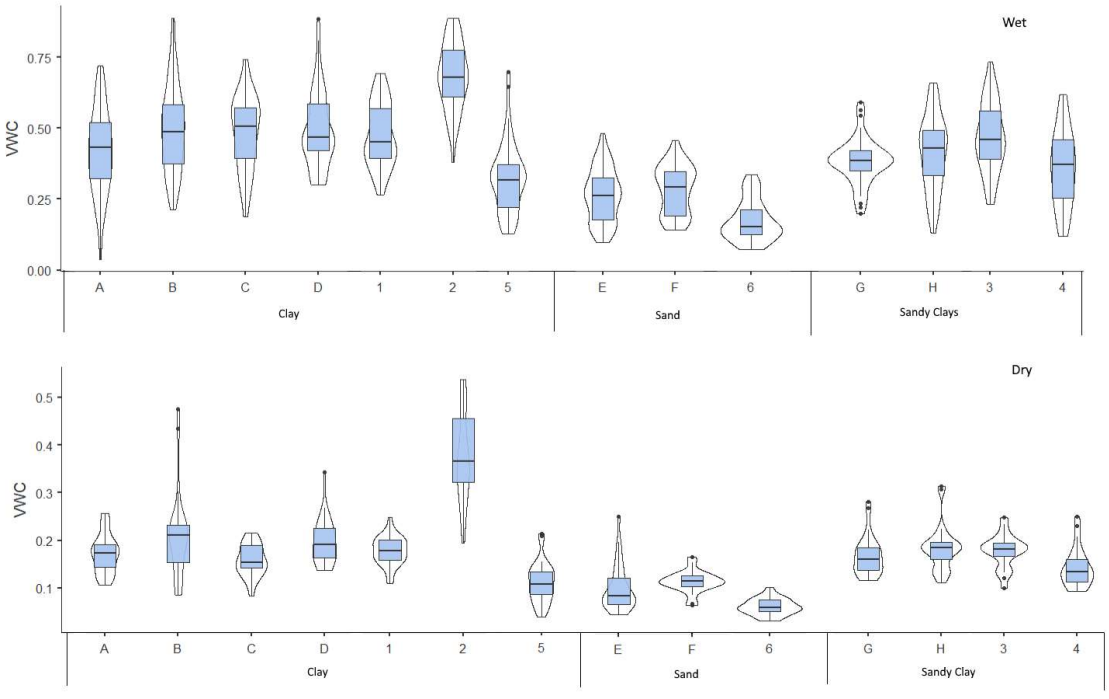


Figure 4.9 Box and Violin plots of Clusters split by wet and dry months

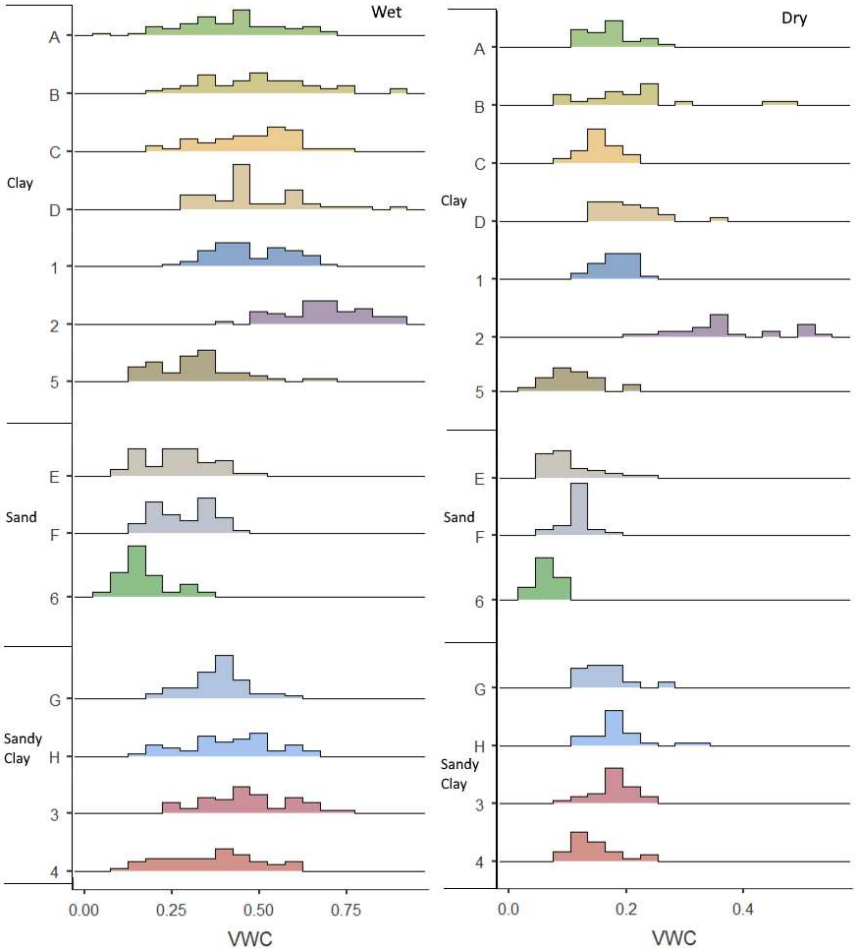


Figure 4.10 Histograms of Clusters split by wet and dry months

The skewness values for the subsets (Figure 4.10, Table 4.6 and Table 4.7) of the data give a more quantitative assessment of the distribution of data within the clusters and during the 'dry' and 'wet' periods. In the 'wet' subset the 'Sandy Clay' class has the most symmetrical data, with skewness values ranging from -0.16 (H) to 0.113 (G). The Sand and Clay classes are less coherent in their skewness. In Sand, E and F are fairly symmetrical, with values of 0.209 and -0.083, whereas 6 is fairly skewed with a value of 0.77. In the Clay subset, C and 5 are positively skewed, with values of 0.821 and 0.828 respectively. The other clusters can be defined as being fairly symmetrical, with skewness values ranging from -0.347 (C) to 0.414 (B). Conversely, the 'dry' subset of data are more skewed than the 'wet' subset. Overall, most of the clusters exhibit a positive skew, with six having a skew that would be defined as 'Highly Skewed' - in Clay 1.37 (B), 1.18 (D), in Sandy Clay 1.47, (E), 1.23, in Sand (G), 1.27 (H), 1.15 (4). It is notable that the skew values for all the clay clusters bar cluster 5 increase the positivity of their skew from wet to dry months.

This is encouraging as it is what would be expected for a clay soil – one that holds water in wetter conditions but can also tend towards dryness during dry periods.

Table 4.6 Descriptive Statistics for 'wet' months

| Soil Type | Cluster | Mean | Median | Minimum | Maximum | Skewness | Kurtosis | Std. dev. |
|---|---|---|---|---|---|---|---|---|
| **Clay** | A | 0.418 | 0.432 | 0.0381 | 0.722 | -0.057 | -0.244 | 0.151 |
| | B | 0.503 | 0.487 | 0.214 | 0.889 | 0.415 | -0.124 | 0.158 |
| | C | 0.484 | 0.508 | 0.188 | 0.743 | -0.347 | -0.469 | 0.131 |
| | D | 0.492 | 0.467 | 0.302 | 0.885 | 0.821 | 0.59 | 0.135 |
| | 1 | 0.477 | 0.451 | 0.264 | 0.694 | 0.193 | -0.942 | 0.112 |
| | 2 | 0.685 | 0.68 | 0.382 | 0.889 | -0.242 | -0.314 | 0.119 |
| | 5 | 0.324 | 0.318 | 0.127 | 0.7 | 0.828 | 1.24 | 0.125 |
| **Sand** | E | 0.264 | 0.263 | 0.097 | 0.483 | 0.209 | -0.726 | 0.094 |
| | F | 0.283 | 0.293 | 0.142 | 0.456 | -0.083 | -1.16 | 0.086 |
| | 6 | 0.173 | 0.152 | 0.072 | 0.336 | 0.77 | -0.288 | 0.071 |
| **Sandy Clay** | G | 0.384 | 0.387 | 0.199 | 0.591 | 0.113 | 0.751 | 0.080 |
| | H | 0.413 | 0.429 | 0.13 | 0.66 | -0.16 | -0.621 | 0.132 |
| | 3 | 0.468 | 0.459 | 0.233 | 0.733 | 0.075 | -0.569 | 0.123 |
| | 4 | 0.358 | 0.371 | 0.119 | 0.621 | 0.048 | -0.76 | 0.135 |

Table 4.7 Descriptive Statistics for 'dry' months

| Soil Type | Cluster | Mean | Median | Minimum | Maximum | Skewness | Kurtosis | Std. dev. |
|---|---|---|---|---|---|---|---|---|
| **Clay** | A | 0.173 | 0.174 | 0.107 | 0.257 | 0.384 | -0.431 | 0.0413 |
| | B | 0.214 | 0.211 | 0.085 | 0.475 | 1.37 | 2.48 | 0.0955 |
| | C | 0.158 | 0.154 | 0.0836 | 0.216 | -0.193 | -0.146 | 0.0342 |
| | D | 0.199 | 0.192 | 0.138 | 0.343 | 1.18 | 2.1 | 0.0481 |
| | 1 | 0.179 | 0.178 | 0.11 | 0.249 | -0.138 | 0.524 | 0.0308 |
| | 2 | 0.374 | 0.366 | 0.195 | 0.538 | 0.231 | -0.717 | 0.0955 |
| | 5 | 0.111 | 0.107 | 0.0387 | 0.213 | 0.635 | 0.471 | 0.0439 |
| **Sand** | E | 0.101 | 0.0858 | 0.0464 | 0.251 | 1.47 | 2 | 0.0478 |
| | F | 0.115 | 0.116 | 0.066 | 0.167 | -0.0866 | 1.16 | 0.0227 |
| | 6 | 0.061 | 0.0592 | 0.032 | 0.101 | 0.355 | -0.0010 | 0.017 |
| **Sandy Clay** | G | 0.169 | 0.161 | 0.116 | 0.281 | 1.23 | 1.5 | 0.0427 |
| | H | 0.185 | 0.185 | 0.111 | 0.314 | 1.27 | 2.42 | 0.0485 |
| | 3 | 0.178 | 0.182 | 0.0992 | 0.248 | -0.326 | 0.314 | 0.0349 |
| | 4 | 0.143 | 0.135 | 0.0931 | 0.251 | 1.15 | 1.02 | 0.0415 |

## 4.3 Summary of dataset overviews

Having undertaken this descriptive assessment of the spatio-temporal statistics at an inter-cluster level, it is possible to make some recommendations regarding the necessary format for remotely monitoring soil moisture at a site of this kind. These analyses have shown several important relationships. They have shown that the spatial distribution of surface soil moisture values is strongly associated with soil type and that the wettest area, namely Cluster 2, corresponds to the most geomorpically active areas of the site.

One area that has been specifically highlighted in the summary statistics review above has been the Cluster 2 area. This area of the slope was specifically targeted

as an area that had been identified during preliminary site visits and from BGS site reports (Jenkins *et al.* 2006; Chambers *et al.*, 2008) as being likely to be influential in the hydrology and instability of the slope, sitting at the foot of the scar and above the mobile mass. In each of the previous analyses it has behaved in a markedly different way to the rest of the clusters, even within its soil class – clay. This cluster, given that it is the wettest on the site is important in directing recommendation about the range of soil moisture values is it necessary for remote sensing applications to be able to assess as it represents one extreme of the range of soil moisture values present on site. The highest value at this cluster was 0.889 $m^3.m^{-3}$, which shows that these values are present in mobile soil masses and, as such, sensors should be calibrated with this in mind. It is also important to note that this value is not an outlier, as is seen in some of the other clay clusters, where maxima of 0.889 and 0.885 are recorded for Clusters B and D respectively, but rather, these high VWC values are repeated in this cluster. That this area exhibits consistently high VWC values both in 'wet' and 'dry' subsets gives confidence that this is a feature of the slope that behaves consistently, holding considerably more water than areas further down the slope to it. Given that other studies show (Jenkins *et al.* 2006; Chambers *et al.*, 2008) that the movement of the slope is initiated from the high soil moisture values in this area of the slope, it is a clear indicator of the high VWC of value it is important to be able to measure.

The availability of soil moisture data at three different depths is novel in the context of soil remote sensing applications. For, while there has been much focus on the groundtruthing of remote sensing estimations of *surface* soil moisture, there has been no reference to the relationship to soil moisture deeper than the remote sensing platform can penetrate (Choi and Jacobs, 2007; Vereecken *et al.*, 2008).

Having looked at this, let us now turn our attention to directly addressing how this section of analysis meets Objective 1.

## 4.4 Objective 1

It is attested in landslide hydrology literature that there is no guarantee that surface soil moisture is well related to deeper moisture values (Van Asch *et al.* 1999; Thiebes, 2012). This section examines the relationship between the surface soil moisture measurements (depth ~0-5 cm) taken during the field campaign with the DeltaT probe, shallow subsurface (depth ~ 10 cm) moisture measurements taken by the automated SensorNET 5TE probes and deeper subsurface moisture measurements

from the COSMOS Cosmic-Ray Neutron Sensor (CRNS). The single-value nature of the COSMOS data for each month means that most of the small-scale analysis will be undertaken with just the SensorNET and ThetaProbe data, with a short discussion of the way these data sets relate to the deeper moisture being undertaken at the end of this section. As with the previous section, the SensorNET and COMSOS values are from 0900 hours on the day of the acquisition, to be as close as possible to the *in situ* acquisition time. First, the subsurface soil moisture data for clusters D (clay), E (Sand) and G (Sandy clay) is presented, then the data for each soil type individually, and then the surface-subsurface relationships are explored for each cluster.

Table 4.8 shows that the descriptive statistics of the two datasets are very similar, which gives confidence that it might be possible to model the relationship between the two successfully, and also that the data from both datasets does not feature any significant unique outliers or artefacts.

Table 4.8 Descriptive statistics of SensorNET and ThetaProbe

| | SensorNet | Thetaprobe |
|---|---|---|
| **N** | 163 | 163 |
| **Missing** | 0 | 0 |
| **Mean** | 27.0 | 26.2 |
| **Median** | 26.3 | 23.9 |
| **Standard deviation** | 15.8 | 14.0 |
| **Minimum** | 2.81 | 4.64 |
| **Maximum** | 63.1 | 60.2 |
| **Skewness** | 0.228 | 0.353 |
| **Kurtosis** | -0.908 | -0.931 |
| **Shapiro-Wilk p** | < .001 | < .001 |

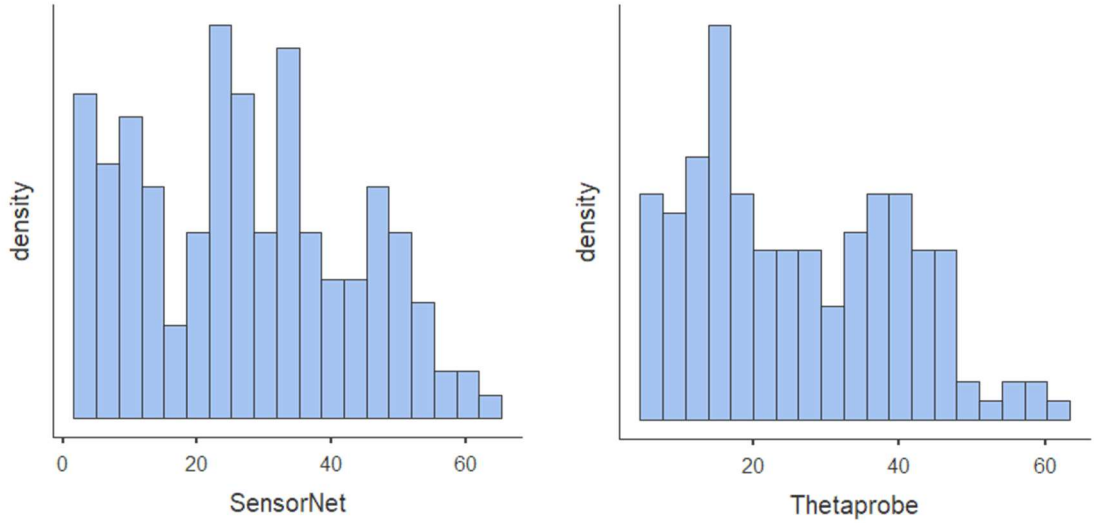

Figure 4.11 Distribution of VWC SensorNET and ThetaProbe values

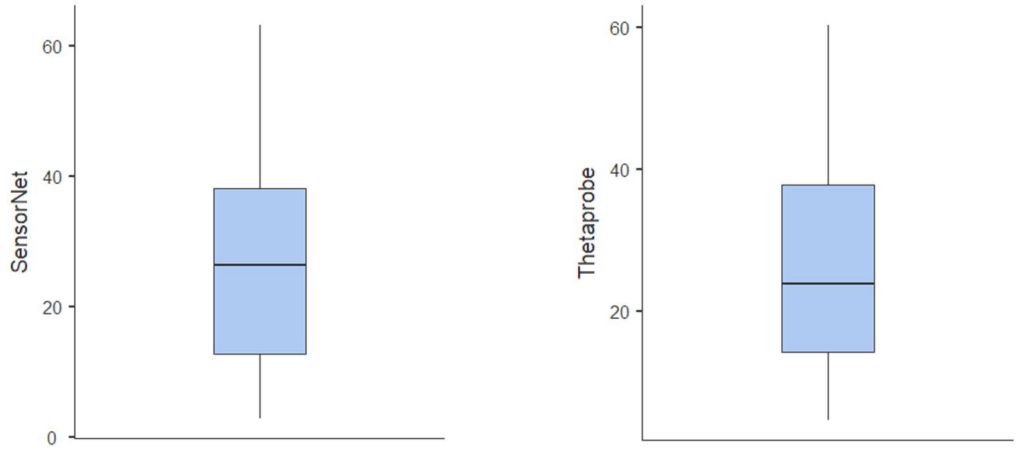


Figure 4.12 Boxplot of VWC values of SensorNET and ThetaProbe

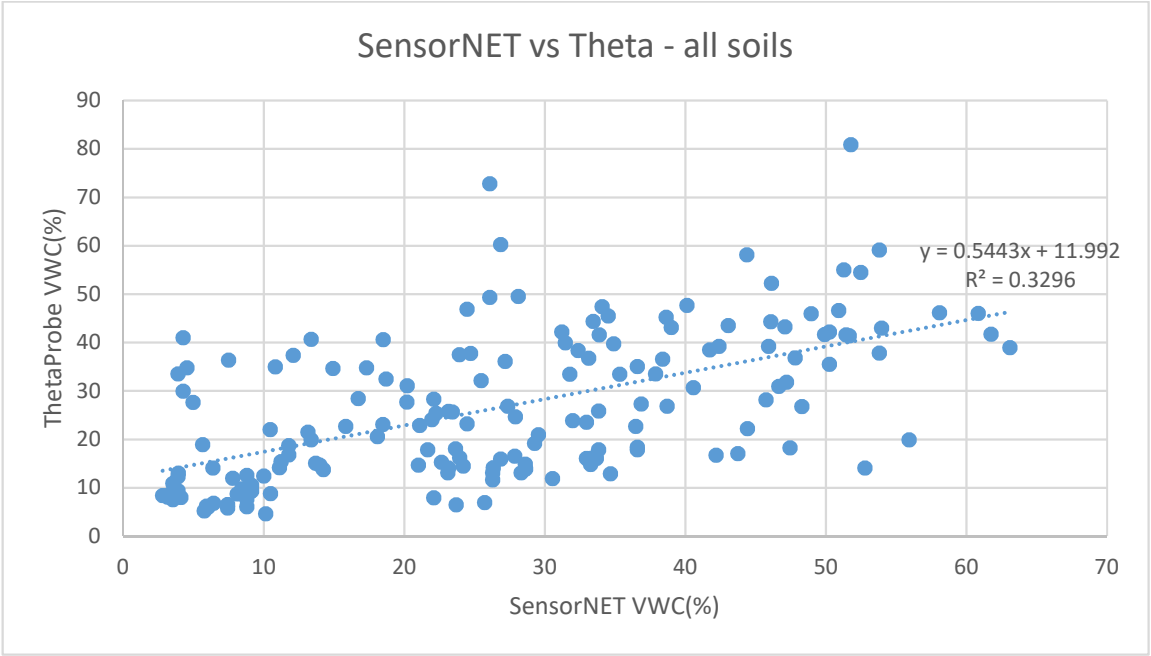


Figure 4.13 Comparison of SensorNet and ThetaProbe VWC values for all soil types

As anticipated, there is a positive correlation between the SensorNET and ThetaProbe VWC datasets (Figure 4.13). It is not, however, as strong as expected. This could be due to sensor error, or different surface-subsurface relationships existing in each soil type, or indeed, that there is a time lag between transfers of moisture between the layers. The following analyses explore relationships in each soil type, and then at each sensor node, culminating in a discussion of the relationship between surface and sub-surface moisture at the site.

Table 4.9 shows the comparative descriptive statistics of each of the soil types at the site. It shows that for most metrics Sand has the most similar values between the

two datasets. Indeed, it is the only soil type which does not exhibit a normal distribution in both datasets. The SensorNET data have lower minima than the ThetaProbe, and higher maxima, with the exception of Clay. They also have higher skewness and normality values, with the exception of Sand, as already mentioned.

Table 4.9 Descriptive Statistics of all three soil types for SensorNET and ThetaProbe

| | Soil | SensorNet | Thetaprobe |
|---|---|---|---|
| **Mean** | Clay | 27.7 | 34.0 |
| | Sand | 15.0 | 18.6 |
| | Sandy Clay | 41.3 | 31.1 |
| **Median** | Clay | 26.6 | 33.0 |
| | Sand | 11.8 | 15.2 |
| | Sandy Clay | 42.2 | 35.0 |
| **Standard deviation** | Clay | 10.1 | 14.2 |
| | Sand | 10.3 | 10.8 |
| | Sandy Clay | 11.2 | 12.9 |
| **Minimum** | Clay | 5.67 | 13.8 |
| | Sand | 2.81 | 4.64 |
| | Sandy Clay | 10.8 | 11.6 |
| **Maximum** | Clay | 51.3 | 60.2 |
| | Sand | 43.7 | 41.0 |
| | Sandy Clay | 63.1 | 59.1 |
| **Skewness** | Clay | 0.356 | 0.148 |
| | Sand | 0.805 | 0.587 |
| | Sandy Clay | -0.259 | -0.0276 |
| **Kurtosis** | Clay | 0.518 | -1.32 |
| | Sand | -0.269 | -0.921 |
| | Sandy Clay | -0.223 | -1.14 |
| **Shapiro-Wilk p** | Clay | 0.587 | 0.036 |
| | Sand | < .001 | < .001 |
| | Sandy Clay | 0.645 | 0.003 |

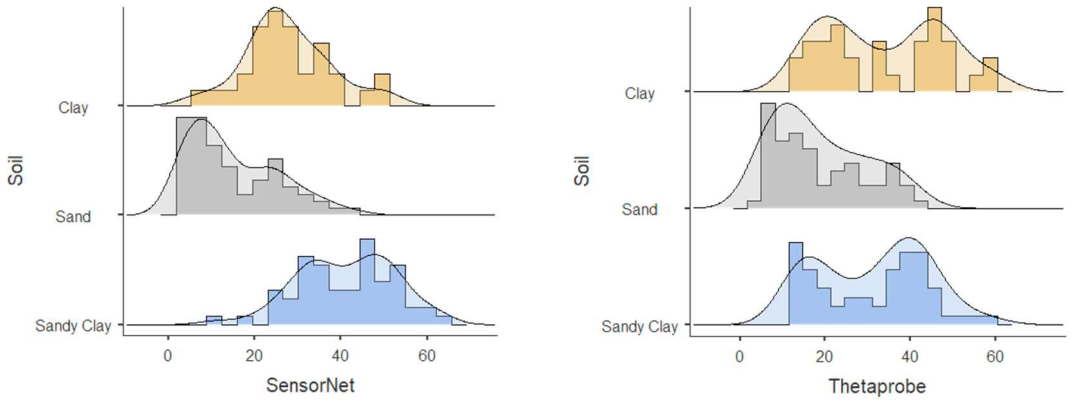


Figure 4.14 Histograms of three different soil types for SensorNET and ThetaProbe

The histograms in Figure 4.14 show the SensorNET and ThetaProbe distributions are similar for the Sand data. In the Clay and Sandy Clay datasets, however, the ThetaProbe shows a stronger bi-modal distribution than the SensorNET. If the bimodal distribution is accepted as a function of seasonal variability, this increased

strength in the bimodal distribution suggests that the surface exhibits stronger responses to wet and dry periods than the subsurface. Here the data of the four clusters are briefly described. There follows an analysis of what these data mean for relating surface and shallow moisture in the slope.

### 4.4.1 Cluster D (Clay)

Sensors D1, D2, D7 and D9 did not function throughout the fieldwork, while sensors D3 and D6 stopped working after September. Likewise, the surface dataset is incomplete, with no values having been recorded for D11, and some sensor locations sporadically missed. Of those sensors where surface and subsurface recording occurred on the same acquisition day, brief summary statistics of the difference between the surface and subsurface values are found in Table 4.10, where a positive value represents surface soil moisture being higher than subsurface soil moisture.

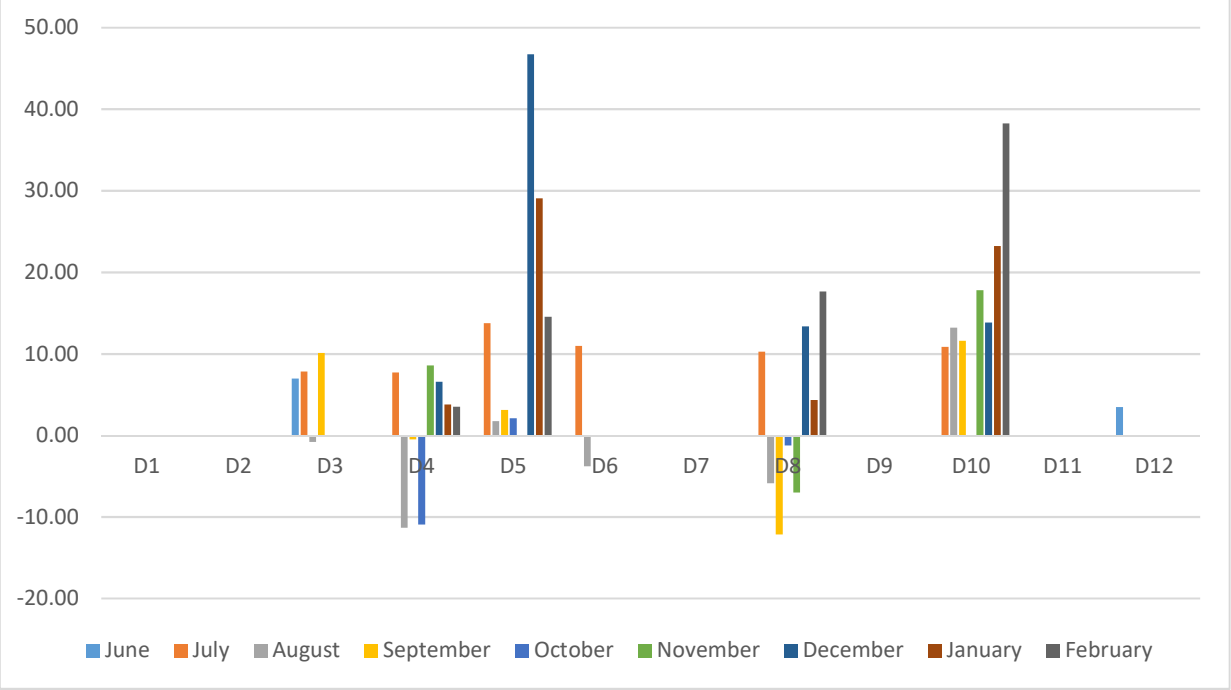


Figure 4.15 Difference between surface and subsurface soil moisture at cluster D

Table 4.10 Summary statistics of surface and sub-surface soil moisture variation at Cluster D

| Sensor | Count | Missing | Mean | Median | Minimum | Maximum | St. Dev. | Range |
|---|---|---|---|---|---|---|---|---|
| **D1** | 0 | 9 | - | - | - | - | - | - |
| **D2** | 0 | 9 | - | - | - | - | - | - |
| **D3** | 4 | 5 | 6.01 | 7.38 | -0.828 | 10.1 | 4.75 | 10.9 |
| **D4** | 8 | 1 | 0.922 | 3.64 | -11.3 | 8.58 | 7.97 | 19.9 |
| **D5** | 8 | 1 | 8.58 | 8.44 | -42.5 | 46.7 | 25.8 | 89.2 |
| **D6** | 2 | 7 | 3.58 | 3.58 | -3.8 | 11 | 10.4 | 14.8 |
| **D7** | 0 | 9 | - | - | - | - | - | - |
| **D8** | 8 | 1 | 2.41 | 1.54 | -12.1 | 17.6 | 10.7 | 29.8 |
| **D9** | 0 | 9 | - | - | - | - | - | - |
| **D10** | 7 | 2 | 18.4 | 13.8 | 10.9 | 38.3 | 9.74 | 27.4 |
| **D11** | 0 | 9 | - | - | - | - | - | - |
| **D12** | 1 | 8 | 3.47 | 3.47 | 3.47 | 3.47 | - | 0 |

### 4.4.2 Cluster E (Sand)

Cluster E performs best in an assessment of difference between surface and subsurface moisture. For, not only are the differences between the two datasets lower (Table 4.11), they also demonstrate variability in whether that difference is positive or negative (Figure 4.16). Or rather, there are sensors which have both positive and negative differences, rather than just one or the other. There are, however, four sensors which should be considered carefully. E7 and E8 have low difference values until November, when the difference values significantly increase, and remain increased. It is possible this is due to a partial failure in the sensors, or that the sensors behave differently when a moisture threshold is passed, as the surface measurements show that soil moisture increases significantly from October to November. Sensor E3, likewise, has anomalously large difference values for the three months it recorded. E10 has higher than average difference values, with one peak difference value in November. Whether this is indicative of a systematic error associated with this sensor or not, it is difficult to confidently assert.

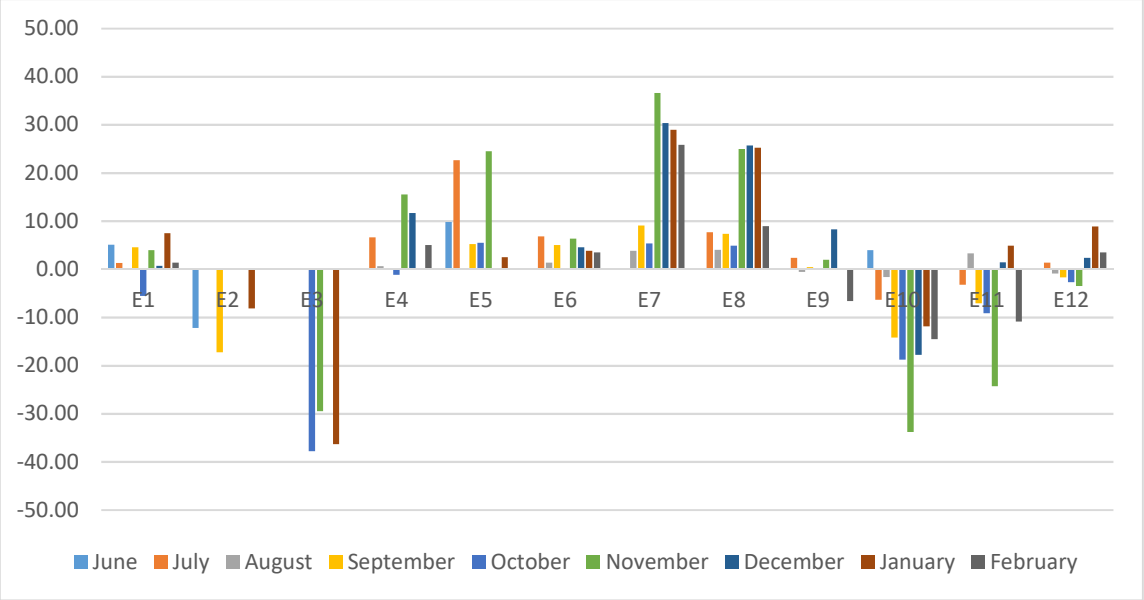


Figure 4.16 Difference between surface and subsurface soil moisture at cluster E

Table 4.11 Summary statistics of surface and sub-surface soil moisture variation at Cluster E

| Sensor | Count | Missing | Mean | Median | Minimum | Maximum | St. Dev. | Range |
|---|---|---|---|---|---|---|---|---|
| **E1** | 9 | 0 | 2.1 | 1.36 | -5.51 | 7.49 | 3.76 | 13 |
| **E2** | 3 | 6 | -12.5 | -12.2 | -17.2 | -8.1 | 4.58 | 9.14 |
| **E3** | 4 | 5 | -37.1 | -37.1 | -44.8 | -29.5 | 6.29 | 15.3 |
| **E4** | 6 | 3 | 6.4 | 5.85 | -1.17 | 15.5 | 6.39 | 16.7 |
| **E5** | 6 | 3 | 11.7 | 7.65 | 2.51 | 24.5 | 9.52 | 22 |
| **E6** | 8 | 1 | 3.96 | 4.21 | 0.197 | 6.82 | 2.29 | 6.62 |
| **E7** | 7 | 2 | 20 | 25.8 | 3.84 | 36.6 | 13.5 | 32.8 |
| **E8** | 8 | 1 | 13.6 | 8.32 | 4.02 | 25.7 | 9.81 | 21.7 |
| **E9** | 7 | 2 | 0.89 | 0.455 | -6.59 | 8.3 | 4.41 | 14.9 |
| **E10** | 9 | 0 | -12.8 | -14.2 | -33.8 | 3.93 | 10.9 | 37.7 |
| **E11** | 9 | 0 | -4.96 | -3.21 | -24.3 | 4.87 | 9.12 | 29.1 |
| **E12** | 8 | 1 | 0.927 | 0.24 | -3.47 | 8.92 | 4.06 | 12.4 |

### 4.4.3 Cluster G (Sandy Clay)

The plot (Figure 4.17) for G shows that for all bar G8 and five other one-off instances at G4, G5, G10 and G11, all the subsurface readings are lower than the surface readings. G1 is the sensor with the greatest offset, while G2, G3, G4 and G9 have similar offsets to each other. The mean offset from the surface measurements ranges from -24.5 (G1) to 13.7 (G8) (Table 4.12), with six of the clusters having a difference of less than -10 (G4, G5, G6, G10, G11, G12). Despite many of the clusters seeming to have distinctive offsets, the range in the offset value for each cluster is high, with values ranging from 15.1 (G11) to 26.2 (G4).

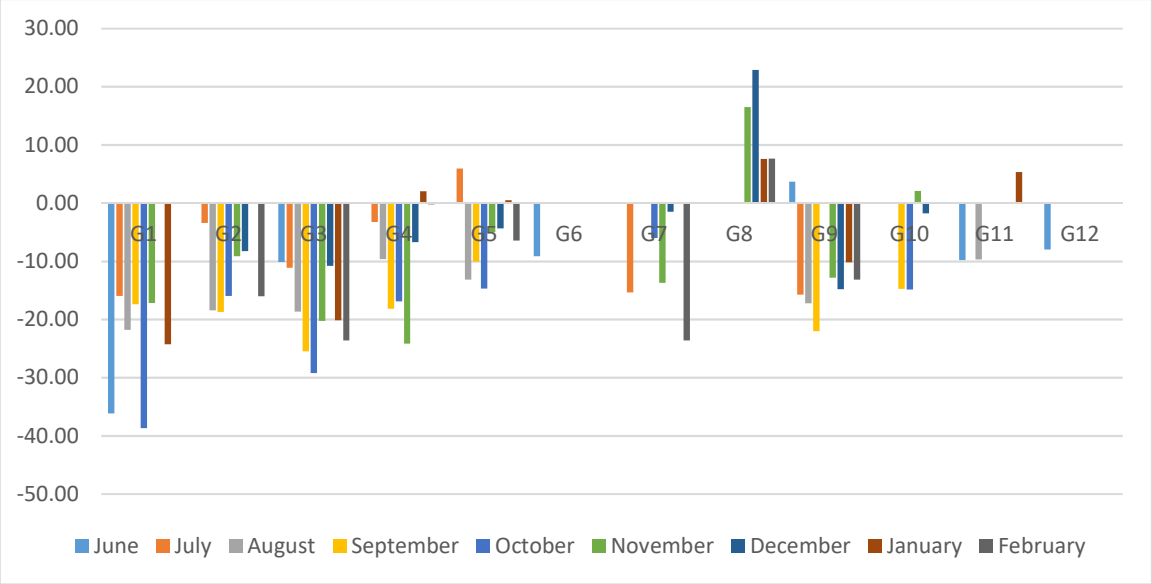


Figure 4.17 Difference between surface and sub-surface soil moisture at cluster G

Table 4.12 Summary statistics of surface and sub-surface soil moisture variation at Cluster G

| Sensor | Count | Missing | Mean | Median | Minimum | Maximum | St. Dev. | Range |
|---|---|---|---|---|---|---|---|---|
| **G1** | 7 | 2 | -24.5 | -21.8 | -38.7 | -16 | 9.33 | 22.7 |
| **G2** | 7 | 2 | -12.9 | -16 | -18.7 | -3.39 | 5.91 | 15.3 |
| **G3** | 9 | 0 | -18.8 | -20.2 | -29.2 | -10.1 | 6.87 | 19.1 |
| **G4** | 8 | 1 | -9.63 | -8.16 | -24.2 | 2.02 | 9.34 | 26.2 |
| **G5** | 8 | 1 | -5.92 | -5.75 | -14.7 | 5.96 | 6.89 | 20.6 |
| **G6** | 1 | 8 | -9.15 | -9.15 | -9.15 | -9.15 | - | 0 |
| **G7** | 5 | 4 | -12 | -13.7 | -23.6 | -1.49 | 8.6 | 22.1 |
| **G8** | 4 | 5 | 13.7 | 12.1 | 7.57 | 22.9 | 7.45 | 15.3 |
| **G9** | 8 | 1 | -12.8 | -14 | -22 | 3.69 | 7.52 | 25.7 |
| **G10** | 4 | 5 | -7.34 | -8.28 | -14.9 | 2.07 | 8.78 | 16.9 |
| **G11** | 3 | 6 | -4.72 | -9.69 | -9.8 | 5.33 | 8.71 | 15.1 |

It is difficult to draw meaningful conclusions from these data as they appear to show, as is seen most clearly in Figure 4.15 and Figure 4.17, that the amount of variability between surface and subsurface measurements is a function of the behaviour of each sensor or is specific to the conditions at that location, rather than being the product of global soil moisture variations. It is necessary, therefore, to question, whether it is possible to use this SensorNET dataset for understanding the relationship between surface soil moisture and subsurface soil moisture and, indeed, whether a modelling of this relationship is even appropriate to undertake. To better visualise the variability in the data, each of the three data subsets – Clay, Sand and Sandy Clay have been plotted and discussed below.

Figure 4.18, Figure 4.19, and Figure 4.20 show that the relationship between the SensorNET and Thetaprobe values is distinctive for each soil type. Clay has the

strongest positive correlation of the three, followed by Sandy Clay and then Sand. Standard error for each soil type is highest at the minima and maxima of each dataset, and greatest for Clay.

The expectation of the relationship between surface and subsurface VWC is that there should be a very strong positive correlation, in the form of a linear relationship, with a gradient of approximately 1 and passing through the origin. The Clay data (Figure 4.18) best equate to this expectation, with a gradient of the best fit line of 1.0692, and an intercept of 6.2746. It also has the highest $R^2$ value of the three datasets, with a value of 0.4378. The Sandy Clay has a shallower gradient of 0.609, though a similar intercept of 6.018 and an $R^2$ value of 0.2806. Sand has the shallowest gradient, at 0.3538, and a similar, though higher intercept at 13.244. The $R^2$ is the lowest of the three datasets, at 0.1148. It should be noted that the trendline is heavily influenced by the tight grouping of low values. Outside of this grouping, the data are seemingly randomly scattered.

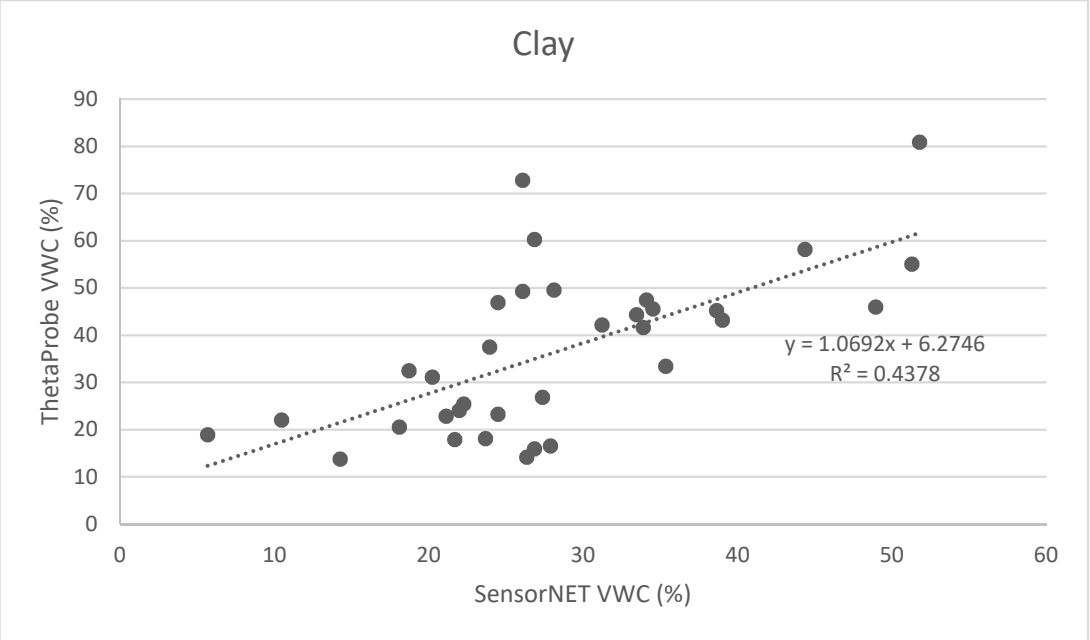


Figure 4.18 Plot of Surface VWC against Shallow VWC for Clay

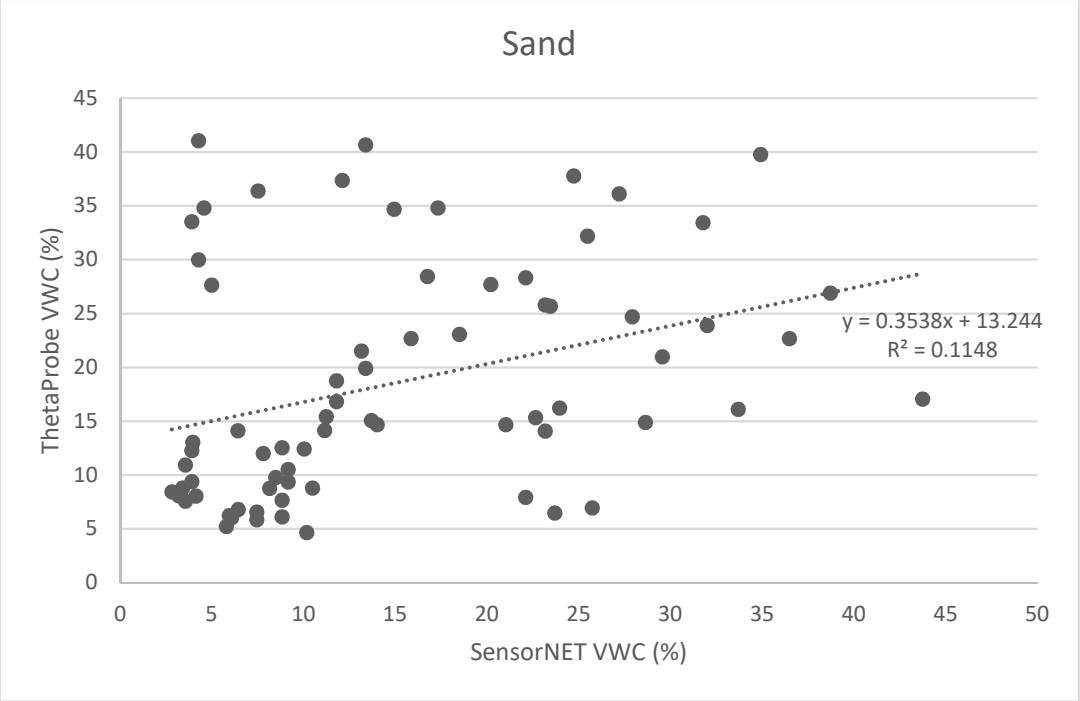


Figure 4.19 Plot of Surface VWC against Shallow VWC for Sandy Clay

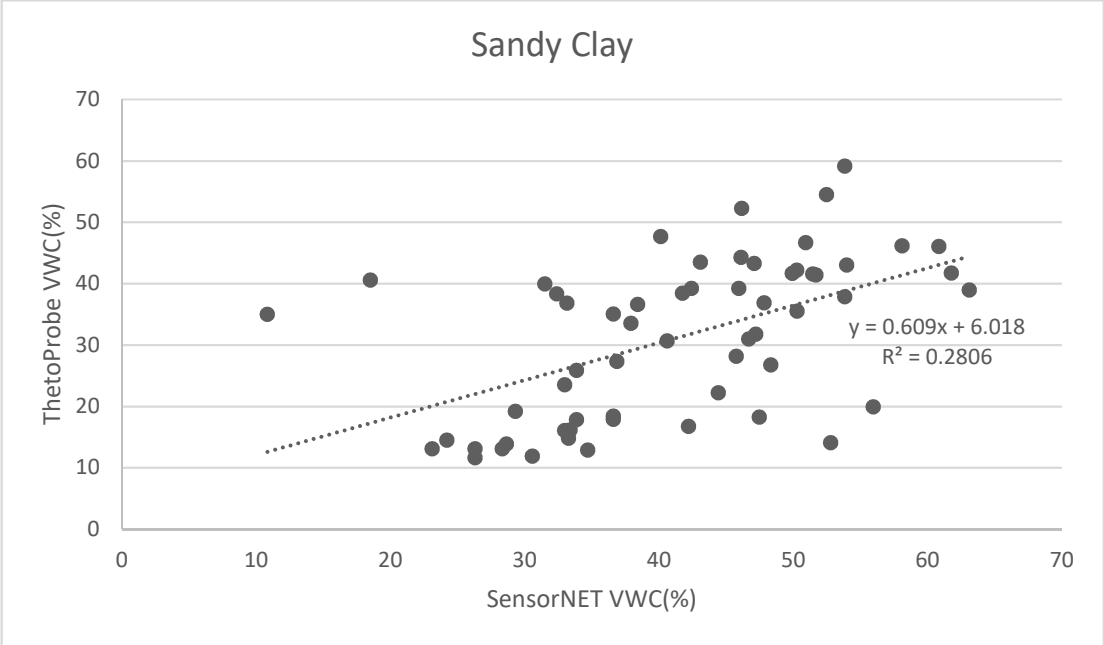


Figure 4.20 Plot of Surface VWC against Shallow VWC for Sand

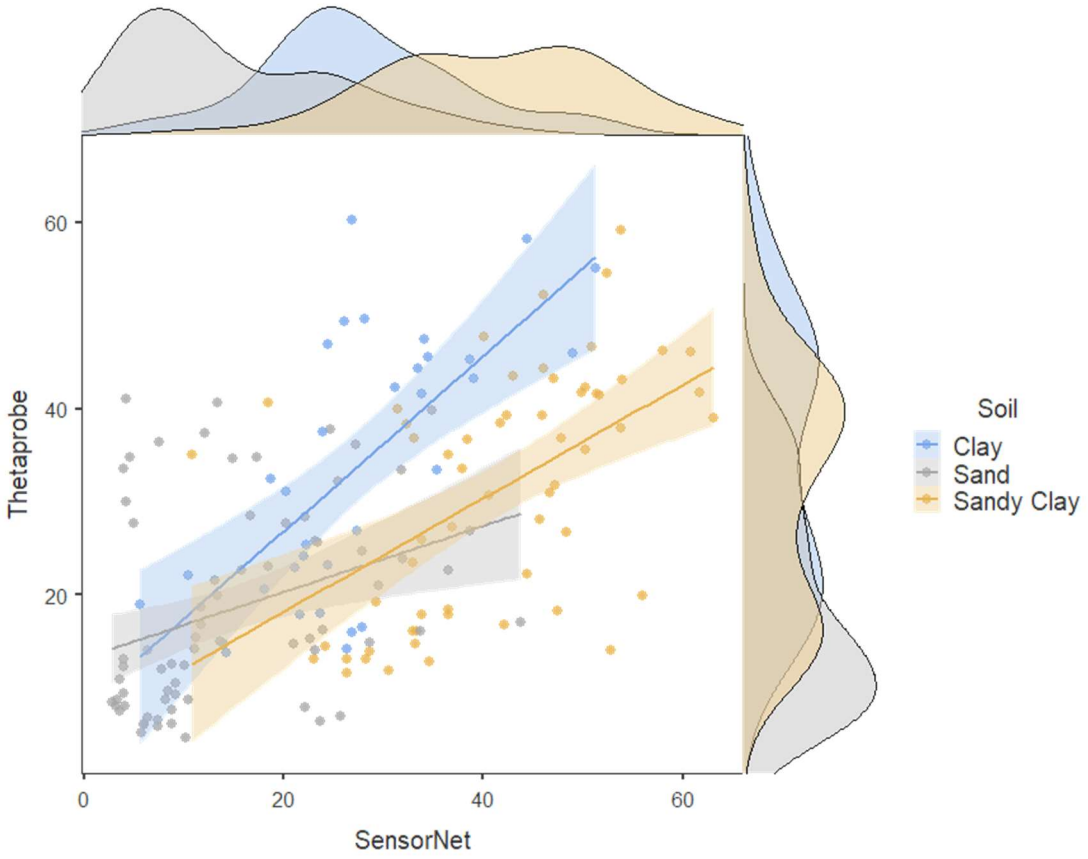


Figure 4.21 Plot of Surface VWC against Shallow VWC for all soil types

Figure 4.21 shows that each of the three soil types at the site exhibits a different surface-subsurface relationship. This is most likely due to the different rates of wetting or drying that the pore spacings of each material allows. That Clay has the strongest relationship between the three is unsurprising given that it is known from Gunn *et al.*'s study (2013) and the presence of sag pond features in its vicinity to be extremely poorly draining, and, by extrapolation, limited in the flow from near surface to subsurface due to sitting at capacity.

### 4.4.4 Relating COMSOS data and surface and shallow data

Having assessed the relationships between surface and shallow measurements, it is valuable to assess the relationship with deeper soil moisture values, closer to the supposed failure surface. Although the Hollin Hill Landslide has a shallow shear surface, estimated by Gunn *et al.* (2013) to be at a depth of approximately 2 m, it is valuable to understand how deeper moisture measures relate to surface measurements for several reasons. First, to establish what the difference is, and whether the surface or shallow measurements better relate to the COSMOS data, second to assess whether large-scale soil moisture readings like COMSOS have a value in calibrating SAR or other remote sensing products (RS2). In this analysis

only surface and shallow data are used from the locations the SensorNET sensors were working, to enable a better comparison between the two datasets and COSMOS.

Figure 4.22 and Figure 4.23 show that most ThetaProbe measurements are lower than COSMOS data, but that above a threshold between 33.42% and 42.46% some ThetaProbe values exceed the COSMOS values. The SensorNET values both exceed and are lower than the COSMOS data at all COSMOS values. The spread of the SensorNET data is greater than that of the ThetaProbe data for most of the monthly datasets.

That the COSMOS readings are generally higher than the other two datasets is not wholly surprising. At depth, the impact of surface drying processes like evapotranspiration are not present. Likewise, COSMOS is not a measurement of a point, but rather a measurement of the moisture of a volume, at depths ranging from approximately 0.4 m by the sensor, to 0.15 at the extent of its range. Although this makes comparison of the quasi-point datasets with it more complicated than the comparison directly between them, there are some valuable comments that can be made on the relationship. First, the COSMOS sensor is positioned close to the western edge of the active eastern lobe, near the slope transition from clay to sandy clay. This is significant for the measurements of the CRNS have been found to be most affected by the moisture values within a few meters of the probe (Köhli *et al.*, 2015). Its position, therefore, close to the intersection of significantly different hydrologies at the site is valuable as it means that one soil type, and therefore hydrology, is not over-represented. That being said, it must be noted that the sand soils are, perhaps, under-represented, which might explain why CRNS values are higher than those from the SensorNET and ThetaProbe data.

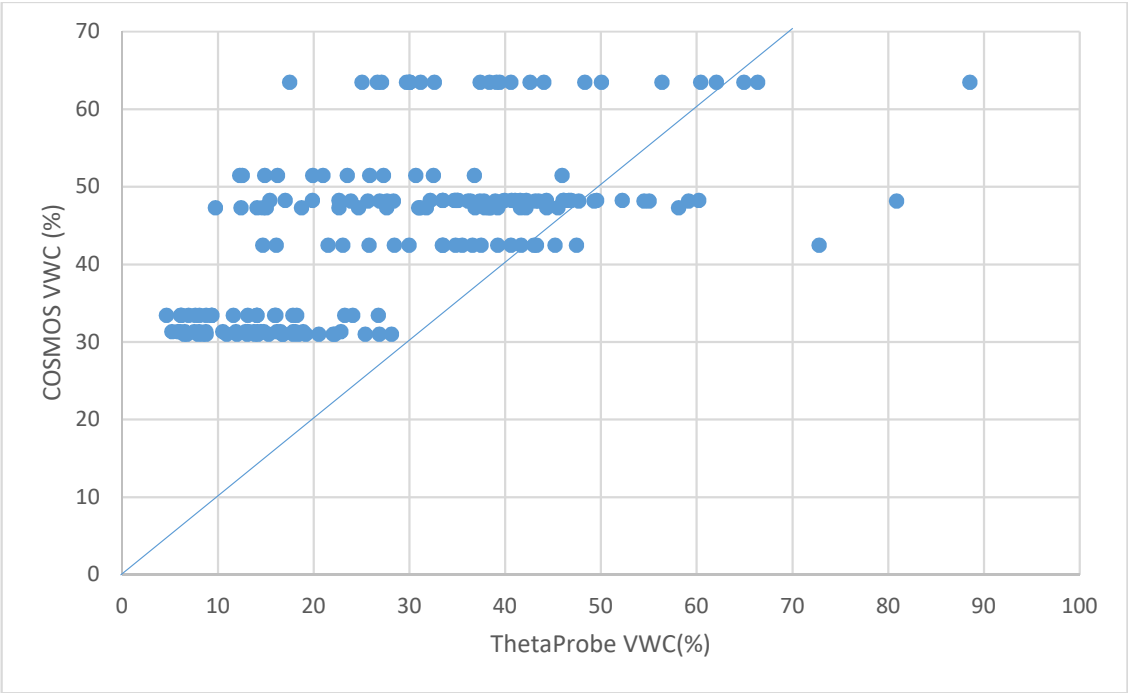


Figure 4.22 Plot of COSMOS VWC against ThetaProbe VWC

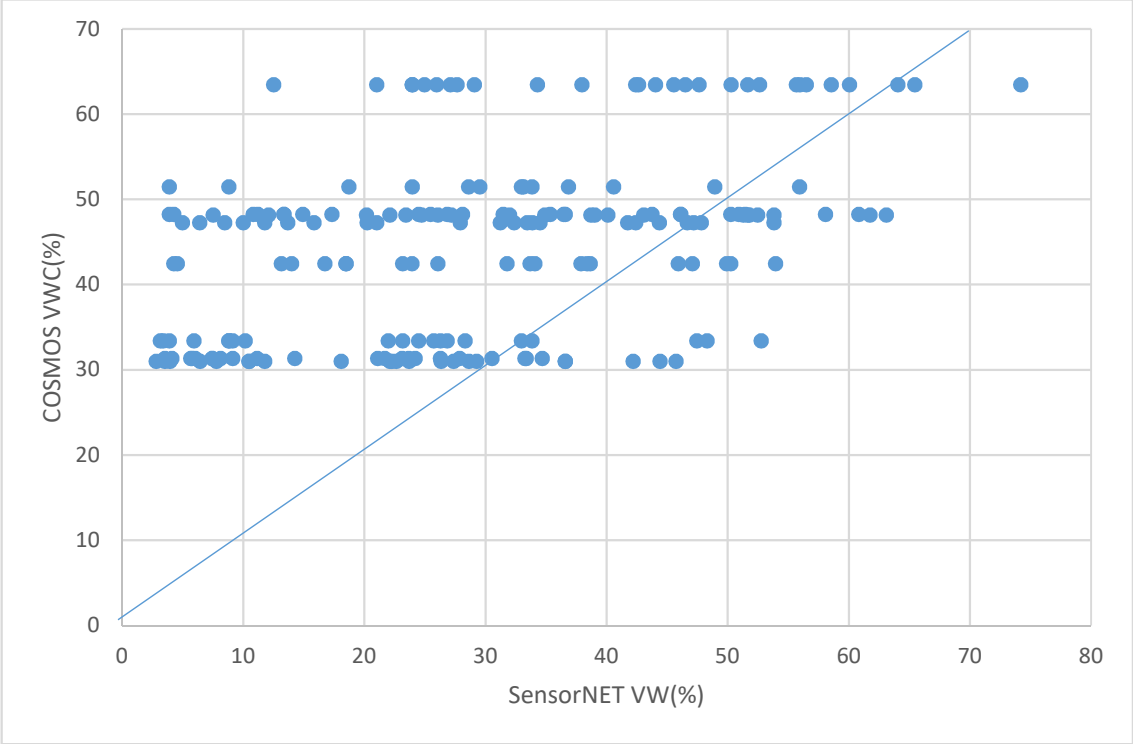


Figure 4.23 Plot of COSMOS VWC against SensorNET VWC

### 4.4.5 Objective 1 Discussion

Surface-shallow relationship

It was envisaged that the SensorNET data would enable the meeting of Objective 1 and then be used to model subsurface soil moisture across the site. Two factors do,

however, preclude this course of action. First, the data that BGS are able to provide are limited to three out of eight clusters. It would not be appropriate to interpolate a global moisture surface from this few data points in this clustered arrangement. Likewise, of those data that BGS have provided – those which they deem to be the most reliable – the comparison of them with the surface Delta T values indicates that much of the variability between surface and subsurface is likely due to an error in the VWC measurement by the 5TE sensor, rather than being due to unusual moisture routing in the soil mass, given the small vertical distance between the two measurement volumes. It is not possible, of course, presume that the surface soil moisture values are entirely trustworthy and without error, but the way that each sensor has a relatively distinct error each month is indicative of a systematic error in the SensorNET data rather than the DeltaT data. The only cluster that it might be possible to use the data of to model surface-subsurface soil moisture relationships is cluster E, if some of the suspicious data points are discarded; but, given the paucity of data points that leaves, and given that E covers the most stable area of the site, the value of such an attempt is questionable given the focus of this study on soil moisture in an active landslide setting.

Surface-Deep relationship

As already mentioned, relating such different volumes of soil measured by the ThetaProbe and the CRNS makes quantitative assessment of the relationship between surface soil moisture values and the deeper CRNS values problematic, especially given the known heterogeneity of the hydrogeology in the area the CRNS probe measures. It can, however, be said that the VWC values from the surface measurements are lower than those measured by the calibrated CRNS sensor. This is significant for remote sensing, as the wavelength of most SAR platforms means that the backscatter of most products does not penetrate more than a few centimetres into the soil mass (Kerr, 2007; Eineder *et al.*, 2009; Beven, 2011), and therefore, is not affected by the slope material that is wettest, and therefore most indicative of slope conditions.

Objective 1 Conclusions

This section has assessed the surface, shallow and deep soil moisture relationships at Hollin Hill. It must be recognised that there are issues regarding some of the sensors in the SensorNET array, and that the difference in the soil volumes the quasi-point measurements and CRNS sensors measure makes the establishment of

absolute relationships complex. However, the relationships between CRNS and the point measurements show that, while not fully understood, there appears to be a strong relationship between surface/shallow values and deeper subsurface values.

## 4.5 Objective 2

There is an assumption in geographical literature that things that are close together will be more similar than things that are further apart (Legendre, 1993). This is referred to as spatial autocorrelation. Correlations lengths are typically expected to be between 30 and 60 m for soil moisture (Western *et al.*, 2004). The following section assesses the scales at which autocorrelation occurs at this site, and the site characteristics that define and limit those scales. To assess spatial autocorrelation, measures of semivariance were undertaken for each monthly dataset using the Geostatistical Wizard in ESRI's ArcMap 10.3.1. The scale at which autocorrelation occurs is important for decision making in remote sensing as it informs both the scale of window averaging appropriate to apply during image processing and also allows better understanding of the range of soil moisture values that might be contained within a pixel of a given size. This section begins with exploring autocorrelation at the site-wide scale, and then moves on to explore it at a cluster-scale, thereby reporting on both the larger-scale patterning of soil moisture, but also the small-scale variability at a pixel-specific scale.

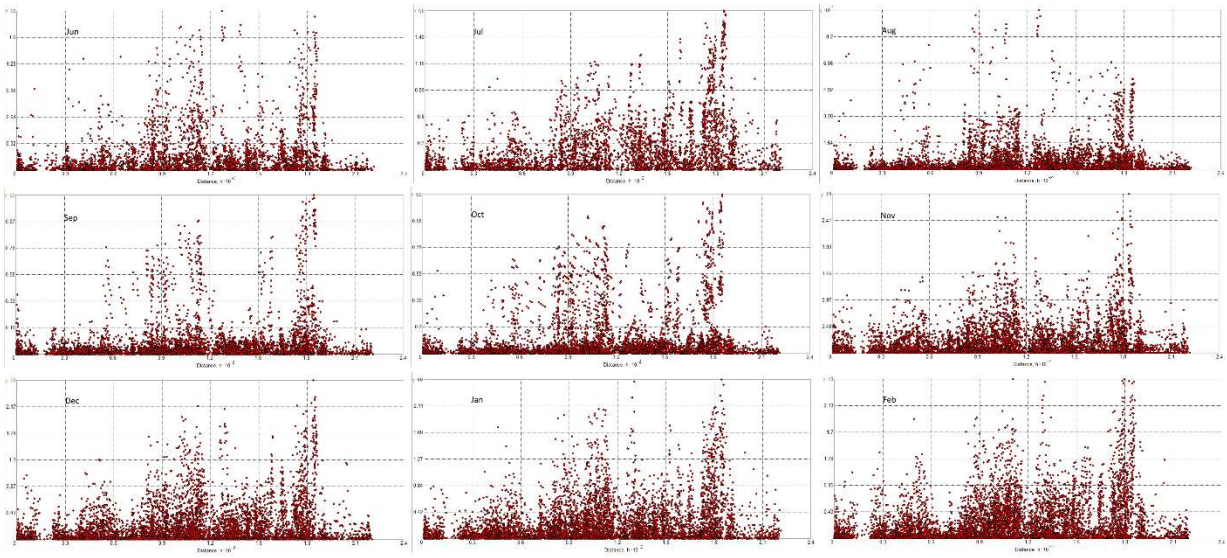


Figure 4.24 Unbinned semivariograms for each month of data featuring all data points

The raw, unbinned semivariograms (Figure 4.24) show that while there is an overall trend for the more dissimilar pairs of points to be further apart, there is also significant complexity to this finding. For, in each semi variogram it is apparent

that at distances of above ~ 200 metres the difference in paired values decreases to close to those values seen in the closest pairs. Indeed, the high density of points close to the x axis along its full 220 m range indicates that there is complexity to the spatial patterning of soil moisture at this site. It is likely that this complexity is, in part, caused by the different soil types at the site. The boundaries between these soil types are distinct and so clusters that are close together can have distinctly different hydrological properties, likewise clusters far apart can have relatively similar material characteristics. Indeed, the low variance values at the furthest distance are exclusively from pairs of points from clusters A and D – both on Clay soils (Figure 4.25), which indicates that within the same soil type there can be considerable similarity even at a distance, as long as there are similar hydrological processes ongoing in that area.

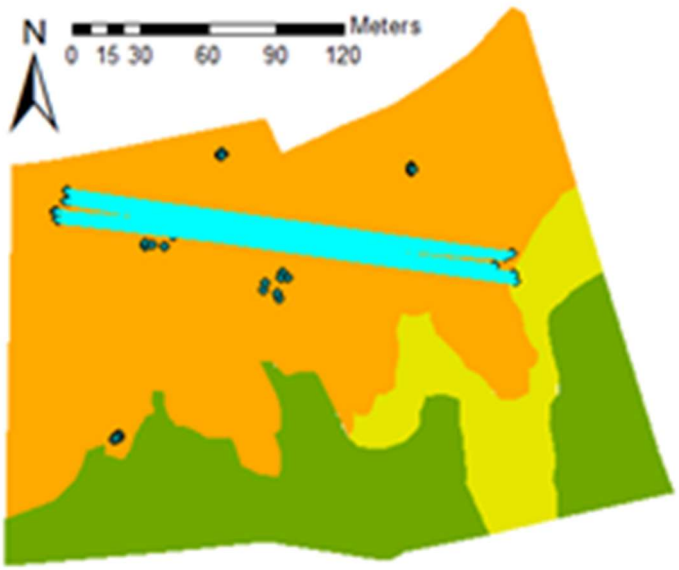


Figure 4.25 Map of pairs with high spatial dissimilarity, but high VWC similarity. The blue lines show the pairings in question

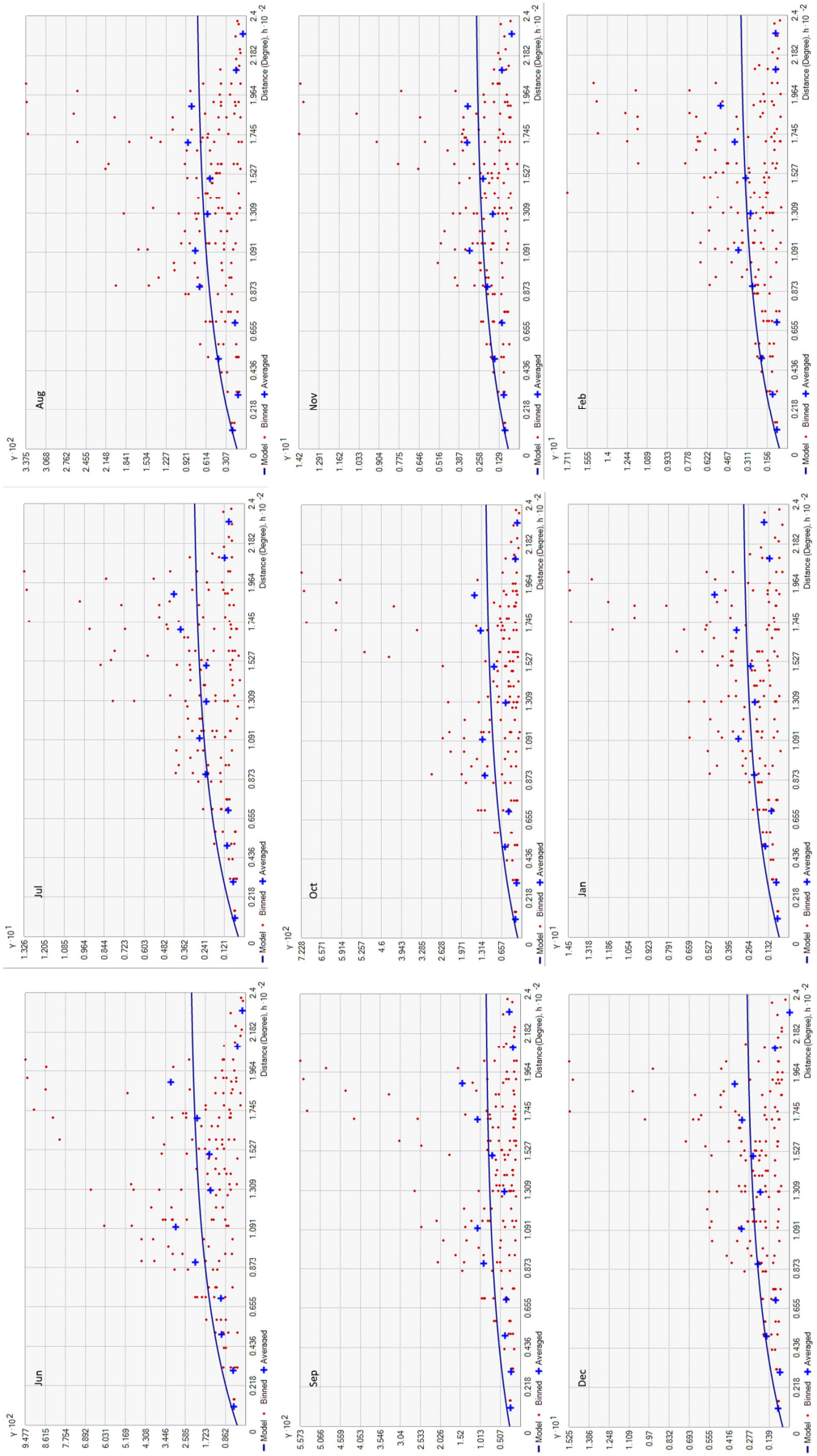


Figure 4.26 Monthly semivariograms with binned data and fitted exponential models

There are strong similarities between the monthly semivariograms which rules out the potential for moisture thresholds by which autocorrelation is limited. In the variogram models produced with the averaged binned data and fitted with an exponential model, as seen in Figure 4.26, flattening out of the model does not occur within the data range. This suggests that autocorrelation is not evident in these data sets. The nugget value – normally indicative of measurement error - is inconsistent across the datasets (Table 4.13), ranging from 0.00144 in august to 0.721 in November. Given the standardised measuring procedure undertaken across the data, this is further evidence of the high spatial variability of soil moisture at the site.

Table 4.13 Descriptors of semivariogram models

| Month | Partial Sill | Nugget | Major Range | Lag size | Lag Number |
|---|---|---|---|---|---|
| **June** | 0.0205 | 0.0037 | 240 | 20 | 12 |
| **July** | 0.0276 | 0.0037 | 240 | 20 | 12 |
| **August** | 0.0063 | 0.0014 | 240 | 20 | 12 |
| **September** | 0.0062 | 0.0027 | 240 | 20 | 12 |
| **October** | 0.0109 | 0.0013 | 240 | 20 | 12 |
| **November** | 0.0214 | 0.0072 | 240 | 20 | 12 |
| **December** | 0.0258 | 0.0046 | 240 | 20 | 12 |
| **January** | 0.0245 | 0.0063 | 240 | 20 | 12 |
| **February** | 0.0312 | 0.0064 | 240 | 20 | 12 |

### 4.5.1 Cluster-scale autocorrelation

To better understand autocorrelation at the site, semivariogram analysis has been undertaken on a cluster-by cluster basis using two case-study months - one 'dry' and one 'wet' – October (Figure 4.27) and December (Figure 4.28) respectively. In the previous, whole-site assessment the results were not clear because of multiple variables, like soil type and slope angle, not being consistent from cluster-to-cluster. Within each cluster there is, however, minimal variability in factors which can affect VWC.

Even though it would be expected that a clearer autocorrelation signature would be present in the semivariograms due to the reduction in variables, in many cases this in not evident. Cluster 2 shows no autocorrelation in October, with a pattern-less scattering of values within the plot. In December, there is also little evidence of a standard autocorrelation pattern in the Cluster 2 data. Conversely, some clusters do have semivariograms that indicate spatial autocorrelation in both October and

December. Clusters 3 and D, both of which sit to the Eastern side of the mobile Eastern Lobe have plots indicative of spatial autocorrelation. The number of data points in each cluster is quite small (~8), so it is hard to be confident in assessing the autocorrelation cut-off. The semivariogram for Cluster 4 in October shows that a tight grouping of most values close to the X axis, with a few outliers. This is caused by one data point that is significantly different from the rest. The December data from this cluster shows, however, much less similarity point-to-point.


Figure 4.27 Semivariogram plots for each cluster (1-6, A-H) in dry case study month, October

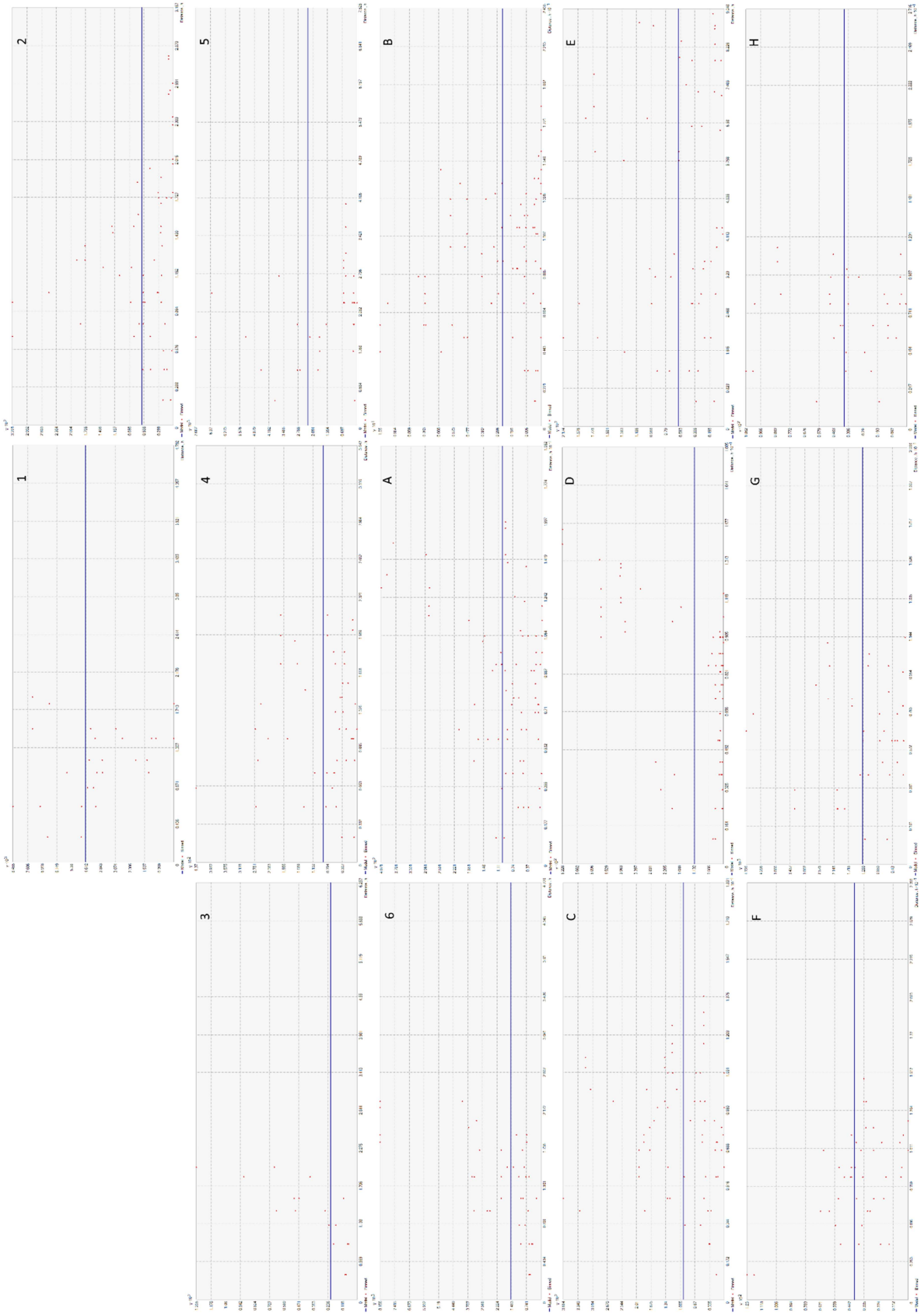


Figure 4.28 Semivariogram plots for each cluster (1-6, A-H) in wet case study month, December

### 4.5.2 Predicted soil moisture surfaces

To meet Objective 2, an assessment of the anticipated soil moisture spatial distribution over the whole site kriged soil moisture surfaces were created using the Ordinary Kriging function in the Geostatistical Wizard in ArcMap and *in situ* data from each month. Although other work on kriging soil moisture has advocated use of a Gaussian model (Obroślak and Dorozhynskyy, 2017), an exponential model was used for the kriging for two reasons, first that the descriptive statistics show that the data cannot be assumed to be normally distributed, second, that tests with data from two sample months (September - 'dry' - and June - 'wet') showed that this was the best model type, based on the Root-Mean-Square Standardised Error and the Mean Standardised Prediction Error. Other model types that were assessed but rejected were: Circular, Spherical, Rational Quadratic and Stable.

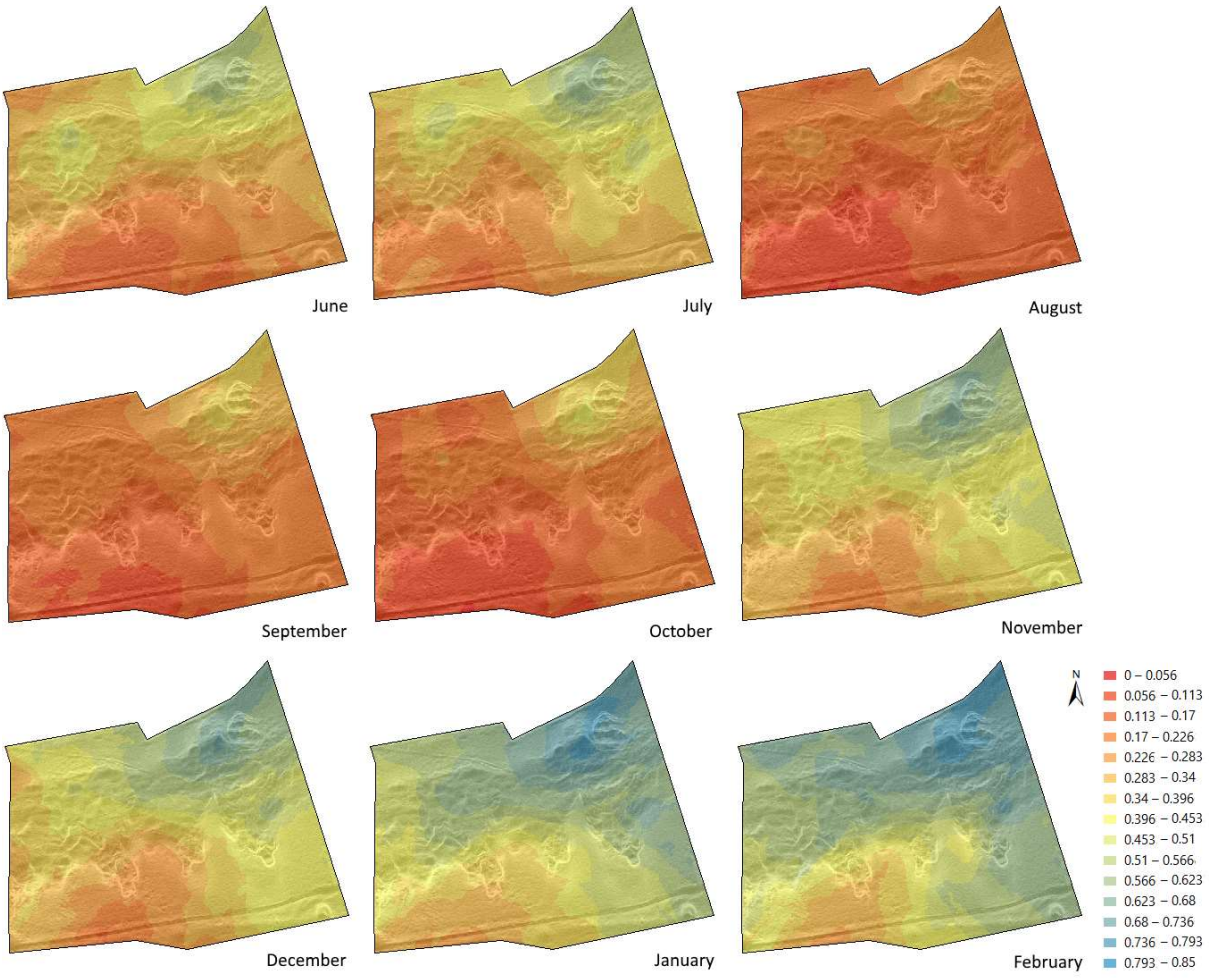


Figure 4.29 Kriged VWC surfaces for each month, with topography underlying

The kriged VWC surfaces (Figure 4.29) show strong similarities in moisture patterning, with the North Eastern quadrant being consistently the wettest and the area with the 'Sand' soil class being consistently the driest. The kriging was

undertaken without any barriers and yet the moisture patterns, particularly in the southern half of the site show some similarity to the topography. Although the clay at the North of the site is considered as being uniform in its composition across the site, it is of interest that the Western part of the slope is considerably drier than the Eastern part, where most of the slope deformation is initiated.

While the clustered design of the data will inevitably create artefacts in the kriged surfaces, the prediction error scores (Table 4.14) are such that it is possible to be confident in the quality of the surfaces in Figure 4.29. The proximity of the Mean predicted error to 0 indicates that the overall error for the kriged surfaces is low and although the RMSE standardised error is slightly lower than optimum, it is just necessary to be aware that variability is slightly under-predicted by these surfaces.

Table 4.14 Prediction Errors for kriged surfaces in Figure 16

| Month | Mean | Root-Mean-Square | Mean Std. | Root-Mean-Square Std. | Ave Std Error | Mean Std. from optimum | RMS Std. from optimum |
|---|---|---|---|---|---|---|---|
| June | -0.0003 | 0.08197 | -0.00321 | 1.0957 | 0.07249 | 0.00329 | 0.09574 |
| July | -0.0015 | 0.08368 | -0.0144 | 1.1149 | 0.07471 | 0.01441 | 0.11495 |
| August | -0.0002 | 0.05129 | -0.0015 | 1.1522 | 0.04371 | 0.00157 | 0.15222 |
| September | -0.0001 | 0.05446 | -0.0021 | 0.9394 | 0.05858 | 0.00212 | -0.0605 |
| October | 2.40E-05 | 0.05059 | -0.0007 | 1.1243 | 0.0451 | 0.00071 | 0.12438 |
| November | -0.0014 | 0.10449 | -0.0119 | 1.0883 | 0.09552 | 0.01195 | 0.08834 |
| December | -0.0032 | 0.0904 | -0.011 | 1.1144 | 0.07994 | 0.01105 | 0.11441 |
| January | -0.0012 | 0.09355 | -0.0101 | 1.0196 | 0.09106 | 0.01017 | 0.01963 |
| February | -0.0009 | 0.09668 | -0.0073 | 1.0364 | 0.09296 | 0.00734 | 0.03642 |

### 4.5.3 Objective 2 Discussion

The rationale behind this objective was to assess the appropriate scales of multi-looking or adaptive filtering which could appropriately be undertaken with remote sensing products. This is challenging to answer as, on the one hand, this study has shown through the data from the smaller surface clusters (1-6) that within the area of a CSK cell (~1x1 m) the soil moisture can vary considerably, whereas, the autocorrelation analysis has shown that the limit of autocorrelation is about 190 meters, which is two orders of magnitude greater than the scale of the CSK pixels. The recommendation on this, therefore, has to be that the appropriateness of multilooking and adaptive or non-adaptive filtering approaches and the scales of their use is defined by the objectives of the research being undertaken. If projects are investigating the soil moisture content of soils at a field scale, then the choice of

multilooking and filtering techniques and their scale can be free to the discretion of the user, based on the availability of data and the computational capacity, given the multi-order of magnitude difference in the autocorrelation length and pixel size. However, if targeted, quasi-point information about moisture is required, then it should be noted that within the area of the pixel it is probable that there is variation in soil moisture values.

### 4.5.4 Objective 2 Conclusions - Interpreting spatial autocorrelation and its impact on Remote Sensing decision making

The findings from this section have, however, been inconclusive, both when assessing spatial autocorrelation at a site scale and a cluster scale. This problem, due to small-scale variability in soil moisture, is not uncommon in studies seeking to interpret point-measure soil moisture data (Vereecken et al., 2008). Although this is frustrating in that it does not allow specific recommendations to be made with regards to parameters for processing the COSMO-SkyMed data in later chapters, it does serve to highlight that even when multiple site variables are thought to be accounted for in the development of a project plan, the highly stochastic nature of this variable in a geomorphically active context cannot be fully accounted for.

This analysis has shown the difficulty in drawing clear conclusions about the scale at which autocorrelation exists and is indicative of the complex stochastic nature of soil moisture. This difficulty does, however, have implications for meeting Objective 2 as it is not possible to confidently assert the scale to which satellite products need to be produced to well characterise the spatial variability in soil moisture at site similar to this one.

## 4.6 Chapter discussion and conclusions

In addressing Objective 1, it was found that while there is a positive correlation between surface and sub-surface soil moisture readings, the strength of the relationship is weaker than anticipated. Given that the routing of moisture below the surface is important to understand in the context of modelling slope deformation and factors of safety, this presents problems in interpreting what surface readings of soil moisture mean for sub-surface moisture and any deformation caused by it. This, in and is therefore indicative that should CSK data be used for monitoring surface soil moisture as a pre-cursory condition of a large rainfall event, or, indeed, as a proxy for any other environmental monitoring, it should be noted that surface conditions do not necessarily well define sub-surface conditions and that, therefore,

some kind of modelling should be undertaken if subsurface conditions are important to the project aim.

Spatial autocorrelation of soil moisture values was tested in this chapter and the threshold for autocorrelation was 190 m. This is within the scales found in Wester and Blöschl's (1999) survey of studies of autocorrelation, though higher than the more commonly cited and found distances of 30-60 m (Western *et al.*, 2004). However, as mentioned above, this does not represent a realistic scale to apply filtering or other such post-processing techniques for CSK data due to the fine spatial resolution of the imagery. Rather, the intra-cluster variability analysis has shown that there is significant variability in soil moisture at distances below the scale of a pixel.

To summarise, this chapter has highlighted the heterogeneity of soil moisture distributions at this active landslide site and shown that modelling of expected soil moisture at the site did not characterise the measured soil moisture well. It has also shown that surface geometry is an important characteristic to account for, and as such SAR acquisition should be tasked with a geometry that is most favourable for diminishing the impact of shadowing and foreshortening on the slope that is being imaged.

# 5

# CHAPTER 5: ESTABLISHING THE PERFORMANCE OF COSMO-SKYMED PRODUCTS AT ESTIMATING SOIL MOISTURE ON VEGETATED SLOPES

This chapter explores the potential of using single polarised X-band COSMO-SkyMed (CSK) Synthetic Aperture RADAR (SAR) imagery for sensing surface soil moisture in a bare soil / lightly vegetated active slope setting. The investigation focuses on the potential of CSK being used for monitoring soil moisture in a similar-to-real-world scenario with the following parameters: multiple satellites from the constellation are used, and no *a priori* knowledge of the micro-roughness of the site is available. The purpose of this is to investigate how useful a short (~2.5 cm) wavelength product can be in the monitoring of a parameter that is spatially and temporally highly variable (see Chapter 4) when X-band backscatter return is known to be strongly influenced by both surface geometry and soil moisture (Gorrab *et al.*, 2015). The underlying context for this chapter and the questions that it asks is that in a changing climate context, the monitoring of soil moisture is increasingly important, in the context of understanding precursory conditions of major rainfall events affecting large areas and assessing the potential hazard impact that rainfall event might have. In most cases where SAR imagery, such as CSK, might be used for estimating these precursory conditions it is unlikely that *a priori* surface models of a high-enough resolution to account for surface scattering for a wavelength of this length are available, despite the increase in coarser-resolution and longer-wavelength SAR products being deployed in recent years (Attema *et al.*, 2009; Snoeij *et al.*, 2009; Torres *et al.*, 2012; Balenzano *et al.*, 2013).

## 5.1 Objective 3 – Part 1

There have been some accounts in the literature that the CSK satellites do not show close agreement with each other (Pettinato *et al.*, 2013; Baghdadi *et al.*, 2015). This chapter rigorously examines the data product delivered by ASI and interrogates the quality of the inter- and intra- sensor calibration quality.

## 5.2 Sensor Calibration

During the commissioning phase of the CSK constellation, extensive work was undertaken in absolute radiometric calibration of the sensors using corner reflectors and test sites of flat, sparsely vegetated characteristics across Italy (Calabrese *et al.*, 2008; Grimani *et al.*, 2008) using a calibration and validation of image quality module (CALVAL) to rigorously assess the data being acquired by the satellites. The process included using an iterative calibration technique to ensure good calibration and quality of images. Following on from commissioning, the operational phase has been run such that the monthly acquisition schedule accommodates imaging of the same areas used during commissioning to enable continued testing of the image products being delivered (Grimani *et al.*, 2008). The active transponder continues to be used during the operational phase of the project, and the corner reflectors were due to remain in use for the early stages at least of the operational phase (Calabrese *et al.*, 2008), though their current status is unknown.

It has, however, been recognised that there is a need for good inter-calibration of SAR sensors for the measurement of vegetation condition and soil moisture (Pettinato *et al.*, 2013). Previous studies have shown that within the CSK constellation there is significant variation in image brightness from sensor to sensor with Baghdadi *et al.* (2015) finding differences in HH polarisation at an incidence angle of 28.3 of CSK3 being 1.6 dB darker than CSK4, with CSK2 very similar to CSK3 (only one CSK3 image was used in the study), and CSK1 having the lowest returns, around 1.1 dB darker than CSK2.

It has been found that the CSK sensors require further inter-calibration, with consistent differences between sensors being quoted as being in the range of 3-5 dB (Gorrab *et al.*, 2014). This section explores the extent to which this is the case with the data used in this study, using two tests. First, backscatter returns from areas of anticipated year-round homogeneous vegetation – in this case, conifer

plantations - are compared across the sensors. Second, strong scatterers from areas of the scene which, following analysis of optical imagery, are judged to be permanent perfect reflectors, like building corners or similar structures, are compared. Third, the constructive and destructive interference (speckle) on each sensor is examined through analysis of returns from a managed large-scale water body.

### 5.2.1 Invariant scatterer studies

Conifer stands are recognised as being a valuable asset within a multi-temporal set of scenes, as the minimal change in geometry and water content throughout the year means they exhibit very little seasonal change, unlike bare earth or deciduous forestry. Given this, to test the inter-calibration of the four CSK sensors being used in this study, optical imagery from Google Earth was used to locate mature homogeneous conifer stands within the scene (Figure 5.1). The CSK scenes were then subsetted to these areas (Figure 5.2) and the statistics of each image in the conifer areas were calculated in QGIS. The expectation of this test would be that either all the images have very similar statistics, or that, as with the study by Gorrab *et al.*, (2014), each sensor would have good agreement within itself, but be offset from the other sensors.


Figure 5.1 Example of heterogeneous conifer stand used in study using optical imagery from Google Earth (2020).

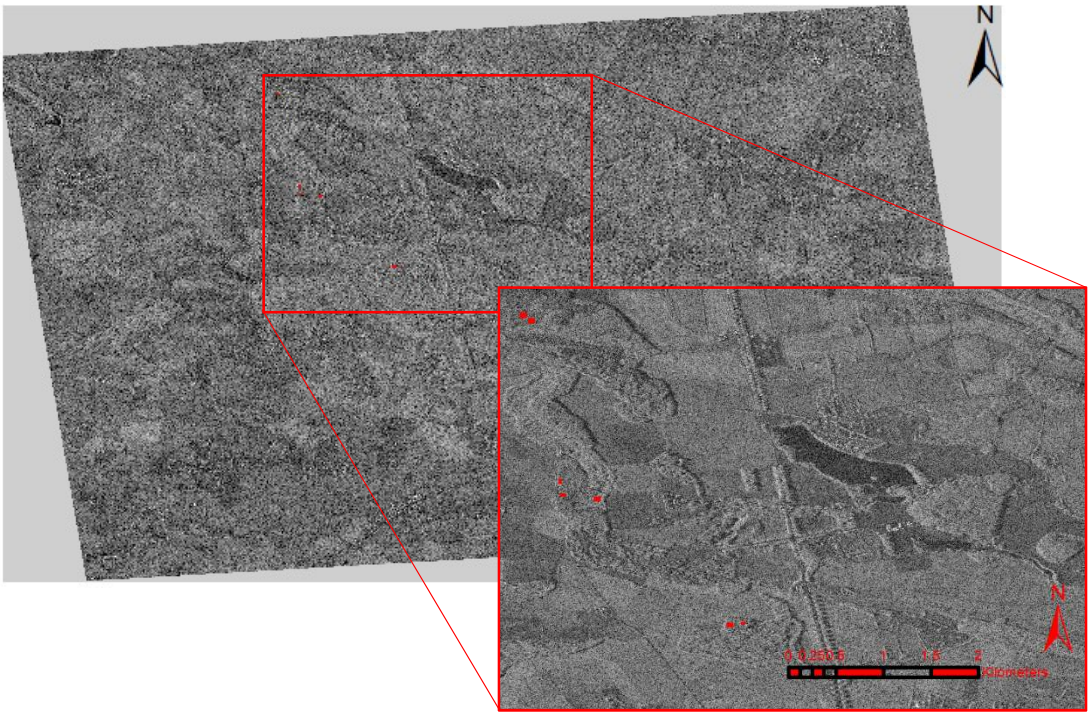


Figure 5.2 Full scene with spatial subset; homogeneous conifer areas used in red

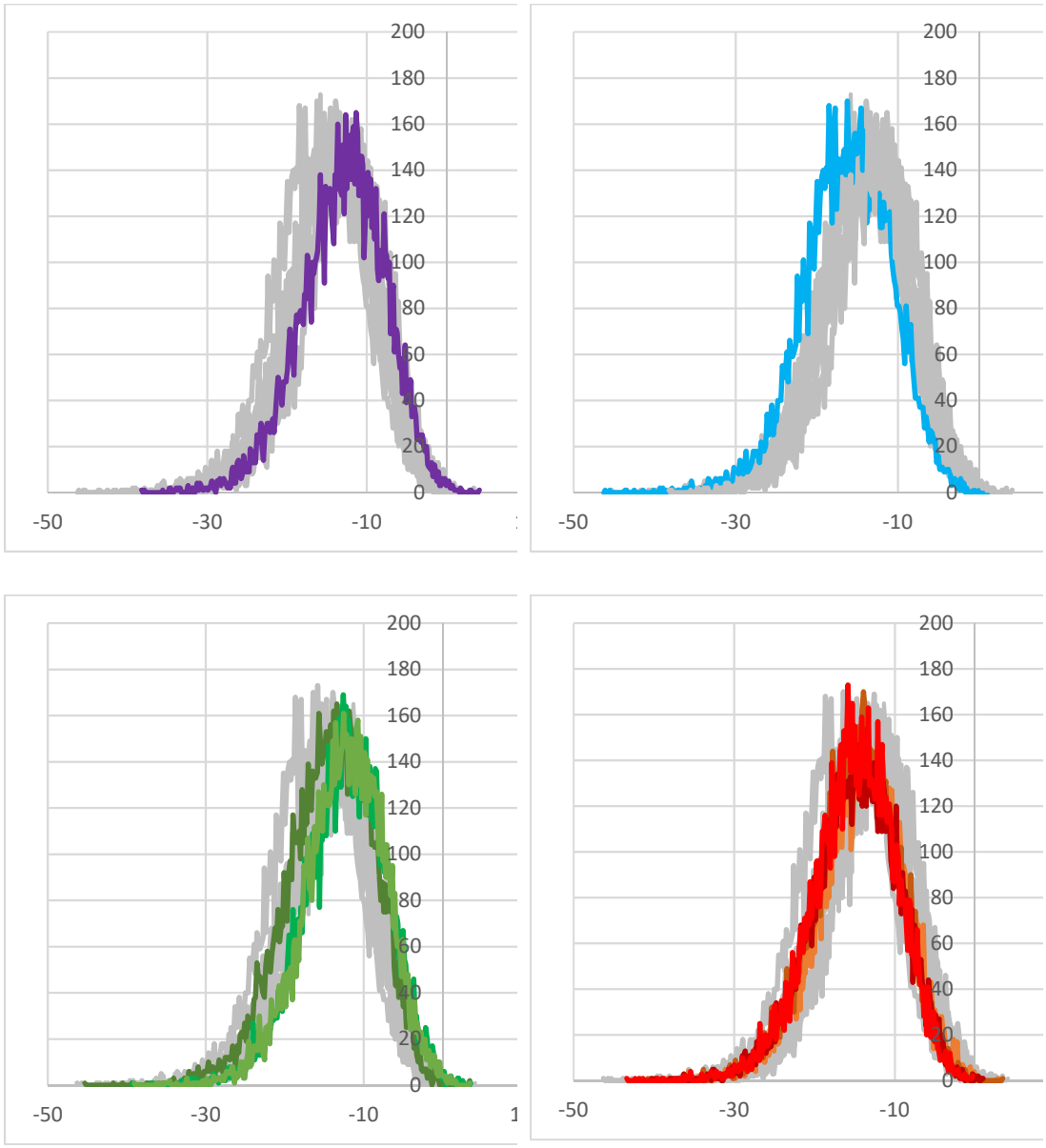


Figure 5.3 Histograms of $\sigma^0$ values of conifer areas, colour-coded by sensor (Purple, Sensor 1; Blue, Sensor 2; Green, Sensor 3; Red, Sensor 4)

Table 5.1 Summary statistics of $\sigma^0$ values of conifer stand areas

| | Max | Mean | Min | Median | Standard Deviation | Sensor |
|---|---|---|---|---|---|---|
| June | 1.225 | -16.491 | -46.196 | -22.579 | 5.453 | 2 |
| July | -0.354 | -15.105 | -43.293 | -21.908 | 5.249 | 4 |
| August | 0.940 | -14.969 | -40.227 | -19.724 | 5.420 | 4 |
| September | 3.318 | -14.332 | -45.228 | -21.051 | 5.520 | 3 |
| October | 3.358 | -14.845 | -40.699 | -18.757 | 5.209 | 4 |
| November | 3.474 | -12.477 | -39.234 | -17.964 | 5.168 | 3 |
| December | 2.766 | -14.259 | -38.707 | -18.052 | 5.443 | 4 |
| January | 3.347 | -12.480 | -38.968 | -17.894 | 5.095 | 3 |
| February | 4.025 | -13.028 | -38.152 | -17.147 | 5.288 | 1 |

The summary statistics (Figure 5.3, Table 5.1) from this test show that there is intra- as well as inter-sensor variability. The median values for Sensor 4 (red) range from -21.908 (July) to -18.052 (December). Likewise, the medians for Sensor 3 (green) range from -21.051 (September) to -17.894 (January). Although there is a trend in increasing median values through the time series, this is still a concern to note, and one which is replicated in strong scatterer assessment below. Just as intra-sensor variation is apparent, so, inter-sensor variability is too. While caution should be observed given Sensors 1 and 2 provide only one image for this study, it is notable that the average median value for the four sensors ranges from -22.579 dB (Sensor2) to -17.147 dB (Sensor 1), with a difference of 0.641 dB between Sensors 3 and 4 (Table 5.1). The similarity of the averaged medians of Sensors 3 and 4 suggests that the co-calibration of the satellites is not necessarily a significant concern and can, if deemed necessary, be accounted for by applying a simple, linear, calibration adjustment. Of more significant concern is the variability in the intra-sensor values.

In Table 5.1 it is notable that January and November (both Sensor 3) are significantly lower than their antecedent months - December and October (Sensor 4). Considering each sensor in turn, Sensor 2 has the highest backscatter return of the three sensors, Sensor 4 (July, August, October, December) has consistent median returns, and Sensor 3 (September, November, January) has lower returns than the other sensors and a marked difference between September and the other two images.

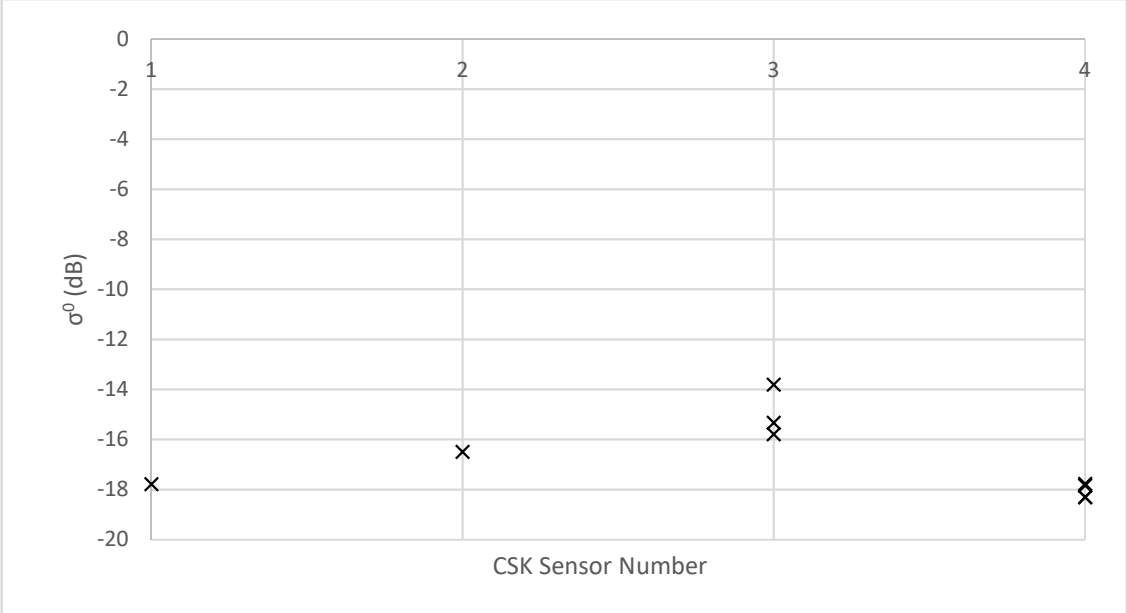


Figure 5.4 Median $\sigma^0$ values for each image, by sensor

Whereas the September image (Sensor 3) was anomalously positively offset relative to the other curves, in this case it sits in the midst of the curves. Conversely, July is notable for a higher peak and narrower body than the other images. Although there is greater agreement between the images, there is still the suggestion of an offset between the sensors. This is not, however, consistent. January and November (Sensor 3) are very similar, but distinct from September (Figure 5.4). Likewise, October, August and December have similar profiles, yet July's is different. It is not, therefore possible simply to adjust the brightness values of one sensor to align it with other Sensors' outputs and thereby undertake relative soil moisture estimation.

### 5.2.2 Strong scatterers

A further test of sensor co-calibration was undertaken, using a different type of artefact in the imaged scenes. To be able to calibrate reflectance values for the SAR images it is necessary to have points of known reflectance value in the image (Gray *et al.*, 1990). Conventionally, these points are provided through the placement of trihedral corner reflectors. Trihedral corner reflectors are formed of three conducting plates intersecting at right angles, the reflectance of which, if its relative alignment to the satellite overpass is known, can be calculated (Ulaby, Moore and Fung, 1982) and thereby used as a known value within the image from which other values in that image can be inter-calibrated. The orthogonal structure of the trihedral corner reflector ensures that the reflected waves exit in

the same direction as the original incident waves entered (Shaeffer *et al.*, 2004), meaning that it functions as a strong scatterer and appears very bright in the image (Sabins, 1996).

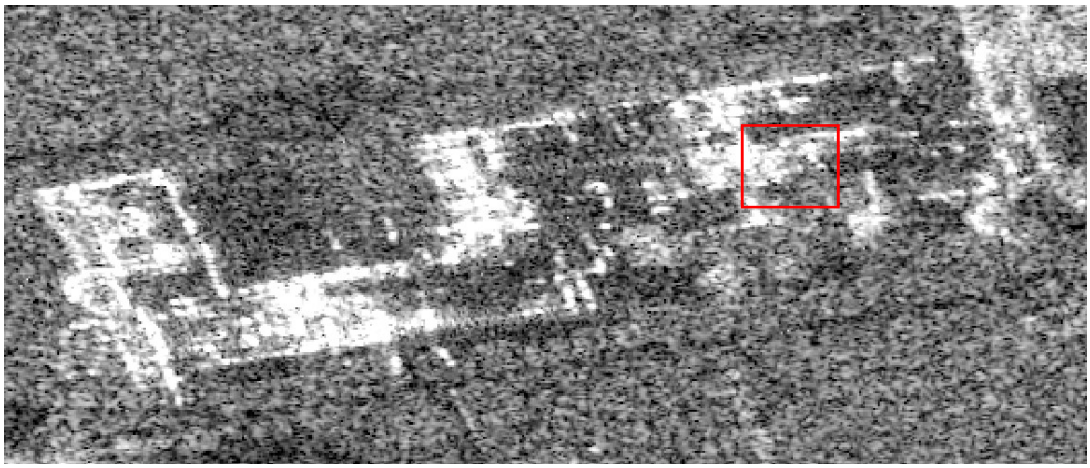

Figure 5.5 Example strong scatterer on roof of Castle Howard complex. Note the brighter pixels extending orthogonal to the pixel


Figure 5.6 Optical image of Castle Howard complex. Area of presumed double bounce effect highlighted.

Although it was not possible to implement the placement of corner reflectors during the field campaign, several candidate structures within the scene provide radar returns similar to those of corner reflectors. These structures are found in the scenes as pixels with very high backscatter values, and with pixels orthogonal to them much brighter through constructive interference. Seven strong scatterers

were chosen from within the whole scene to assess the variability in radar returns. Locations were chosen that from optical imagery appeared to be permanent, fixed, features like buildings (Figure 5.5 and Figure 5.6), and where backscatter brightness extended orthogonal to the central pixel. A buffer with radius of 5 pixels was created around the supposed source pixel, and the highest return value from within that buffer zone was recorded in Figure 5.7. This method was undertaken to ensure that, given the presence of multiple high-value pixels in the proximity of the supposed strong scatterer, the source pixel was not missed. The backscatter values for these supposed strong scatterers are presented in Figure 5.7, and colour-coded by sensor number – Purple for Sensor 1, Blue for Sensor 2, Red for Sensor 3, and Green for Sensor 4. The plot shows that there is variability location-to-location, but also, more importantly, there is variation within each location. Of particular note for this are locations 4 and 5. Locations 2,3,6 and 7 are the only points that have somewhat consistent readings.

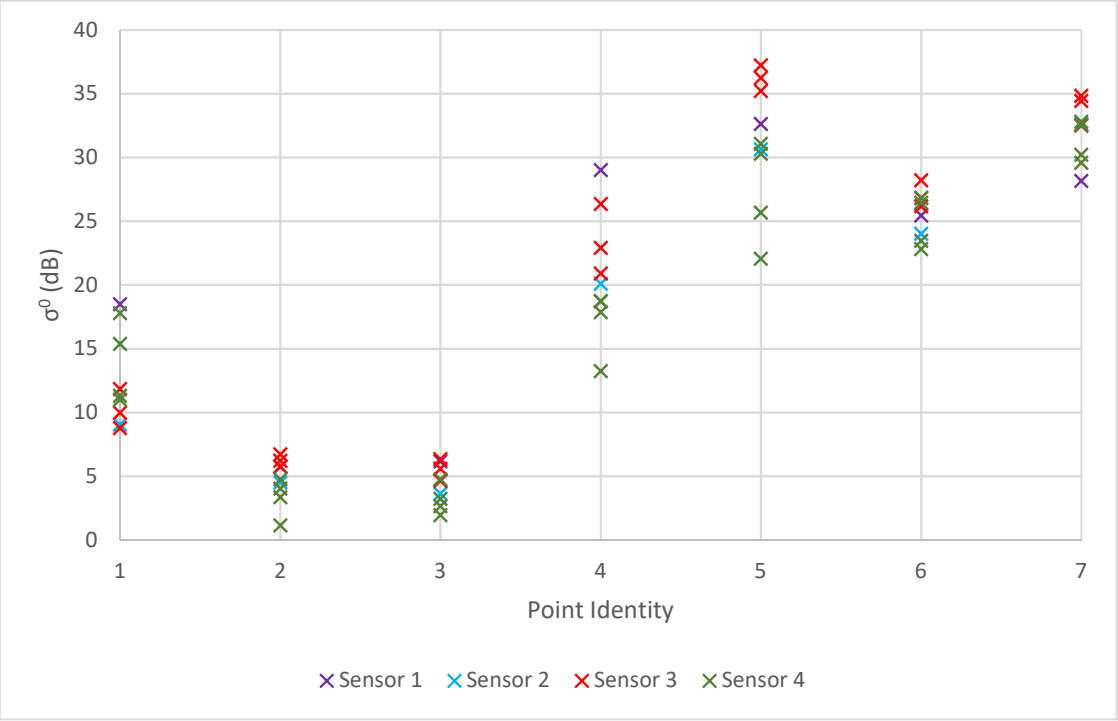


Figure 5.7 Backscatter values at presumed strong scatterer locations, colour-coded by sensor

Figure 5.7 shows that all points have high values, and that some, namely points 6 and 7 show tight bunching across sensors. Also apparent is that Sensor 3 (red) tends to have amongst the highest returns for each point (3,5,6,7), although it has

some of the lowest values for point 1. Conversely, sensor 4 generally has the lowest returns at most points.

Although values at locations 6 and 7 are tightly grouped, and therefore can be assessed with the greatest confidence as being true strong scatterers, and worthy of most attention, the other points have a much wider spread of values. There are two possible reasons for this being the case. First, that the scatterers are inconsistent throughout the year, which is unlikely given the careful choice of the targets using both optical and radar imagery. Second, and perhaps more likely, is that this is an artefact of satellite viewing angle being variable, despite the grant design specifying a repeated look angle.

It is significant that for the same scatterer and the same sensor there is such large variation in backscatter returns. Even if points 1-5 were to be discounted as poorly chosen targets, the variation between sensors at points 6 and 7, which seem to perform much better as strong scatterers, is still sufficient that consideration needs to be given to the quality of the inter-calibration of the constellation. If each sensor had performed reliably relative to the other sensors across all scatterers, it would, again, be possible to confidently make a linear offset to inter-calibrate the sensors, but the fact that sensors 3 and 4, in particular, demonstrate variable returns relative to the other sensors, this does not appear to be an option.

### 5.2.3 Speckle assessment

Another useful form of assessment for calibration is that of speckle. Speckle is caused by irregular constructive and destructive interference caused by scatterers in adjacent pixels. Speckle was assessed by examining the backscatter statistics for an area of managed waterbody, presumed to be a reservoir, in the scene (Figure 5.8). The image was calibrated and terrain corrected with 3 arcsec SRTM imagery. Water bodies are expected to have consistently low returns due to specular reflection (Sabins, 1996). Assessing water bodies is a useful tool for assessing the inter-calibration of sensors, as the returns should be very similar. Any deviation in the amount of speckle between the sensors is necessary to be accounted for.

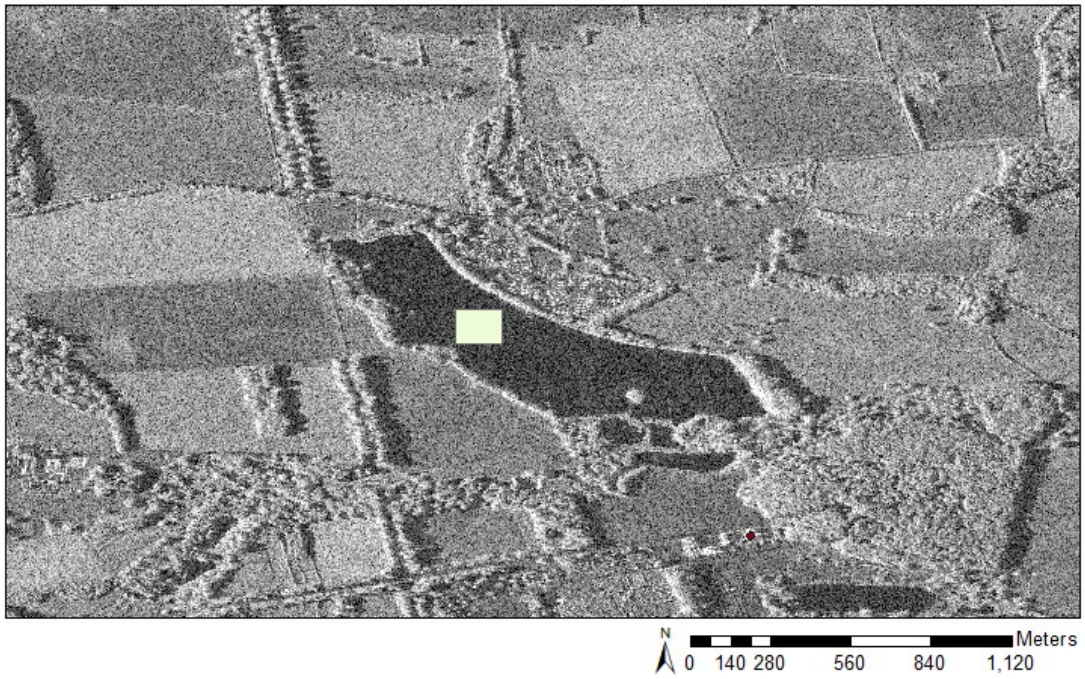


Figure 5.8 Subset of example CSK image. The yellow box represents the area of the lake used for speckle assessment

Figure 5.9 and Table 5.2 show that although there is good agreement between most of the images, the images for November and January (Sensor 3) have a markedly different distribution of backscatter values to the other months and, most importantly, to the other image from Sensor 3. The means of November and January (-18.199, -18.938) are significantly lower than those of the other months, which range from -23.482 (February) to -25.129 (July). Interpretation of this different backscatter signature is difficult. The two images were visually inspected to ensure there were no anomalies from processing like striping of the image, and they were found to be clear from any anomalies. Freezing of the water, or other issues that might accompany winter, can also be ruled out due to the known ambient temperature preceding and during the acquisition. There is the potential that seasonal changes associated with changes of inflow and outflow might be affecting the water quality, but given that the water body is artificial and managed, and the variability exists in later studies as well, it is possible to be confident that this is not an artefact of water conditions; the Castle Howard estate management team, who maintain the lake, were contacted to find out whether there were any significant inflow-outflow events associated with the period around the image acquisitions, but were not able to access this information. Wind strength and direction were checked using the COSMOS data

from Hollin Hill, and found to be similar for the November and January images (4.99 m/s, 180.32°; 2.63 m/s, 165.45°) as the other Sensor 3 image (1.134 m/s, 169.325°).

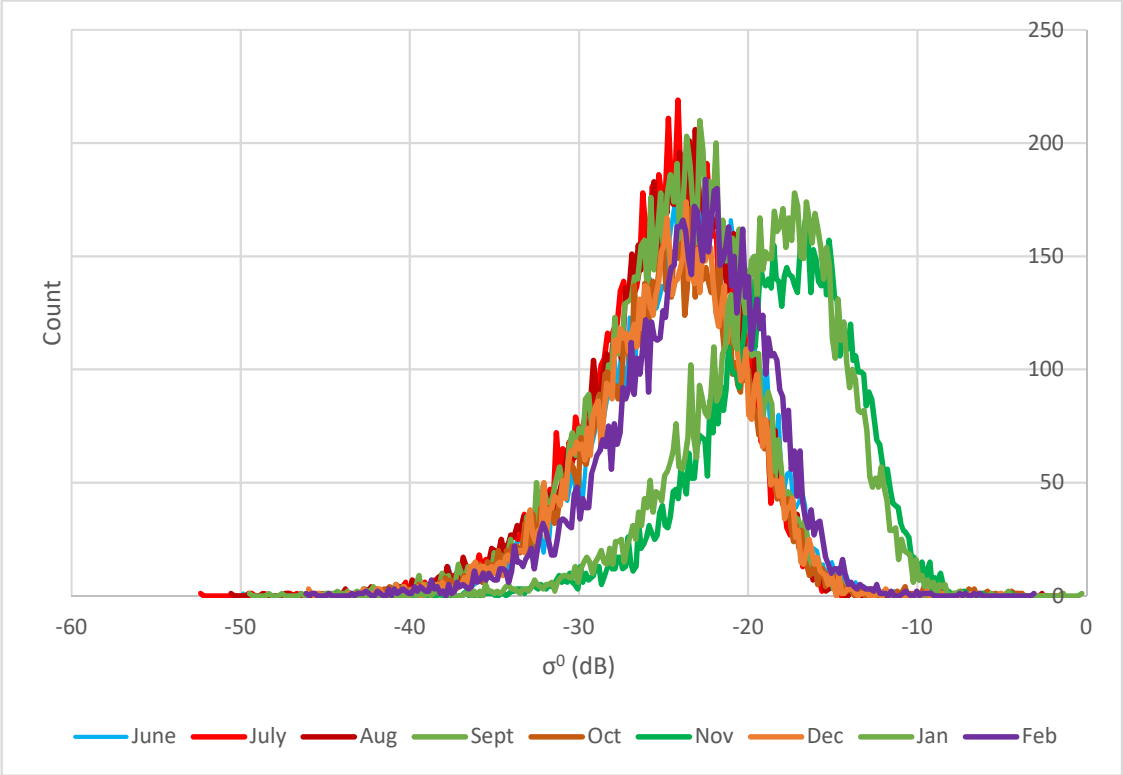


Figure 5.9 Frequency distributions of backscatter from lake, colour-coded by sensor

The distributions in Figure 5.9 are not as expected, both because of the different distributions in the November and January data, but also because of the length of the tails in the data sets and the lack of normality in the distributions. It is likely that the shortness of the wavelength and the smallness of the pixels causes the length of tails as the impacts of destructive and constructive interference are made more apparent with these parameters. The position of the curves is also of some surprise, with the median values of these frequency distributions being not much lower than the medians of the field site, as shown in Figure 5.4.

Table 5.2 summary statistics of lake area

| | Maximum | Mean | Minimum | Median | Standard Deviation |
|---|---|---|---|---|---|
| June | -5.127 | -24.196 | -49.759 | -27.53 | 4.486 |
| July | -4.174 | -25.129 | -52.271 | -28.506 | 4.416 |
| August | -2.721 | -25.002 | -50.477 | -26.881 | 4.491 |
| September | -0.376 | -24.69 | -49.395 | -24.981 | 4.554 |
| October | -1.528 | -24.75 | -41.435 | -21.717 | 4.585 |
| November | -4.895 | -18.199 | -44.241 | -24.443 | 4.365 |
| December | -4.843 | -24.845 | -45.911 | -25.457 | 4.499 |
| January | -1.457 | -18.938 | -44.833 | -23.23 | 4.48 |
| February | -3.197 | -23.482 | -46.057 | -24.711 | 4.478 |

The relationship seen in Figure 5.9 was unexpected in terms of the offset of the November and January images so the metadata of all the images was rechecked and all images were reprocessed to ensure it wasn't an artefact from unintentional inconsistencies in the processing. Indeed, given the dynamic range of the backscatter in these images is roughly 50 dB, an offset of roughly 5dB is statistically significant and needs to be acknowledged.

### 5.2.4 Summary of Objective 3 – Part 1

The first part of meeting Objective 3 has explored the inter-calibration of the four sensors on the COSMO-SkyMed constellation and whether further calibration was required during processing as other papers using images from a smaller subset of the four sensors have found (Gorrab *et al.*, 2014).

The three studies have each shown that where a well-calibrated constellation would have minimal inter- and intra-sensor variability in studies of this type, there is marked inter-sensor variability across the constellation, as well as intra-sensor variability for Sensor 3 in particular. The conifer-stand assessment showed variability in the intra-sensor values, which are found particularly in Sensor 3, and the November and January images, in all three of the tests undertaken in this section. The marked difference in the November and January backscatter returns for the open water body in the speckle assessment present concerns given that external environmental factors have been ruled out as the cause. If such a deviation from the rest of the images was specific to all the images from one sensor then a calibration correction could be applied to all the images from that sensor. But the fact that it is only two images from the sensor that are

affected is cause for concern regarding the consistency of the sensor. These concerns are replicated in the strong scatterer assessment, though less conclusively. Few studies that have explicitly explored the calibration of the sensors have used multiple CSK3 images, and the variation in backscatter found in those was minimal, with Pettinato *et al.* (2013) finding a slight difference (0.59 dB) in the mean between their two CSK3 images, although the incidence angle between the two images was different by four degrees, which automatically means there would be a difference between the two.

## 5.3 Chapter Summary

This chapter has explored two key questions regarding the use of CSK data in a real-world scenario. First, how well calibrated is the constellation, and are there any concerns about this calibration?

The findings from the first question - using the speckle and conifer studies - are fairly conclusive – that the inter-sensor calibration is not as simple as applying a linear offset as some studies (Baghdadi *et al.*, 2015; Gorrab *et al.*, 2015) undertaken early in the operational phase of the constellation have indicated. This chapter is certainly not the first study to examine the inter-correlation of X-band SAR sensors. Some of the earliest papers following the launch of the CSK platform examined this (Paloscia *et al.*, 2012; Pettinato *et al.*, 2013; Baghdadi *et al.*, 2015; Gorrab *et al.*, 2015), often with respect to TerraSAR-X – the other X-band platform operational at the time. However, it is unique in the distribution of images across the four satellites. Baghdadi *et al.*'s (2015) study which has been cited widely in the community (Gorrab *et al.*, 2015) only made use of one CSK3 image, which is the sensor which has been found in this study to have the most variability. Baghdadi *et al.*'s 2015 research into using multiple X-band SAR sensors (TerraSARX, CSK1, CSK2, CSK3, CSK4) with forestry stands as targets and using five CSK1 images (four descending, one ascending), four CSK2 images (all descending) one CSK3 image (descending), and five CSK4 images (all descending), all with an incidence angle of 28.3° and acquired between June and October 2013 found that each sensor was stable, with variation of less than 1dB, but that there was variation between the sensors both across the two platforms, and across the CSK platform itself, with variation across the constellation of between 1.5dB and 2.7dB. Rather, the intra-sensor variability, seen particularly in sensor 3, which Baghdadi *et al.* were not able to comment upon because of their

access to a single image (2015), makes estimation of appropriate inter-calibration methods challenging.

## 5.4 Conclusions

COSMO-SkyMed has been shown by many studies to be a useful and exciting tool for use in environmental remote sensing projects in multiple different problem settings (see review at the start of the chapter), with its high resolution data and short return periods, the constellation has overcome the traditional remote-sensing trade-off between resolution and return period. However, attention needs to be paid by researchers, in particular by those using multi-temporal and multi-sensor datasets in the context of increasing use of constellations, to ensure that they understand the quality of calibration between their images, particularly if they have very few images from one sensor.

This study has been novel in the delivery of the data across all four satellites in the constellation. The data ordering process did not make reference to whether there was a requirement or desire for the images to be collected using just one or any of the satellites. It could be inferred from this that ASI assumed an inter-calibration quality that rendered whether the data came from the same sensor or not immaterial. This study has, however, shown that it is material, and also that for confident inter-sensor calibration to be undertaken, a better understanding of the intra-sensor variability is attained.

Looking forwards, as constellations of remote sensing satellites become more prevalent, as a means of reducing revisit times while providing increasingly high resolution data products, attention needs to be given during the testing and build processes by manufacturers to ensure either good inter-calibration of sensors before launch, or undertaken during the processing prior to delivery of products to the end user, or a well-publicised and thoroughly tested set of calibration methods for end users. It is worth noting that the second generation of COSMO-SkyMed satellites (CSG) has been commissioned and the first satellite launched, but that only two satellites have been commissioned for this supplementary constellation. The rationale is not known, but it is possible that it could be in recognition of the challenge of inter-calibrating a large constellation.

# 6

# CHAPTER 6: THE VIABILITY OF USING SAR TO MONITOR SOIL MOISTURE

Multiple studies have shown that there is potential for SAR to be used for monitoring soil moisture (Shi *et al.*, 1991; Pettinato *et al.*, 2013; Santi *et al.*, 2013). However, the parameters within which this is possible and useful are limited. This project has already shown that there are challenges associated with the use of CSK data. This chapter explores the relationships found between backscatter and surface and subsurface *in situ* soil moisture measurements in the second part of Objective 3. It then goes on to explore the viability of SAR SM estimation through a discussion of the results from this analysis and those from other published studies. The chapter concludes with a diagrammatic schema for assessment of viability of SAR usage for soil moisture estimation.

## 6.1 Context for this part of the project

When using RS in the context of pre-event monitoring, the amount and quality of surface geometry data available often leaves much to be desired. This question explores whether, when so much of the backscatter response is due to micro-roughnesses of the surface, much advantage is achieved in using higher-resolution DTMs compared to more easily accessible lower-resolution DTMs. To this end, the correlation between *in situ* VWC measurements and the backscatter coefficient ($\sigma^0$) values of images terrain corrected with 25 cm, 50 cm, 1 m, 2 m DTMs and 90m SRTM are compared.

Noise is recognised as significantly hindering the utilisation of SAR imagery for soil moisture estimation. A common technique for minimising the impact of speckle, is applying one of several filtering techniques at different scales. Low pass filtering has long been seen as an appropriate approach for minimising the impact of surface roughness anomalies and constructive interference between pixels to improve agreement between backscatter and VWC. There is an exploration of what, if any,

improvement different scales of kernel averaging have on VWC-dB correlation at this site, and what the findings from this analysis means in the context of the findings relating to spatial variability of soil moisture as shown in the previous chapter.

## 6.2 Relationships between backscatter and surface and subsurface soil moisture measurements

This opening section presents the relationships between the CSK backscatter values and the surface and subsurface *in situ* soil moisture data that was described in chapter 5.

### 6.2.1 Correlation between *in situ* surface soil moisture measurements and unfiltered backscatter values

Surface roughness and topography are well attested (Ulaby *et al.* 1982; Sabins, 1996) as having high degrees of importance in the amount of backscatter return. Indeed, studies using X-band data have noted that backscatter returns are particularly affected by these and soil moisture (El Hajj *et al.*, 2015; Gorrab *et al.* 2015) due to the short wavelength of X-band and therefore the increased roughness of surfaces relative to longer wavelengths. Increased relative roughness causes increased volumetric scattering. On account of this, Baghdadi and many other SAR users argue for the use of high resolution digital elevation model (DEM) use in the processing of SAR data (Baghdadi *et al.* 2002). It had been anticipated that the effective roughness of the site could be derived interferometrically from consecutive images. Preliminary work on this in conjunction with Andy Sowter at Geomatic Ventures, Nottingham using this CSK dataset, however, found that due to the length of time between images that this was not possible as the incoherence of phase was too great. This subsection of the objective explores whether the scale of open source DTMs generally available in the UK are viable sources for Terrain Correction for SAR data with this resolution and in this type of terrain. The resolutions tested approximate to 10x, 20x, 40x, 80x and 3600x the length of the incident wavelength of COSMO-SkyMed's X-band product, which has a spatial resolution of approximately 1 m.

#### 6.2.1.1 Results

This study showed that there is poor correlation between backscatter value and *in situ* VWC values at all DTM scales. It is expected that the higher the VWC, the greater the attenuation of the incident energy, thereby resulting in a negative correlation between VWC and backscatter. Contrary to this expectation, very weak

positive correlations are found at all resolutions (Table 6.1). The Pearson's *r* value increases with DTM scale from 0.011 for the 0.25 m DTM to 0.028 for the 2 m DTM, with the value decreasing to 0.016 for the SRTM image. The *r* value is marginally greater for the coarsest resolution compared to the three finest resolutions. Ultimately, these r values are so low, that the variability is due to noise rather than being indicative of anything further.

Table 6.1 Correlation Matrix of VWC and terrain corrected images

| | | VWC | 025DTM | 050DTM | 1DTM | 2DTM | SRTM |
|---|---|---|---|---|---|---|---|
| VWC | Pearson's r | — | | | | | |
| | p-value | — | | | | | |
| 0.25m DTM | Pearson's r | 0.011 | — | | | | |
| | p-value | 0.731 | — | | | | |
| 0.50m DTM | Pearson's r | 0.013 | 0.995 *** | — | | | |
| | p-value | 0.673 | < .001 | — | | | |
| 1m DTM | Pearson's r | 0.014 | 0.981 *** | 0.989 *** | — | | |
| | p-value | 0.667 | < .001 | < .001 | — | | |
| 2m DTM | Pearson's r | 0.028 | 0.797 *** | 0.793 *** | 0.783 *** | — | |
| | p-value | 0.378 | < .001 | < .001 | < .001 | — | |
| SRTM | Pearson's r | 0.016 | 0.619 *** | 0.614 *** | 0.619 *** | 0.587 *** | — |
| | p-value | 0.602 | < .001 | < .001 | < .001 | < .001 | — |

Note. * p < .05, ** p < .01, *** p < .001

Table 6.1 shows that an analysis of the correlation between *in situ* measurements of VWC and backscatter is weak at all the DTM resolutions used in this study, with none of the correlations being significant. However, given the very small variability between the best and worst performing DTMs, it can be taken that any scale of DTM, when an order of magnitude greater than the incident wavelength, performs as well as any other even when the site is geometrically complex.

The distribution of data was assessed through box and violin plots (Figure 6.2). These showed that the distribution of values changes between the different terrain correction resolutions, with the 0.25 m, 0.50 m and 1 m resolutions having similar distributions, the 2 m DTM dataset having more values grouped around the mean than the other datasets, and the SRTM-corrected values being less distributed around the mean.

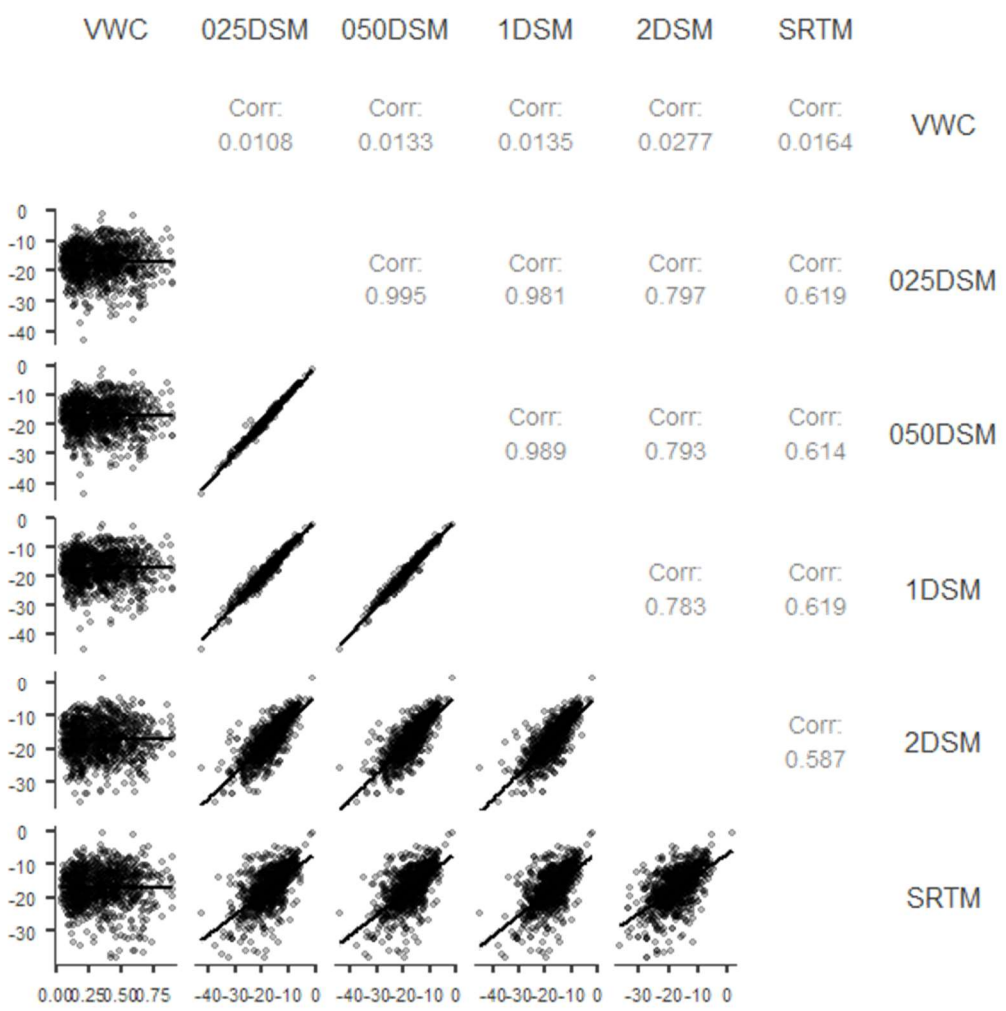


Figure 6.1 Correlation matrix for pixel values and surface soil moisture measurements from all months at all terrain corrections

The correlation matrices in Figure 6.1 show that although the *r* values for the resolutions are similar when the data from all months are looked at as a whole, it is clear that for each month there are clear differences in values from resolution to resolution. That is, the correlation between the resolutions themselves, rather than their correlation with VWC, shows that as the difference in scale increases, the correlation reduces. It is also worth noting that November and January – the months with anomalous backscatter responses in these studies do not display markedly different correlations to the other months.

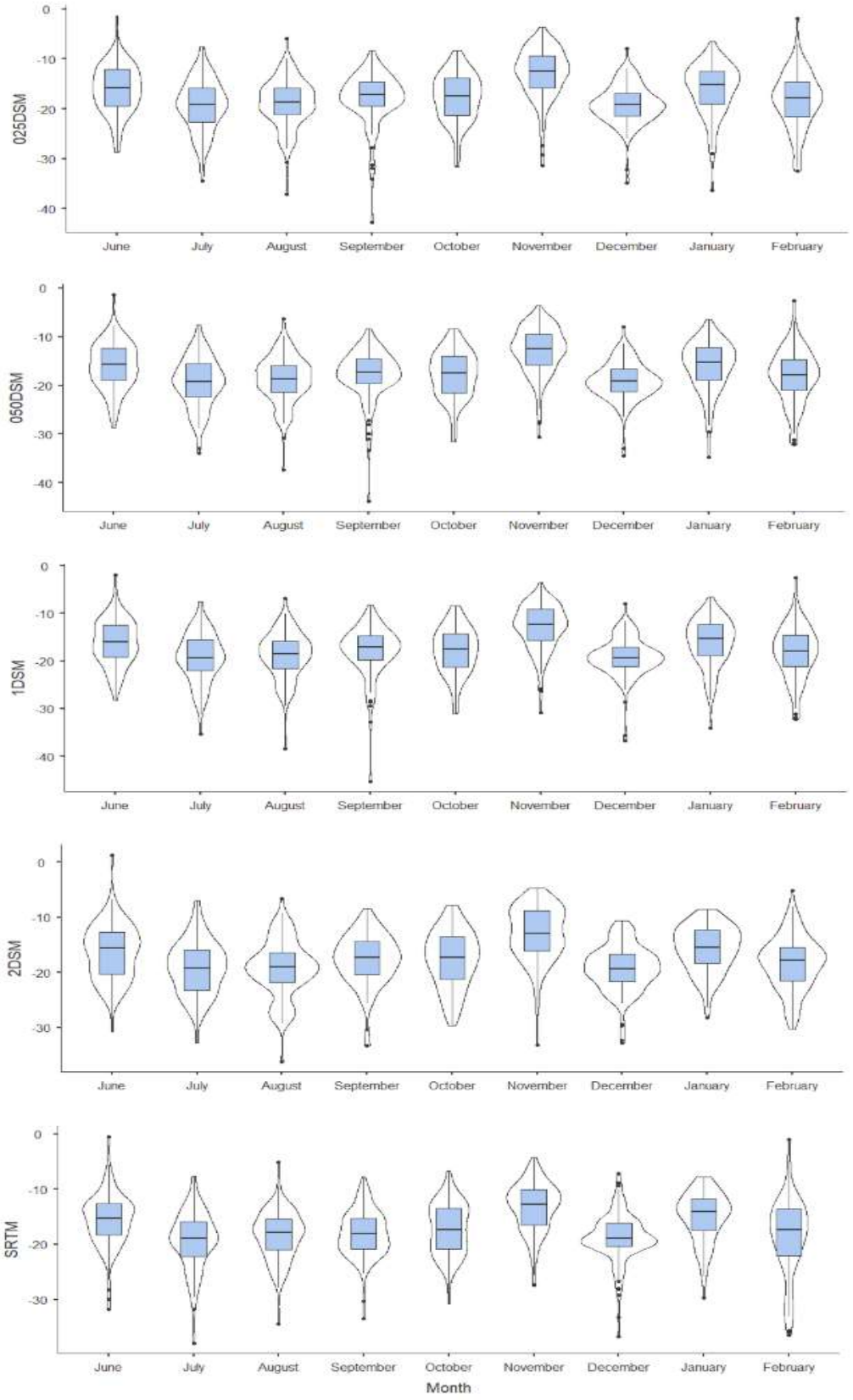


Figure 6.2 Box and violin plots of data distribution at five different terrain correction scales

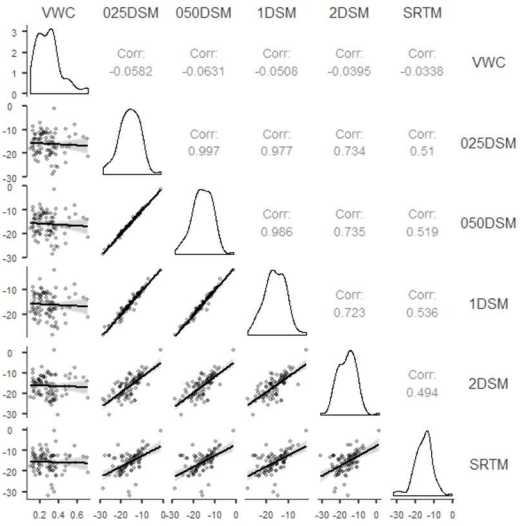


June

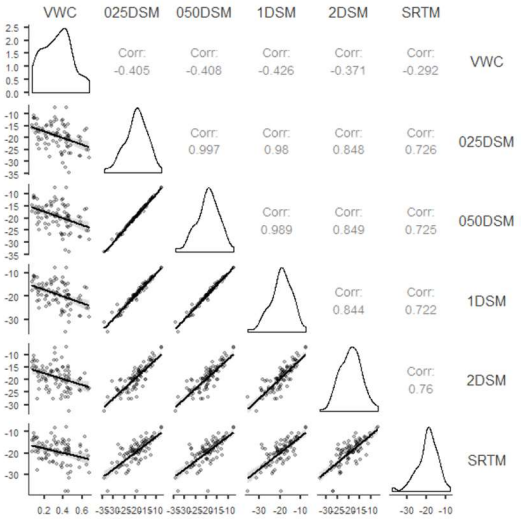


July

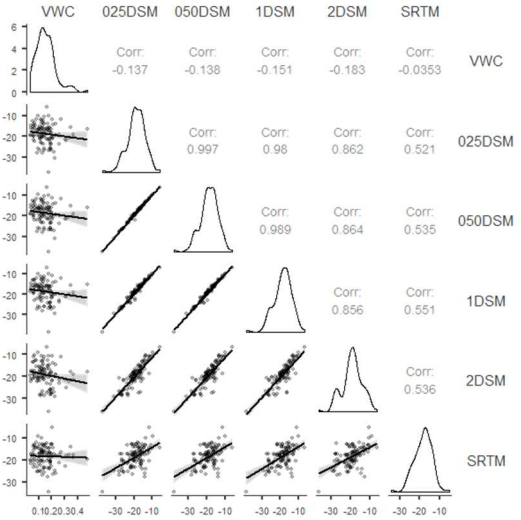


August

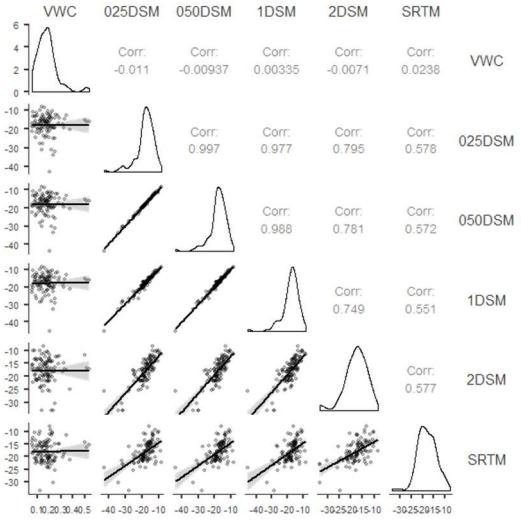


September

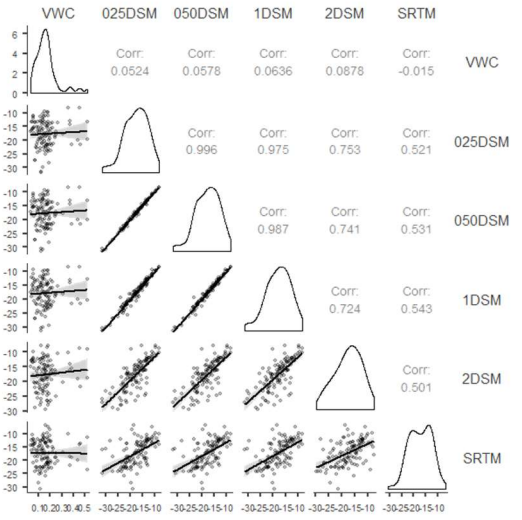


October

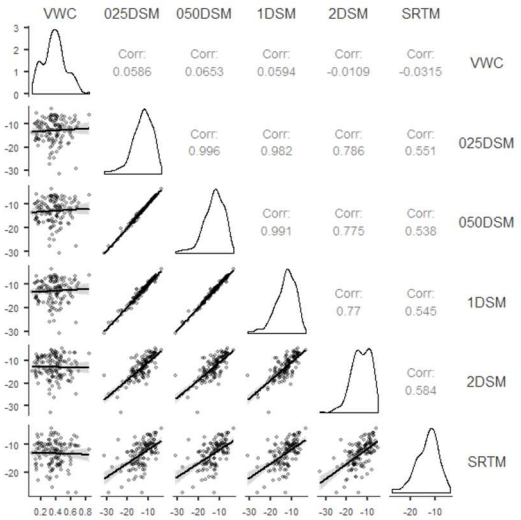


November

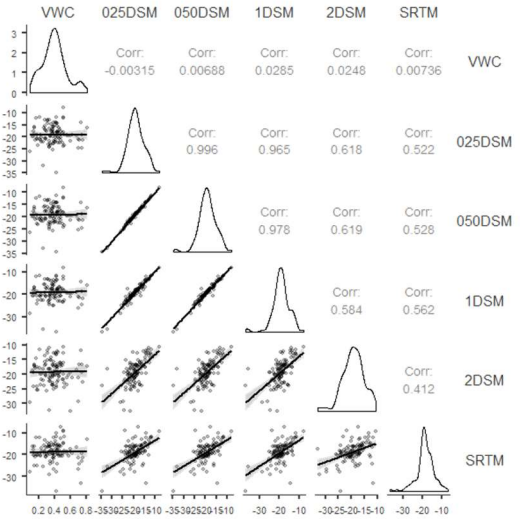


December

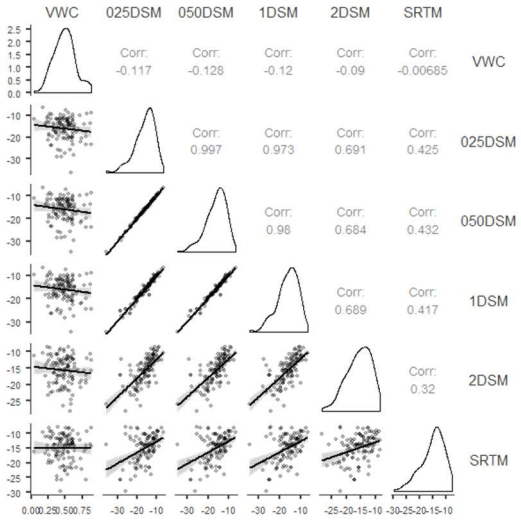


January

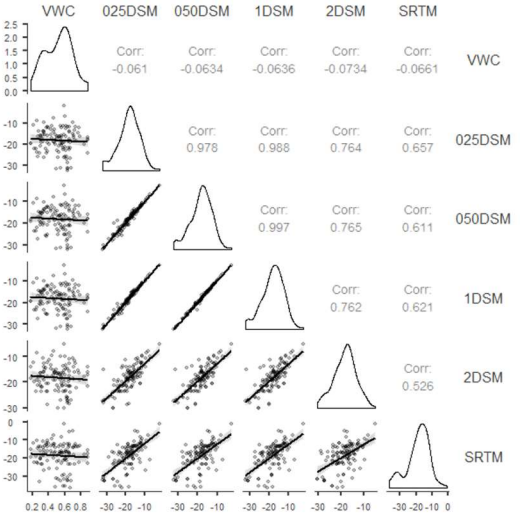


February

Figure 6.3 correlation matrices of VWC with 5 terrain correction scales by month

#### 6.2.1.2 Summary of the relationship between *in situ* soil moisture values and unfiltered backscatter values

This section has shown that for terrain correction using open source, accessible terrain models, there is marginal benefit in reducing the coarseness of the imagery, if the imagery you have access to is more than an order of magnitude greater than the incident wavelength. It is recommended, if possible, to utilise terrain models at a resolution as close to the length of the incident wave as possible, to ensure that roughness and surface geometry is well accounted for. There is significant noise in the data, making relating surface soil moisture and backscatter challenging. Nevertheless, the results for some images in this study show similar relationships to those described by Balenzano *et al.* (2011) who found a 5-6% retrieval accuracy over vegetated soil.

### 6.2.2 Optimising backscatter-soil moisture relationships through applying different filtering types and parameters

Filtering has long been seen as an appropriate approach for minimising the impact of surface roughness anomalies and constructive and destructive interference between pixels to improve agreement between backscatter and VWC (Lee, 1980; Frost *et al.*, 1982; Lopes *et al.* 1990). This section explores the impact of different scales of filtering, using both non-adaptive and adaptive filters, for processing CSK data and establishing the relationship between $\sigma^0$ pixel values and *in situ* VWC values. There is also a discussion, in light of the findings in the previous chapter regarding soil moisture spatial variability, about appropriate limits on the size of kernels used in these techniques.

#### 6.2.2.1 Non-adaptive filtering

Non-adaptive mean spatial domain filtering was undertaken to assess the extent to which this technique improved the correlation between *in situ* soil moisture and $\sigma^0$. The CSK imagery used was calibrated and terrain-corrected with the 2m DTM. A mean approach was chosen because although it can cause a loss of image feature integrity – like the loss of linear features – it preserves the radiometric integrity of the image better than a median filtering approach. Kernel sizes of 3, 5 and 7 pixels were used and compared with the relationship between the non-filtered pixel and ground truthed data – referred to in Figure 6.4 as "Window_1".

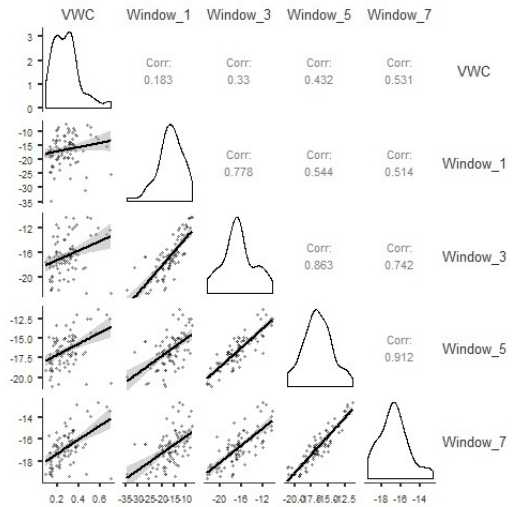


June

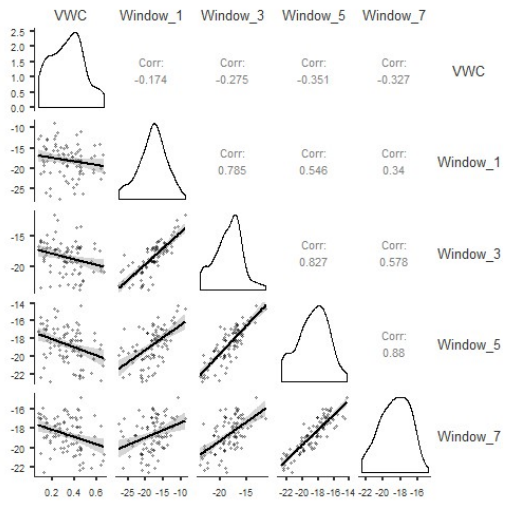


July

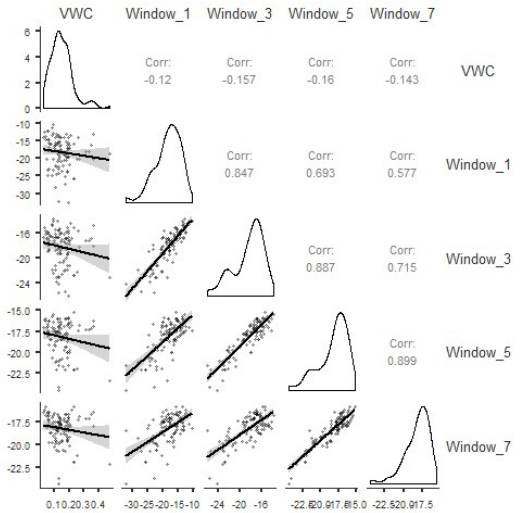


August

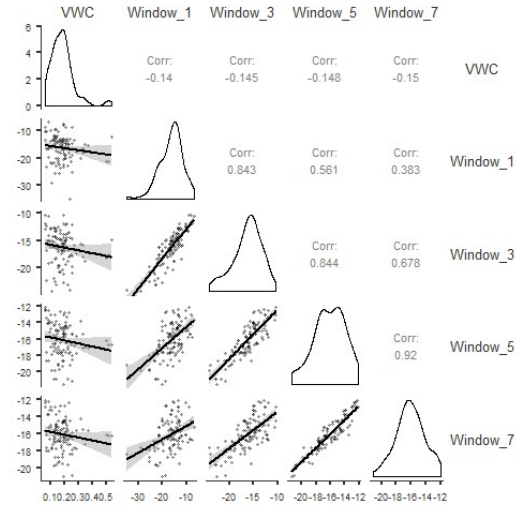


September

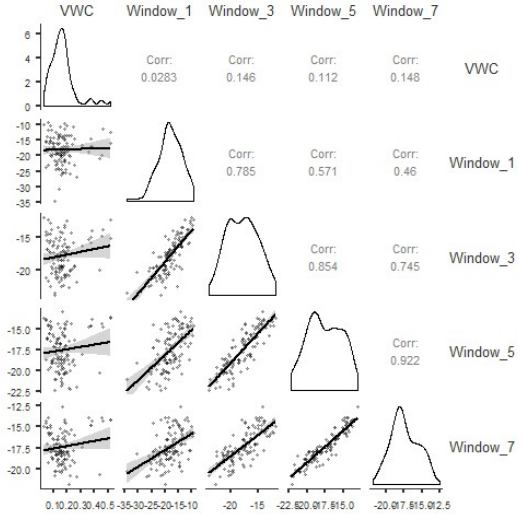


October

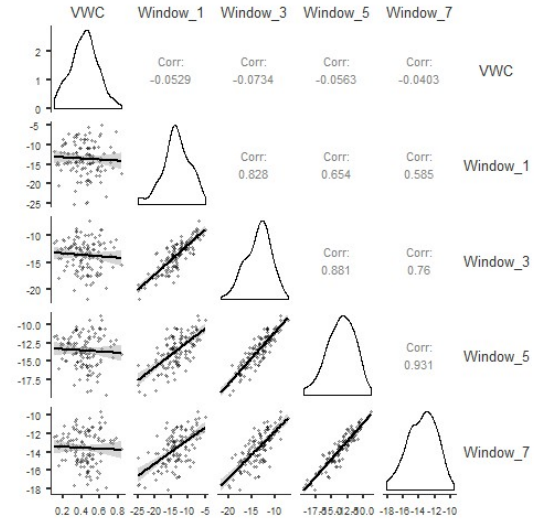


November

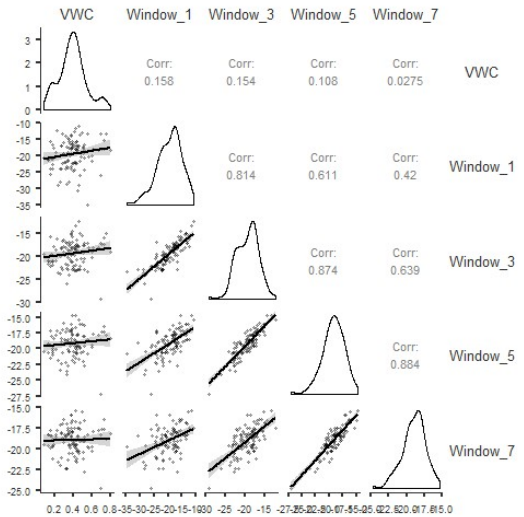


December

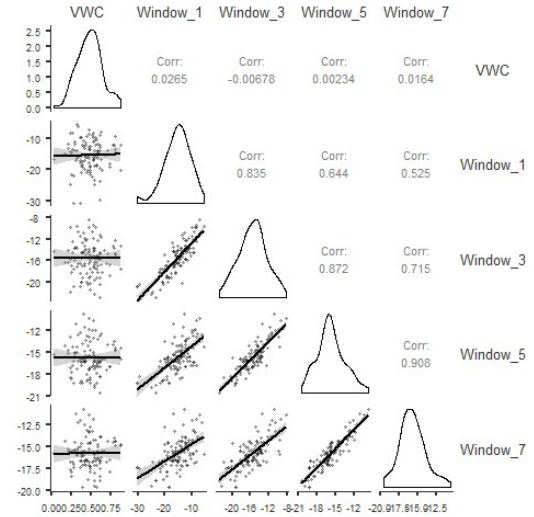


January

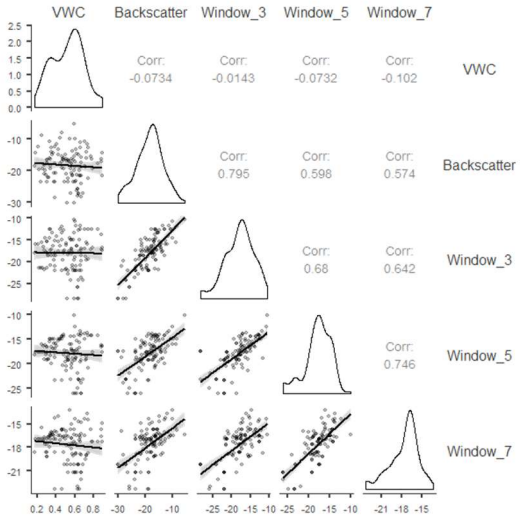


February

Figure 6.4 Backscatter-VWC relationships for each image (June-February) at kernel sizes of 1,3,5,7 pixels.

Table 6.2 Backscatter-VWC correlations at 4 different kernel sizes

| **Kernel Size** | **Point** | **3** | **5** | **7** |
|---|---|---|---|---|
| **June** | 0.183 | 0.33 | 0.432 | 0.531 |
| **July** | -0.174 | -0.275 | -0.351 | -0.327 |
| **August** | -0.12 | -0.157 | -0.16 | -0.143 |
| **September** | -0.14 | -0.145 | -0.148 | -0.15 |
| **October** | 0.0283 | 0.146 | 0.112 | 0.148 |
| **November** | -0.0529 | -0.0734 | -0.0563 | -0.0403 |
| **December** | 0.158 | 0.154 | 0.108 | 0.0275 |
| **January** | 0.0265 | -0.00678 | 0.00234 | 0.0164 |
| **February** | -0.0734 | -0.0143 | -0.0732 | -0.102 |

In most cases, the increase in kernel size led to an increase in correlation (Table 6.2 Backscatter-VWC correlations at 4 different kernel sizes). This was, however, not the case for all images. January, in particular, the correlation switches from very weakly positive to very weakly negative when the frame of reference is increased from just the individual pixel to a three-pixel square kernel, and back again to positive when the size increases again to 5. November, likewise, does not follow expectations. Rather, the correlation increases as kernel size increases to 3, but reduces with each subsequent kernel size increase. June shows the strongest improvement in correlation as kernel size increases, improving from 0.183 for the single pixel, to 0.531 for a 7 pixel kernel. October, likewise, shows an improvement as kernel size increases, however, this improvement is not linear.

#### 6.2.2.2 Adaptive filtering

Adaptive filters, like non-adaptive ones reduce the impact of speckle but are also better at maintaining edge information. To do this, they exploit local statistics in the moving window, or kernel. Four of the most commonly applied methods of adaptive filtering – Frost, Gamma, Lee and Local Sigma – were employed to assess the impact they had on the correlation between $\sigma^0$ and VWC. The CSK imagery used was the August image, calibrated and terrain corrected with the 2m DTM. Three kernel sizes were used in this analysis (Figure 6.5, Table 6.3) – 3 pixels, 5 pixels and 7 pixels. These filters, the parameters of which are described below, were chosen both due to their popularity for use in environmental remote sensing (Lopes *et al.*, 1990; Mondini *et al.*, 2019; Shi & Fung, 1994), but also because they cover the range of different adaptive filtering philosophies.

The Lee filter is a weighted sum of the observed central pixel and the mean of the kernel values. The weighting coefficient is a function of heterogeneity in the kernel, which is measured with the coefficient of variation (Lee *et al.*, 1998; Lee, 1980). Like the Lee filter, the Frost filter uses the Minimum Mean Square Error (MMSE) approach. It does, however, differ on one fundamental point, namely, that it uses the measure of local heterogeneity to adapt the size of the kernel. (Frost *et al.*, 1982). The Gamma Filter assumes that the values of the scene underlying the speckle have a gamma distribution. The filter functions similarly to the enhanced Lee filter in that it is designed to minimise the loss of radiometric and textural information, but with a different filtering model for heterogeneous areas. It minimises the loss of texture better than the Frost and Lee filters for gamma-distributed areas (oceans, forested and agricultural areas). Where there is not a gamma distribution, it leaves the original pixel value (Shi & Fung, 1994). Local sigma filters preserve fine texture using the local standard deviation of the kernel to establish which pixels are appropriate to use for adjusting the central pixel value. The central pixel is replaced using a weighted mean of the pixels deemed appropriate by the standard deviation test (Eliason and McEwen, 1990; Harris Geospatial, 2020).

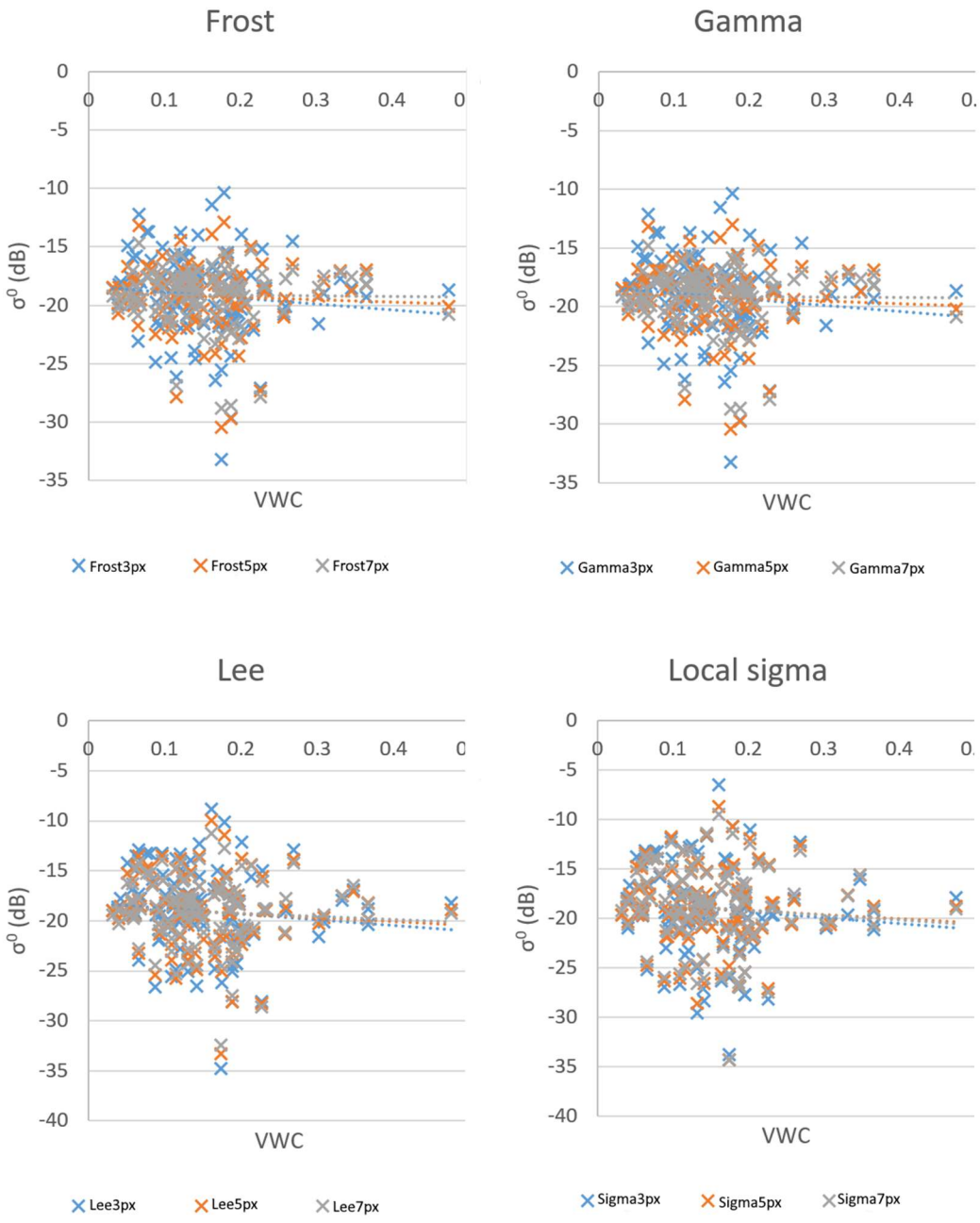


Figure 6.5 $\sigma^0$ - VWC correlations using Frost, Gamma, Lee and Local Sigma adaptive filters at kernel sizes of 3,5,7 pixels.

Table 6.3 Correlation coefficients for Adaptive filters at three kernel sizes.

| Kernel size | Frost | Gamma | Lee | Local Sigma |
|---|---|---|---|---|
| **3** | 0.0121 | 0.0122 | 0.0108 | 0.0093 |
| **5** | 0.003 | 0.003 | 0.0073 | 0.0054 |
| **7** | 0.0001 | 0.00007 | 0.0053 | 0.0083 |

This assessment found that correlation between VWC and $\sigma^0$ decreased as the kernel size increased, with a kernel size of 3 providing the highest correlation values. None of the correlation values were significant.

#### 6.2.2.3 Filtering summary

This study has explored the extent to which adaptive and non-adaptive filtering, as a method for reducing the impact of constructive and destructive interference, is valuable in the context of remotely sensing soil moisture, and the scale to which this filtering can appropriately be undertaken. The non-adaptive low-pass filter approach showed an increase in correlation with the increase in size of the kernel for most datasets. This was not, however, the case, with the adaptive filters, where the optimum kernel size appeared to be three, with the correlation values of all filters reducing with each size increase with the exception of Local Sigma, where correlation increased from kernel size five to size seven.

This study has explored the extent to which adaptive and non-adaptive filtering, as a method for reducing the impact of constructive and destructive interference, is valuable in the context of remotely sensing soil moisture, and the scale to which this filtering can appropriately be undertaken. The non-adaptive low-pass filter approach showed an increase in correlation with the increase in size of the kernel for most datasets. This was not, however, the case, with the adaptive filters, where the optimum kernel size appeared to be three, with the correlation values of all filters reducing with each size increase with the exception of Local Sigma, where correlation increased from kernel size five to size seven.

### 6.2.3 Summary of Part 2 of Objective 3

This section has explored a key question regarding the use of CSK data in a real-world scenario – namely, how viable estimation of relative soil moisture values from single-polarised COSMO-SkyMed data is if limited *a priori* surface knowledge is available. Asking, if low resolution terrain data are the only ones available, because the site in question has not been imaged in high resolution before and a high resolution surface model cannot be made from available SAR imagery, to what extent does the scale of the terrain model matter? Similarly, to what extent and which parameters of filtering techniques enhance that soil moisture estimation?

The findings in the previous section were not straightforward. The anticipated relationship (Ulaby *et al.* 1981) between $\sigma^0$ and *in situ* VWC was not found with any scale of terrain correction being applied, although neither was the application of

adaptive and non-adaptive filtering on the data, as undertaken in this chapter, much benefit in reducing the impact of speckle on the assessment of this. Rather, weak positive and negative correlations were found between VWC and $\sigma^0$ values at all scales of terrain correction utilised, which are similar to findings of others (Zribi *et al*. 2019) where weak positive relationships have been found. Although this gives confidence in this project's results, the low coefficients of determination associated with these relationships challenges the idea that it is possible to reliably use SAR for SM estimation. The finding regarding the scale of DTM used in terrain correction is indicative that, to account for the impact of variable terrain on a geometrically complex site, it is necessary to terrain correct using a terrain model that is at least the same order of magnitude in vertical and horizontal scale as the incident SAR wavelength. This outcome is particularly important given the impact of vegetation on increasing the effective roughness of a surface when using very short wavelength SAR. Without recourse to such a terrain correction method, it is inappropriate to estimate soil moisture from backscatter returns, whether other forms of processing have been undertaken or not because the roughness component has not been well quantified and therefore the problem of equifinality presents itself in interpreting the backscatter values. With regards to filtering methodologies, the optimum approach will always, in part, be defined by the goal of the research being undertaken. This study found Frost and Gamma filters to perform the best of the four approaches and with a kernel size of three, but none of the correlations were significant, and therefore, it should not be taken that these are necessarily optimum methods for all soil moisture estimation approaches.

Answering part 2 of Objective 3 has shown that with the parameters of this study, there are challenges associated with using X band SAR for monitoring soil moisture, particularly when using imagery with the temporal coarseness of the dataset used in this project and the limited constraint of surface roughness in the project design. As mentioned in the introduction to this project, some of these limitations are ones which external circumstances caused – namely the Covid-19 pandemic. The following section outlines the impact these limitations have had on this project and also what these restrictions have enabled to be ascertained regarding the parameters for soil moisture estimation viability for CSK.

## 6.3 Objective 3 conclusions

This section draws together the findings from the two parts of Objective three. Objective 3's focus has been on analysing the viability of using COSMO-SkyMed data

for soil moisture estimation. Part 1, in Chapter 5 established that there are issues associated with inter- and intra- sensor variability within the CSK constellation, and discussed the implications of these for using the data product both as a stand-alone image, and as part of a time series. Part 2, in this chapter, has established whether using CSK in a coarse time series is viable when limited *a priori* information is available relating to surface roughness, and whether any mitigation of the impacts of the constructive and destructive interference that affects SAR images can be mitigated in post-processing by using non-proprietary software packages available to non-expert SAR users.

## 6.4 Contextualising the findings from Objective 3

Meeting part 2 of Objective 3 has shown that in the context of this research, and with these research parameters, that the viability of CSK for SM monitoring has significant challenges. These are seen most clearly in Figure 6.1, which shows that for each image the correlation between dB and sigma nought has a small correlation coefficient, and the relationship varies between slightly positive and slightly negative, meaning that essentially the mean is the best model for the variability data. Although it might be argued that this result is indicative of a need for further processing of the data and application of backscattering models to improve the fit of the data, a survey of studies which related backscatter and *in situ* soil moisture measurements has shown that these results are similar to those achieved by studies which undertook modelling, and an anticipated slope is expected as being between 0.1 and 0.3 (Zribi & Baghdadi, 2015). A further point to this, is that there is so much scatter in the data, as evidenced by Figure 6.1, that any model applied would have to do a lot of work to remove the impacts of this, and would, therefore, have the potential of reducing the validity of the results.

The following section assesses the parameters of projects where SAR has been found to be a viable tool for SM estimation. This investigation follows three strands – first, establishing projects that have found SM estimation with SAR to be possible, and setting out the data that was used by these projects and discussing the confidence it is possible to have in their findings. Second, in discussing these findings relative to this project, and third, in combining these two strands into the creation of a decision-tree for assessing the viability of SAR usage for SM estimation. The projects are summarised in Table 6.4.

Table 6.4 Summary of SAR-SM studies - their parameters and their results

| **Papers** | **Platform** | **Polarisation** | **Number of images** | **Processing method** | **Image interval** | **Fieldwork/ imagery timing** | **Surface** | **Landcover** | In situ **measurements** | **Roughness measurements** | **Result Bare** | **Result Vegetated** | **Result Slope** |
|---|---|---|---|---|---|---|---|---|---|---|---|---|---|
| Balenzano 2103 | CSK, PALSAR1 | HH, 26deg | 8 (4 in 2010, 4 in 2011) | SMOSAR algorithm (temporally dense images) | ~1 week | 1-5 days (no precipitation between) | Flat | Vegetated – (Wheat, Tomato, Sugar beet) | Mv measurements. Method undefined | - | 5%-7% $m^3/m^3$ accuracy (X-,L-Band) | 5%-7% $m^3/m^3$ accuracy (L Band) | - |
| Mattia *et al*. 2012 | CSK; PALSAR1 | HH, HV Pingpong; HH spotlight | 8 | SMOSAR (Balenzano *et al*. 2011) | ~8 days | unspecified | Flat | Wheat; corn and alfalfa; | Mv measurements. Method undefined | Soil texture maps, DEMs (scale unspecified), vegetation height and fresh biomass | n/a | 6% to DREAM hydrological model | - |
| Zribi *et al*. 2019 | L band, PALSAR | HH, HV | 10 | AIEM; IEM; Oh (1992); Dubois; Baghdadi | 2 weeks | 2 hours | flat | Marigold, sorghum, turmeric | Mv – Theta Probe; 3 measurements per 0.5 ha field | soil moisture, soil roughness, and leaf area index (LAI) | 0.21 dB/(vol.%) | ~0.1 dB/(vol.%) RMSE: AIEM 2.2 IEM 2.9 Oh'92 5.4 Dubois 2.1 Baghdadi 1.2 | - |
| Balenzano 2011 | C band | HH, HV 25 deg | 26 (16 HH, 10 HV) | SMOSAR | ~10 days | 3-54 days | flat | winter crops, maize and sugar beet | - | - | - | 5-6% retrieval accuracy | - |
| El Hajj *et al*. 2016 | TerraSAR-X; CSK | HH,HV | TSX-7; CSK - 16 | Water cloud model | 1-60 days | 2hrs | Flat | Irrigated grass | 5-30 VWC TDR measures ~ 20 m apart | LAI, NDVI derived from optical imagery | N/A | RMSE 3.6 Vol.% for NDVI 0.45-0.75, and 6.1 Vol.% for NDVI 0.75- 0.9 | - |
| Ryu *et al*. 2020 | KOMPSAT-5; X band; Spotlight | VV | 3 | Linear Water Cloud Model (WCM) | 1-2 months | 0-3 days | Flat | Wheat | 30-11 points for calibration; 16-6 points for validation | Not specified | N/A | 0.22-0.52 $R^2$ | - |

Table 6.5 shows a selection of studies that have been undertaken using SAR imagery for SM estimation during the last decade. Studies have been selected to be presented because they cover a range of SAR data types and approaches to handling the data. The findings in the table have been fed into the production of a set of guidelines for when viability of SAR for soil moisture can be established (Figure 6.6).

Where studies have found X band SAR to be somewhat viable, they have not had the amount of ground truthed data, either in terms of number of points, or in terms of density of points, that my project has had, with the densest measurements that were found to be recorded being every 20 metres (El Hajj *et al.*, 2016). These papers have quoted results that show a relationships between backscatter and soil moisture e.g. weak positive correlation (Zribi *et al.*, 2019), of 5-6% accuracy (Balenzano *et al.*, 2011; Mattia *et al.*, 2012), 3.6%-6.1% RMSE (El Hajj *et al.*, 2016), and 0.22-0.52 $R^2$ (Ryu *et al.*, 2020), that compare favourably with this project's. However, the results in these papers do not, necessarily, indicate that SAR can be used as a tool for reliably relating backscatter to soil moisture conditions. Each of these studies accounted for surface roughness, and vegetation biomass – both components that have a significant impact on backscatter, and yet it can be argued that their results are not considerably better than those presented here, nor are they necessarily sufficiently strong for SAR to be confidently classed as a viable tool for estimating SM reliably. Likewise, the spatial density of the ground-truthing data utilised by these studies means that it is likely that the ground truthing data does not accurately represent the soil moisture heterogeneity, and that, therefore, the quality of agreement with actual surface conditions is not, necessarily, as strong as they have presented.

The brief summary of projects investigating the potential of SAR-SM estimation has shown that the quality of the relationship between backscatter and SM is generally limited. Where backscatter and *in situ* measurements have been compared in these projects, there has often been very limited ground truthing data, with only a few measurements per hectare (Zribi *et al.*, 2019).

### 6.4.1 Recommendations for assessing viability of SAR

On the basis of the literature survey outlined above, and the findings from this project, there are certain key criteria that need to be considered when assessing

the viability of SAR for SM estimation, which are presented with respect to two groups of researchers – those who do not specialise in SAR usage, and those who do.

#### 6.4.1.1 SAR non-specialists

First, is the question being asked one that SAR can be used to answer? If small-scale, high resolution SM data, with a high degree of accuracy regarding the values of the SM is required – e.g. if the project is looking at remotely monitoring a slope with a known SM threshold at which instability occurs, and the slope often sits close to that threshold – SAR is unlikely to be an appropriate tool, unless the roughness and vegetation parameters can be really well accounted for, and the conditionally stable area is large enough that filtering can be undertaken.

Figure 6.6 provides a rough decision tree for assessing the viability of SAR –SM estimation based on the findings from this study and those of the other studies covered in this review. This is aimed, particularly, at those who are looking to use SAR as a data product for soil moisture-related study, rather than Remote Sensing specialists who are looking to further develop capabilities within the technology. The recommendations are directed towards this group for two reasons; first, because the increasing availability of open source SAR data is making it increasingly commonly used outside of the dedicated SAR-remote sensing community, and second, because the majority of SAR specialists are exploring methods of optimising and developing tools to enhance SAR usage capabilities, so the question of viability is one which they themselves are working to push.

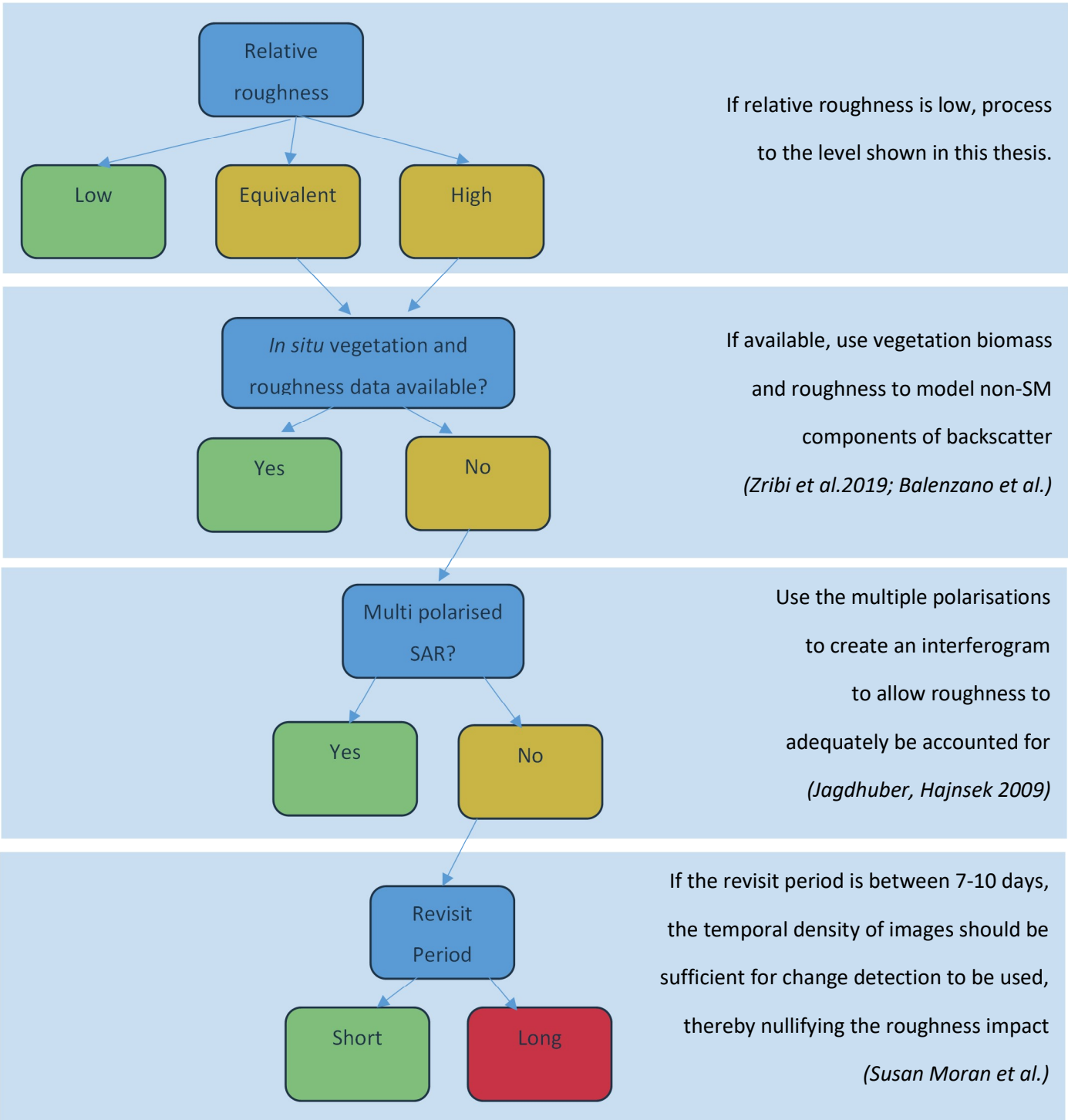


Figure 6.6 Flow chart showing viability of SAR SM estimation, colour-coded by viability, where green is good, orange dependent, and red, severely limited.

Figure 6.6 highlights the importance of relative roughness. This is a very important parameter in the assessment criteria for the viability of SAR. Roughness has a significant effect on BS returns, but this effect is greatest when the roughness of a surface is high relative to the wavelength of the incident wave. That is, depending on the length of the incident wave, the relative roughness of same surface varies. Given this, it is recommended that if roughness is going to

be poorly constrained, or is known to be high at the site being imaged, that a multi-polarised SAR product is utilised, or additional ground truthing data that enables roughness to be well described is obtained.

#### 6.4.1.2 SAR Specialists

It is possible, however, make some comments to this specialist group regarding how they quantify viability of an approach. First, are the parameters by which they judge viability useful in a real-world situation? That is, is the quality of agreement between backscatter and soil moisture actually useful in real terms – does the quality of agreement enable a user of the methodology to answer a valuable research question? Likewise, is the researcher using *in situ* or modelled soil moisture data that is of a sufficient spatial density that it well-describes the spatial variability of the soil moisture in that location? If not, how confident can they actually be of their results? A third, and wider-ranging question that is worth exploring with this specialist group is the value of their research to the wider non-specialist body. Given that the processing of SAR data is often undertaken using a tool developed within the research group, and that is not well described in the research, how valuable is it for the rest of the research community if a lack of access to that tool - which almost exists as a black-box in the context of the reading public – means that the work that the research group has done cannot be replicated by the wider research community in their own studies? This ties in with the wider issues of reproducibility in the wider scientific community, and is worthy of attention both within the RS community and beyond (Baker, 2016).

## 6.5 Summary of viability assessment

SAR is often lauded as a tool that can be used in contexts where optical imagery cannot, and particularly in contexts where the provision of results has the potential to significantly impact on situations – for example in hazard contexts. Although SAR is theoretically viable and its use seems valuable, this needs to be caveated by the recognition that there needs to be sufficient additional data available to enable key parameters like surface roughness and vegetation scattering to be well accounted for in the backscatter signal. Without this, it will be hard to utilise SAR for timely, real-world, uses in understanding and mitigating hazards.

Though many studies using SAR have shown that SM estimation from SAR is possible, the constraints on this are significant. It is notable that the majority of studies where dB/$\sigma^0$ relationship is reported as being valuable have used systems with longer wavelengths, where effective surface roughness is much lower (Mattia *et al.*, 2009; Balenzano *et al.*, 2013; Zribi *et al.*, 2019). Recent studies with shorter wavelength SAR have made use of multi-polarised data (Zhang *et al.*, 2012) or image series with small temporal gaps between the images (Balenzano, *et al.*, 2011a; Balenzano *et al.*, 2011b, Dille *et al.*, 2021) to reduce the impact of vegetation change (Notarnicola *et al.*, 2010; Marin *et al.* 2015; Zhu *et al.*, 2019; Punithraj *et al.,* 2020) or enable the creation of a surface model through interferometry, thus enabling the impact of surface roughness to be well accounted for. It is not possible, therefore, to say that SM estimation with SAR is not viable. It should, however, not be assumed that it is viable in all system criteria. This project has attempted to estimate SM using the hardest combination of parameters currently available– single polarised, shortest wavelength, images taken over a time series with irregular, large intervals between the images. Indeed, it is notable that many of those who work most with SAR tend towards using the longer wavelength C- (Hornacek *et al.*, 2012; Rodionova, 2019; Sangwoo *et al.,* 2019; Mattia *et al.*, 2020; Zakharov *et al.*, 2020) and L- (Ouellette *et al.*, 2017; Zhu *et al.*, 2018, 2019; Zribi *et al.*, 2019) band products because they are recognised as being less challenging to use for soil moisture estimation due to the reduced impact of roughness on them.

# 7

# CHAPTER 7: DISCUSSION AND CONCLUSION

The introduction to this thesis set out the environmental context for this project – namely that under modelled changed climates precipitation regimes were likely to cause more hydraulically driven landslides, and that there was a need to assess methods of monitoring slopes to assess potential failures. SAR constellations, with their reduced return times between images, and high resolution imagery, unhampered by the restrictions of optical or other passive sensing technologies were recognised as having the potential to enable monitoring of these slopes. This thesis has explored the complexity of soil moisture – a key GCOS parameter in the context of climate change (GCOS-138, 2010) – and the complexity of its monitoring using novel X-band Synthetic Aperture Radar data from the COSMO-SkyMed platform. The thesis has presented, analysed and discussed four key datasets – an *in situ* surface soil-moisture measurement, an *in situ* shallow subsurface soil-moisture measurement, an *in situ* sub-surface CRNS soil moisture dataset and a satellite-based X-band high-resolution Spotlight2 SAR data product. The geographic context of the study was novel – a geomorphically active, slow-moving landslide site in a temperate, maritime climate, grazed, and comprising of three different soil types.

The project has enabled the exploration of the capabilities of, and ideal methodology for, using CSK Spotlight2 data for estimating soil moisture in an environmental context that previous studies had not explored. It was couched in the terms of seeking to establish the limits of soil moisture sensing capabilities of the sensor and whether these aligned with the requirements needed based on the hydraulic properties of the slope at Hollin Hill. As part of this, the variability of soil-moisture values, as measured *in situ* using Theta Probes and the SensorNet array, were analysed in Chapter 4, and the spatio-temporal relationships explored alongside the VWC values in areas most associated with deformation. It was found, unsurprisingly, that the geomorphically active areas of the site had high VWC values, often higher than those anticipated in the literature (Centre for Ecology and Hydrology, 2018), and that the VWC values in these areas were

uniformly higher than the stable areas of the slope throughout the time series. In addition, the project found high heterogeneity of soil moisture within clusters as well as between clusters, which presented a challenge regarding the appropriate interpretation of this variation for directing CSK image improvement parameters.

Initial assessments of the CSK data led to the project taking a different route from that originally envisaged. Despite the rigorous work undertaken by ASI and their partners during the commissioning phases of each satellite (Calabrese *et al.*, 2008), it had been anticipated from reading the research of other projects working with CSK data (Baghdadi *et al.*, 2015) that there might be a need for a simple, linear, offset of backscatter returns that would require some post-processing inter-sensor calibration before further studies using the data could be undertaken. It was, however, found in this thesis that there was not just inter-sensor variability, but also intra-sensor variability, in particular on Sensor 3, which showed in the persistent scatterer tests to have provided two images which had significantly different $\sigma^0$ returns. This result seems to contradict the expectations of ASI and the projects they provided data for in the early operational phases of the project to establish the usability and inter-calibration of the constellation (Balenzano *et al.*, 2011), which found some linear offsets needed to be applied between sensors (as indeed was found in this study), but that where multiple images from the same satellite were used, that there was good inter-calibration there. It is not possible to say whether intra-sensor variability is present in Sensors 1 and 2 in the constellation as this project only used one image from each of these sensors. However, given the presence of intra-sensor variability in Sensor 3, it is important that researchers using multiple CSK images perform initial tests - like the ones undertaken in this thesis - before they seek to employ the data products in their research. This is particularly pertinent in the case of time series studies, for, as has been evidenced by recent re-appraisals of studies using the NOAA AVHRR catalogue, where a lack of awareness of inter-calibration between sensors occurs, trends and relationships can wrongly be interpreted (Van Leeuwen *et al.*, 2006; Alcaraz-Segura *et al.*, 2010).

Indeed, given the increasing predominance of multi-satellite constellations being used for environmental remote sensing (Kelly *et al.*, 2009), including the second

generation of COSMO-SkyMed (CSG) – the first satellite of which launched in December 2019 (Telespazio, 2019) – it is necessary to ensure that those using data from multiple sensors, whether within the same constellation, or across platforms, ensure that their data are rigorously and robustly inter-calibrated before use. Indeed, CSK data have been used in studies published recently (Silva Guimarães *et al.*, 2020) where no mention is given to which satellites in the constellation have been used in the imaging, nor of the potential for inter-calibration issues as SAR moves from being a specialist technology, where much of the research around it is how to use it, to being a technology that is used by those for whom radar remote sensing is not their background, awareness of the necessary checks that need to be performed on data should be increased.

Despite the inter-calibration issues which necessarily directed the thesis in a slightly different direction to the one originally intended, all three Objectives that were set out in the Introduction were met. The results of these are recapitulated below, and discussed in the context of other research.

*Objective 1: Describe the relationship between surface soil moisture at a penetration depth equal to that of X-band SAR and moisture at depths closer to the failure plain and more representative of the wider soil mass.*

The relationship between co-located surface (~5 cm) soil moisture capacitance probe readings and those at a depth of ~ 10 cm was found to be strong. Generally, the deeper measurements were higher than those at the surface, which is to be expected given the well-attested surface drying or preferential routing processes occurring in the vadose zone (Calvet and Noilhan, 2000; Robinson *et al.*, 2008; Vereecken *et al.*, 2008). The processes behind the linking of these two depths of moisture, nor the more geometrically complex volumetric measurement provided by the CRNS probe at the COSMOS station, were established during this project. However, that the moisture levels are generally higher at depth is an important consideration for those using SAR soil moisture estimations for assessing potential slope stability implications of this measurement, as the soil mass may be wetter than the near-surface that SAR interacts with.

*Objective 2: To assess the spatial variability of surface and subsurface soil moistures in the soil mass.*

Chapter 4 explored the spatio-temporal soil moisture relationships at Hollin Hill. The findings – that each soil type had different surface-subsurface relationships – was not surprising. The repeated spatial distributions of relative soil moisture values across the site throughout the time series (Figure 4.29) is common to many studies of spatio-temporal soil moisture. Vachaud *et al.*'s (1985) 'temporal stability' (TS) concept of continuous relative ranking of points by wetness has been seen to exist at the site.

The autocorrelation length of surface soil moisture variability was found to be in the region of 190 m, which sits within the range of values from 1 m to 600 m found by Western and Bloschl (1999) in their survey of soil moisture spatial variability patterns. It was, however, longer than the common distance range found in a later summary of spatial soil moisture distribution by Western *et al.* (2004), which quotes the most common lengths as being between 30 and 60 m. The use of quasi-point based data at multiple distances allowed for a robust assessment of spatial patterns but also highlighted the challenges of using point-based data, due to the high heterogeneity of soil moisture at very small scales. This is an issue which has been echoed in several studies in terms of how to interpret and use that interpretation of spatial variability of soil moisture (Vereecken *et al.*, 2008; Biswas, 2014).

*Objective 3: To explore the viability of using SAR for monitoring soil moisture on a geometrically complex site.*

Chapter 5 explored the Spotlight2 CSK data provided to the project by ASI, and its utility for estimating soil moisture at Hollin Hill. The findings were somewhat inconclusive due to the intra-sensor variability found through persistent scatterer testing of conifer stands and water bodies, where it was found that one sensor at least exhibited significant backscatter return variability. This problem has not, to our knowledge, been recognised in other studies using CSK data, although it should be noted that studies that have assessed *inter*-sensor variability have not necessarily had access to sufficient images from all sensors in the constellation to assess *intra*-sensor variability on all sensors. A survey of recently published papers using images from multiple CSK sensors has, however, shown that while some papers by those who have worked extensively with CSK data (Pettinato *et al.*, 2019) do explicitly state their careful calibration work, those who are newer to the field, or who are using SAR purely as a tool to answer a question rather

than exploring SAR's potential as a tool, do not necessarily show evidence of rigour in assessing the inter-calibration of their data prior to using it (Silva Guimarães *et al.*, 2020). The persistent scatterer studies did show that if the two seemingly problematic images (November and January) were removed, a similar post-processing linear offset would be required to inter-calibrate the images from the four sensors, as Baghdadi *et al.* (2015) and Gorrab *et al.* (2015) had found in their own assessments of their data. An assessment of the correlation between backscatter value and measured surface *in situ* soil moisture was undertaken, using four different scales of open source DTM data for terrain correction. The results of this were disappointing, though not necessarily surprising. No significant improvement in the correlation was found as the scale of the DTM decreased. This is not necessarily surprising, given Baghdadi *et al.*'s 2002 study regarding the scale of surface corrections needed, but it does highlight the challenges of using SAR for soil moisture estimation in a mock-up hazard monitoring situation where high-resolution DTMs aren't necessarily available through interferometry or other methods. It is further backing to Wagner *et al.*'s (2005) assertion that SAR has, so far, in many societally important contexts, failed to live-up to the potential it is often touted as having for soil moisture estimation.

This study has not fully answered the question regarding the ideal resolution parameters for remote sensing platforms for monitoring soil moisture. While variability in *in situ* surface soil measurements was found to be high at short distances, the necessity of resolving soil moisture measurements to such a resolution is dependent on the goals of the research being undertaken. It can, however, be said, that the effect of micro-roughness on the backscatter of an X-band SAR product and the high impact of speckle relative to the impact of dielectric constant on backscatter might warrant the choice of a coarser resolution product if undertaking projects without access to appropriate measurements of the effective roughness of the site.

COSMO-SkyMed has been found by many to be an excellent platform for environmental remote sensing, with multiple papers showing strong correlations between backscatter values and *in situ* moisture measurements, predominantly using SAR platforms with longer wavelengths like ERS (C–band) (Griffiths and Wooding, 1996; Quesney *et al.*, 2000) or ALOS PALSAR (Balenzano *et al.*, 2013;

Zribi *et al.*, 2019b). These papers achieve such results after extensive focus on establishing the roughness and vegetation scattering parameters at their study sites, and focussing on areas that have easily definable geometries and ground covers. Without this *a priori* knowledge, and extensive modelling of vegetation structures, such time-series based projects would not be able to produce such strong backscatter – *in situ* VWC correlation values. The current requirement for such detailed *a priori* knowledge for soil moisture estimation using single-polarised SAR products is one that led Wagner and Pathe (2005) a decade and a half ago to query whether SAR is fulfilling the promise that it was thought to have a few decades ago. The reliance on empirical *in situ* observations and modelling to enable soil moisture inversion, rather than just relative soil moisture estimation offered by change detection mechanisms, renders SAR still to be a very unwieldy tool for the estimation of soil moisture. This is particularly the case when using the shorter wavelengths, as has been done in this study; for, the impact of change in surface roughness and vegetation is more considerable for these wavelengths (Baghdadi *et al.*, 2002).

## 7.1 Areas for further research

### 7.1.1 Irregularities in CSK CALVAL

As already highlighted, a further examination into the causes and implications of variability within the CSK constellation is pertinent. Likewise, it would be valuable for those involved in the CSK and CSG projects to assess the continued functionality of the CALVAL image quality assessment tool being used during the operational phase of the constellations.

### 7.1.2 Connecting surface soil moisture readings with locations of known or highly probable preferential routing.

Although the additional clusters designed for the manual surface soil moisture measurements proved valuable in targeting areas of the landslide that field assessments had identified as hydraulically significant for the development of slope deformation, these locations did not have any corresponding sub-surface point measurements associated with them. Given that one of these clusters was near the sag ponds at the site and would have experienced significant subsurface turbation during deformation events, it would be useful to better understand whether the necessarily changed structure of the soil there and possible

preferential routing associated with the cracking in the area and further up the slope at the back-scarp changed the relationship between subsurface and surface moisture. Likewise, it would be useful to understand the full moisture profile of that area of the slope better to enable improved understanding of how surface soil moisture relates to the full depth of the mobile mass.

### 7.1.3 Assessment of the need for high-resolution data for landslide monitoring

The development of constellation platforms over the last 15 years has been lauded by many as it has reduced the trade-off between resolution and return period (Kelly *et al.*, 2009; Snoeij *et al.*, 2009; Kornelsen and Coulibaly, 2013), which had previously been seen as a disadvantage for active remote sensing platforms. It should be questioned whether, in the context of monitoring landslides, where the conditions of a large mass are important, rather than point-scale measurements, high resolution imagery is as valuable as has been argued. A better approach might well be to use a longer wavelength SAR product, like ALOS PALSAR and benefit from reduced effective roughness and greater soil penetration. High resolution for high resolution's sake is not always necessary, particularly when products are not free and open source, as is the case with the CSK and CSG products.

An extension of this is to comment on the need for more extensive access and utilisation of the NovaSAR-S product - the airborne emulator of which was used in the research undertaken prior to this thesis (Chapter 3) – for the estimation of soil moisture. The high resolution S-band product should perform as a valuable dataset, with a mid-range wavelength but better spatial resolution than is generally available from L-band products.

The high resolutions of CSK, CSG and TerraSAR-X have been touted as highly valuable for environmental remote sensing. While this is absolutely the case for some applications, there is need for recognition of which environmental remote sensing objectives actually are enhanced by such high-resolution data. Given the stochastic nature of many environmental parameters, it is valuable for parameters and project goals to be assessed in advance of ordering high-resolution data, for that imaging mode might not actually be optimal. For example, given that mass movements are driven not by changes at points, but by

changes at much larger scales, it might be worth using much coarser resolution imagery.

## 7.2 Conclusions

There follows a set of conclusions aimed at two different audiences. While the conclusions are valid and valuable for both groups, it was felt important to highlight specifics to each group. This is because the project has highlighted

This project has shown that at the Hollin Hill landslide – a slide which has been established as being representative, both in terms of materials and function, of slides common in the UK and beyond – exhibited greater complexity spatio-temporal complexity in its surface soil moisture characteristics than is commonly cited within the literature on this topic (Objective 1). This, in combination with the study relating surface soil moisture with soil moisture at greater depths in the soil mass of the slope, showed that assumptions about spatial heterogeneity of soil moisture and autocorrelation of the same are not necessarily appropriate in the context of developing soil moisture estimation tools using radar remote sensing (Objective 2).

The project found that the challenges associated with soil moisture estimation using X-band SAR are significant when using a time series with roughly monthly gaps without *in situ* roughness measurements. That being said, it has also challenged the positive results that other scholars have presented regarding their development of SAR processing algorithms, by highlighting that the quality of agreement that they present is little better than that presented in this study, and almost certainly is insufficient to represent a processing methodology that could be used in hazard assessment or in conditions where *a priori in situ* measurements are lacking.

The viability of X band SAR usage for soil moisture estimation was further called into question due to the inter- and intra- sensor variability found in the data provided by the ASI as part of the project. The variability in returns from sensor 3 within the constellation provided significant concerns regarding how images can be used – either as stand-alone images, or as part of a time series, when there is discrepancy between the backscatter returns between sensors in a constellation and between images from the same sensor (Objective 3).

Nonetheless, SAR is a really valuable tool, with huge potential for use by environmental scientists to enable the further development of current research areas where the operation or utilisation of optical imagery is insufficient. In certain situations, SAR offers an alternative to traditional proxies for soil moisture, while also offering the potential for DEM creation using interferometry.

This project has highlighted several key points for RS specialists. First, that while constellations are offering solutions to many of the problems the RS community has long recognised in SAR (e.g. return periods, spatial resolution), these constellations do not come without potential problems of inter-sensor variability. Second, this project has shown that there are multiple scales at which SM varies, and therefore that it is valuable to understand this through *in situ* or optical RS SM proxies in advance of accessing SAR data to enable assessment of the most appropriate parameters for the SAR imagery that is being sought for use.

## 7.3 Recommendations

This research was undertaken in a context where SAR imagery and the tools to manipulate it has become increasingly available through freeware platforms like Google Earth Engine and the freeware data repositories from which it can directly pull. While the accessibility of RS data is a fantastic step in increasing possible research directions, it is important to be mindful that we are also entering into a new epoch where remotely sensed data is being used by people for whom remote sensing is not their primary research area. Where previously SAR was the domain of those who do research into remote sensing, it is now commonly being used by those who have only a rudimentary understanding of the complexities and issues associated with the data type. There are, increasingly, going to be more projects that do not necessarily take into account data issues, not because there is not an academic integrity in those projects but because the issues are unrecognised by non-remote sensing specialists. With a recognition of the breadth of backgrounds of those now using SAR, the recommendations are categorised not just by theme, but also by user. For a more extensive set of recommendations and a tool for assessing viability of using SAR when designing a project, please see sections 6.4.1 and 6.4.2.

### 7.3.1 Users

As the assessment of the calibration of the CSK data in this project has shown, there should not be an assumption made by users that despite the rigorous calibration and validation procedures undertaken by data providers that careful assessment of the data does not need to be undertaken prior to use.

#### 7.3.1.1 Non-specialist academics

The increasing access of easily downloaded SAR imagery from platforms like Google Earth Engine and the Sentinel Hub, combined with the increasingly high resolution of imagery and shorter return times offered by constellations has made SAR a valuable data source, particularly given some of the issues that optical imageries have, and that SAR does not. There is not always information available on best practice for calibrating imagery. It is, therefore, recommended that undertaking due diligence in assessing the calibration of imagery before beginning using it for projects is essential. As a minimum, it is recommended that:

- Open source freeware processing methods like ESA's SNAP and Google Earth Engine make processing of imagery quick and relatively straightforward. However, these are to some extent a black box approach, where not all the processing parameters are specified or adaptable. It is important to ensure that the objective and rationale for each type of pre-processing undertaken is well understood in terms of the impact it will have on the utility of the processed data product.
- Radiometric assessment is a valuable tool to use after pre-processing data and before engaging in any analysis planned for the data, as this provides the opportunity to assess whether the data are well calibrated and whether there is the need for any additional calibration to be undertaken. Recommended methods for doing this would be to undertake comparative radiometric assessments of water bodies or other features in the image – for example roads – as shown in Section 5.2.3 124.
- Care should be taken when using this data that the complexity of relationships between backscatter and soil moisture is understood and that there needs to be rigor in the engagement with these complexities.

#### 7.3.1.2 SAR Specialists

- In undertaking work where the assessment of tools for estimating soil moisture is done, consider whether the parameters used for consideration of whether a tool is successful map onto parameters which exist in real-world scenarios.
- As constellations become more popular there is a need for dedicated remote sensing practitioners to ensure that research is accessible not just within the remote sensing community but to those whose research interests are to use SAR rather than optimise SAR – that is, people for whom SAR is becoming a means to an end, rather than the focus of their research. It is important to consider the accessibility – both in terms of publication locations and publication style and content – to ensure that those in the academic community for whom remote sensing is not their primary focus, are able to make informed decisions on SAR data and processing methodologies.

### 7.3.2 Industry and Developers

#### 7.3.2.1 CSK developers

- CALVAL – can the performance of this continue to be assessed during the operational phase of satellites? Is there a method for highlighting to users when calibration issues are picked up? Is there a method for assessing how long a calibration issue has existed when it is spotted?
- How do you share the inter-calibration issues with users? Currently the ASI documentation does not mention inter- or intra-sensor calibration as being a potential issue. With more users being non-specialists in RS, what do they have in place to make sure service users use data appropriately?

#### 7.3.2.2 Other Developers

- This project has benefitted greatly from the availability of freeware SAR processing packages in the form of ESA's SNAP software and its associated toolboxes. The provision of these by ESA is to be commended and makes the use of SAR products viable for those whose specialism is not in their processing. While this is a great advantage and one which should be lauded for the way it opens these datasets up to environmental scientists from around the world, a greater set of guidance on how to use SAR data and

appropriate checks and calibration steps to be undertaken in advance of undertaking analysis with it should be provided. For, as has been noted often in this thesis, SAR behaves quite differently to optical imagery, and cannot be used as straightforwardly as many optical products.

- The project has shown that there are a variety of scales at which surface soil moisture varies. These scales are important to different scientific user groups. Recourse should be given to the findings presented in chapter 4 to assess the scales at which it is useful for environmental scientists to be able to monitor soil moisture, and future sensor design should take these parameters into account during the design and feasibility study phases.
- The project has also shown that there is a greater range of SM values than literature generally recognises and that those values which sit outside the expected are the ones most associated with slope instability. It is, therefore, recommended that consideration is given to how systems are designed, and processing methodologies are optimised, such that the high values which often correspond to greatest instability potential are not processed-out or disregarded.

## 7.4 Final remarks

Soil moisture is a valuable parameter to be able to estimate for a range of key environmental monitoring or forecasting undertakings including, but not limited to agriculture (Engman, 1991), hazard prediction (Gritzner *et al.*, 2001; Ray and Jacobs, 2007, 2008; Balenzano *et al.*, 2013; Hassaballa *et al.* 2014; Sangwoo *et al.* 2019), weather forecasting (Calvet and Noilhan, 2000) and climate monitoring (Huszár *et al.*, 1999; Seneviratne *et al.*, 2010). It is anticipated that the monitoring of it will increase in importance over the coming decades as climate change impacts precipitation regimes. This thesis has highlighted considerations to be made in using high resolution, short wavelength SAR products to meaningfully monitor soil moisture in the context of an active landslide site. Although some limitations have been found in its use in the particular parameters employed in this study, in part due to problems with the data provided, it is possible to state that SAR can be viable for the monitoring of relative surface moistures at sites similar to Hollin Hill if the response of the slope to changes in moisture is well understood, and precursory conditions of the imaging are also taken into account when assessing the functional stability of the slope.

## Data Citations

COSMO-SkyMed Spotlight2 data was provided to this project through the UK Satellite Applications Catapult Corsair agreement with the Italian Space Agency, Project Corsair008.

Lidar Composite Digital Terrain Model England 25cm resolution [ASC geospatial data], Scale 1:1000, Tiles: se6768,se6868, Updated: 5 January 2016, Open Government Licence, Using: EDINA LIDAR Digimap Service, <https://digimap.edina.ac.uk>

Lidar Composite Digital Terrain Model England 50cm resolution [ASC geospatial data], Scale 1:2000, Tiles: se6768,se6868, Updated: 5 January 2016, Open Government Licence, Using: EDINA LIDAR Digimap Service, <https://digimap.edina.ac.uk>

Lidar Composite Digital Terrain Model England 1m resolution [ASC geospatial data], Scale 1:4000, Tiles: se6768,se6868, Updated: 5 January 2016, Open Government Licence, Using: EDINA LIDAR Digimap Service, <https://digimap.edina.ac.uk>

Lidar Composite Digital Terrain Model England 2m resolution [ASC geospatial data], Scale 1:8000, Tiles: se6768,se6868, Updated: 5 January 2016, Open Government Licence, Using: EDINA LIDAR Digimap Service, <https://digimap.edina.ac.uk>

# References

Agenzia Spatiale Italiana (2009) *COSMO-SkyMed SAR Products Handbook*.

Agenzia Spaziale Italiana (2016) *COSMO-SkyMed Mission and Products Description*.

Albergel, C. *et al.* (2012) 'Evaluation of remotely sensed and modelled soil moisture products using global ground-based in situ observations', *Remote Sensing of Environment*, 118, pp. 215–226.

Alcaraz-Segura, D. *et al.* (2010) 'Evaluating the consistency of the 1982-1999 NDVI trends in the Iberian Peninsula across four time-series derived from the AVHRR sensor: LTDR, GIMMS, FASIR, and PAL-II', *Sensors*, 10(2), pp. 1291–1314. doi: 10.3390/s100201291.

Allison, R. J. and Brunsden, D. (1990) 'Some mudslide movement patterns', *Earth Surface Processes and Landforms*, 15(4), pp. 297–311. doi: 10.1002/esp.3290150402.

Álvarez-Mozos, J. *et al.* (2006) 'Assessment of the operational applicability of RADARSAT-1 data for surface soil moisture estimation', in *IEEE Transactions on Geoscience and Remote Sensing*, pp. 913–923. doi: 10.1109/TGRS.2005.862248.

Andreasen, M. *et al.* (2016) 'Modeling cosmic ray neutron field measurements', *Water Resources Research*, 52(8), pp. 6451–6471. doi: 10.1002/2015WR018236.

Angeli, M.-G., Gasparetto, P. and Bromhead, E. (2004) 'Strength-regain mechanisms in intermittently moving slides', in *Landslides, Evaluation and Stabilization. Proceedings of the 9th International Symposium on Landslides*, pp. 689–696.

Archer, N. A. L. *et al.* (2016) 'Approaches to calibrate in-situ capacitance soil moisture sensors and some of their implications', *Soil Discussions*. doi: 10.5194/soil-2016-40.

van Asch, T. W. J., Van Beek, L. P. H. and Bogaard, T. A. (2007) 'Problems in predicting the mobility of slow-moving landslides', *Engineering Geology*, 91(1), pp. 46–55. doi: 10.1016/j.enggeo.2006.12.012.

Van Asch, T. W. J., Buma, J. and Van Beek, L. P. H. (1999) 'A view on some

hydrological triggering systems in landslides', *Geomorphology*, 30(1), pp. 25–32.

Attema, E. (1991) 'The active microwave instrument on-board the ERS-1 satellite', *Proceedings of the IEEE*.

Attema, E. *et al.* (2009) 'Sentinel-1 mission overview', in *Geoscience and Remote Sensing Symposium, 2009 IEEE International, IGARSS 2009*, pp. I--36.

Azzam, R. M. A. and Bashara, N. M. (1987) *Ellipsometry and polarized light*. North-Holland. sole distributors for the USA and Canada, Elsevier Science Publishing Co., Inc.

Baghdadi, N. *et al.* (2002) 'An empirical calibration of the integral equation model based on SAR data, soil moisture and surface roughness measurement over bare soils', *International Journal of Remote Sensing*, 23(20), pp. 4325–4340.

Baghdadi, N. *et al.* (2015) 'Signal level comparison between TerraSAR-X and COSMO-SkyMed SAR sensors', *IEEE Geoscience and Remote Sensing Letters*, 12(3), pp. 448–452. doi: 10.1109/LGRS.2014.2342733.

Baghdadi, N., Gaultier, S. and King, C. (2002) 'Retrieving surface roughness and soil moisture from synthetic aperture radar (SAR) data using neural networks', *Canadian Journal of Remote Sensing*, 28(5), pp. 701–711. doi: 10.5589/m02-066.

Baker, M. (2016) 'Is there a reproducibility crisis?', *Nature*, 533(7604), pp. 452–454. doi: 10.1038/533452A.

Balenzano, A., Mattia, F., *et al.* (2011) 'Dense Temporal Series of C- and L-band SAR Data for Soil Moisture Retrieval Over Agricultural Crops', *IEEE Journal of Selected Topics in Applied Earth Observations and Remote Sensing*, 4(2). doi: 10.1109/JSTARS.2010.2052916.

Balenzano, A., Satalino, G., Belmonte, A., *et al.* (2011) 'On the use of multi-temporal series of cosmo-skymed data for Landcover classification and surface parameter retrieval over Agricultural sites', in *2011 IEEE International Geoscience and Remote Sensing Symposium*, pp. 6511–6514.

Balenzano, A., Satalino, G., Pauwels, V., *et al.* (2011) 'Soil moisture retrieval from dense temporal series of C-band SAR data over agricultural sites', in *International Geoscience and Remote Sensing Symposium (IGARSS)*. doi:

10.1109/IGARSS.2011.6049883.

Balenzano, A. *et al.* (2013) 'On the use of temporal series of L- and X-band SAR data for soil moisture retrieval. Capitanata plain case study', *European Journal of Remote Sensing*, 46(1), pp. 721–737. doi: 10.5721/EuJRS20134643.

Barbera, E. (2014) *COSMO-SkyMed polarimetric data for soil moisture retrieval: capability of SAR data for landslide monitoring*. Universit{à} degli Studi di Napoli Federico II.

Bertini, T. *et al.* (1984) 'Climatic conditions and slow movements of colluvial covers in Central Italy', in *Proc. IV Int. Symp. on Landslides, Toronto*, pp. 367–376.

Beven, K. J. (1981) 'Kinematic subsurface stormflow', *Water Resources Research*, 17(5), pp. 1419–1424. doi: 10.1029/WR017i005p01419.

Beven, K. J. (2011) *Rainfall-runoff modelling: the primer*. John Wiley & Sons.

BGS (2015a) 'How does BGS classify landslides?' Available at: http://www.bgs.ac.uk/landslides/how_does_BGS_classify_landslides.html.

BGS (2015b) 'Rainfall and landslide data for the UK, England, Scotland and Wales: updated monthly'. Available at: http://www.bgs.ac.uk/research/engineeringGeology/shallowGeohazardsAndRisks/landslides/landslidesAndRainfall.html.

BGS (2016) *The Hollin Hill Landslide Observatory, Yorkshire*. Available at: http://www.bgs.ac.uk/research/engineeringGeology/shallowGeohazardsAndRisks/landslides/hollinHill.html.

Bhandari, R. K. (1988) 'Special lecture: Some lessons in the investigation and field monitoring of landslides', in *5th International Symposium on Landslides*, pp. 1435–1457.

Biswas, A. (2014) 'Season- and depth-dependent time stability for characterising representative monitoring locations of soil water storage in a hummocky landscape', *Catena*, 116, pp. 38–50. doi: 10.1016/j.catena.2013.12.008.

Boerner, W.-M., Mott, H. and Luneburg, E. (1997) 'Polarimetry in remote sensing:

Basic and applied concepts', in *Geoscience and Remote Sensing, 1997. IGARSS'97. Remote Sensing-A Scientific Vision for Sustainable Development., 1997 IEEE International*, pp. 1401–1403.

Born, M. and Wolf, E. (1980) *Principles of Optics*. 6th edn. Cambridge: Cambridge University Press.

Bovenga, F. *et al.* (no date) 'Using COSMO/SkyMed X-band and ENVISAT C-band SAR interferometry for landslides analysis'. doi: 10.1016/j.rse.2011.12.013.

Brabb, E. (1991) 'The World Landslide Problem', *Episodes*, 14(1), pp. 52–61.

Brand, E. W. (1981) 'Some thoughts on rain-induced slope failures', in *Proceedings of the 10th International Conference on Soil Mechanics and Foundation Engineering, Stockholm*, pp. 373–376.

Brunsden, D. and Thornes, J. B. J. (1979) 'Landscape Sensitivity and Change', *Transactions of the Institute of British Geographers*, 4(4), pp. 463–484. doi: 10.2307/622210.

Bulmer, M. G. (1979) *Principles of Statistics*. New York: Dover.

Caine, N. (1980) 'The rainfall intensity-duration control of shallow landslides and debris flows', *Geografiska Annaler: Series A, Physical Geography*, 62(1), pp. 23–27.

Calabrese, D. *et al.* (2008) 'COSMO-SkyMed: Calibration & validation resources and activities', in *2008 IEEE Radar Conference, RADAR 2008*. doi: 10.1109/RADAR.2008.4721099.

Calvet, J. C. and Noilhan, J. (2000) 'From near-surface to root-zone soil moisture using year-round data', *Journal of Hydrometeorology*, 1(5), pp. 393–411. doi: 10.1175/1525-7541(2000)001<0393:FNSTRZ>2.0.CO;2.

Capodici, F. *et al.* (2011) 'On the influences of vegetation biomass on COSMO-Skymed X-band', in *SPIE Remote Sensing*.

Carlson, T. N., Gillies, R. R. and Perry, E. M. (1994) 'A method to make use of thermal infrared temperature and NDVI measurements to infer surface soil water content and fractional vegetation cover', *Remote Sensing Reviews*, 9(1–2),

pp. 161–173. doi: 10.1080/02757259409532220.

Casagli, N. *et al.* (1999) 'Pore water pressure and streambank stability: results from a monitoring site on the Sieve River, Italy', *Earth Surface Processes and Landforms*, 24(12), pp. 1095–1114.

Cascini, L., Fornaro, G. and Peduto, D. (2010) 'Advanced low- and full-resolution DInSAR map generation for slow-moving landslide analysis at different scales', *Engineering Geology*, 112(1–4), pp. 29–42. doi: 10.1016/j.enggeo.2010.01.003.

Centre for Ecology and Hydrology (2018) *COSMOS-UK User Guide v.2.10*.

Chambers, J. E. *et al.* (2008) 'Geophysical anatomy of the Hollin Hill landslide, North Yorkshire, UK', in *Near Surface 2008, Krakow, Poland, 15-17 Sept 2008*.

Chambers, J. E. *et al.* (2011) 'Three-dimensional geophysical anatomy of an active landslide in Lias Group mudrocks, Cleveland Basin, UK', *Geomorphology*, 125(4), pp. 472–484.

Chatwin, S. (1994) 'A guide for management of landslide-prone terrain in the Pacific Northwest'.

Chauhan, N. S., Miller, S. and Ardanuy, P. (2003) 'Spaceborne soil moisture estimation at high resolution: A microwave-optical/IR synergistic approach', *International Journal of Remote Sensing*, 24(22), pp. 4599–4622. doi: 10.1080/0143116031000156837.

Choi, M. and Jacobs, J. M. (2007) 'Soil moisture variability of root zone profiles within SMEX02 remote sensing footprints', *Advances in Water Resources*, 30(4), pp. 883–896.

Ciervo, F. *et al.* (2011) 'Use of high-resolution SAR data for the monitoring of water resources in Burkina Faso', in *SPIE Remote Sensing*, p. 817909.

Coe, J. A. (2012) 'Regional moisture balance control of landslide motion: Implications for landslide forecasting in a changing climate', *Geology*, 40(4), pp. 323–326.

Cohen, M., Hall, D. and Semedo, P. L. (2016) 'NovaSAR-S low cost SAR Payload', in *Proceedings of the European Conference on Synthetic Aperture Radar, EUSAR*.

Hamburg: VDE.

Colesanti, C. *et al.* (2003) 'SAR monitoring of progressive and seasonal ground deformation using the permanent scatterers technique', in *IEEE Transactions on Geoscience and Remote Sensing*, pp. 1685–1701. doi: 10.1109/TGRS.2003.813278.

Colesanti, C. and Wasowski, J. (2006) 'Investigating landslides with space-borne Synthetic Aperture Radar (SAR) interferometry', *Engineering Geology*, 88(3–4), pp. 173–199. doi: 10.1016/j.enggeo.2006.09.013.

Corominas, J. *et al.* (1999) 'Monitoring of the Vallcebre landslide, Eastern Pyrenees, Spain', *Yagi, Yamagami and Jiang Eds., Slope Stability Engineering, Balkema, Rotterdam*, pp. 1239–1244.

Corominas, J. *et al.* (2005) 'Prediction of ground displacements and velocities from groundwater level changes at the Vallcebre landslide (Eastern Pyrenees, Spain)', *Landslides*, 2(2), pp. 83–96. doi: 10.1007/s10346-005-0049-1.

Corsini, A. *et al.* (2006) 'Space-borne and ground-based SAR interferometry as tools for landslide hazard management in civil protection', *International Journal of Remote Sensing*, 27(12), pp. 2351–2369. doi: 10.1080/01431160600554405.

Coulomb, C. A. (1776) 'Essai sur une application des regles de maximis es minimis a quelques problemes de statique relatifs a l'architecture', *Memoires Academie Royale des Sciences*, 7.

Craig, R. F. (1995) *Soil mechanics*. Springer.

Crosta, G. B. and Frattini, P. (2001) 'Rainfall thresholds for the triggering of soil slips and debris flows', in *Mediterranean Storms 2000*, pp. 463–488.

Cruden, D. (1991) 'A simple definition of a landslide', *Bulletin of Engineering Geology and the Environment*.

Cruden, D. and Varnes, D. (1996) 'Landslide Types and Processes', in Turner, A. and Schuster, R. (eds) *Landslides Investigation and Mitigation*. Washington, DC: Transportation Research Board, US National Research Council, pp. 36–75.

Curlander, J. C. and Mcdonough, R. N. (1991) *Synthetic Aperture Radar*. New York: John Wiley & Sons.

D'Urso, G. and Minacapilli, M. (2006) 'A semi-empirical approach for surface soil water content estimation from radar data without a-priori information on surface roughness', *Journal of Hydrology*, 321(1–4), pp. 297–310. doi: 10.1016/j.jhydrol.2005.08.013.

Dahal, R. K. and Hasegawa, S. (2008) 'Representative rainfall thresholds for landslides in the Nepal Himalaya', *Geomorphology*, 100(3–4), pp. 429–443. doi: 10.1016/j.geomorph.2008.01.014.

Davidson, M. W. J. *et al.* (2000) 'On the characterization of agricultural soil roughness for radar remote sensing studies', *IEEE Transactions on Geoscience and Remote Sensing*, 38(2 I), pp. 630–640. doi: 10.1109/36.841993.

Davidson, M. W. J. *et al.* (2001) 'Improving soil moisture retrieval by incorporating a priori information on roughness parameters', in *International Geoscience and Remote Sensing Symposium (IGARSS)*, pp. 1306–1308. doi: 10.1109/igarss.2001.976827.

Decagon Devices (2016) *5TE, Water Content, EC and Temperature Sensor*.

Delta T Devices (1999) *Theta Probe Soil Moisture Sensor, Type ML2x User Manual ML2x-UM-1.21*. Cambridge.

Dille, A. *et al.* (2021) 'When image correlation is needed: Unravelling the complex dynamics of a slow-moving landslide in the tropics with dense radar and optical time series', *Remote Sensing of Environment*, 258, p. 112402. doi: 10.1016/j.rse.2021.112402.

Dobson, M., Ulaby, F. and Hallikainen, M. (1985) 'Microwave dielectric behavior of wet soil—Part II: Dielectric mixing models', *IEEE Trans. Geosci.*

Dubois, P. C., Van Zyl, J. and Engman, T. (1995) 'Measuring soil moisture with imaging radars', *Geoscience and Remote Sensing, IEEE Transactions on*, 33(4), pp. 915–926.

e-geos (no date) *COSMO-SkyMed Image Calibration*. Available at: https://egeos.my.salesforce.com/sfc/p/#1r000000qoOc/a/1r000000kUNA/tm1AYuYs45y6AUb9E5bJZc8Dp8dWNIa0nxE8ZaJCms4.

Eineder, M. *et al.* (2009) 'Spaceborne spotlight SAR interferometry with

TerraSAR-X', *IEEE Transactions on Geoscience and Remote Sensing*, 47(5), pp. 1524–1535. doi: 10.1109/TGRS.2008.2004714.

Eliason, E. M. and McEwen, A. S. (1990) 'Adaptive box filters for removal of random noise from digital images', *Photogrametric Engineering and Remote Sensing*, 56(4), pp. 453–458.

Engman, E. T. (1991) 'Applications of microwave remote sensing of soil moisture for water resources and agriculture', *Remote Sensing of Environment*, 35(2), pp. 213–226.

Engman, E. T. and Chauhan, N. (1995) 'Status of microwave soil moisture measurements with remote sensing', *Remote Sensing of Environment*, 51(1), pp. 189–198.

Eriksson, M. *et al.* (2009) *Impact of Climate Change on Water Resources and Livelihoods in the Greater Himalayas*, *The Changing Himalayas*. Kathmandu: ICIMOD.

ESA (2020) 'SNAP 7.0'.

Evans, H. *et al.* (2013) 'Mapping a nation's landslides: A novel multi-stage methodology', in *Landslide Science and Practice: Landslide Inventory and Susceptibility and Hazard Zoning*. Springer Science and Business Media Deutschland GmbH, pp. 21–27. doi: 10.1007/978-3-642-31325-7_2.

Fersch, B. *et al.* (2018) 'Synergies for Soil Moisture Retrieval Across Scales From Airborne Polarimetric SAR, Cosmic Ray Neutron Roving, and an In Situ Sensor Network', *Water Resources Research*, 54(11). doi: 10.1029/2018WR023337.

Fontanelli, G. *et al.* (2013) 'HydroCosmo: The monitoring of hydrological parameters on agricultural areas by using Cosmo-SkyMed images', *European Journal of Remote Sensing*, 46, pp. 875–889.

Foster, C., Jenkins, G. O. and Gibson, A. (2007) 'Landslides and mass movement processes and their distribution in the York District (Sheet 63)'. British Geological Survey.

Freer, J. *et al.* (2002) 'The role of bedrock topography on subsurface storm flow', *Water Resources Research*, 38(12), pp. 5-1-5–16. doi: 10.1029/2001WR000872.

Frost, V. S. *et al.* (1982) 'A Model for Radar Images and Its Application to Adaptive Digital Filtering of Multiplicative Noise', *IEEE Transactions on Pattern Analysis and Machine Intelligence*, PAMI-4(2), pp. 157–166. doi: 10.1109/TPAMI.1982.4767223.

Froude, M. J. (2011) *Capturing and characterising pre-failure strain on failing slopes*. Durham University.

Fung, A. (1994) *Microwave Scattering and Emission Models and their Applications*. Boston: Artech House, Inc.

Gallart, F. *et al.* (1997) 'Hydrological functioning of mediterranean mountain basins in Vallcebre, Catalonia: Some challenges for hydrological modelling', *Hydrological Processes*, 11(9), pp. 1263–1272. doi: 10.1002/(SICI)1099-1085(199707)11:9<1263::AID-HYP556>3.0.CO;2-W.

Gallart, F. *et al.* (2008) 'Investigating hydrological regimes and processes in a set of catchments with temporary waters in Mediterranean Europe', *Hydrological sciences journal*, 53(3), pp. 618–628.

Gallart, F., Llorens, P. and Latron, J. (1994) 'Studying the role of old agricultural terraces on runoff generation in a small Mediterranean mountainous basin', *Journal of Hydrology*, 159(1–4), pp. 291–303. doi: 10.1016/0022-1694(94)90262-3.

GCOS-138 (2010) *Implementation Plan for the Global Observing System for Climate in Support of the UNFCCC*.

Gerrard, J. and Gardner, R. a. M. (2000) 'Relationships between rainfall and landsliding in the Middle Hills, Nepal', *Norsk Geografisk Tidsskrift - Norwegian Journal of Geography*, 54(2), pp. 74–81. doi: 10.1080/002919500423807.

Giacomelli, A. *et al.* (1995) 'Evaluation of surface soil moisture distribution by means of SAR remote sensing techniques and conceptual hydrological modelling', *Journal of hydrology*, 166(3), pp. 445–459.

Gibson, A. D. *et al.* (2013) 'Landslide management in the UK-the problem of managing hazards in a "low-risk" environment', *Landslides*, 10(5), pp. 599–610. doi: 10.1007/s10346-012-0346-4.

González, D. A., Ledesma, A. and Corominas, J. (2008) 'The viscous component in

slow moving landslides: A practical case', *Landslides and engineered slopes: from the past to the future*, 1, pp. 237–242.

Gorrab, A. *et al.* (2014) 'X-band Terrasar-X and COSMO-SkyMed SAR data for bare soil parameters estimation', in *Geoscience and Remote Sensing Symposium (IGARSS), 2014 IEEE International*, pp. 3224–3227.

Gorrab, A., Zribi, M., Baghdadi, N., Mougenot, B. and Chabaane, Z. L. (2015) 'Potential of X-Band TerraSAR-X and COSMO-SkyMed SAR Data for the Assessment of Physical Soil Parameters', *Remote Sensing*, 7(1), pp. 747–766.

Gorrab, A., Zribi, M., Baghdadi, N., Mougenot, B., Fanise, P., *et al.* (2015) 'Retrieval of both soil moisture and texture using TerraSAR-X images', *Remote Sensing*, 7(8), pp. 10098–10116. doi: 10.3390/rs70810098.

Gorrab, A. *et al.* (2016) 'Mapping of surface soil parameters (roughness, moisture and texture) using one radar X-band SAR configuration over bare agricultural semi-arid region', in *International Geoscience and Remote Sensing Symposium (IGARSS)*, pp. 3035–3038. doi: 10.1109/IGARSS.2016.7729785.

Granger, J. (1983) 'Shuttle Imaging Radar: A/B sensors', *Spaceborne Imaging Radar Symposium*.

Gray, A. *et al.* (1990) 'Synthetic aperture radar calibration using reference reflectors', 28(3), pp. 374–383. doi: 10.1109/36.54363.

Griffiths, G. and Wooding, M. (1996) 'Temporal Monitoring of Soil Moisture Using ERS-1 SAR Data', *Hydrological Processes*, 10(9), pp. 1127–1138.

Grimani, V. *et al.* (2008) *Cosmo-SkyMed end to end system calibration strategies and Evolution.*

Gritzner, M. L. *et al.* (2001) 'Assessing landslide potential using GIS, soil wetness modeling and topographic attributes, Payette River, Idaho', *Geomorphology*, 37(1), pp. 149–165.

Gunn, D. A. *et al.* (2013) 'Rapid observations to guide the design of systems for long-term monitoring of a complex landslide in the upper lias clays of North Yorkshire, UK', *Quarterly Journal of Engineering Geology and Hydrogeology*, 46(3), pp. 323–336. doi: 10.1144/qjegh2011-028.

Guzzetti, F. *et al.* (2009) 'Analysis of ground deformation detected using the SBAS-DInSAR technique in Umbria, Central Italy', *Pure and Applied Geophysics*, 166(8–9), pp. 1425–1459. doi: 10.1007/s00024-009-0491-4.

El Hajj, M. *et al.* (2015) 'Estimation of soil moisture using radar and optical images over Grassland areas', in *EGU General Assembly Conference Abstracts*, p. 1794.

El Hajj, M. *et al.* (2016) 'Soil moisture retrieval over irrigated grassland using X-band SAR data', *Remote Sensing of Environment*, 176. doi: 10.1016/j.rse.2016.01.027.

Hajnsek, I. *et al.* (2009) 'Potential of estimating soil moisture under vegetation cover by means of PolSAR', *Geoscience and Remote Sensing, IEEE Transactions on*, 47(2), pp. 442–454.

Hallikainen, M. T. *et al.* (1985) 'Microwave Dielectric Behavior of Wet Soil-Part I: Empirical Models and Experimental Observations', *IEEE Transactions on Geoscience and Remote Sensing*, GE-23(1), pp. 25–34. doi: 10.1109/TGRS.1985.289497.

Harris Geospatial (2020) *Adaptive Filters*. Available at: https://www.harrisgeospatial.com/docs/AdaptiveFilters.html.

Hassaballa, A. A., Althuwaynee, O. F. and Pradhan, B. (2014) 'Extraction of soil moisture from RADARSAT-1 and its role in the formation of the 6 December 2008 landslide at Bukit Antarabangsa, Kuala Lumpur', *Arabian Journal of Geosciences*, 7(7), pp. 2831–2840.

Hegarat-Mascle, L. *et al.* (2002) 'Soil moisture estimation from ERS/SAR data: Toward an operational methodology', *Geoscience and Remote Sensing, IEEE Transactions on*, 40(12), pp. 2647–2658.

Hobbs, P. R. N. *et al.* (2012) *Engineering geology of British rocks and soils: Lias Group*. British Geological Survey.

Hornacek, M. *et al.* (2012) 'Potential for high resolution systematic global surface soil moisture retrieval via change detection using Sentinel-1', *Selected Topics in Applied Earth Observations and Remote Sensing, IEEE Journal of*, 5(4), pp.

1303–1311.

Horton, R. E. (1933) 'The Rôle of infiltration in the hydrologic cycle', *Eos, Transactions American Geophysical Union*, 14(1), pp. 446–460. doi: 10.1029/TR014i001p00446.

Huisman, J. A. *et al.* (2001) 'Soil water content measurements at different scales: accuracy of time domain reflectometry and ground-penetrating radar', *Journal of Hydrology*, 245(1), pp. 48–58. doi: 10.1016/S0022-1694(01)00336-5.

Hungr, O., Leroueil, S. and Picarelli, L. (2014) 'The Varnes classification of landslide types, an update', *Landslides*, 11(2), pp. 167–194.

Huszár, T. *et al.* (1999) 'Climate change and soil moisture: A case study', *Physics and Chemistry of the Earth, Part A: Solid Earth and Geodesy*, 24(10), pp. 905–912. doi: 10.1016/S1464-1895(99)00134-9.

Hutchinson, D. G. and Moore, R. D. (2000) 'Throughflow variability on a forested hillslope underlain by compacted glacial till', *Hydrological Processes*, 14(10), pp. 1751–1766. doi: 10.1002/1099-1085(200007)14:10<1751::AID-HYP68>3.0.CO;2-U.

Iacobellis, V. *et al.* (2013) 'Inter-comparison of hydrological model simulations with time series of SAR-derived soil moisture maps', *European Journal of Remote Sensing*, 46, pp. 739–757.

Jagdhuber, T. *et al.* (2008) 'Pol-SAR time series for soil moisture estimation under vegetation', in *Synthetic Aperture Radar (EUSAR), 2008 7th European Conference on*, pp. 1–4.

Jebur, M. N., Pradhan, B. and Tehrany, M. S. (2014) 'Optimization of landslide conditioning factors using very high-resolution airborne laser scanning (LiDAR) data at catchment scale', *Remote Sensing of Environment*, 152, pp. 150–165.

Jenkins, G., Jones, L. D. and Gibson, A. D. (2006) 'Analysis of the Hollin Hill Landslide, Low Mowthorpe, North Yorkshire: field reconnaissance survey and proposed survey recommendations'.

Jenkins, G. O. *et al.* (2005) *Landslide Survey of North Yorkshire : Reconnaissance Report*. Available at: http://nora.nerc.ac.uk/7412/.

Jones, D. K. C. and Lee, E. M. (1994) *Landsliding in Great Britain*. Stationery Office Books (TSO).

Jordan, C. J. (2015) 'AS14-17: Hollin Hill Landslide Observatory: Performance assessment and validation of calibrated soil moisture products from S-/X-band full-pol airborne data for landsliding and soil erosion mapping', in *RSPSoc Conversazione 2015*.

Jordan, R. (1980) 'The Seasat-A synthetic aperture radar system', *IEEE Journal of Oceanic Engineering*.

Jordan, R., Huneycutt, B. and Werner, M. (1991) 'The SIR-C/X-SAR synthetic aperture radar system', *Proceedings of the IEEE*.

Kane, W. and Beck, T. (2000) 'Instrumentation practice for slope monitoring', *Engineering Geology Practice in Northern California*, pp. 1–20.

Kelly, A. C. *et al.* (2009) 'Constellations: A new paradigm for earth observations', in *International Geoscience and Remote Sensing Symposium (IGARSS)*. doi: 10.1109/IGARSS.2009.5418144.

Kerr, Y. H. (2007) 'Soil moisture from space: Where are we?', *Hydrogeology journal*, 15(1), pp. 117–120.

Kerr, Y. H. *et al.* (2010) 'The SMOS mission: New tool for monitoring key elements ofthe global water cycle', *Proceedings of the IEEE*, 98(5), pp. 666–687.

Kirk, T. (2003) *Physics for the IB Diploma: Standard and Higher Level*. Oxford University Press.

Knox, R. *et al.* (1991) 'Lower and Middle Jurassic sediments of the Cleveland Basin, NE England: shallow marine and paralic facies seen in their sequence stratigraphic context.', in British Sedimentological Research Group (ed.) *13th International Sedimentological Congress, Field Guide No. 5*.

Köhli, M. *et al.* (2015) 'Footprint characteristics revised for field-scale soil moisture monitoring with cosmic-ray neutrons', *Water Resources Research*, 51(7), pp. 5772–5790. doi: 10.1002/2015WR017169.

Koppen, W. (1936) *Handbuch der Klimatologie*. Edited by W. Koppen and R.

Geiger. Berlin. doi: 10.2307/200498.

Kornelsen, K. C. and Coulibaly, P. (2013) 'Advances in soil moisture retrieval from synthetic aperture radar and hydrological applications', *Journal of Hydrology*, 476, pp. 460–489.

Krieger, G., Moreira, A. and Fiedler, H. (2007) 'TanDEM-X: A satellite formation for high-resolution SAR interferometry', *on Geoscience and ….*

Kuras, O. *et al.* (2009) 'Monitoring hydraulic processes with automated time-lapse electrical resistivity tomography (ALERT)', *Comptes Rendus Geoscience*, 341(10), pp. 868–885.

Kweon, S.-K., Hwang, J.-H. and Oh, Y. (2012) 'COSMO SkyMed AO projects-soil moisture detection for vegetation fields based on a modified water-cloud model using COSMO-SkyMed SAR data', in *Geoscience and Remote Sensing Symposium (IGARSS), 2012 IEEE International*, pp. 1204–1207.

Kweon, S.-K., Hwang, J.-H. and Oh, Y. (2013) 'Development of a simple scattering model for radar backscatters of agricultural fields to be used in retrieving soil moisture', in *Geoscience and Remote Sensing Symposium (IGARSS), 2013 IEEE International*, pp. 2720–2723.

Kweon, S.-K. and Oh, Y. (2014) 'Estimation of soil moisture and surface roughness from single-polarized radar data for bare soil surface and comparison with dual- and quad-polarization cases', *Geoscience and Remote Sensing, IEEE Transactions on*, 52(7), pp. 4056–4064.

Lacasse, S. and Nadim, F. (2009) 'Landslide risk assessment and mitigation strategy', in *Landslides–disaster risk reduction*. Springer. doi: 10.1201/b15621.

Lark, R. M. (2011) 'Spatially nested sampling schemes for spatial variance components: Scope for their optimization', *Computers & Geosciences*, 37(10), pp. 1633–1641.

Latron, J. and Gallart, F. (2007) 'Seasonal dynamics of runoff-contributing areas in a small mediterranean research catchment (Vallcebre, Eastern Pyrenees)', *Journal of Hydrology*.

Lee, J.-S. *et al.* (1998) 'A new technique for noise filtering of SAR interferometric

phase images', *Geoscience and Remote Sensing, IEEE Transactions on*, 36(5), pp. 1456–1465.

Lee, J. Sen (1980) 'Digital Image Enhancement and Noise Filtering by Use of Local Statistics', *IEEE Transactions on Pattern Analysis and Machine Intelligence*, PAMI-2(2), pp. 165–168. doi: 10.1109/TPAMI.1980.4766994.

Van Leeuwen, W. J. D. *et al.* (2006) 'Multi-sensor NDVI data continuity: Uncertainties and implications for vegetation monitoring applications', *Remote Sensing of Environment*, 100(1), pp. 67–81. doi: 10.1016/j.rse.2005.10.002.

Legates, D. R. *et al.* (2011) 'Soil moisture: A central and unifying theme in physical geography', *Progress in Physical Geography*, 35(1), pp. 65–86.

Legendre, P. (1993) 'Spatial Autocorrelation: Trouble or New Paradigm?', *Ecology*, 74(6), pp. 1659–1673. doi: 10.2307/1939924.

Leroueil, S. (2004) 'Geotechnics of slopes before failure', *Landslides: evaluation and stabilization*, 1, pp. 863–884.

Liu, P. *et al.* (2013) 'Using advanced InSAR time series techniques to monitor landslide movements in Badong of the Three Gorges region, China', *International Journal of Applied Earth Observation and Geoinformation*, 21, pp. 253–264.

Lopes, A., Touzi, R. and Nezry, E. (1990) 'Adaptive Speckle Filters and Scene Heterogeneity', *IEEE Transactions on Geoscience and Remote Sensing*, 28(6), pp. 992–1000. doi: 10.1109/36.62623.

Malamud, B. D. *et al.* (2004) 'Landslide inventories and their statistical properties', *Earth Surface Processes and Landforms*, 29(6), pp. 687–711.

Malet, J., Maquaire, O. and Calais, E. (2002) 'The use of Global Positioning System techniques for the continuous monitoring of landslides', *Geomorphology*, 43(1–2), pp. 33–54. doi: 10.1016/S0169-555X(01)00098-8.

Malone, A. W. (2004) 'The Story of Quantified Risk and its Place in Slope Safety Policy in Hong Kong', in Glade, T., Anderson, M., and Crozier, M. J. (eds) *Landslide Hazard and Risk*. John Wiley & Sons.

Marchant, B. *et al.* (2013) 'A semi-wireless network to monitor soil moisture over

disparate spatial and temporal scales.', in *EGU General Assembly Conference Abstracts*, p. 5150.

Marin, C., Bovolo, F. and Bruzzone, L. (2015) 'Building change detection in multitemporal very high resolution SAR images', *IEEE Transactions on Geoscience and Remote Sensing*, 53(5), pp. 2664–2682. doi: 10.1109/TGRS.2014.2363548.

Martone, M. *et al.* (2010) 'Modified scattering decomposition for soil moisture estimation from polarimetric X-band data', in *IEEE GOLD Remote Sensing Conference*.

Massonnet, D. and Feigl, K. (1998) 'Radar interferometry and its application to changes in the Earth's surface', *Reviews of geophysics*. Available at: http://onlinelibrary.wiley.com/doi/10.1029/97RG03139/full (Accessed: 9 February 2017).

Matsuura, S., Asano, S. and Okamoto, T. (2008) 'Relationship between rain and/or meltwater, pore-water pressure and displacement of a reactivated landslide', *Engineering Geology*, 101(1–2), pp. 49–59. doi: 10.1016/j.enggeo.2008.03.007.

Mattia, F. *et al.* (2003) 'A comparison between soil roughness statistics used in surface scattering models derived from mechanical and laser profilers', in *IEEE Transactions on Geoscience and Remote Sensing*, pp. 1659–1671. doi: 10.1109/TGRS.2003.813359.

Mattia, F. *et al.* (2009) 'Soil moisture retrieval through a merging of multi-temporal L-band SAR data and hydrologic modelling', *Hydrology and Earth System Sciences*, 13(3), pp. 343–356. doi: 10.5194/hess-13-343-2009.

Mattia, F. *et al.* (2012) 'Time series of COSMO-SkyMed data for landcover classification and surface parameter retrieval over agricultural sites', in *Geoscience and Remote Sensing Symposium (IGARSS), 2012 IEEE International*, pp. 6511–6514.

Mattia, F. *et al.* (2020) 'Field Scale Soil Moisture from Time Series of Sentinel-1 Sentinel-2', in *2020 Mediterranean and Middle-East Geoscience and Remote Sensing Symposium, M2GARSS 2020 - Proceedings*. Institute of Electrical and Electronics Engineers Inc., pp. 176–179. doi:

10.1109/M2GARSS47143.2020.9105290.

McDonnell, J. J. (1990) 'The influence of macropores on debris flow initiation', *Quarterly Journal of Engineering Geology*, 23(4), pp. 325–331. doi: 10.1144/GSL.QJEG.1990.023.04.06.

Merritt, A. (2014) *4D geophysical monitoring of hydrogeological precursors to landslide activation*. University of Leeds.

Merritt, A. J. *et al.* (2013) '3D ground model development for an active landslide in Lias mudrocks using geophysical, remote sensing and geotechnical methods', *Landslides*, pp. 1–14.

Milledge, D. G. (2008) *Modelling shallow landslides: the importance of hydrological controls and lateral reinforcement*. Durham University.

Mironov, V. L. *et al.* (2004) 'Generalized refractive mixing dielectric model for moist soils', *IEEE Transactions on Geoscience and Remote Sensing*, 42(4), pp. 773–785. doi: 10.1109/TGRS.2003.823288.

Mironov, V. L. (2004) 'Spectral dielectric properties of moist soils in the microwave band', in *International Geoscience and Remote Sensing Symposium (IGARSS)*, pp. 3474–3477. doi: 10.1109/igarss.2004.1370455.

Mironov, V. L., Bobrov, P. P. and Mandrygina, V. M. (2004) 'Bound water spectroscopy for the soils with varying mineralogy', in *International Geoscience and Remote Sensing Symposium (IGARSS)*, pp. 3478–3480. doi: 10.1109/igarss.2004.1370456.

Mondini, A. *et al.* (2019) 'Sentinel-1 SAR Amplitude Imagery for Rapid Landslide Detection', *Remote Sensing*, 11(7), p. 760. doi: 10.3390/rs11070760.

Moon, W. *et al.* (2010) 'RADARSAT-2 and coastal applications: Surface wind, waterline, and intertidal flat roughness', *Proceedings of the*.

Moran, M. S. *et al.* (2000) 'Soil moisture evaluation using multi-temporal synthetic aperture radar (SAR) in semiarid rangeland', *Agricultural and Forest meteorology*, 105(1), pp. 69–80.

Morgenstern, N. R. and Price, V. E. (1965) 'The analysis of the stability of general

slip surfaces'.

Nemoto, Y. *et al.* (1991) 'Japanese Earth Resources Satellite-1 Synthetic Aperture Radar', *Proceedings of the IEEE*, 79(6), pp. 800–809. doi: 10.1109/5.90159.

Newton, R. W. *et al.* (1982) 'Soil Moisture Information and Thermal Microwave Emission', *IEEE Transactions on Geoscience and Remote Sensing*, GE-20(3), pp. 275–281. doi: 10.1109/TGRS.1982.350443.

Njoku, E. G. *et al.* (2003) 'Soil moisture retrieval from AMSR-E', *Geoscience and Remote Sensing, IEEE Transactions on*, 41(2), pp. 215–229.

Notarnicola, C. *et al.* (2010) 'Exploitation of C-and X-band SAR images for soil moisture change detection estimation in agricultural areas (Po Valley, Italy)', in *Remote Sensing*, pp. 78290G--78290G.

Obrośląk, R. and Dorozhynskyy, O. (2017) 'Selection of a semivariogram model in the study of spatial distribution of soil moisture', *Journal of Water and Land Development*, 35(1), pp. 161–166. doi: 10.1515/jwld-2017-0080.

Oh, Y., Kweon, S.-K. and Hwang, J.-H. (2013) 'Soil moisture retrieval from single-polarized measurements of well-calibrated radars for bare soil surfaces', in *Synthetic Aperture Radar (APSAR), 2013 Asia-Pacific Conference on*, pp. 45–48.

Oh, Y., Kwon, S.-G. and Hwang, J.-H. (2011) 'Soil moisture detection algorithm at X-band', in *Synthetic Aperture Radar (APSAR), 2011 3rd International Asia-Pacific Conference on*, pp. 1–4.

Oh, Y., Sarabandi, K. and Ulaby, F. T. (2002) 'Semi-empirical model of the ensemble-averaged differential Mueller matrix for microwave backscattering from bare soil surfaces', *IEEE Transactions on Geoscience and Remote Sensing*, 40(6), pp. 1348–1355. doi: 10.1109/TGRS.2002.800232.

Oh, Y., Sarabandi, K. and Ulaby, F. T. F. F. T. (1992) 'An empirical model and an inversion technique for radar scattering from bare soil surfaces', *Geoscience and Remote Sensing, IEEE Transactions on*, 30(2), pp. 370–381. doi: 10.1109/36.134086.

Olsen, R. C. (2007) *Remote sensing from air and space*. SPIE Press.

Ouchi, K. (2013) 'Recent trend and advance of synthetic aperture radar with selected topics', *Remote Sensing*, pp. 716–807. doi: 10.3390/rs5020716.

Ouellette, J. D. *et al.* (2017) 'A Time-Series Approach to Estimating Soil Moisture from Vegetated Surfaces Using L-Band Radar Backscatter', *IEEE Transactions on Geoscience and Remote Sensing*, 55(6), pp. 3186–3193. doi: 10.1109/TGRS.2017.2663768.

Paloscia, S. *et al.* (2012) 'Comparison of COSMO-SkyMed and TerraSAR-X data for the retrieval of land hydrological parameters', in *Geoscience and Remote Sensing Symposium (IGARSS), 2012 IEEE International*, pp. 5510–5513.

Paloscia, Simonetta *et al.* (2014) 'The Sensitivity of Cosmo-SkyMed Backscatter to Agricultural Crop Type and Vegetation Parameters', *Selected Topics in Applied Earth Observations and Remote Sensing, IEEE Journal of*, 7(7), pp. 2856–2868.

Paloscia, S *et al.* (2014) 'The use of COSMO-SkyMed images for retrieving snow depth and soil moisture in mountainous areas', in *Geoscience and Remote Sensing Symposium (IGARSS), 2014 IEEE International*, pp. 3654–3657.

Paloscia, S., Pettinato, S. and Santi, E. (2012) 'Combining L and X band SAR data for estimating biomass and soil moisture of agricultural fields', *European Journal of Remote Sensing*, 45(1).

Pelletier, J. D. *et al.* (1997) 'Scale-invariance of soil moisture variability and its implications for the frequency-size distribution of landslides', *Engineering Geology*, 48(3), pp. 255–268.

Pennington, C. *et al.* (2015) 'The National Landslide Database of Great Britain: Acquisition, communication and the role of social media', *Geomorphology*, 249, pp. 44–51. doi: 10.1016/j.geomorph.2015.03.013.

Peplinski, N. R., Ulaby, F. T. and Dobson, M. C. (1995) 'Dielectric Properties of Soils in the 0.3–1.3-GHz Range', *IEEE Transactions on Geoscience and Remote Sensing*, 33(3), pp. 803–807. doi: 10.1109/36.387598.

Petley, D. *et al.* (2005) 'The use of surface monitoring data for the interpretation of landslide movement patterns', *Geomorphology*.

Petley, D. N. (2008) 'The global occurrence of fatal landslides in 2007', *Geophysical*

*Research Abstracts*, 10(EGU2008–A–10487).

Pettinato, S. *et al.* (2013) 'The intercomparison of x-band SAR images from COSMO-SkyMed and TerraSAR-X satellites: Case studies', *Remote Sensing*, 5(6), pp. 2928–2942. doi: 10.3390/rs5062928.

Pettinato, S. *et al.* (2019) 'Exploiting the Synergy between Sentinel-1 and Cosmo Sky-Med Data for Snow Monitoring in Alpine Areas', in *International Geoscience and Remote Sensing Symposium (IGARSS)*. Institute of Electrical and Electronics Engineers Inc., pp. 5738–5741. doi: 10.1109/IGARSS.2019.8898945.

Phillips, J. D. (2006) 'Deterministic chaos and historical geomorphology: A review and look forward', *Geomorphology*, 76(1–2), pp. 109–121. doi: 10.1016/j.geomorph.2005.10.004.

Picarelli, L. (2007) 'Considerations about the Mechanics of Slow Active Landslides in Clay', in *Progress in Landslide Science*. Berlin, Heidelberg: Springer Berlin Heidelberg, pp. 27–45. doi: 10.1007/978-3-540-70965-7_3.

Pierson, T. C. (1983) 'Soil pipes and slope stability', *Quarterly Journal of Engineering Geology and Hydrogeology*, 16(1), pp. 1–11.

Powell, J. H. (1984) 'Lithostratigraphical nomenclature of the Lias Group in the Yorkshire Basin', in *Proceedings of the Yorkshire Geological and Polytechnic Society*, pp. 51–57.

Pratola, C. *et al.* (2014) 'Evaluation of a Global Soil Moisture Product from Finer Spatial Resolution SAR Data and Ground Measurements at Irish Sites', *Remote Sensing*, 6(9), pp. 8190–8219.

Punithraj, G., Pruthviraj, U. and Shetty, A. (2020) 'Surface Soil Moisture Retrieval Using C-Band Synthetic Aperture Radar (SAR) over Yanco Study Site, Australia—A Preliminary Study', in *Lecture Notes in Civil Engineering*. Springer, pp. 107–121. doi: 10.1007/978-981-13-7067-0_8.

QGIS.org (2020) 'QGIS Geographic Information System'. Open Source Geospatial Foundation Project. Available at: http://qgis.org.

Quesney, A. *et al.* (2000) 'Estimation of watershed soil moisture index from ERS/SAR data', *Remote Sensing of Environment*, 72(3), pp. 290–303. doi:

10.1016/S0034-4257(99)00102-9.

Quinn, P., Beven, K. and Chevallier, P. (1991) 'The prediction of hillslope flow paths for distributed hydrological modelling using digital terrain models', *Hydrological Processes*, 5, pp. 59–79.

Raney, R., Luscombe, A. and Langham, E. (1991) 'RADARSAT (SAR imaging)', *Proceedings of the Institute of British Geographers*, 79(6), pp. 839–849.

Ray, R. L. and Jacobs, J. M. (2007) 'Relationships among remotely sensed soil moisture, precipitation and landslide events', *Natural Hazards*, 43(2), pp. 211–222.

Ray, R. L. and Jacobs, J. M. (2008) 'Landslide susceptibility mapping using remotely sensed soil moisture', in *Geoscience and Remote Sensing Symposium, 2008. IGARSS 2008. IEEE International*, pp. III--47.

Ray, R. L., Jacobs, J. M. and Cosh, M. H. (2010) 'Landslide susceptibility mapping using downscaled AMSR-E soil moisture: A case study from Cleveland Corral, California, US', *Remote sensing of environment*, 114(11), pp. 2624–2636.

Reigber, A. *et al.* (2013) 'Very-high-resolution airborne synthetic aperture radar imaging: Signal processing and applications', *Proceedings of the IEEE*, 101(3), pp. 759–783.

Riccio, D. *et al.* (2012) 'Calibration of COSMO-SkyMed SAR data for hydrology applications', in *Geoscience and Remote Sensing Symposium (IGARSS), 2012 IEEE International*, pp. 844–847.

Robinson, D. A. *et al.* (2008) 'Soil Moisture Measurement for Ecological and Hydrological Watershed-Scale Observatories: A Review', *Vadose Zone Journal*, 7(1), pp. 358–389. doi: 10.2136/vzj2007.0143.

Rodionova, N. V. (2019) 'Correlation of the Sentinel 1 Radar Data with Ground-Based Measurements of the Soil Temperature and Moisture', *Izvestiya - Atmospheric and Ocean Physics*, 55(9), pp. 939–948. doi: 10.1134/S0001433819090421.

Rosenqvist, A., Shimada, M. and Ito, N. (2007) 'ALOS PALSAR: A pathfinder mission for global-scale monitoring of the environment', *IEEE Transactions on*.

Rosser, N. J. (2010) 'Landslides and Rockfalls', in Burt, T. and Allison, R. (eds) *Sediment Cascades: An Integrated Approach*. John Wiley & Sons, Ltd, pp. 55–87.

Ryu, D. *et al.* (2020) 'Multi-Temporal Assessment of X-Band SAR Soil Moisture Retrievals Across Growth Stages of a Dryland Wheat Field', in *International Geoscience and Remote Sensing Symposium (IGARSS)*. doi: 10.1109/IGARSS39084.2020.9323970.

Sabins, F. F. (1996) *Remote Sensing: Principles and Interpretation*. WH Freeman and Company, San Francisco, USA.

Sahebi, M. R. and Angles, J. (2010) 'An inversion method based on multi-angular approaches for estimating bare soil surface parameters from RADARSAT-1', *Hydrology and Earth System Sciences*, 14(11), pp. 2355–2366. doi: 10.5194/hess-14-2355-2010.

Sangwoo, K., Taehwa, L. and Yongchul, S. (2019) 'Estimation of High Resolution Soil Moisture Based on Sentinel-1 SAR Sensor', *Journal of the Korean Society of Agricultural Engineers*, 61(5), pp. 89–99. doi: 10.5389/KSAE.2019.61.5.089.

Santi, E. *et al.* (2011) 'The potential of multi-temporal COSMO-Skymed SAR images in monitoring soil and vegetation', in *Geoscience and Remote Sensing Symposium (IGARSS), 2011 IEEE International*, pp. 1532–1535.

Santi, E. *et al.* (2012) 'The retrieval and monitoring of vegetation parameters from COSMO-SkyMed images', in *Geoscience and Remote Sensing Symposium (IGARSS), 2012 IEEE International*, pp. 7031–7034.

Santi, E. *et al.* (2013) 'Comparison between SAR Soil Moisture Estimates and Hydrological Model Simulations over the Scrivia Test Site', *Remote Sensing*, 5(10), pp. 4961–4976.

Sarma, S. (1979) 'Stability analysis of embankments and slopes', *Journal of Geotechnical and Geoenvironmental*.

Satalino, G. *et al.* (2012) 'COSMO-SkyMed multi-temporal data for land cover classification and soil moisture retrieval over an agricultural site in Southern Australia', in *Geoscience and Remote Sensing Symposium (IGARSS), 2012 IEEE International*, pp. 5701–5704.

Schmugge, T. J. *et al.* (2002) 'Remote sensing in hydrology', *Advances in water resources*, 25(8), pp. 1367–1385.

Schmugge, T. J., Jackson, T. J. and McKim, H. L. (1980) 'Survey of methods for soil moisture determination', *Water Resources Research*, 16(6), pp. 961–979.

Schuster, R. L. and Highland, L. M. (2007) 'Overview of the effects of mass wasting on the natural environment', *Environmental & Engineering Geoscience*, 13(1), pp. 25–44.

Sekertekin, A., Marangoz, A. M. and Abdikan, S. (2020) 'ALOS-2 and Sentinel-1 SAR data sensitivity analysis to surface soil moisture over bare and vegetated agricultural fields', *Computers and Electronics in Agriculture*, 171, p. 105303. doi: 10.1016/j.compag.2020.105303.

Selby, M. J. (1983) 'Hillslope materials and processes.', *Hillslope materials and processes*.

Seneviratne, S. I. *et al.* (2010) 'Investigating soil moisture–climate interactions in a changing climate: A review', *Earth-Science Reviews*, 99(3), pp. 125–161. doi: 10.1016/j.earscirev.2010.02.004.

Serway, R. A., Beichner, R. J. and Jewett, J. W. (2000) *Physics for scientists and engineers with modern physics*. Saunders College.

Shaeffer, Tuley and Knott (2004) *Radar Cross Section*. 3rd edn, *Radar Cross Section*. 3rd edn. Edited by M. Skolnik. McGraw-Hill. doi: 10.1049/sbra026e.

Shi, H. *et al.* (2021) 'Soil moisture retrieval over agricultural fields from L-band multi-incidence and multitemporal PolSAR observations using polarimetric decomposition techniques', *Remote Sensing of Environment*, 261. doi: 10.1016/j.rse.2021.112485.

Shi, Jiancheng *et al.* (1991) 'Soil moisture measurements from airborne SAR', in *JPL Proceedings of the Third Airborne Synthetic Aperture Radar (AIRSAR) Workshop*.

Shi, J *et al.* (1991) 'Soil Moisture Measurements from Airborne SAR', in van Zyl, J. J. (ed.) *Proceedings from the Third Airborne Synthetic Aperture Radar (AIRSAR) Workshop, May 23-24, 1991, Pasadena*. (JPL publication), pp. 68–77.

Shi, J. *et al.* (1997) 'Estimation of bare surface soil moisture and surface roughness parameter using L-band SAR image data', *IEEE Transactions on*.

Shi, Z. and Fung, K. B. (1994) 'Comparison of digital speckle filters', in *International Geoscience and Remote Sensing Symposium (IGARSS)*. IEEE, pp. 2129–2133. doi: 10.1109/igarss.1994.399671.

Shimada, M. (2006) 'SAR programmes in JAXA: From JERS-1 to the future', in *IEE Proceedings: Radar, Sonar and Navigation*, pp. 122–128. doi: 10.1049/ip-rsn:20045125.

Shimada, M. (2010) 'Ortho-Rectification and Slope Correction of SAR Data Using DEM and Its Accuracy Evaluation', *IEEE Journal of Selected Topics in Applied Earth Observations and Remote Sensing*, 3(4), pp. 657–671. doi: 10.1109/JSTARS.2010.2072984.

Shoshany, M. *et al.* (2000) 'The relationship between ERS-2 SAR backscatter and soil moisture: generalization from a humid to semi-arid transect', *International Journal of Remote Sensing*, 21(11), pp. 2337–2343.

Shroder, J. F., Cvercková, L. and Mulhern, K. L. (2005) 'Slope-failure Analysis and Classification: Review of a Century of Effort', *Physical Geography*, 26(3), pp. 216–247. doi: 10.2747/0272-3646.26.3.216.

Sidle, R. C. and Swanston, D. N. (1982) 'Analysis of a small debris slide in coastal Alaska', *Canadian Geotechnical Journal*, 19(2), pp. 167–174. doi: 10.1139/t82-018.

Silva Guimarães, U. *et al.* (2020) 'Cosmo-SkyMed and TerraSAR-X datasets for geomorphological mapping in the eastern of Marajó Island, Amazon coast', *Geomorphology*, 350, p. 106934. doi: 10.1016/j.geomorph.2019.106934.

Skempton, A. and Hutchinson, J. (1969) 'Stability of natural slopes and embankment foundation. State of the Art Report', *Proceedings of the 7th International Conference on*.

Skempton, A. W. (1985) 'Residual strength of clays in landslides, folded strata and the laboratory', *Géotechnique*, 35(1), pp. 3–18. doi: 10.1680/geot.1985.35.1.3.

Snoeij, P. *et al.* (2009) 'The Sentinel-1 radar mission: status and performance', in

*Radar Conference-Surveillance for a Safer World, 2009. RADAR. International*, pp. 1–6.

Song, K., Zhou, X. and Fan, Y. (2009) 'Empirically adopted IEM for retrieval of soil moisture from radar backscattering coefficients', in *IEEE Transactions on Geoscience and Remote Sensing*, pp. 1662–1672. doi: 10.1109/TGRS.2008.2009061.

Sportouche, H. *et al.* (2012) 'How to combine TerraSAR-X and Cosmo-SkyMed high-resolution images for a better scene understanding?', in *International Geoscience and Remote Sensing Symposium (IGARSS)*, pp. 178–181. doi: 10.1109/IGARSS.2012.6351608.

Srivastava, H. S. *et al.* (2008) 'Retrieval of surface roughness using multi-polarized Envisat-1 ASAR data', *Geocarto International*, 23(1), pp. 67–77. doi: 10.1080/10106040701538157.

Srivastava, H. S. *et al.* (2009) 'Large-area soil moisture estimation using multi-incidence-angle RADARSAT-1 SAR data', *IEEE Transactions on Geoscience and Remote Sensing*, 47(8), pp. 2528–2535. doi: 10.1109/TGRS.2009.2018448.

Stocker, T. F. *et al.* (2013) *IPCC, 2013: Climate Change 2013: The Physical Science Basis. Contribution of working group I to the fifth assessment report of the intergovernmental panel on climate change*. Cambridge University Press.

Strozzi, T. *et al.* (2005) 'Survey and monitoring of landslide displacements by means of L-band satellite SAR interferometry', *Landslides*, pp. 193–201. doi: 10.1007/s10346-005-0003-2.

Telespazio (2019) *The first COSMO-SkyMed Second Generation satellite has been launched successfully*. Available at: https://www.telespazio.com/en/news-and-stories-detail/-/detail/171219-the-first-second-generation-cosmo-skymed-satellite-has-been-launched-successfully?f=%2Fpress-release-detail.

Terlien, M. T. J. (1996) *Modelling Spatial and Temporal Variations in Rainfall-triggered Landslides: The Integration of Hydrologic Models, Slope Stability Models and Geographic Information Systems for the Hazard Zonation of Rainfall-triggered Landslides with Examples from Manizal*. International Institute for Aerial Survey and Earth Sciences (ITC).

Terzaghi, K. (1950) 'Mechanisms of landslides', in Paige, S. (ed.) *Application of geology to engineering practice*. Berkley: Geological Society of America, pp. 83–123.

Terzaghi, K., Peck, R. B. and Mesri, G. (1996) *Soil mechanics in engineering practice*. Wiley.

Terzaghi, K. Van (1936) 'The shearing resistance of saturated soils', in *Proceedings of the 1st International Conference on Soil Mechanics and Foundation Engineering*. Cambridge, MA.

Tetzlaff, D. *et al.* (2008) 'Conceptualizing catchment processes: simply too complex?', *Hydrological Processes*, 22(11), pp. 1727–1730. doi: 10.1002/hyp.7069.

Teuling, A. J. and Troch, P. A. (2005) 'Improved understanding of soil moisture variability dynamics', *Geophysical Research Letters*, 32(5).

The Jamovi Project (2020) 'jamovi'. Available at: https://www.jamovi.org/.

Thiebes, B. (2012) *Landslide Analysis and Early Warning Systems: Local and Regional Case Study in the Swabian Alb, Germany*. Springer.

Torre, A. and Capece, P. (2011) 'COSMO-SkyMed: The advanced SAR instrument', in *RAST 2011 - Proceedings of 5th International Conference on Recent Advances in Space Technologies*, pp. 865–868. doi: 10.1109/RAST.2011.5966966.

Torres, R. *et al.* (2012) 'GMES Sentinel-1 mission', *Remote Sensing of Environment*, 120, pp. 9–24.

Uhlemann, S. *et al.* (2016) 'Assessment of ground-based monitoring techniques applied to landslide investigations', *Geomorphology*, 253, pp. 438–451. doi: 10.1016/j.geomorph.2015.10.027.

Ulaby, F. T., Moore, R. K. and Fung, A. K. (1981) *Microwave Remote Sensing Active and Passive - Volume 1: Microwave Remote Sensing Fundamentals and Radiometry*. Addison-Wesley Publishing CompanyAdvanced Book Program/World Science Division.

Ulaby, F. T., Moore, R. K. and Fung, A. K. (1982) *Microwave Remote Sensing*

*Active and Passive-Volume II: Radar Remote Sensing and Surface Scattering and Emission Theory*. Addison-Wesley Publishing CompanyAdvanced Book Program/World Science Division.

Ulaby, F. T., Moore, R. K. and Fung, A. K. (1986) *Microwave Remote Sensing Active and Passive Volume III: From Theory to Applications*. Edited by D. S. Simonett. Artech House, Inc.

Vachaud, G. *et al.* (1985) 'Temporal Stability of Spatially Measured Soil Water Probability Density Function', *Soil Science Society of America Journal*, 49(4), pp. 822–828. doi: 10.2136/sssaj1985.03615995004900040006x.

Varnes, D. J. (1978) 'Slope movement types and processes', *Transportation Research Board Special Report*, (176).

Vereecken, H. *et al.* (2008) 'On the value of soil moisture measurements in vadose zone hydrology: A review', *Water Resources Research*, 44(4). doi: 10.1029/2008WR006829.

Verhoest, N. E. C. *et al.* (2008) 'On the soil roughness parameterization problem in soil moisture retrieval of bare surfaces from synthetic aperture radar', *Sensors*. MDPI, pp. 4213–4248. doi: 10.3390/s8074213.

Wagner, W. *et al.* (1999) 'A study of vegetation cover effects on ERS scatterometer data', *Geoscience and Remote Sensing, IEEE Transactions on*, 37(2), pp. 938–948.

Wagner, W. *et al.* (2003) 'Evaluation of the agreement between the first global remotely sensed soil moisture data with model and precipitation data', *Journal of Geophysical Research: Atmospheres (1984-2012)*, 108(19).

Wagner, W. and Pathe, G. (2005) 'Has SAR failed in soil moisture retrieval?', in *European Space Agency, (Special Publication) ESA SP*.

Wainwright, J. and Mulligan, M. (2013) *Environmental modelling: finding simplicity in complexity*. John Wiley & Sons.

Wang, H., Magagi, R. and Goita, K. (2017) 'Comparison of different polarimetric decompositions for soil moisture retrieval over vegetation covered agricultural area', *Remote Sensing of Environment*, 199, pp. 120–136. doi: 10.1016/j.rse.2017.07.008.

Wang, S. G. *et al.* (2011) 'Estimation of surface soil moisture and roughness from multi-angular ASAR imagery in theWatershed Allied Telemetry Experimental Research (WATER)', *Hydrology and Earth System Sciences*, 15(5), pp. 1415–1426. doi: 10.5194/hess-15-1415-2011.

Wang, X., Ge, L. and Li, X. (2013) 'Pasture Monitoring Using SAR with COSMO-SkyMed, ENVISAT ASAR, and ALOS PALSAR in Otway, Australia', *Remote Sensing*, 5(7), pp. 3611–3636.

Western, A. W. *et al.* (2004) 'Spatial correlation of soil moisture in small catchments and its relationship to dominant spatial hydrological processes', *Journal of Hydrology*, 286(1–4), pp. 113–134. doi: 10.1016/j.jhydrol.2003.09.014.

Western, A. W. and Blöschl, G. (1999) 'On the spatial scaling of soil moisture', *Journal of Hydrology*, 217(3–4), pp. 203–224. doi: 10.1016/S0022-1694(98)00232-7.

Western, A. W., Grayson, R. B. and Blöschl, G. (2002) 'Scaling of Soil Moisture: A Hydrologic Perspective', *Annual Review of Earth and Planetary Sciences*, 30(1), pp. 149–180. doi: 10.1146/annurev.earth.30.091201.140434.

White, I. *et al.* (1994) 'Comments on "Considerations on the use of time-domain reflectometry (TDR) for measuring soil water content" by W.R. Whalley', *European Journal of Soil Science*, 45(4), pp. 503–508. doi: 10.1111/j.1365-2389.1994.tb00536.x.

Wieczorek, G. (1996) 'Landslide triggering mechanisms', in Turner, K. A. and Schuster, R. L. (eds) *Landslides: investigation and mitigation (Special Report)*, pp. 76–90.

Wieczorek, G. F. (1987) 'Effect of rainfall intensity and duration on debris flows in central Santa Cruz Mountains, California', *Reviews in Engineering Geology*, 7, pp. 93–104.

Wiley, C. A. (1985) 'Synthetic aperture radars: A paradigm for technology evolution', *IEEE Trans. Aerospace Elec. Sys*, 21(3), pp. 440–443. doi: 10.1109/TAES.1985.310578.

Wilheit, T. T. (1978) 'Radiative Transfer in a Plane Stratified Dielectric', *IEEE*

*Transactions on Geoscience Electronics*, 16(2), pp. 138–143. doi: 10.1109/TGE.1978.294577.

Yang, W., Wang, M. and Shi, P. (2013) 'Using MODIS NDVI time series to identify geographic patterns of landslides in vegetated regions', *IEEE Geoscience and Remote Sensing Letters*, 10(4), pp. 707–710. doi: 10.1109/LGRS.2012.2219576.

Zakharov, I. *et al.* (2020) 'Retrieval of Surface Soil Moisture from Sentinel-1 Time Series for Reclamation of Wetland Sites', *IEEE Journal of Selected Topics in Applied Earth Observations and Remote Sensing*, 13, pp. 3569–3578. doi: 10.1109/JSTARS.2020.3004062.

Zhang, H. *et al.* (2012) 'Improvement of pol sar calibration based on the ainsworth algorithm', in *Proceedings of the European Conference on Synthetic Aperture Radar, EUSAR*.

Zhang, H. *et al.* (2015) 'Spatial analysis of Wenchuan Earthquake-damaged vegetation in the mountainous basins and its applications', *Remote Sensing*, 7(5), pp. 5785–5804. doi: 10.3390/rs70505785.

Zhu, L. *et al.* (2018) 'Soil moisture retrieval over agricultural fields from time series multi-angular L-band radar data', in *International Geoscience and Remote Sensing Symposium (IGARSS)*. Institute of Electrical and Electronics Engineers Inc., pp. 6139–6142. doi: 10.1109/IGARSS.2018.8518119.

Zhu, L. *et al.* (2019) 'Roughness and vegetation change detection: A pre-processing for soil moisture retrieval from multi-temporal SAR imagery', *Remote Sensing of Environment*, 225, pp. 93–106. doi: 10.1016/j.rse.2019.02.027.

Zribi, M. *et al.* (2019) 'Analysis of L-Band SAR Data for Soil Moisture Estimations over Agricultural Areas in the Tropics', *Remote Sensing*, 11(9), p. 1122. doi: 10.3390/rs11091122.

Zribi, M. and Baghdadi, N. (2015) 'Analysis of soil properties using high resolution radar remote sensing, Soils and Sediments as Archives of Environmental Change', in Lucke, B., Bäumler, R., and Schmidt, M. (eds) *Geoarchaeology and Landscape Change in the Subtropics and Tropics*. Erlangen, Germany: Fränkische Geographische Gesellschaft.

# Appendix 1 – CSK imagery

This appendix presents the 9 full images CSK Spotlight images and subsets of the field site without any processing. The sensor number for each image is shown.

June – CSK 2 – HH – Spotlight - Full Scene

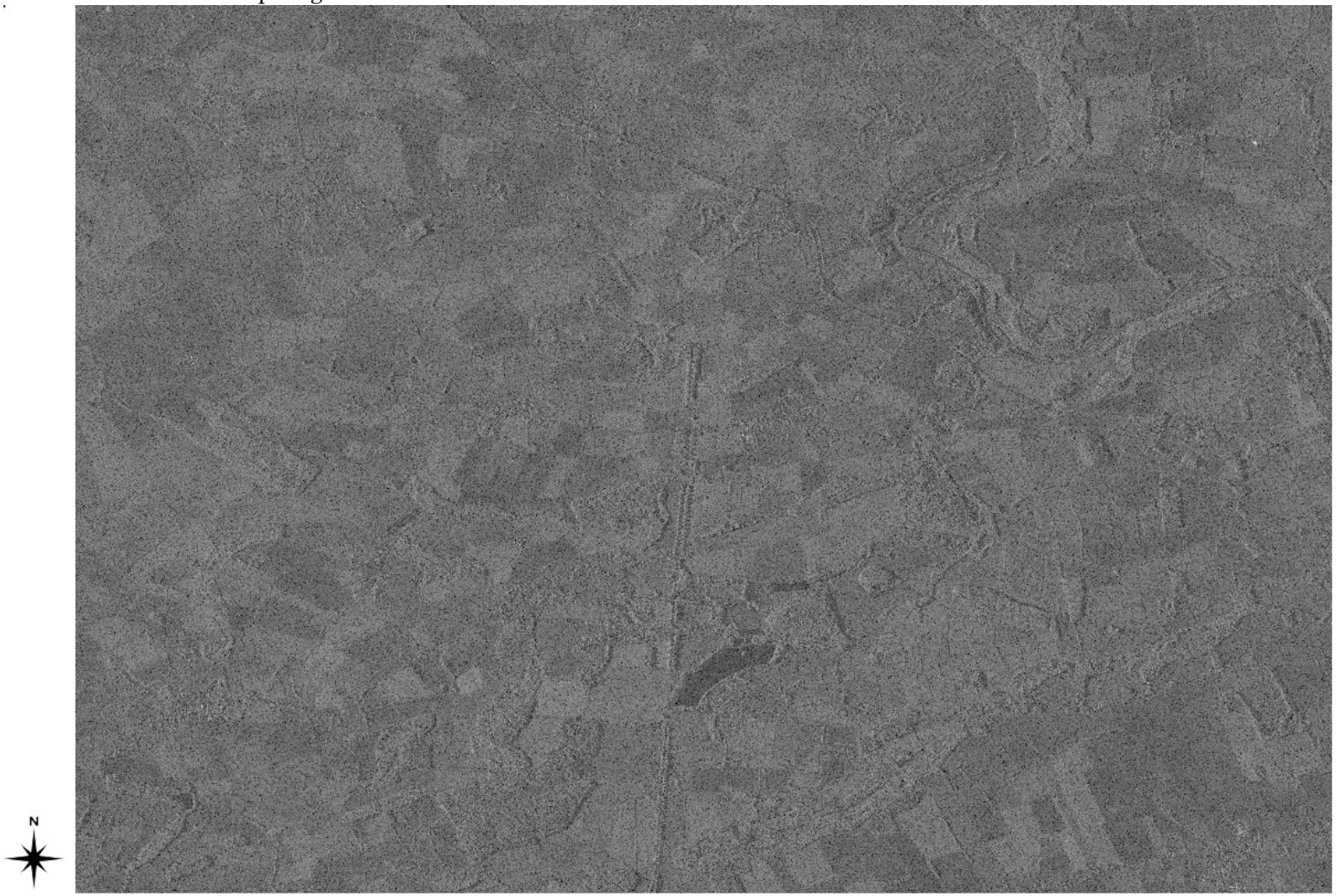

July – CSK4 - HH- Spotlight - Full Scene

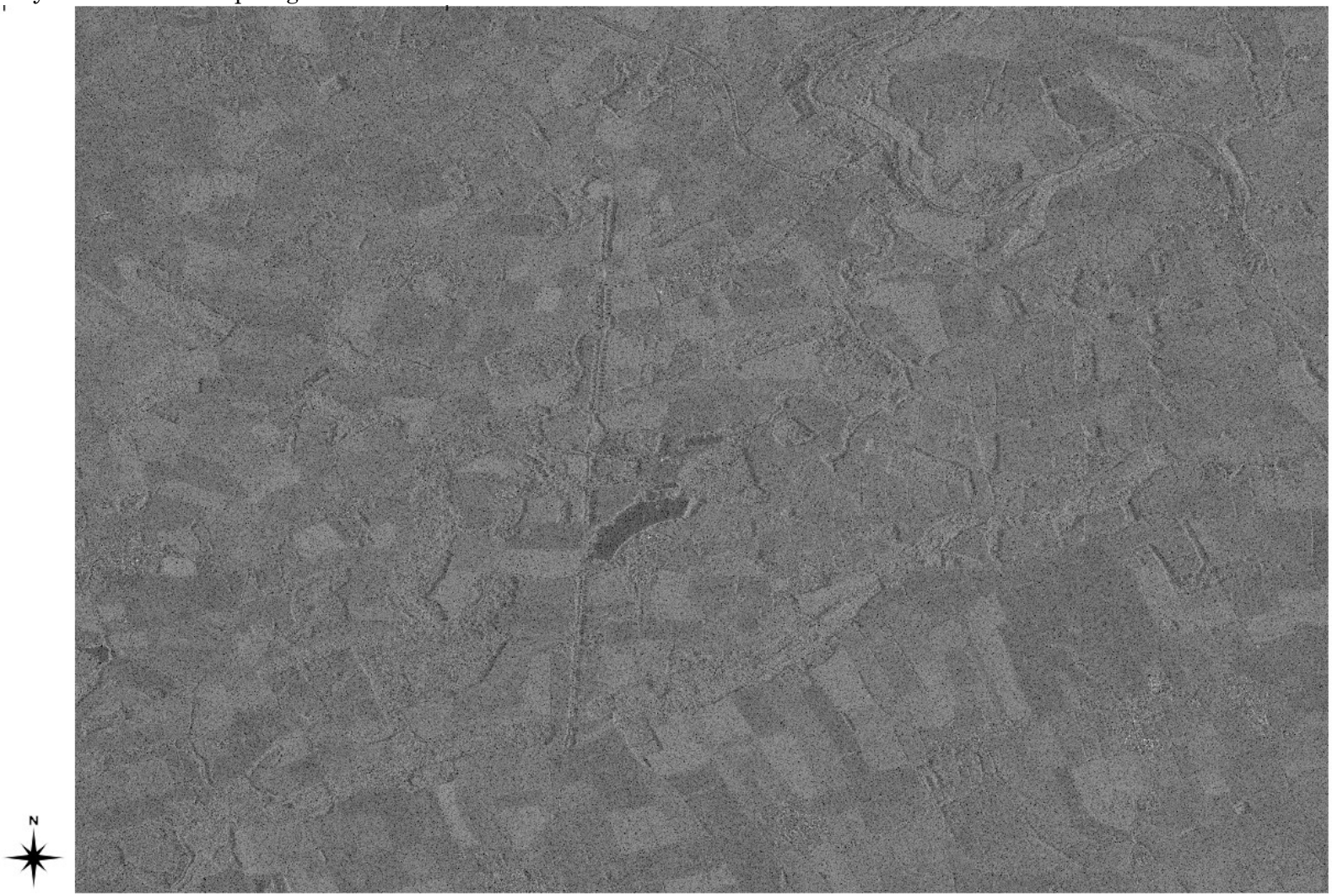

August – CSK4 – HH – Spotlight - Full Scene

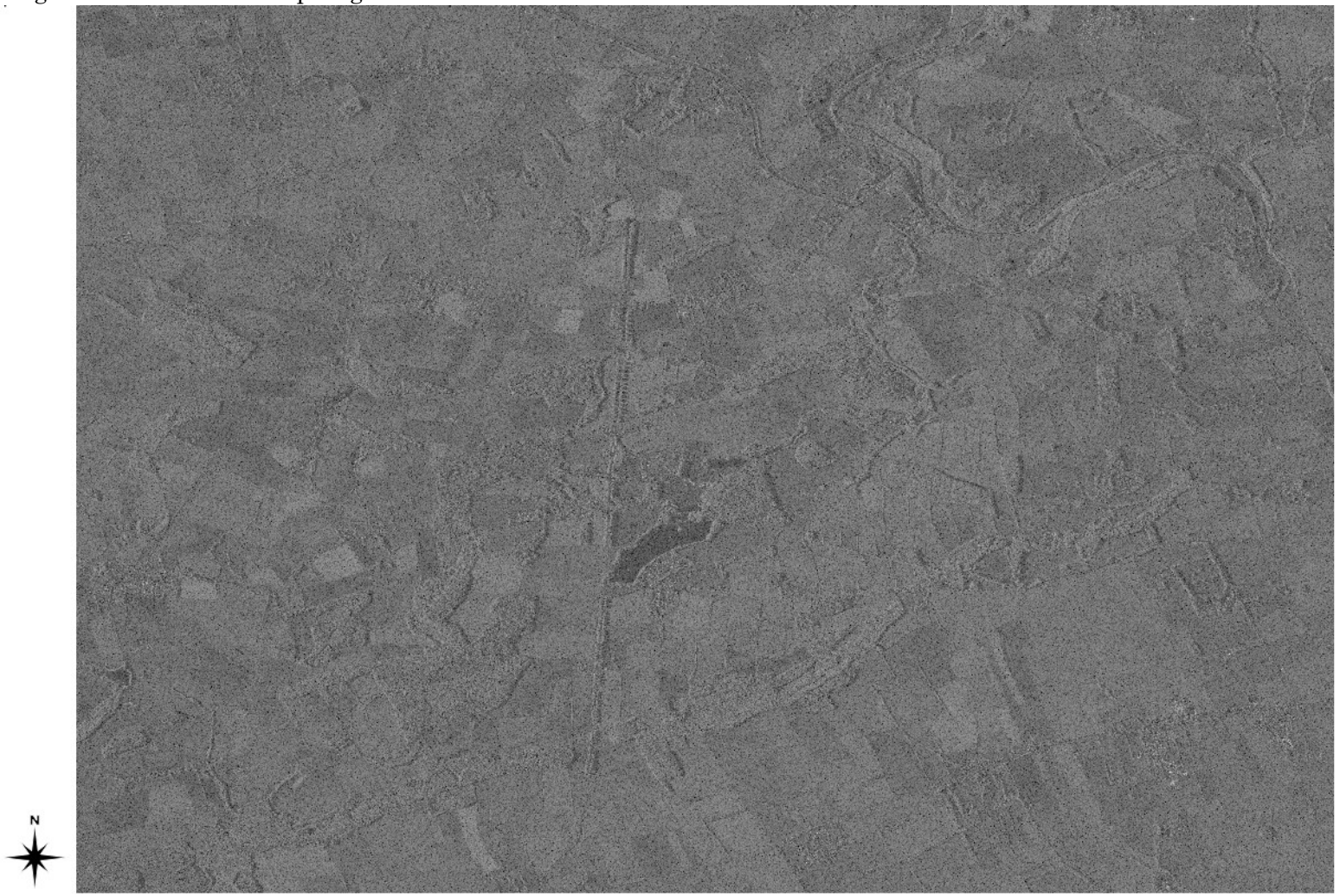

September – CSK3 – HH – Spotlight - Full Scene

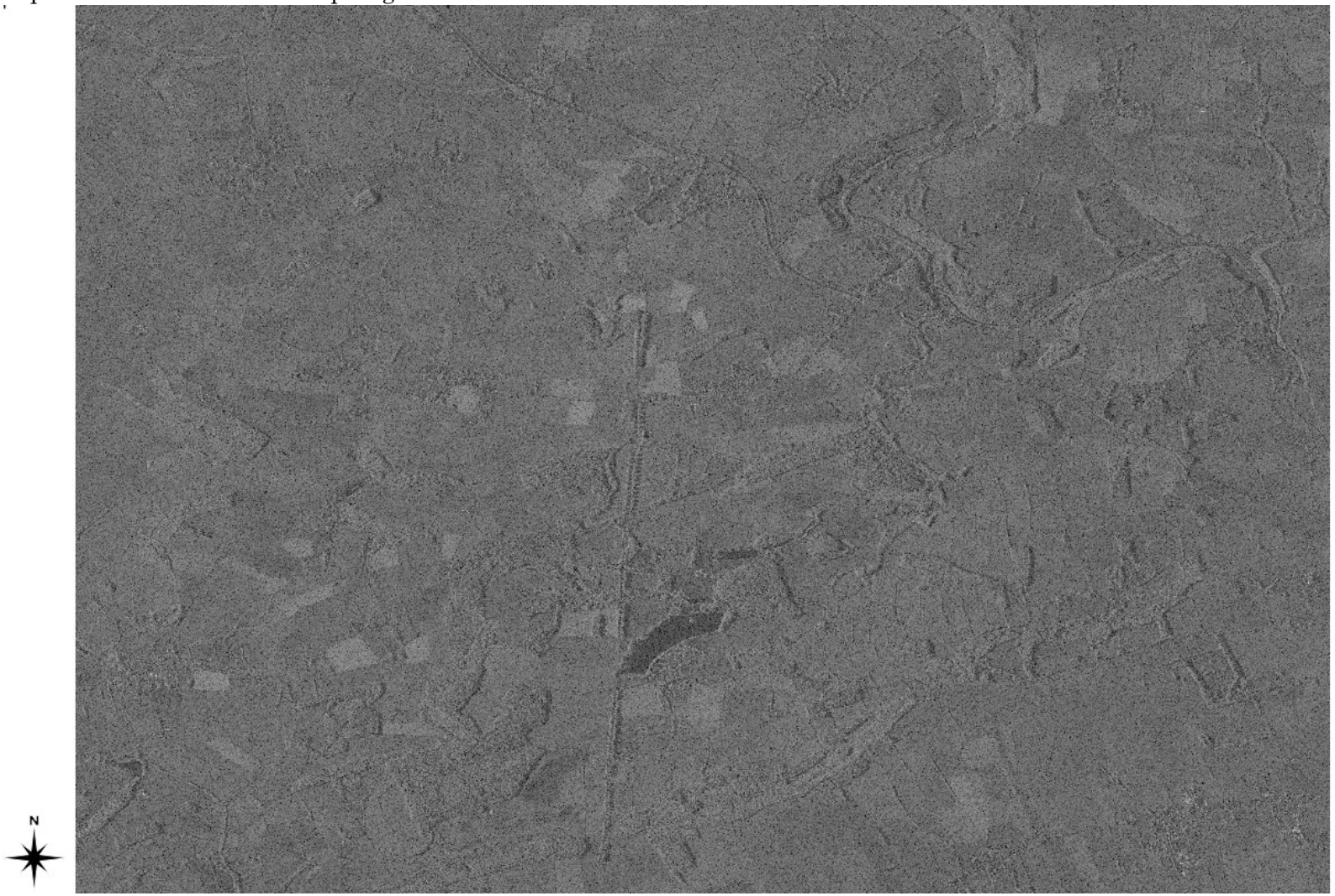

October – CSK4 – HH – Spotlight - Full Scene

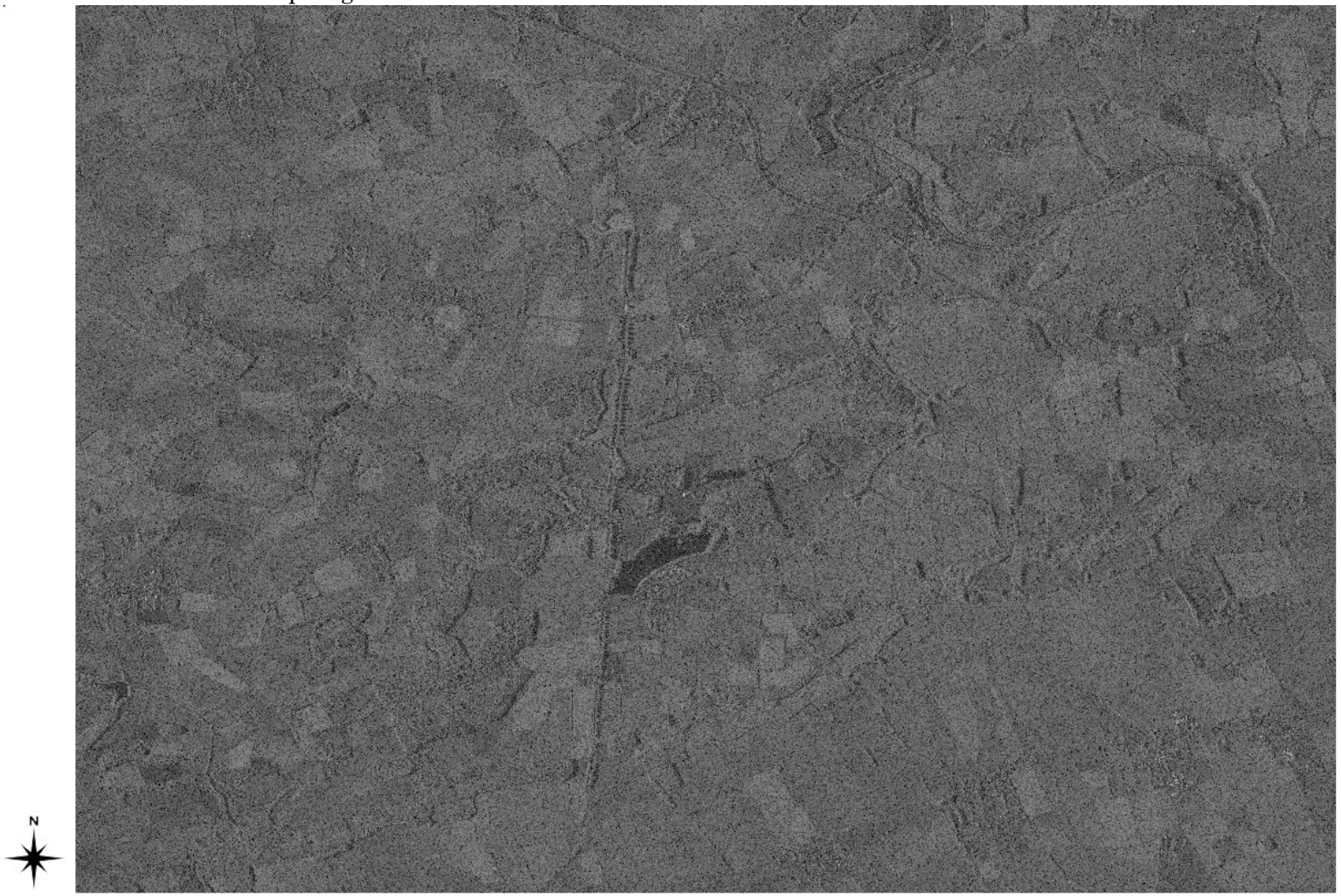

November – CSK3 – HH – Spotlight - Full Scene

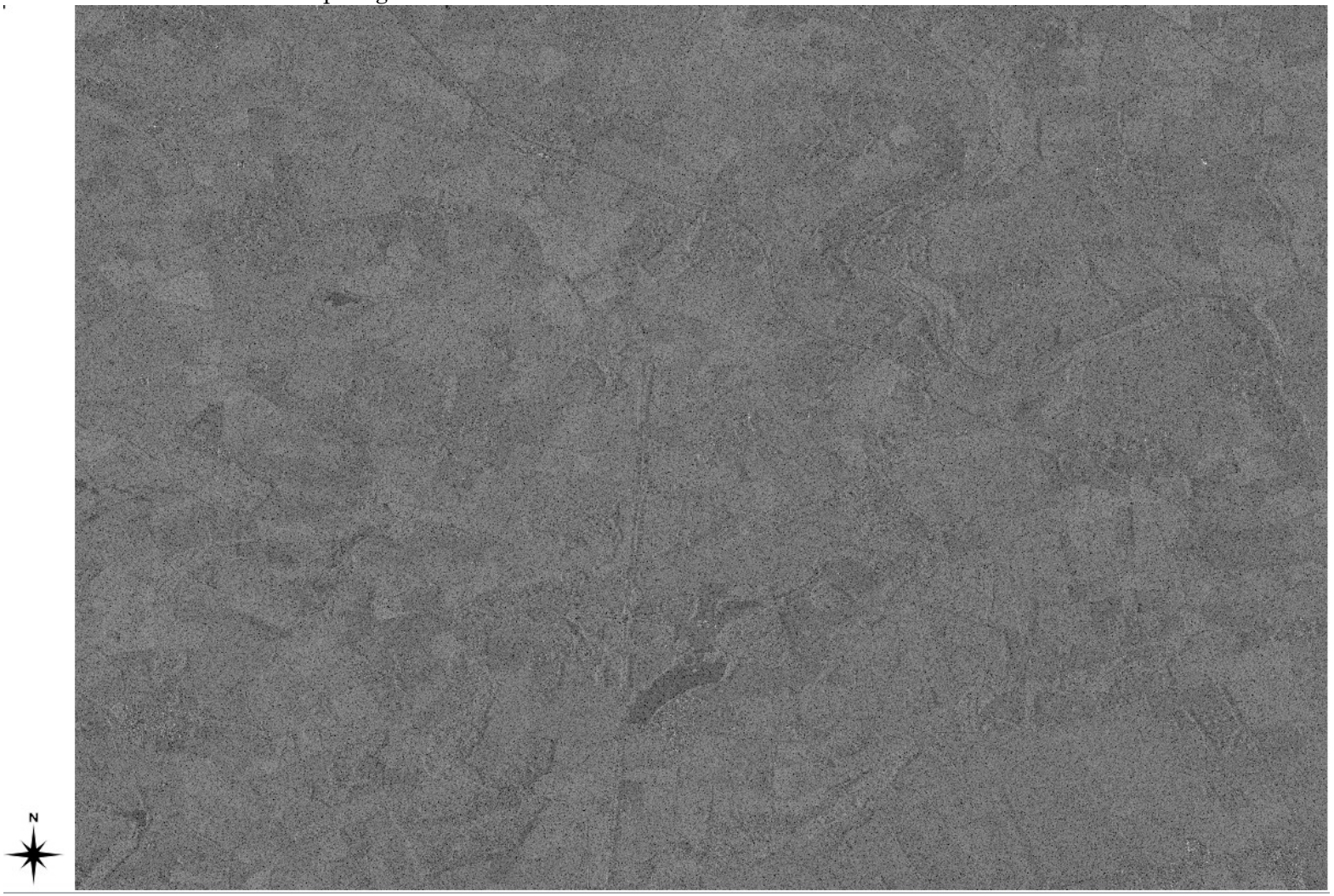

December – CSK4 – HH – Spotlight - Full Scene

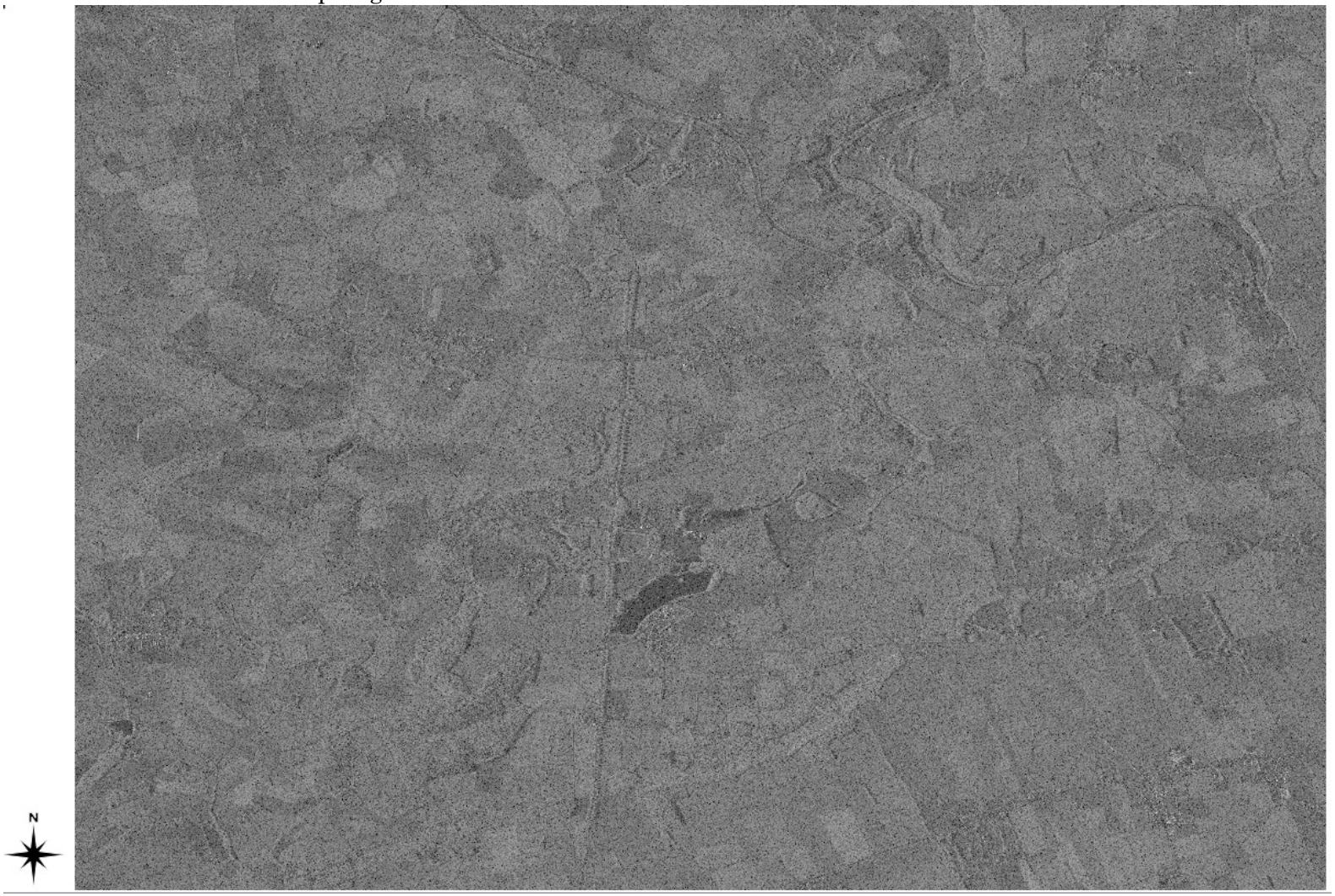

January – CSK3 – HH – Spotlight - Full Scene

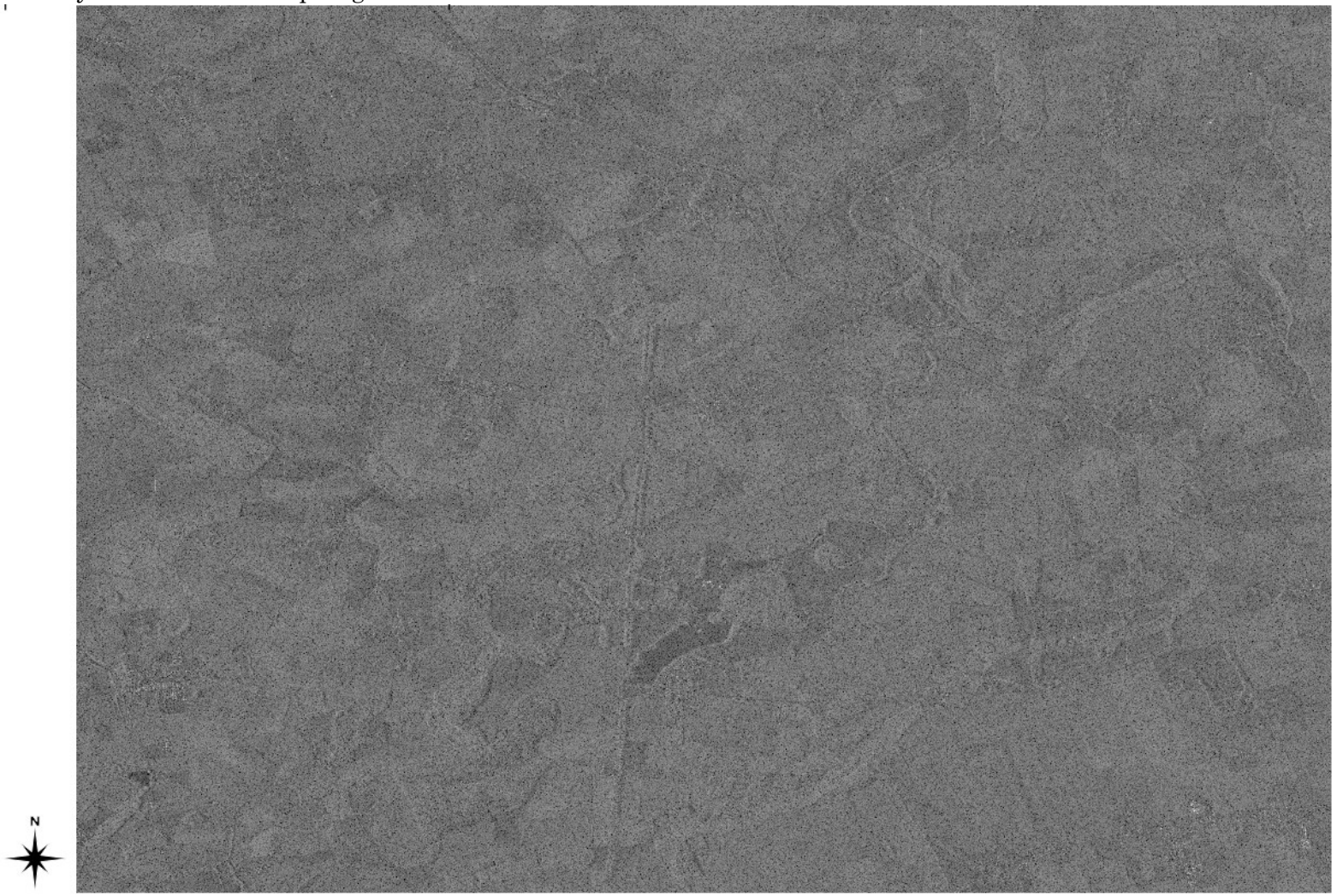

June – CSK2; HH;

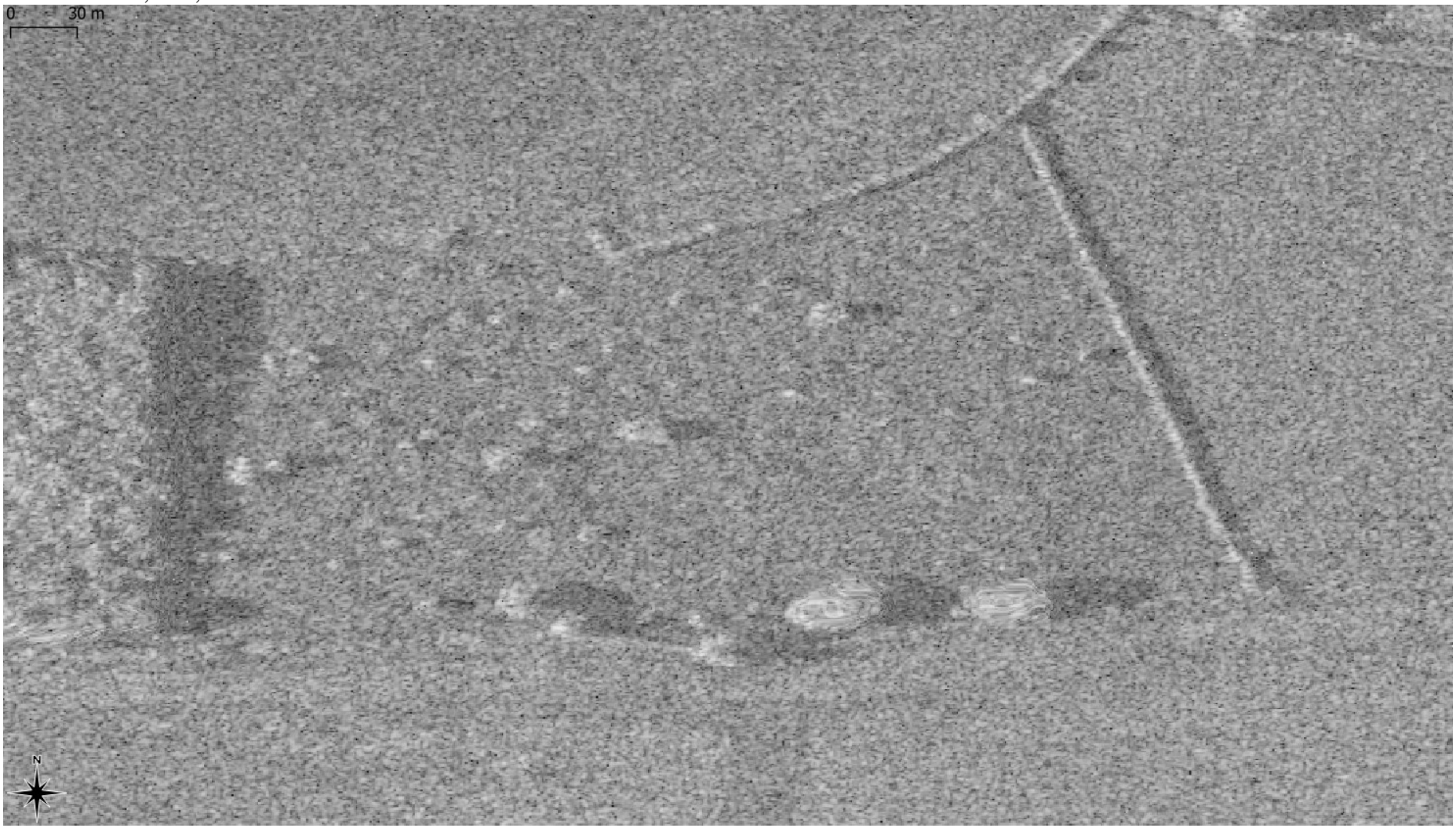

July – CSK4; HH;

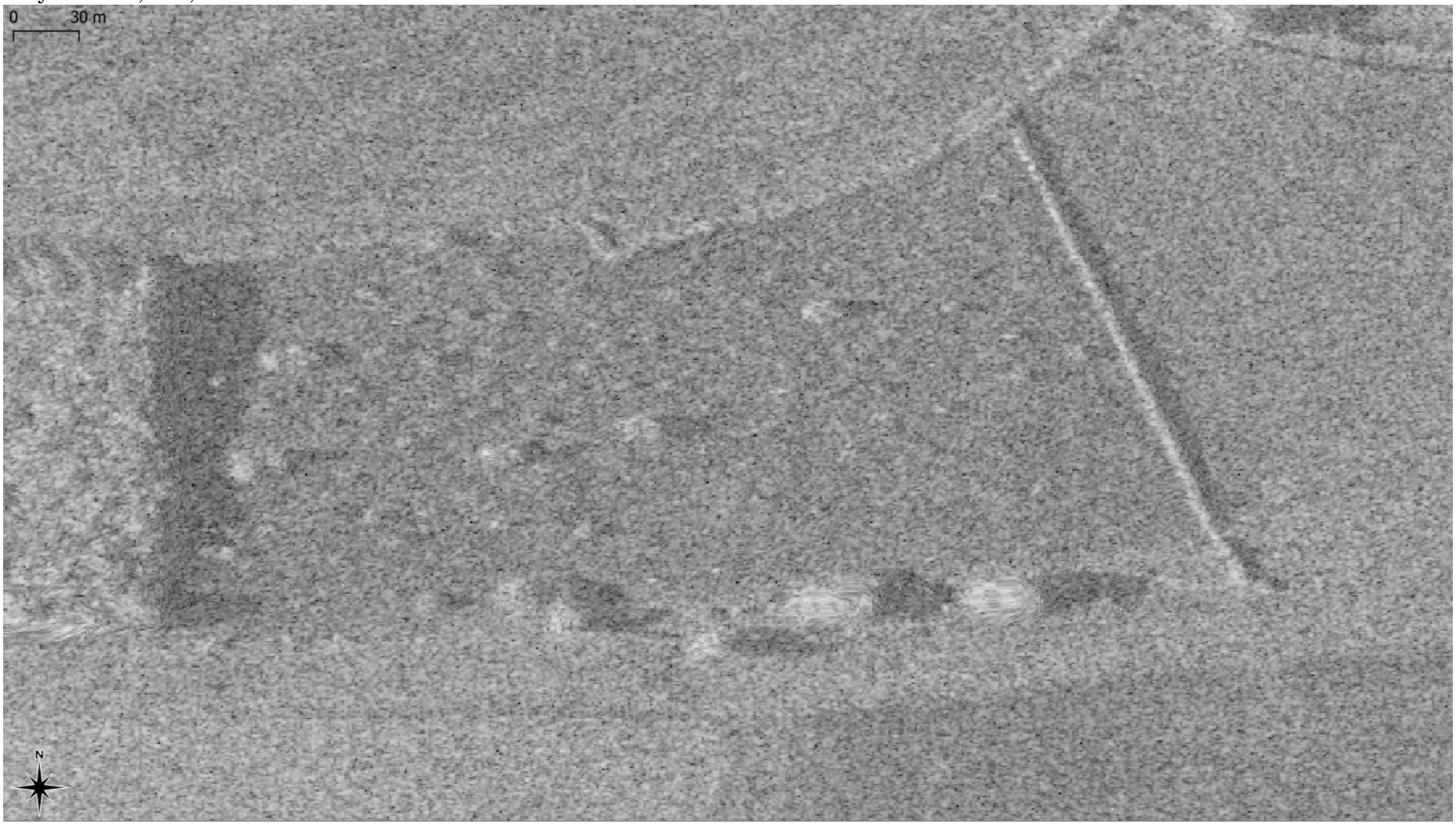

August – CSK4; HH;

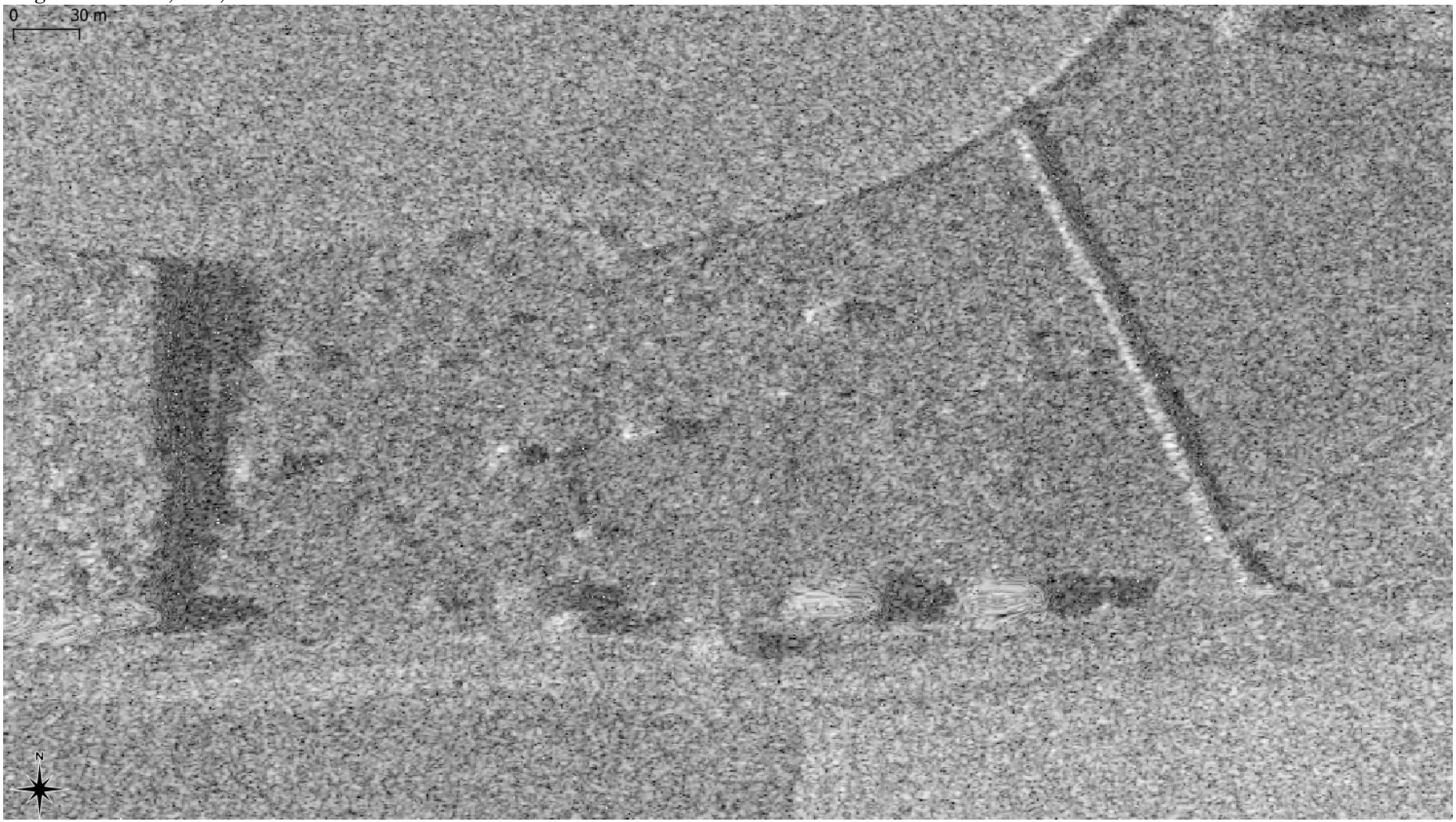

September – CSK3; HH;

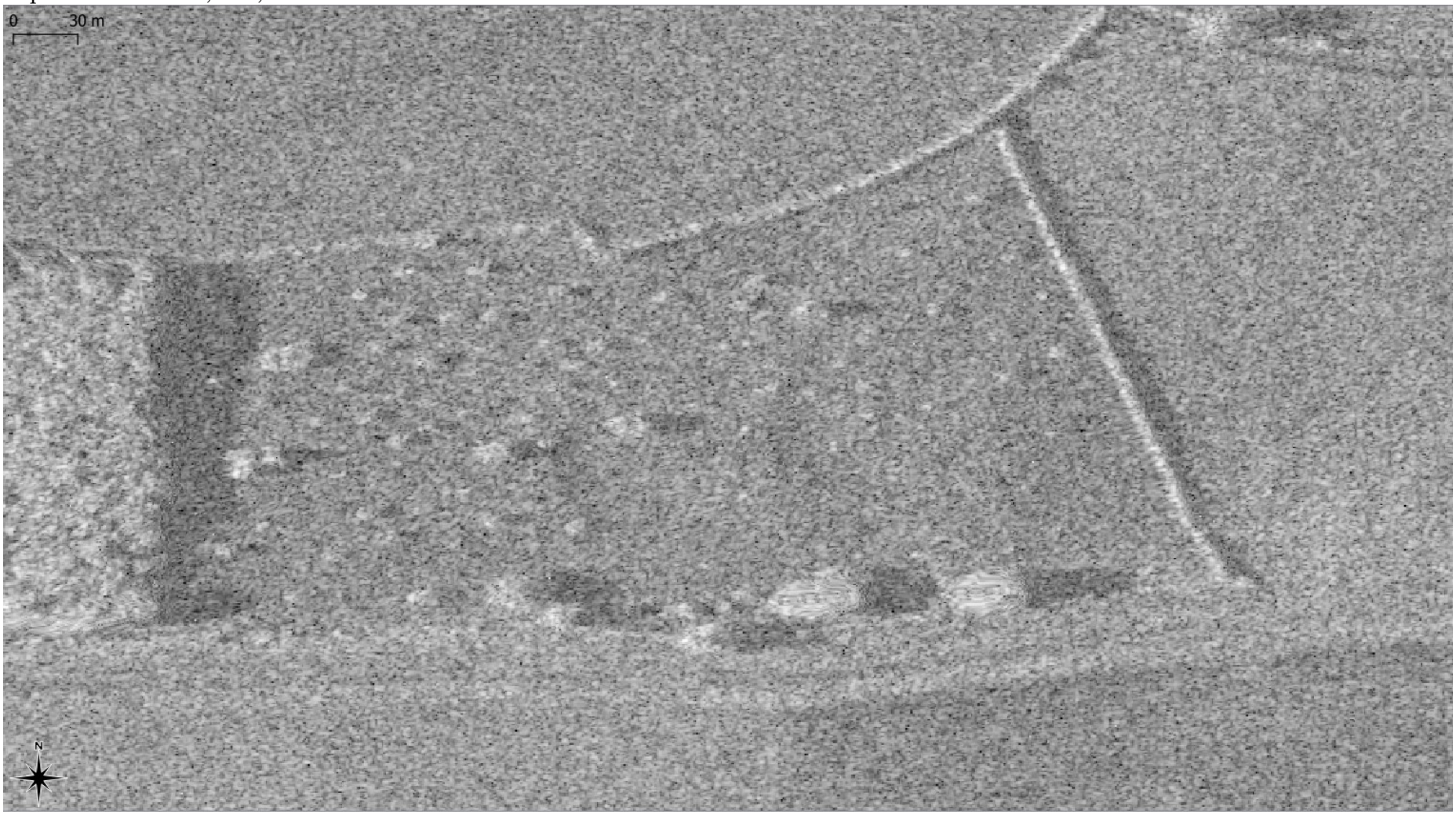

October – CSK4; HH;

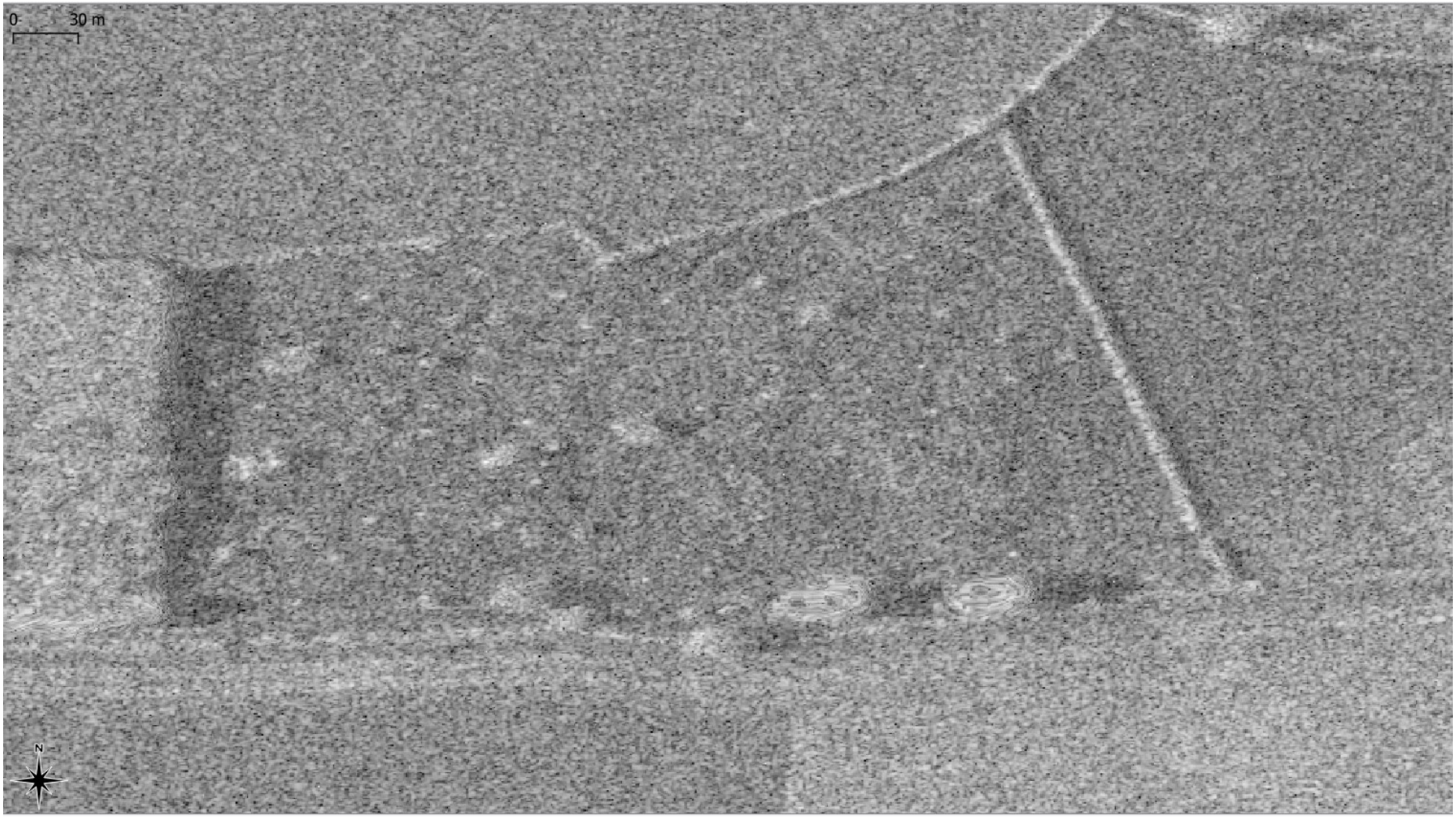

November CSK3; HH;

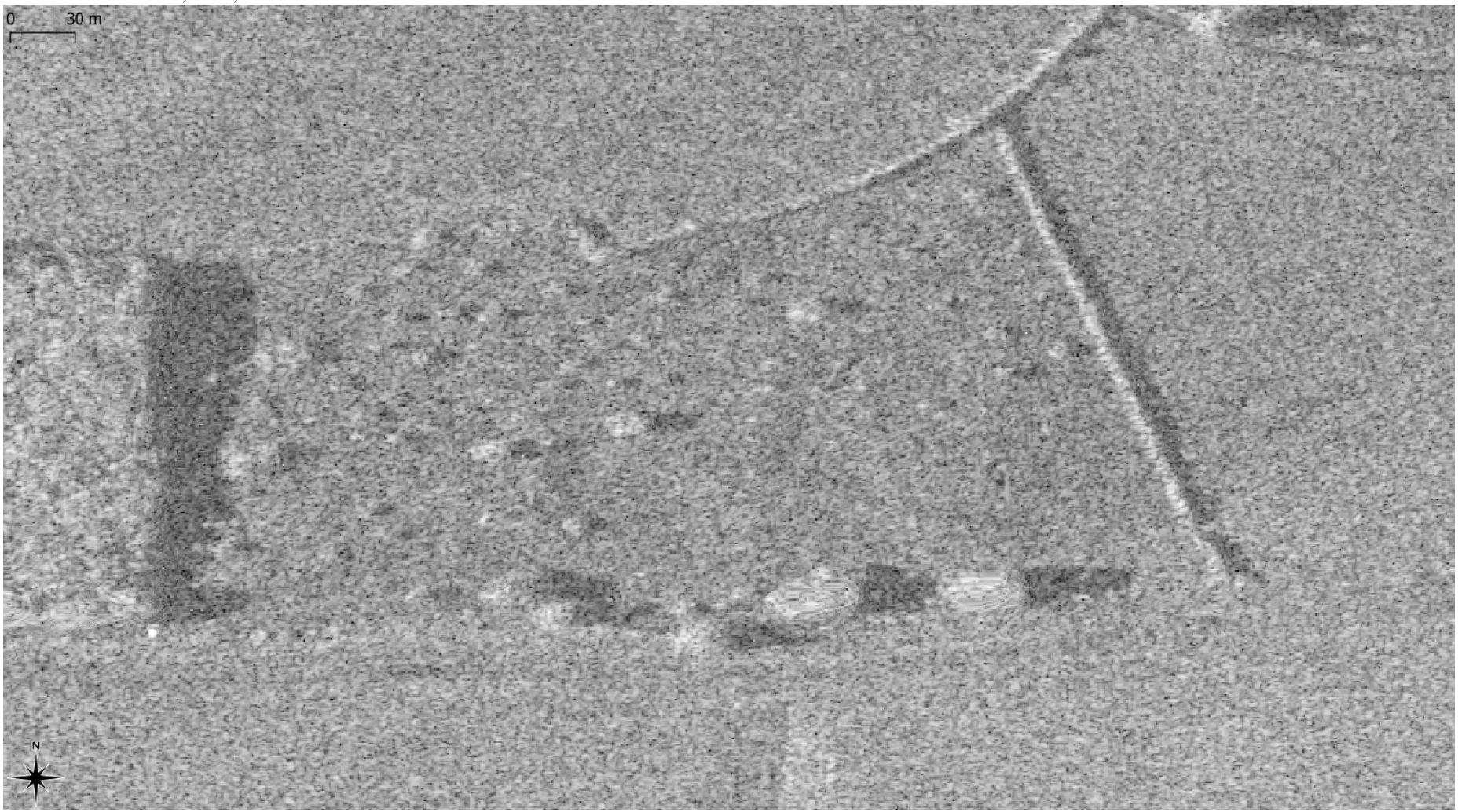

December – CSK4; HH;

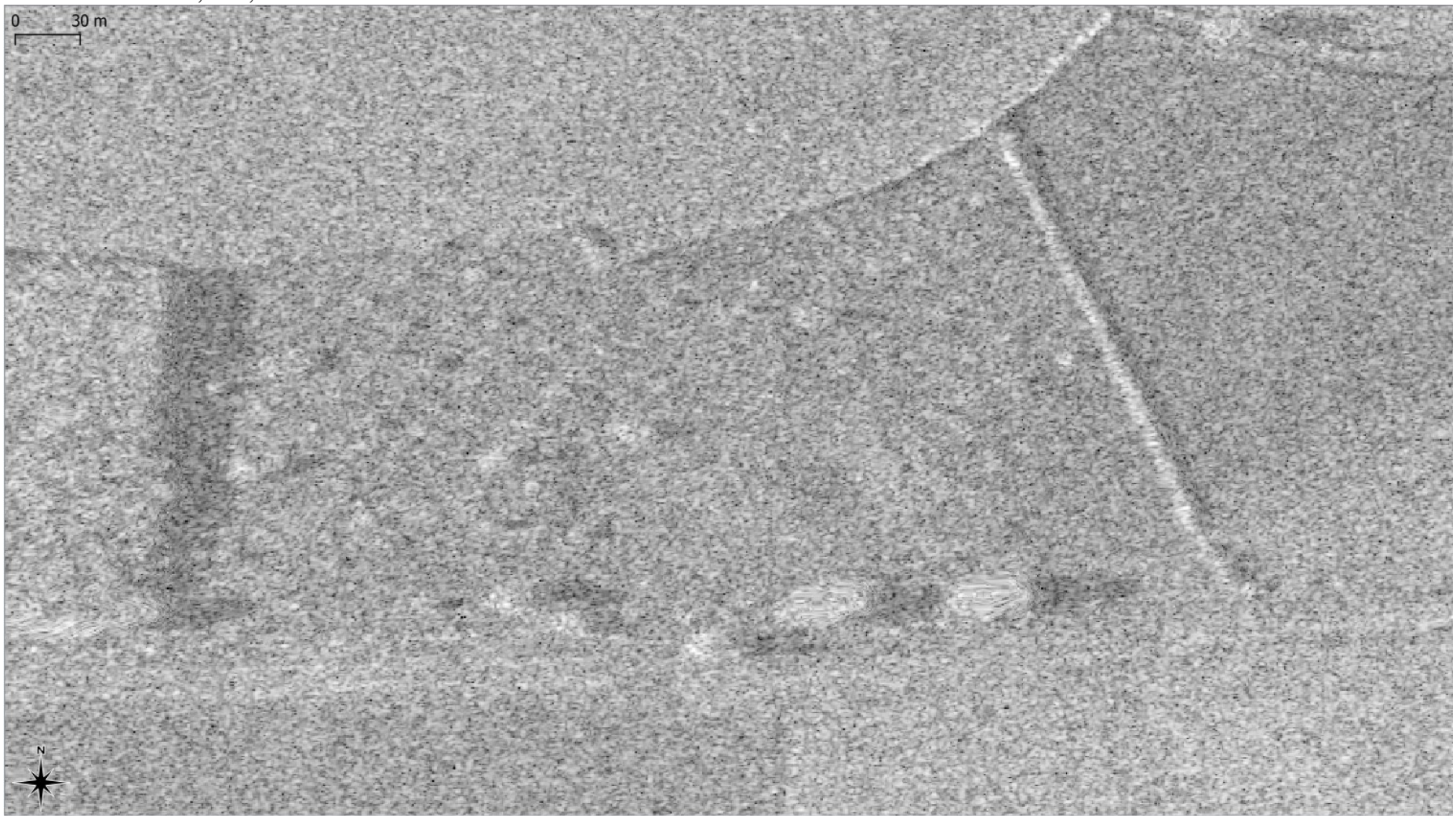

January - CSK3; HH;

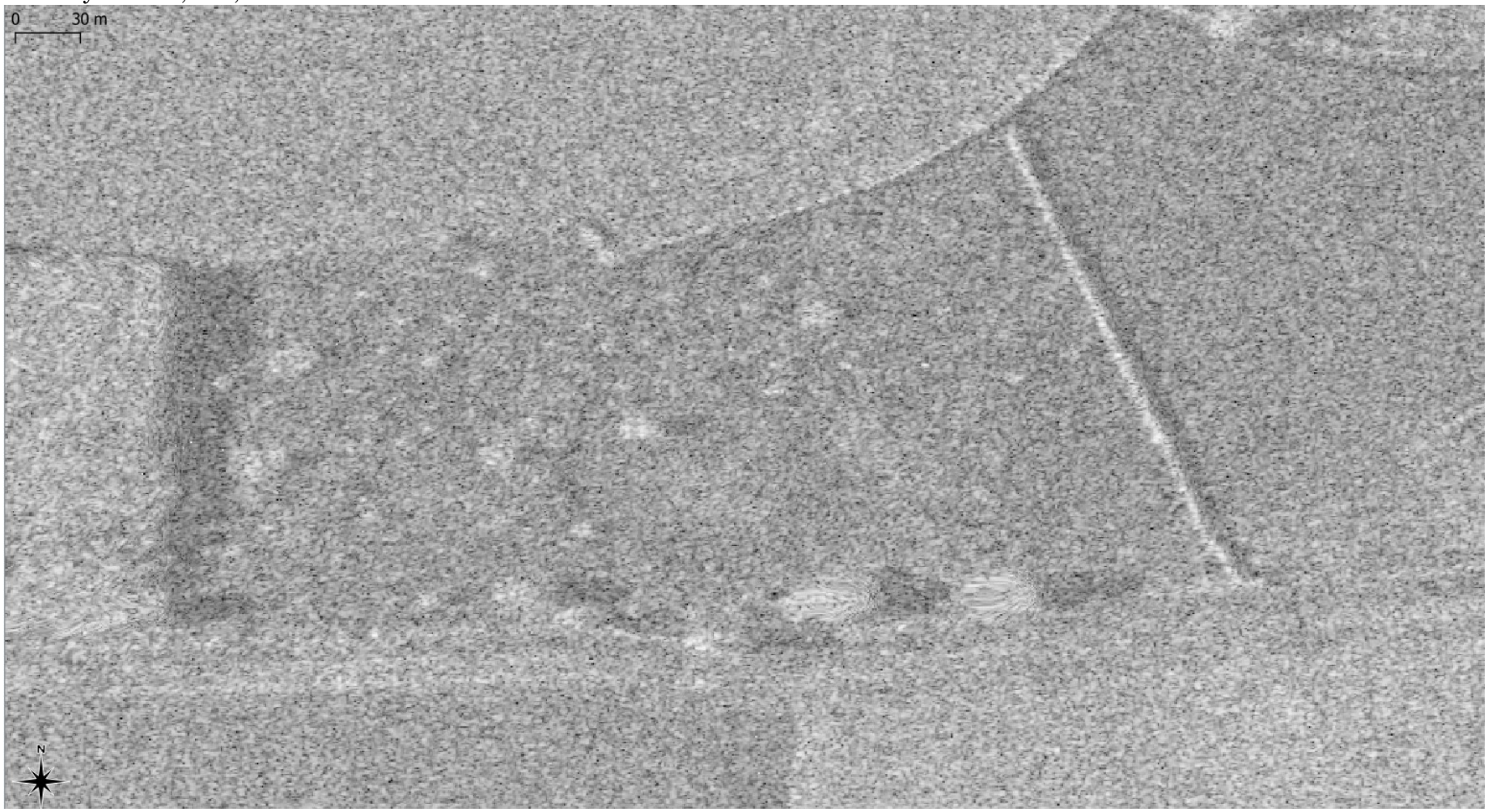


F

# Appendix 2 – COVID-19 Impact

As set out in chapter 1, there was some work that was curtailed due to the COVID-19 pandemic. This appendix briefly sets out the work not undertaken, the methods and rationale for the work, and the impact it would have had on the thesis if it had been undertaken.

There are several techniques that it was intended should be undertaken, but that it was not possible to undertake due to the Coronavirus pandemic, the closing of university facilities and the inability to safely conduct additional fieldwork. These further actions are, therefore, described and explained in the following section and the impact that it is anticipated that they would have had is set out.

## Surface roughness measurement

ACTIONS

As is well attested in the literature, surface roughness has a significant impact on backscatter values. It was intended to use surface profilometers to measure the roughness of the site both parallel to and perpendicular to the look direction of the satellite. Measurements were going to be taken in the area of each of the clusters at which the *in situ* ground truthing measurements had been taken. This work was planned for March 2020.

RATIONALE

It was recognised that a large proportion of the backscatter signal from the CSK would be caused by surface roughness. The intention was to explore how the quality of the estimation improved with surface roughness measurements. A pin-profilometer was chosen as this is a tool commonly used for this type of work (Davidson *et al.*, 2000; Verhoest *et al.*, 2008; Sahebi and Angles, 2010; Zribi *et al.*, 2019).

IMPACT

Doing this would have improved the understanding of the relationship between surface soil moisture and backscatter. Surface roughness has an impact on backscatter that is at least an order of magnitude greater than the impact of soil

moisture. To have surface roughness well established would have made the inferences of relationships between backscatter and soil moisture stronger. Having better relationships established would have enabled better definition of necessary DEM parameters in future.

## Radiometric modelling

It had been intended to take the radar processing further. The project did not use any form of backscatter modelling to improve soil moisture estimation.

Further application of backscatter models was not undertaken. This was due to the COVID-19 pandemic and restrictions this placed on training and processing opportunities. Additionally, there is an argument that because the relationships in the data are very limited already, modelling would have a limited capability to improve the results.

Our intention was to apply a physically based theoretical model. Physically based models account for the dielectric constant of the scattering surface. The disadvantage of these models is that they require *a priori* knowledge of surface roughness. Fung *et al.*'s (1994) Integral Equation Model (IEM) is the most well-known of these and is based on the Physical Optics Model (POM) (Born and Wolf, 1980; Song, Zhou and Fan, 2009).

There are three possible types of model, the small perturbation recently (Baghdadi *et al.*, 2002; Song, Zhou and Fan, 2009) for when surface roughness is small relative to the wavelength and slope is minimal. The physical optics model (Kirchoff model with scalar approximation is valid when the slope is small relative to the wavelength. Geometrical optics model (Kirchoff model under stationary phase approximation) is 'generally valid when the average radius of curvature and the vertical roughness are large relative to the wavelength' (Ulaby *et al.* 1986). Of these three options, the GOM is the most appropriate given the short wavelength (~3cm) and the relatively large roughness due to both vegetation and surface geometry.

The Geometric Optic Model (Kirchoff model under stationary phase approximation) was chosen because it has the best performance where roughness is large relative to the incident wavelength (Shi *et al.* 1991) – which matches the situation at Hollin Hill and is likely to be the case for almost all situations in

which X band SAR is used for monitoring the natural environment. The model is described thus:

$$\sigma^0_{ppn}(\theta) = \frac{\Gamma\,(0)\exp(-tan^2\frac{\theta}{2m^2})}{2m^2cos^4\theta}$$

where, m is RMS slope and Γ(0) is the 'Fresnel reflectivity evaluated at normal incidence' (Ulaby *et al.*, 1986)

It was intended to use the roughness estimates gathered during the final field campaign as an input for the roughness component of this equation.

The application of these models and assessment of the results from them could have given a stronger foundation for comparing the backscatter-soil moisture relationships derived in this study with those from other studies where these approaches have been used. Because some form of model is normally used in studies to relate backscatter and soil moisture, it is hard to assess how the un-modelled relationships in this study compare to those in other studies, because there are very few studies that present their data results without some form of modelling having been undertaken.